Elucidating the Mechanisms of T_H17 Cell Stability and Plasticity in Organ-specific Autoimmunity

Dissertation

with the aim of achieving the doctoral degree *Dr. rer. nat.* at the Faculty of Mathematics, Informatics and Natural Sciences in the Department of Chemistry, University of Hamburg

submitted by

Michael Zinke, M.Sc.

Hamburg, October 7, 2019

Dissertationsgutachter / *dissertation reviewer*:

1. Gutachter / *first reviewer*: **Prof. Dr. med. Wolfram Brune**,
Heinrich Pette Institute (HPI), Leibniz Institute for Experimental Virology,
Hamburg, Germany

2. Gutachter / *second reviewer*: **Prof. Dr. med. Samuel Huber**,
University Medical Centre Hamburg-Eppendorf, I. Department of Medicine and Polyclinic, Section for Molecular Gastroenterology and Immunology,
Hamburg, Germany

Vorgelegt von / *submitted by*: **Michael Zinke, M.Sc.**
Vorgelegt am / *submitted on*: October 7, 2019

Datum der Disputation / *date of thesis defense*: November 22, 2019

Datum der Druckfreigabe / date of print release: November 22, 2019

Diese Arbeit wurde im Zeitraum vom 15. Juni 2016 bis zum 30. August 2019 in der III. Medizinischen Klinik und Poliklinik / Transnationale Immunologie am Universitätsklinikum Hamburg-Eppendorf in der Arbeitsgruppe Autoimmun-vermittelte Nierenerkrankungen von PD Dr. med. Christian F. Krebs angefertigt.

This work was done in the period from 15th of June 2016 until 30th of August 2019 in the III. Department of Medicine / Translational Immunology in the University Medical Center Hamburg-Eppendorf in the research department autoimmune-related kidney diseases of PD Dr. med. Christian F. Krebs.

Universitätsklinikum Hamburg-Eppendorf

DFG Deutsche Forschungsgemeinschaft

SFB 1192 Immune-Mediated Glomerular Diseases

“*I think we're going to the moon because it's in the nature of the human being to face challenges. It's by the nature of his deep inner soul... we're required to do these things just as salmon swim upstream.*”

Neil Alden Armstrong
1930-2012

Den Helden, die vor 50 Jahren das Unmögliche erreicht haben.

Table of contents

Zusammenfassung

Die Niere stellt ein Organ mit vielen wichtigen Funktionen im menschlichen Körper dar. Eine dieser Aufgaben, neben der Synthese wichtiger Hormone und der Regulation des Wasser- und Elektrolythaushalts, ist die Entgiftung über den Urin. Sind diese Funktionen, etwa in Folge von Nierenerkrankungen, wie Glomerulonephritiden (GN), nachhaltig gestört, so kann dies lebensbedrohliche Auswirkungen haben. Neben verschiedenen Formen der GN, welche mit einer beidseitigen Entzündung der Nieren einhergehen und bei denen zunächst die Nierenkörperchen (Glomeruli) geschädigt werden, bilden die GN mit autoimmun-bedingter Genese, und hier speziell der T-Helferzellen (T_H-Zellen), einen wichtigen Anteil aller Nierenerkrankungen. T_H-Zellen sind, wie auch B-Zellen, ein elementarer Bestandteil des adaptiven Immunsystems des Menschen. Ihren Namen erhielten sie nach dem Ort, in dem sie reifen - dem Thymus. T_H-Zellen stellen eine spezielle Klasse von Lymphozyten dar, die B-Zellen die notwenige Unterstützung zur Aktivierung geben können, aber über Zytokine auch selbst direkt Entzündungsreaktionen steuern können.

Die klassische Unterteilung in T_H1- sowie T_H2- Zellen, die bis vor dem Jahr 2005 existierte, wurde durch die Entdeckung von IL-17-produzierenden T_H17-Zellen erweitert. T_H17-Zellen sind substanziell an der Regulierung von Entzündungsprozessen, bei der Abwehr von Bakterien und in autoimmun-vermittelten Erkrankungen beteiligt. Eine besondere Eigenschaft stellt die Fähigkeit dieser Zellen dar, in andere Zellen (T_H-Zellen, T-regulatorische (T_{Reg})-Zellen) zu transdifferenzieren. Diese als *T_H17-Plastizität* bezeichnete Eigenschaft scheint eine wichtige Rolle in der Pathogenese von autoimmune-vermittelten Erkrankungen wie Multiple Sklerose (MS) zu spielen. Bei einem Mausmodell der MS wurde eine erhöhte T_H17-Plastizität gefunden. Im Gegensatz dazu sind T_H17-Zellen in der GN relativ stabil. Es wurde zudem gefunden, dass T_H17-Zellen den Krankheitsverlauf der GN durch die Migration von Neutrophilen in das Nierengewebe vermitteln und so einen entscheidenden Faktor in der Pathogenese dieser Erkrankung darstellen.

Das Ziel dieser Arbeit war es, Mechanismen, die diese hohe T_H17-Stabilität in der GN begründen, aufzuklären und molekulare Ziele zu identifizieren, die die T_H17-Plastizität in der GN modifizieren und so ggf. als therapeutisches Agens dazu genutzt werden können, die Pathogenese der Erkrankung zu hemmen bzw. zu attenuieren.

Um dies zu realisieren, wurde ein unvoreingenommener Ansatz (*unbiased approach*) verfolgt. Dazu wurden in separaten Experimenten verschiedene Krankheitsmodelle (GN, EAE, α-CD3 Duodenitis, Infektion mit *Staphylokokkus Aureus*) induziert. Anschließend wurden mittels RNA-Sequenzierung differenzielle Genexpressionsmuster analysiert und zwischen den verschiedenen Modellen verglichen. Modelle mit hoher T_H17-Plastizität (z.B. EAE) wurden dem GN-Modell mit limitierter T_H17-Plastizität gegenübergestellt. Durch weitere Analysen und Vergleiche konnten so potentielle Ziel-Gene identifiziert werden, die möglicherweise Einfluss auf die T_H17-Plastizität haben. Als einen sehr interessanten Kandidaten selektierten wir den IL-27-Rezeptor α (IL-27ra). Ein weiteres Ziel dieser Arbeit war es, die Rolle der IL-27/IL-27r-Achse in der GN näher zu untersuchen.

Aus vorangegangen Studien ist bekannt, dass die IL-27/IL-27r-Achse, je nach Modell und Situation, sowohl pro- als auch anti-inflammatorische Immunmechanismen aktivieren kann. Um die Rolle dieses biochemischen Signalwegs in der GN zu entschlüsseln, wurden, nach Validierung der Sequenzierungsergebnisse mittels FACS-Analysen, NTN-induzierte IL-17A Reporter-Mäuse mit IL-27 behandelt. Hierbei konnte eine stark verminderte Pathogenität dieser mit IL-27-behandelten Mäuse im Vergleich zu PBS-behandelten Kontrollmäusen nachgewiesen werden. Allerdings konnte in den bisherigen Experimenten kein direkter Einfluss von IL-27 auf den Phänotyp von T_H17-Zellen nachgewiesen werden. Anschließend war es das Ziel, die hinter der verminderten GN-Pathogenese durch IL-27 liegenden biochemischen Signalwege zu verstehen. Dazu wurde der Anteil von phospho-STAT3 (pSTAT3) nach *in vitro*-Stimulation von Nierenzellen mit IL-27 bzw. IL-6 als Positivkontrolle gegen PBS-stimulierte Kontrollzellen ermittelt und miteinander verglichen. Dabei konnte eine leichte Erhöhung des pSTAT3-Anteils bei IL-6-Stimulation gegenüber PBS-Kontrollen, jedoch keine signifikante Erhöhung bei IL-27-Stimulation ermittelt werden, was mit dem allgemein hohen Anteil von pSTAT3 durch andere biochemische Signalwege zu erklären sein könnte.

Zudem konnte in weiteren *in vivo* Experimenten mit konditionalen *tbx21*-(Tbet) knockout-Mäusen gezeigt werden, dass dieser wichtige Transkriptionsfaktor in T_H1-Zellen keinen Einfluss auf die Pathogenität oder die Stabilität von T_H17-Zellen im NTN-Modell hat.

Abstract

The kidney is an organ with various important functions in the human body. One of those functions among the synthesis of important hormones and the regulation of the water and electrolyte balance is the detoxification via the urine. When these functions are disturbed over a longer period like in the case of glomerulonephritis (GN) diseases, life-threatening effects can occur. Among different forms of GN which go along with inflammation of both kidneys and where the renal corpuscles (glomeruli) are damaged, the GNs with autoimmune-related genesis and especially T helper cells (T_H cells) are an important proportion of all kidney diseases.

T_H cells are, like B cells, an elementary part of the human adaptive immune system. Their names originate from the location in the body where they mature – the thymus. T_H cells represent a special class of lymphocytes which can promote B cells in their activation but are also able to mediate inflammatory reactions themselves.

The classic subdivision into T_H1 and T_H2 cells which existed before 2005 was expanded by the discovery of IL-17-producing T_H17 cells. These cells are substantially involved in the regulation of inflammatory processes against bacteria and in autoimmune-mediated diseases. One feature of these cells is the ability to transdifferentiate into other cells like T_H1 and T-regulatory (Treg) cells. This property known as *T_H17 plasticity* seems to play a major role in the pathogenesis of autoimmune-mediated diseases like Multiple Sclerosis (MS). In a MS mouse model a higher T_H17 cell plasticity was found. In contrast, T_H17 cells in GN show more stable behavior. In addition, it was found that T_H17 cells mediate the course of the GN by recruitment of neutrophils into the renal tissue and therefore are an essential factor in the pathogenesis of this disease.

The aim of this work was the elucidation of mechanisms which could explain the high T_H17 cell stability in the GN and to find gene targets which are capable to modify the T_H17 cell plasticity as a potential therapeutic agent and thereby inhibiting or attenuating the pathogenesis of the GN.

In an unbiased experimental approach, different disease models like GN, EAE, α-CD3 duodenitis and infection with *Staphylococcus aureus* were induced in separated experiments.

By RNA bulk sequencing, differential gene expression profiles were analyzed between the different disease models. Models with higher T_H17 cell plasticity (like EAE) were compared to the GN model with limited T_H17 plasticity.

After further data analysis and comparisons, potential target genes which could have an influence on T_H17 cell plasticity were identified. As a very interesting molecular candidate the IL-27 receptor α (IL-27ra) was selected. Another aim of this work was the investigation of the IL-27/IL-27ra-axis in the GN.

From former studies, it is known that the IL-27/IL-27r-axis can activate both pro- and anti-inflammatory immune-mediated mechanisms depending on the model and experimental circumstances. In order to elucidate the role of this biochemical pathway in the GN, NTN-induced IL-17A reporter mice were treated with IL-27, after validation of our sequencing data by FACS analysis. Here, a strongly reduced pathogenesis in IL-27-treated mice compared to PBS-treated control mice could be verified. Although, in recent experiments a direct influence of IL-27 on the phenotype of T_H17 cells could not be found. Afterwards, it was aimed to understand the underlying biochemical pathways behind the reduced GN pathogenesis by IL-27 treatment. Here, the proportion of phospho-STAT3 (pSTAT3) of kidney cells after *in vitro* stimulation with IL-27 and IL-6 as a positive control was determined and compared to PBS-stimulated control cells. As a result, a moderate increase in the pSTAT3 proportion in IL-6-stimulated cells compared to PBS-treated control cells was found. Although, after IL-27 stimulation, a significant increase in pSTAT3 compared to control cells could not be verified. One reason for this finding might be the general high proportion of pSTAT3, caused by other biochemical pathways.

Furthermore, it could be shown in conditional *tbx21*- (Tbet) knockout mice that this essential transcription factor in T_H1 cell has no impact on the NTN-pathogenesis or T_H17 cell stability in this model.

Index of abbreviations

Acronym	Definition
ACR	Albumin-to-creatinine ratio
aqua dest.	(bi-) Distilled water
AF	Alexa Fluor
AHR	Aryl hydrocarbon receptor
APC	Allophycocyanine
BATF	Basic leucine zipper transcriptional factor ATF-like
Bcl11b	B cell lymphoma/leukemia 11b
BLIMP1	B lymphocyte-induced maturation protein 1
bp	Base pairs
BSA	Bovine serum albumin
BUN	Blood urea nitrogen
BV	Brilliant violet
c	Concentration
CD	Cluster of differentiation
CFA	Complete Freund`s Adjuvant
cGN	Crescentic glomerulonephritis
CKD	Chronic kidney disease
CXCR2	CXC-motif chemokine receptor 2
Da	Dalton (atomic mass unit)
DC	Dendritic cell
DDT	Dithiothreitol
DNA	Deoxyribonucleic acid
dNTP	Deoxynucleotide triphosphate
DPBS	Dulbecco’s phosphate buffered saline
EBI3	Epstein-Barr virus induced gene 3
EDTA	Ethylenediaminetetraacetic acid

EGTA	Ethylene glycol-bis(β-aminoethyl ether)-N,N,N′,N′-tetraacetic acid
ELISA	Enzyme-linked immunosorbent assay
ESRD	End-stage renal disease
ESRF	End-stage renal failure
EtOH	Ethanol
eYFP	Enhanced yellow fluorescent protein
FACS	Fluorescence-activated cell sorting
FCS	Fetal calf serum
FITC	Fluorescein isothiocyanate
fm	*Fate-mapped* T_H17 cells
FoxP3	Forkhead-box-protein 3
FCS	Forward scattering
g	G-force [m/s^2]
GBM	Glomerular basement membrane
gDNA	Genomic DNA
GFP	Green fluorescent protein
GFR	Glomerular filtration rate
GOI	Gene of interest
HBSS	Hank′s balanced salt solution
HD	Hemodialysis
HEPES	4-(2-hydroxyethyl)-1-piperazineethanesulfonic acid
Hif1a	Hypoxia-inducible factor 1α
HKG	Housekeeping gene
HLA	Human leucocyte antigen
HPRT1	Hypoxanthine-guanine phosphoribosyltransferase 1
HRP	Horseradish peroxidase
IFN-γ	Interferon gamma
Ig	Immunoglobulin
IL	Interleukin
ILC	Innate lymphoid cell

i.p.	Intraperitoneally
IR	Infrared radiation
IRF4	Interferon regulatory factor 4
ISN	International Society of Nephrology
IUPAC	International Union of Pure and Applied Chemistry
i.v.	Intravenous
IVC	Individually ventilated cage
Kat	Katushka (far-red fluorescent protein)
KO	(gene) Knockout
loxP	Locus of X-over P1
LPS	Lipopolysaccharides
min	Minutes
mA	Milli Ampere
mM	Milli molar (≙1mmol/L)
MOG	Myelin oligodendrocyte glycoprotein
MS	Multiple sclerosis
NIR	Near infrared
NK cell	Natural killer cell
NLR	NOD-like receptor
NTN	Nephrotoxic nephritis
OD	Optical density
PAS (staining)	Periodic acid-Schiff (staining)
PAMP	Pathogen associated molecular pattern
PCA	Principal component analysis
PCR	Polymerase chain reaction
PD	Peritoneal dialysis
PE	Phycoerythrin
PerCP	Peridinin-chlorophyll-protein
PFA	Paraformaldehyde
PMA	Phorbol 12-myristate 13-acetate

PMSF	Phenylmethylsulfonyl fluorid
PRR	Pattern recognition receptors
PTx	Pertussis toxin
RAAS	Renin-angiotensin-aldesteron-system
Rcf	Relative centrifugal force
RIN	RNA integrity number
RNA	Ribonucleic acid
ROSA26* /*R26	Reverse oriented splice acceptor, clone 26
RORγ	RAR-related orphan receptor gamma
RPGN	Rapid progressive glomerulonephritis
rpm	Revolutions per minutes
RPMI	Roswell Park Memorial Institute
RT	Room temperature
RUNX	Runt-related transcription factor 1
S. aureus	Staphylococcus aureus
sec	Seconds
SE-PE	Streptavidin-phycoerythrin
si	Small intestine
SLE	Systemic lupus erythematosus
SH2	Src homology 2 (domain)
SSC	Side scatter
tpm	Transcripts per million
STAT	Signal transducer and activator of transcription
SPF	Specific-pathogen-free
TB	Trypan blue
TCF-1	T cell-specific transcription factor 1
TGF-β	Transforming growth factor-β
TLR	Toll-like receptors
TMB	3, 3', 5, 5'-Tetramethylbenzidine
TNF-α	Tumor necrosis factor-α

Tris-HCl	Tris(hydroxymethyl)aminomethane hydrochlorid
UKE	Universitätsklinikum Hamburg-Eppendorf *(University Medical Center Hamburg-Eppendorf)*
v	Volt
vs.	Versus
wt	Wild type
YFP	Yellow fluorescent protein

List of tables

Table of figures

1 Introduction

1.1 The human immune system - Innate and adaptive immunity

The immune system is a complex combination of different effector cells and molecules in order to protect an organism from disease-causing microorganisms like bacteria, fungi, parasites and viruses and to remove those pathogens from the organism. Classically, this system is separated into the innate and adaptive immunity. Their members originate from myeloid and lymphoid cells. Components of the innate immunity are rather non-specific; however, they are able to very rapidly (minutes, hours) execute a strong immune response in order to eradicate potentially harmful pathogenic intruders by a variety of defense mechanisms. Members of the innate immunity are macrophages, granulocytes and the recently identified group of *innate lymphoid cells* (ILCs) that include natural killer (NK) cells. Macrophages, dendritic cells and neutrophils are an important group of sensor cells, that can recognize infections by which the innate immune system can be activated (Weaver, 2018). In addition, the latter are able to form so called *neutrophil extracellular traps* (NETs) which consist of extracellular fiber networks, primarily chromosomal neutrophil structures which are generated by a pathogen-induced cell death process, known as *NETosis*. As a result, these NETs can trap and eliminate pathogens like bacteria and fungi (Brinkmann et al., 2004; Gupta and Kaplan, 2016; Hoppenbrouwers et al., 2017; Remijsen et al., 2011).

Those previous described cells are able to detect so called damage-associated molecular patterns (DAMPs) like DNA, released by necrotic cells, as well as pathogen associated molecular patterns (PAMPs) as mannose-rich oligosaccharides, (lipopolysaccharides, LPS) via pattern recognition receptors (PRRs) like Toll-like receptors (TLRs) or NOD-like receptors (NLRs). Other receptors are also able to detect different mRNA or DNA structures and locations which is the case in viral infections. Detection of pathogens will eventually result in the activation of effector functions. Macrophages for example are known to protect the organism from bacteria by phagocytosis. They are also able to secret proteins which can affect other cells (like cytokines) or can activate the migration of other immune cells into the center of an inflammation (chemokines) in case of an immune response due to pathogens.

In contrast, the adaptive immunity reacts less rapid (days to weeks). The adaptive memory can last for years. The adaptive immune system displays a pathogen-(/antigen-) specific immunity response mechanism via lymphocytes. The latter are able to recognize and defend against a great variety of pathogen antigens. The recognition and binding of this huge variety of antigens is accomplished by highly variable antigen receptors on the surface of these cells. After maturation, each lymphocyte exhibits one special variant of antigen receptor. This leads to the expression of a great receptor variety among the lymphocyte population (Weaver, 2018). Here, Sir Frank Mcfarlane Burnet made important contributions to the field. With his *clonal selection theory* it was possible to explain this antigen receptor variety. He described that all antibody producing B- cells as well as T- cells are clones of one *mother cell* (Ada, 2008; Burnet, 1957).

B- and T cells can be distinguished by their immunological function as well as by the structure of their antigen receptors. B- cell antigen receptors are produced by the same genes which encode the antibodies, a group of proteins also called immune globulins (Ig′s). The latter are proteins which can very specifically (non-covalently) bind to distinct substances – their antigen. Although, they have a high specificity they all originate from a small group of different Ig sub structures like IgG, IgA, IgM and others. Antibodies do not recognize the whole antigen but rather small and very specific regions called *epitopes*. The sequestration of antibodies can have different immunological consequences like activation of another innate immune mechanism called the *complement system*, *opsonization* (enveloping) of pathogens which leads to antigen neutralization or phagocytosis (*digestion*) of pathogens. The antigen blocking causes masking of this antigen which eventually leads to inhibition of further cell interaction as well as other effects.

However, B cells mature in the **b**one marrow or **b**ursa fabricii in chicken which lead to their name **B** cells. The latter are part of the adaptive humoral immunity which is mediated by macromolecules like anti-microbial peptides, proteins of the complement system and antibodies found in extracellular fluids. Among their function as antibody producers, like dendritic cells, B cells are able to represent antigens to other immune cells. Hence, they belong to a group of so called *professional antigen presenting cells* which also include dendritic cells and

macrophages. For presentation, antigen peptides are loaded onto major histocompatibility complex (MHC) molecules which are presented to T cell receptors. Furthermore, B cells can secrete cytokines which are essential cell signaling proteins in immunity.
The latter is also accomplished by **T** cells which originate from bone marrow progenitors as well. In contrast to B cells, T cells migrate to the **t**hymus in order to undergo maturation, further selection and subsequent export to peripheral tissues. They belong to the *cell-mediated immunity*.
T cell activation is mediated via the T cell receptor (TCR) and requires two signals. First, the binding to an antigen (epitope), presented on MHC molecules, as well as a number of co-inhibitory signals, provided for example by CD28, a surface molecule on T helper cells which initiates T cell proliferation.
In addition, the T cell activation leads to further immunological effector functions described in more detail below (**1.2**).

Another important hallmark of the immune system is the ability to establish an immunological memory which helps to generate a rapid and effective immunological response against a second encounter with the same antigen. There are B- as well as T- memory cells. Representatives are for example tissue-resident memory cells, central memory cells and effector memory cells.

1.2 T helper cells and selected $CD4^+$ subsets

In the course of T cell development, bone marrow progenitors migrate to the thymus for further selection. Here, they undergo selection to exclude self-reactive T cells as well as distinct surface molecule selection, mainly in cluster of differentiation (CD) 4^+ and $CD8^+$ T cells (Koch and Radtke, 2011; Zuniga-Pflucker, 2004).
During this process, T cells mature from $CD4^-CD8^-$ double negative to $CD4^+CD8^+$ double positive cells which will become single positive $CD4^+$ and $CD8^+$ T cells eventually. The commitment to the CD4 or CD8 T cell linage depends on the binding of the alpha beta ($\alpha\beta$) TCR to MHC class I or II molecules. The binding of $\alpha\beta$ TCR MHC I interaction will lead to $CD4^-CD8^+$ T cells which are essential for the

immunological defense against intracellular pathogens including bacteria and viruses. $CD8^+$ T cells are also called *cytotoxic T cells (Weaver, 2018)*.
However, interaction with MHC II molecules will lead to $CD4^+$ single positive T cells.

Among the great variety of T cells, the following short overview will give an insight with regard to important T_H17 cell plasticity-related T cells.

1.2.1 T_H1 and T_H2 cells

In the 1980`s, Coffman and Mosmann published two papers in which they proposed the T_H1/T_H2-hypothesis which divided the known $CD4^+$ T helper subpopulations according to their expressed cytokine profiles, which define their cellular and immunological function (Mosmann et al., 1986; Mosmann and Coffman, 1989).
They proposed the separation into interferon-gamma (IFN-γ)-producing T_H1 cells which induce cell-mediated inflammatory responses and are deepened on STAT1 expression and IL-4-producing T_H2 cells which are depended on STAT6 and provide B cell helper functions.
This important paradigm served immunology for almost 20 years and led to a better immunological understanding. However, new T helper subsets were identified who could fill immunological questions with answers which could not be accomplished by the T_H1/T_H2 model.

T_H1 cells
Type helper cells are important against infection via bacteria and some viruses as well as well as protozoa and fungi. Furthermore, they are able to secrete IFN-γ, IL-2, TNF-α and β. The latter is very important in the activation of macrophages as well as phagocyte-dependent immunity. As the master regulator, T_H1 cells use *tbx21* which encodes a protein called Tbet. The latter is essential for IFN-γ production in T cells (Singh et al., 2017).
In addition, T_H1 cells require IL-12 and IFN-γ for their differentiation which activate the STAT4 signaling pathway (Trinchieri, 2003). Here, STAT4 seems to be

essential for Tbet-mediated T_H1 cell differentiation. Furthermore, T_H1-related immune responses are found to be important in the pathogenesis of organ-specific autoimmune disorders like Crohn`s disease and others (Brand, 2009).

T_H2 cells

T_H2 effector functions are crucial for immune responses against extracellular parasites like gastrointestinal nematodes (e.g. helminths). They are also responsible for eosinophil activation, strong antibody production like IgG_{2A} which is important for bacteria opsonization in mice as well as inhibition of several macrophage functions. These cells secrete IL-4, IL-5, IL-13, IL-21 as well as IL-10. Some important transcription factors are GATA3, STAT5 and STAT6.

1.2.2 T regulatory cells

In general, $CD4^+$ T cells can be divided into two functional subsets. Effector T cells which are responsible for protection against pathogens. These cells show high ability to induce a strong and efficient immune response. On the other site of this spectrum there are $CD4^+$ T cells which regulate and if necessary suppress the immune response by inhibition of cell proliferation and cytokine production. These cells are called *T regulatory* (Treg) cells. Thus, they also play an essential role in prevention of self-tolerance breakdown, also called *auto-immunity* (Hori et al., 2003).

Among regulatory T cells, there are several subpopulations, like $CD4^+CD25^+$ T regulatory cells, $T_R1$cells, $CD8^+$ regulatory T cells and T_H3 lymphocytes (Weaver, 2018). In addition, recently so called *Tr17 cells* were identified (Kim et al., 2017).

$CD4^+$ $CD25^+$ Treg cells

These Treg cells show expression of their key transcription factor *forkhead box protein 3* (FoxP3). In flow cytometry, they can further be identified by their high surface expression of IL-2 receptor, also called CD25 ($CD25^{high}$) as well as low CD127 expression ($CD127^{low}$).

After activation, these cells are capable to produce IL-4, IL-10 and TGF-β which seem to be involved in regulatory effector functions.

It was shown that replacement of Treg cells led to autoimmunity in multiple organs which could be reversed by adoptive transfer of $CD4^+$ $CD25^+$ cells (Sakaguchi et al., 1995).

T_R1 cells

Cells of this subpopulation are characterized by production of L-10, IFN-γ, IL-5 and transforming growth factor (TGF)-β but no production of IL-4 or IL-2. Importantly, they do not express FoxP3. Furthermore, they also show suppression via a IL-10-dependend autocrine pathway. In addition, it was found that IFN-γ, also produced in T_H1 cells, can suppress the production of IL-17 which is thought to be another immune-regulatory effector function of Treg cells (Langrish et al., 2005; Murphy et al., 2003). Moreover, TGF-β/IL-10 was shown to suppress pro-inflammatory immune responses via both T_H1 and T_H2 cells. T_R1 cells also show the ability to suppress B cell-mediated antibody production (Weaver, 2018).

Tr17 cells

Recently Kim et al. identified another regulatory T cell population called *Tr17 cells*. These $ROR\gamma t^+FoxP3^+$ cells were induced in lymph nodes and seem to be generated from thymic Treg cells via STAT3 upon antigen-specific activation. Furthermore, they suggest that these Tr17 cells could play a pivotal role in the regulation of T_H17 cell-dependent autoimmunity (Kim et al., 2017).

In addition, Huber et al. could show, that IL-17A-producing $CD4^+$ T cells are able to express the IL-10 receptor α (IL-10Rα). Further, they could show that the T cell-specific inhibition of IL-10 signaling increased IL-17A-producing and IL-17A/IFN-γ double producing cell populations in a mouse model of small intestinal inflammation. The group could also show that $FoxP3^-$ Tr1 cells as well as $FoxP3^+$ Treg cells were able to suppress both T_H17 IL-17A-single producing cells and T_H17/T_H1 IL-17A/IFN-γ double producers via IL-10. These findings directly showed that IL-10 is an essential suppressor for T_H17 and T_H17/T_H1 cells (Huber et al., 2011).

1.2.3 γδ-TCR cells

In contrast to other T cells which contain T cell receptors composed of αβ-glycoproteins, gamma delta (γδ) T cells (or γδ-T cell receptor, γδ-TCR) cells provide receptors composed of one γ and one δ chain.
Additionally, most of the γδ-T cells are activated in an MHC-independent manner. Their different effector functions show abilities to directly affect pathogenic targets by their cytotoxic activity (e.g. by cytolysis or production of granulysin, an effective anti-microbial protein) or indirectly by activation of other immune cells (Lawand et al., 2017). Thus, γδ-T cells contribute to both innate and adaptive immunity.

Among T_H17 cells, γδ-TCR cells are also able to produce IL-17 as well as IFN-γ and TNF-α. Furthermore, IL-17 produced from both T_H17 cells and from γδ T cells seem to be important in kidney injury in crescentic glomerulonephritis - cGN (Turner et al., 2012).

1.2.4 T_H17 cells

In 2005 $CD4^+$ T_H17 cells were identified as a T helper linage distinct from T_H1- and T_H2 cells (Harrington et al., 2005).
Since the discovery of IL-17-producing T_H17 cells, these cells were closely related to (1) their induction via interleukin 23 (IL-23) and (2) their role in infection and inflammation (Harrington et al., 2005; Langrish et al., 2005; Park et al., 2005).

In addition, many studies proved the pivotal role of T_H17 cells in autoimmune-mediated diseases such as psoriasis, rheumatoid arthritis, multiple sclerosis and chronic kidney disease – CKD (Krebs et al., 2016b; Langrish et al., 2005; Nakae et al., 2003; van der Fits et al., 2009).
T_H17 cells were originally described as a IL-23-induced cell population with a unique inflammatory gene signature which encompass different IL-17 genes (IL-17 isoforms see **1.2.4.1**), *IL6*, *Csf2* (encoding *colony-stimulating factor 2* which is also known as GM-CSF), *Ccl20* (encoding CCL20), *Tnf* (encoding tumor necrosis factor, TNF), *Il23r* (encoding IL-23 receptor, IL-23r) and *Il1r1*

(encoding IL-1 receptor type 1, IL-1r1). Furthermore, T_H17 cells were characterized by their expression of CCR6 and signal transducer and activator of transcription (STAT) 3 and their main transcription factor *RAR-related orphan receptor gamma t* (RORγt) encoded by *Rorc* (Acosta-Rodriguez et al., 2007; Langrish et al., 2005).

Among RORγt which was identified as a T_H17-defining transcription factor, there is another isotype called RORα (Ivanov et al., 2006; Matysiak-Scholze and Nehls, 1997). It was further shown that these isoforms are generated by alternative exon splicing as well as usage of different promoter (Matysiak-Scholze and Nehls, 1997; Villey et al., 1999).
Here, RORγt plays an essential role for IL-17 production, not only in T_H17 cells. It is also expressed in other IL-17-producing cells (see below).
With regard to the immune system, RORα is expressed in lymphoid and myeloid cells and is furthermore also induced in T_H17 cell differentiation (Dzhagalov et al., 2004a; Dzhagalov et al., 2004b). In addition, it was shown that RORα has some abilities as a negative regulator of NF-κB-related inflammatory responses (Delerive et al., 2001).

In addition, more transcription factors were found in T_H17 cells: *Runt-related transcription factor 1* (RUNX1), important in generation of hematopoietic stem cells and further (T) cell differentiation, *basic leucine zipper transcriptional factor ATF-like* (BATF), *aryl hydrocarbon receptor* (Ahr), *interferon regulatory factor 4* (IRF4), and c-maf, an important anti-inflammatory IL-10-inducer. Key transcription factors are also involved in T_H17 cell differentiation as described in detail in **1.2.4.1**.

For further experiments it is of note that T_H17 cells are $CD4^+$ $CD3^+$ γδ-TCR^- cells.

1.2.4.1 IL-17 isoforms and T_H17 cell differentiation

The cytokine IL-17A was long known before the designation "T_H17 cells" (from its signature cytokine IL-17) and was scientifically established by Harrington et al. in 2005. In 1993, IL-17A (formerly known as *CTLA-8*) was cloned and in 1993 the first

IL-17-binding receptor was discovered (Gaffen et al., 2014; Rouvier et al., 1993; Yao et al., 1995a; Yao et al., 1995b).
Although T_H17 cells are known for effector functions, related to defense against clearance of extracellular pathogens and fungi, the different IL-17 isoforms can perform a variety of different immune functions.

By screening of homologous genes, further IL-17 isoforms were identified, namely: IL-17B, IL-17C, IL-17D, IL-17E (also known as IL-25) and IL-17-F. It was also found that IL-17A and IL-17F which are the best understood IL-17 isoforms, share the highest homology in terms of sequence among the whole IL-17 family. The genes encoding both cytokines are located in close proximity to each other on the same chromosome, in human and mice (Wang et al., 2012b). Further, they both signal via the IL-17RA/RC receptor heterodimer.
Although, both isoforms are known for their pro-inflammatory responses their functionality is depended on the site and type of inflammation (Ishigame et al., 2009).
With the least sequence similarity compared to IL-17A, IL-25 (IL-17E) is more known for its T_H2-regulatory responses against allergic inflammation and helminthic parasites (Fort et al., 2001; Owyang et al., 2006).
IL-17B has been shown to have an anti-inflammatory function during mucosal inflammation (Reynolds et al., 2015). However, in murine models it was shown that IL-17B mediated via IL-17 receptor B (IL-17RB) promoted survival, migration and proliferation of cancer cells (Bie et al., 2017; Wu et al., 2015). In line with these findings in mice, humans with high IL-17B has shown poor prognosis in breast or lung cancer (Laprevotte et al., 2017; Yang et al., 2018). However, IL-17C and IL-17D are rather elusive with regard to their biological functions. But recently studies in patients with severe autoimmune-mediated chronic kidney disease (ANCA-GN) showed elevated IL-17C levels in blood serum (Krohn et al., 2018).
In an according animal model it was found that IL-17C deficiency had positive clinical outcomes in mice which implies a significance in this condition.

IL-17 signaling is accomplished by a number of different IL-17 receptors (IL-17R), as depicted in **Figure 1**. All so far identified IL-17 receptors share a common

cytoplasmic motif, called *similar expression of fibroblast growth factor* (SEFIR) domain. Further, they consist of an inhibitory *C/EBP-β activation* domain *(CBAD)*.

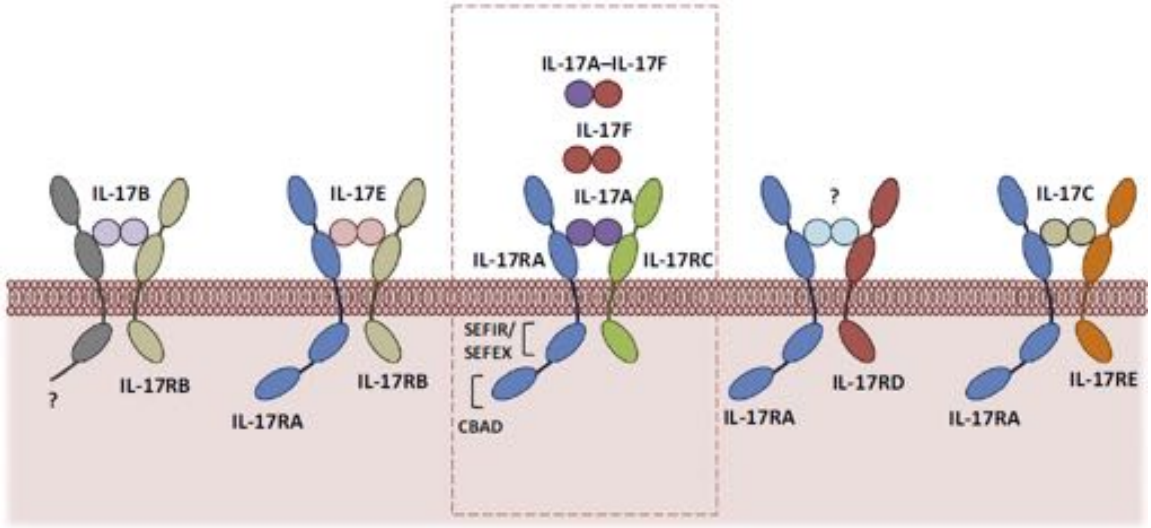

Figure 1: IL-17 signaling via IL-17 receptor family

In order to perform IL-17 signaling by the different isoforms (IL-A to -F), a group of different IL-17 receptors were identified as illustrated here. These receptors share a common cytoplasmic motif, called *similar expression of fibroblast growth factor* (SEFIR) domain. It was found that there is a common subunit (IL-17 receptor a, IL-17RA) for all known IL-17 receptors. The latter consist of an inhibitory *C/EBP-β activation* domain - CBAD. (Illustration adopted from Amataya et al., 2017)

In addition to T_H17 cells, also other immune cells show ability to produce IL-17. For example, innate immune cell subsets like some natural killer T (NKT) cells, γδ-TCR cells, TCRß$^+$ cells as well as type 3 *innate lymphoid cells* (ILC3s) and CD8$^+$ "Tc17" cells (Amatya et al., 2017; Cua and Tato, 2010).

IL-23, IL-6, TGF-β and transcription factors in T_H17 cell differentiation

Since the beginning of research on what was later called *T_H17 cells*, it was known that IL-23 is able to promote the secretion of IL-17 in activated T cells (Aggarwal et al., 2003). Furthermore, it was shown that *IL23a*$^{-/-}$ mice have only few cells which are able to produce IL-17 (Langrish et al., 2005; Murphy et al., 2003). Later it was found that IL-23 is indispensable for promoting autoimmunity in other models (Cua et al., 2003; Kastelein et al., 2007; Parham et al., 2002).

Although, IL-23 was able to induce IL-17 production, IL-23 alone was not sufficient to drive T_H17 cell differentiation from naïve $CD4^+$ T cell precursors (Bettelli et al., 2006). This led to the assumption that other factors were necessary for T_H17 linage fate decision.

In 2006, different groups were able to show that addition of IL-6 as well as TGF-β during T cell recognition via antigen contact promoted T_H17 cell differentiation (Bettelli et al., 2006; Mangan et al., 2006; Veldhoen et al., 2006). Further studies revealed the importance of STAT3 activation via IL-6 during this differentiation (Yang et al., 2007). As a result, STAT3 directly mediates the transcription of T_H17 linage-specific genes including *Rorc*, *Il23* and *Il17*. In addition, STAT3 activation leads to inhibition of expression of the important T regulatory transcription factor FoxP3 and thus suppresses the generation of T regulatory (Treg) cells, illustrated in **Figure 2**.

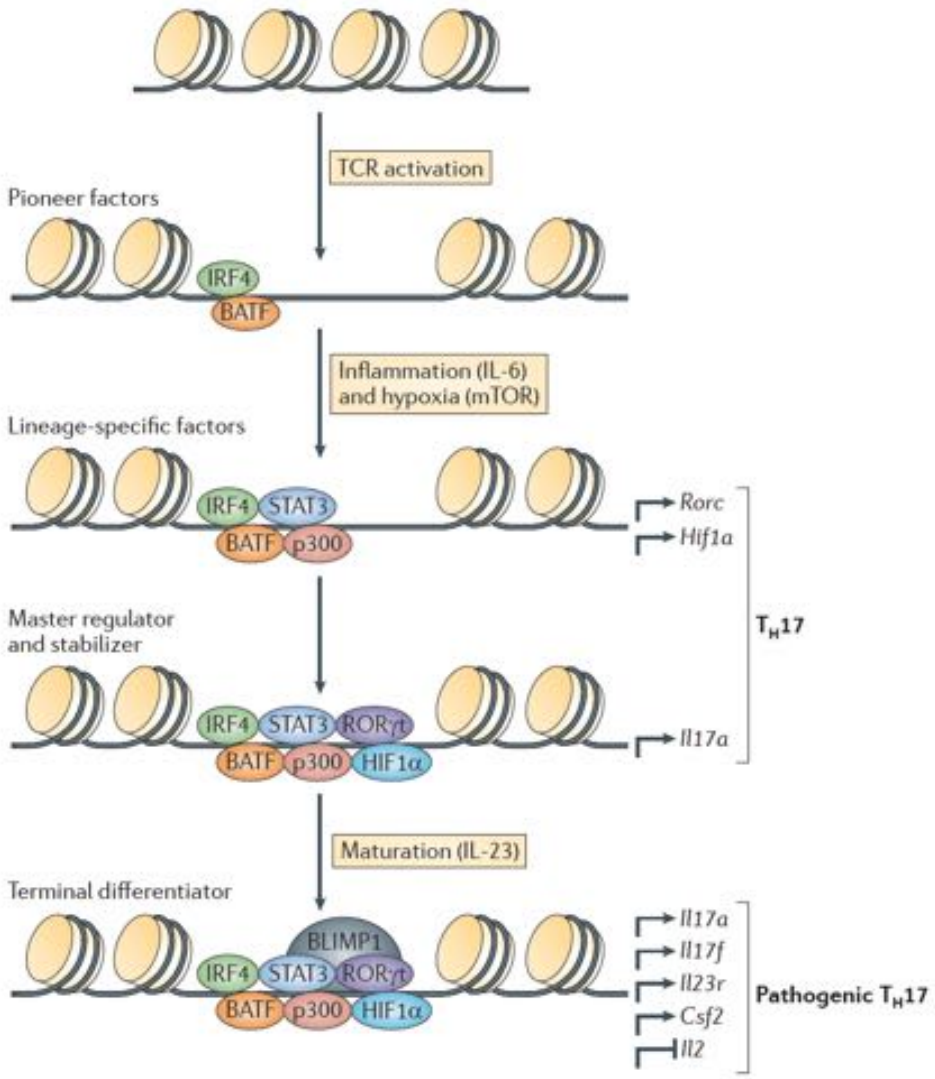

Figure 2: Transcription factor regulation during T_H17 cell differentiation

After initial TCR activation, the transcription factors interferon regulatory factor 4 (IRF4) and basic leucine zipper transcriptional factor ATF-like (BATF) mediate the accessibility of the chromatin structure. Next, STAT3 and the co-activator histone acetyltransferase p300 both promote the gene expression of *Rorc* and hypoxia-inducible factor 1α (*Hif1a*), followed by expression of *Il17a*. Further IL-23 exposure leads to activation and recruitment of *B lymphocyte-induced maturation protein* 1 (BLIMP1). BLIMP1 then binds to the STAT3-RORγt complex, resulting in expression of further T_H17-related signature genes. (Illustration adopted from Gaffen et al., 2014).

Control of gene expression does not only depend on binding of specific transcription factors but also and initially on the accessibility of chromatin structures. The latter is controlled by packaging of DNA and nucleosomes (forming the chromatin) within the cell nucleus.

It was shown that the initial step after TCR signaling during T_H17 cell linage specification is performed by IRF4 and BATF (Ciofani et al., 2012; Li et al., 2012). These proteins cooperatively bind to open the closed chromatin (heterochomatin) and make it accessible for further gene expression-related processes. The open chromatin structure is called euchromatin. In recent studies it was also shown that this initial step is important also for early T cell fate decisions, mediated by two proteins called T cell-specific transcription factor 1 - TCF-1, encoded by *Tcf7,* and B cell lymphoma/leukemia 11b - BCL11B, encoded by *BCL11b* (Hu et al., 2018; Johnson et al., 2018). However, in T_H17 cells it was found that the latter restrain T_H17 cell immunity by inhibition of IL-17 gene expression (Zhang et al., 2018). These findings imply a chromosomal-modifying, epigenetic role in T_H17 cell linage commitment.
After chromatin remodeling by BATF and IRF4, STAT3 mediates transcription of T_H17 genes via the co-activator histone acetyltransferase p300 which further promotes the transcription of *Rorc*. Here, also *hypoxia-inducible factor 1a* (*Hif1a)* is expressed upon TCR activation which is important for further gene expression. Continuous IL-23 exposure recruits and activates *B lymphocyte-induced maturation protein 1* (BLIMP1) which then binds to the STAT3-RORγt complex and initiates further expression of T_H17-related signature genes as well as repression of other T cell genes.

As a poof of principle for the importance of IL-6 in the course of T_H17 cell differentiation, it was also shown that $IL6^{-/-}$ mice were unable to generate T_H17 cells. In a mouse model for multiple sclerosis (MS) which is called *experimental autoimmune encephalomyelitis* (EAE) these mice were protected from development of this neurodegenerative disease (Samoilova et al., 1998).

Since T_H17 cells are involved in many autoimmune-mediated disorders, these findings gave rise for the development of a variety of drugs to treat T_H17/IL-17-mediated disease like rheumatoid arthritis, psoriasis and others. Some of these drugs which showed different clinical outcomes, included antibodies against IL-6 or IL-17A as well as RORγt inhibitors (Amatya et al., 2017; Gaffen et al., 2014; Gooderham et al., 2015).

1.2.4.2 T_H17 cell plasticity in autoimmune disease

Beside activated IL-17-producing pro-inflammatory T_H17 cells which produce IFN-γ, IL-22 and IL-22 there are also RORγt$^+$/FoxP3$^+$ co-expressing T cells which are able to express both cytokines IL-17 as well as the important immune regulatory cytokine IL-10. Accordingly, these cell populations were found to have a rather host-protective phenotype (Hirota et al., 2013; McGeachy et al., 2007).

In addition, as mentioned earlier (**1.2.2**, ***Tr17 cells***), RORγt$^+$ T cells show the ability to express the IL-10 receptor α which can be suppressed in an IL-10-dependent manner (Huber et al., 2011).

These findings provided evidence for the existence of both pro- *and* inflammatory T_H17 cell signaling. Thus, it was suggested that T_H17 cells are able to stay pro-inflammatory with distinct T_H17 signature cytokine profile, to become pro-inflammatory IFN-γ-producing effector T_H1 cells (Bending et al., 2009) or to transdifferentiate into other more regulatory, IL-10-produnging T cell subsets like regulatory T cells which show a rather protective phenotype (Diller et al., 2016; Gagliani et al., 2015; Krebs et al., 2016b). This model is illustrated in **Figure 3**, **A** (left: *plastic* T_H17 phenotype with ability to transdifferentiate into other T cell subtypes and right: more *stable* phenotype with limited ability for transdifferentiation).

This phenomenon is called *T_H17 cell plasticity*. Importantly, the balance of these different T_H17-mediated effector functions is of high clinical interest.
However, in renal samples from mice with experimental crescentic glomerulonephritis, also called *nephrotoxic nephritis* (NTN), it was shown that T_H17 cells show only a limited ability to transdifferentiate into T_H1 cells (also called T_H1 *ex-T_H17* or *non-classical T_H1 cells)* or IL-17/IFN-γ *double producers (Krebs et al., 2016b).* In contrast, in other autoimmune mediated disease like EAE, anti-CD3 duodenitis (sepsis model) or in *S.aureus* infection, the degree of T_H17 plasticity is significantly higher (Krebs and Panzer, 2018), also illustrated in **Figure 3**.

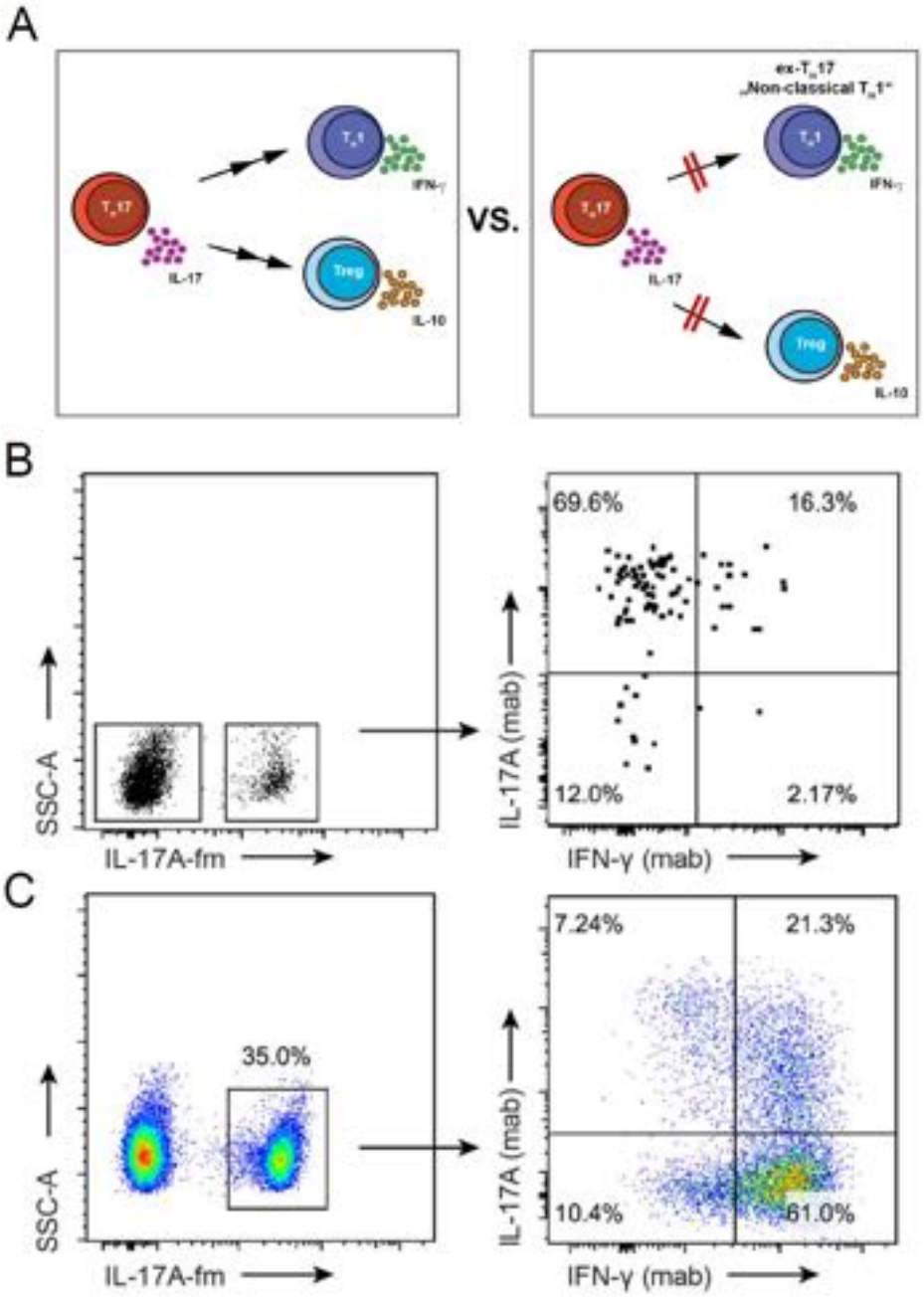

Figure 3: T_H17 cell plasticity in NTN, EAE & others in IL-17A Fate Reporter

In general, IL-17-producing T_H17 cells show the ability to transdifferentiate into other T cell subtypes like IFN-γ producing T_H1 cells (*T_H1 ex-T_H17 cells*), IL-10-producing T regulatory (Treg) cells or so called *double producers* which are able to produce both IL-17 *and* IL-10, depicted in (**A, left**). This tendency to transdifferentiate into other T cell subtypes is called *T_H17 cell plasticity*. However, in disease models like EAE, *S.aureus* infection or anti-CD3 duodenitis T_H17 cells show a high degree of cell plasticity (**A, left** and **C**). In contrast, in the nephrotoxic nephritis (NTN) mouse model T_H17 cells show a limited cell plasticity (**A, right** and **B**).

B and **C**: After FACS gating for $CD4^+$ $CD3^+$ renal T cells from NTN-induced IL-17A Fate Reporter mice (IL-17A^{cre} x *Rosa26*^{YFP}), cells were further gated for populations in which the IL-17A promotor was activated and thus caused the permanent mark of these cells with a $eYFP^+$ tag (IL-17A fm^+), shown the FACS plots (**B, left** and **C**, **left**). 10 days after NTN induction, these mice show a high proportion of IL-17-producing cells (IL-17A mab, antibody-stained, 69,6%) and less

transdifferentiation into IFN-γ-producing T_H1 cells (2,17%) or T_H1 ex-T_H17 cells (called *double producers*, 16,3%) as shown in **B, right**. These T_H17 cells are more "stable" compared to $CD4^+$ $CD3^+$ T cells from brain samples of EAE mice (MS mouse model) 14 days after disease induction, depicted in the FACS plot in **C, right**. These cells show a higher tendency to transdifferentiate into T_H1 cells (61%) or T_H1 ex-T_H17 cells (21,3%) and a lower proportion IL-17A-only producing cells (7,24%). (FACS plot depicted in **B** adopted from Krebs et al., 2016.)

Since, T_H17 cells as well as T_H1 cells are crucially involved in the pathogenesis of not only chronic kidney diseases but in a variety of organ-specific autoimmune disorders (Dolff et al., 2019; Krebs et al., 2017; Yasuda et al., 2019) and other chronic inflammatory diseases as mentioned (**1.2.4, *T_H17 cells***), it is of high clinical importance to elucidate the mechanisms behind T_H17 cell stability.

However, the underlying principles and mechanisms that are responsible for T_H17 cell stability and plasticity are still elusive and incompletely understood.

1.3 The kidney and chronic kidney disease

The kidney is a paired organ with multiple functions but their most common known function is the excretion of toxic waste products from the blood via the urine.
In addition, the kidney also generates important hormones like renin and erythropoietin (EPO) which are essential for blood pressure (via the renin-angiotensin-aldosterone-system, RAAS) and blood formation respectively. The kidneys also regulate the body`s water and base/acid- balance. Furthermore, they regulate the electrolyte balance via angiotensin and aldosterone (Kurts et al., 2013).

The nephrons are the functional units responsible for removal of toxic waste products from the blood via the urine. There are approximately 1 million nephrons in a human kidney.
In addition, each nephron contains one glomerulus which acts as a size-selective filter and a double-shaped tubule through which the filtrate is drained into the renal pelvis. The nephron is surrounded by parietal cells (forming the *Bowman capsule*) and tubular epithelial cells. The essential glomerular filtration barrier contains

endothelial cells, the glomerular basement membrane (GBM) and visceral epithelial cells which are also known as *podocytes*. During filtration, molecules smaller than albumin (< 68kDa) can pass the filter via the tubules, the loop of Henle and the distal convoluted tubule. This filtrate, called primary urine is further concentrated via a high osmotic pressure gradient in the kidney medulla. Furthermore, epithelial cells are capable to re-absorb water, amino acids and small proteins. Thus, they are also essential for the body's water-, acid/base- and electrolyte homeostasis. Intra-renal immune cells (macrophages, fibroblasts and dendritic cells mainly) are located in the inter-tubular space, illustrated in **Figure 4**.

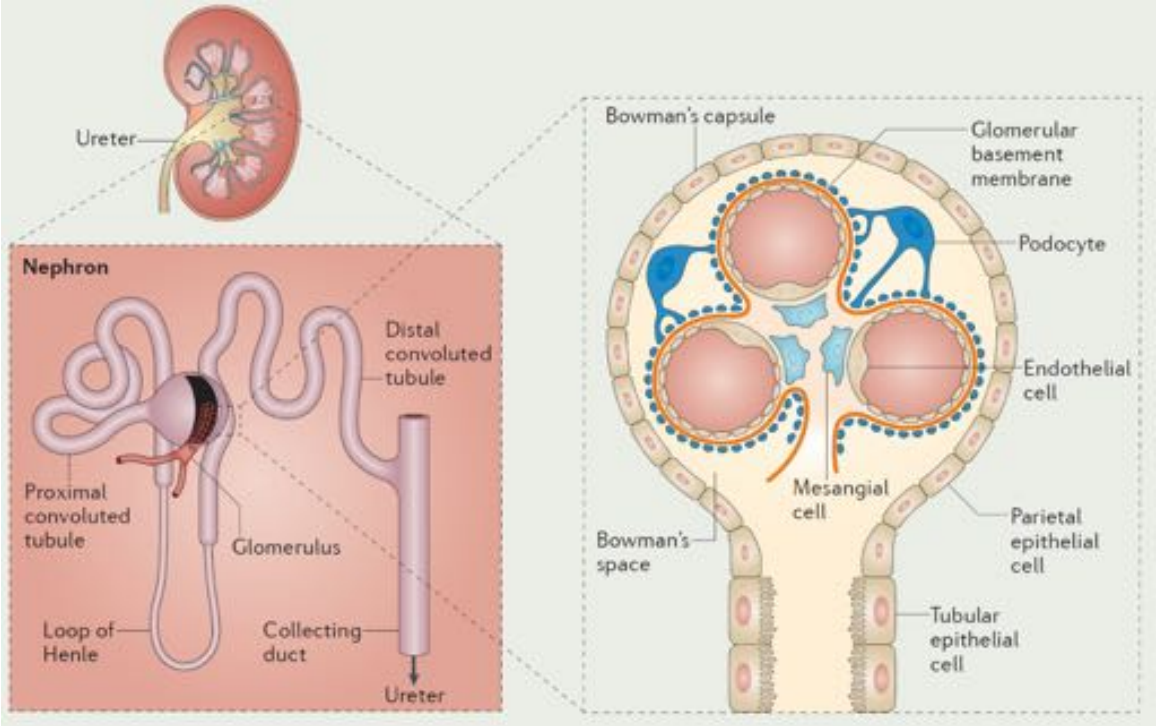

Figure 4: Physiology of kidney, nephron and glomerulus

This illustration shows a simple slice through a human kidney. Here, approximately 1 million nephrons are responsible for the removal of toxic products from the blood via urine secretion. Each nephron contains 1 glomerulus and 1 double hairpin-shaped tubules through which the filtrate is drained into the renal pelvis (**left** side of the illustration). A glomerulus (**right**) has a size of about 0,2mm and is a round-shaped structure which is surrounded by parietal cells (called *Bowman`s capsule*) and tubular epithelial cells. Here, the glomerular filtration barrier encompasses endothelial cells, the glomerular basement membrane (GBM) and podocytes (visceral epithelial cells).
In the course of glomerular filtration, small molecules (< 68kDa, albumin) pass the filter via the tubules, the loop of Henle and the distal convoluted tubule. The concentration of the primary urine is performed via high osmotic pressure gradient in the kidney medulla (not shown). Epithelial cells are able to re-absorb water, amino acids and small proteins etc. and are responsible for the blood pressure, body`s water-, base/acid- and electrolyte balance. The intrarenal immune system which consists mainly of dendritic cells, fibroblasts and macrophages is located in the inter-tubular space. (Illustration adopted from Kurts et al., 2013.)

In general, the inflammation of the kidney is called nephritis which comprise a number of inflammatory kidney diseases. Depending on the type of inflamed issue there are many forms like inflammation of the urethral channel and surrounding tissue (interstitial nephritis), renal pelvis inflammation (pyelonephritis) and glomerular inflammations (glomerulonephritis, GN). The different forms are classified by their pathogenesis and differentiation between acute and chronic disease progression.

Here, glomerular inflammation is a very severe form of chronic kidney disease (CKD) which is a condition characterized by damage of the glomerular filtration barrier, gradual and irreversible loss of nephrons causing progressive loss of kidney function over time. The end state of CKD is characterized by kidney fibrosis in which functional nephrons are restored by fibrotic tissue, depicted in **Figure 6**. However, CKD can progress to end-stage renal failure (ESRF) by a variety of ways, for example by high blood pressure or hypertension. Angiotensin receptor blockers (ARBs) and angiotensin-converting enzyme (ACE) inhibitors and can have a positive effect on kidney function by reduction of proteinuria and blood pressure as well as dietary changes like reduced sodium intake, reduced protein intake and increase of physical exercise (James et al., 2010; Jones-Burton et al., 2006; McMahon et al., 2013; Saran et al., 2017).

The glomerular filtration rate

The glomerular filtration rate (GFR) is a widely accepted scale unit to assess the filtering capacity of the kidneys. Here, the GFR is the volume of primary urine which is filtered by all podocytes in both kidneys in a time unit. The GFR of a healthy individual is $\geq$ 90mL/min/1,73m^2. (The latter considers the kidney area.)

According to the US-*National Kidney Foundation (Daugirdas, 2011)*, the definition of CKD is:

- GFR < 60 mL/min/1.73m^2 over a period of 3 months with or without evidence of kidney damage - **OR**
- Evidence of kidney damage for 3 months with or without decreased GFR, as evidenced by any of the following:
    - Albuminuria
    - Proteinuria
    - Persistent hematuria (where other causes such as urologic conditions have been excluded)
    - Pathologic abnormalities (e.g. abnormal renal biopsy)
    - Radiologic abnormalities (e.g. scarring or polycystic kidneys seen on renal imaging)

(Adopted from Daugirdas, 2011.)

According to the US-*National Kidney Foundation (Daugirdas, 2011)*, kidney function state is divided into 6 groups, depicted in **Table 1** (Modified after Daugirdas, 2011.).

Table 1: Kidney function states according to the National Kidney Foundation

Kidney function state	GFR [mL/min/1,73m^2]	Description
1	≥ 90	Normal or increased GFR
2	60-89	Normal or slightly increased GFR
3a	45-59	Mild-moderate decrease in GFR
3b	30-44	Moderate-severe decrease in GFR
4	15-29	Severe decrease in GFR
5	< 15 or on dialysis	End-stage renal failure (ESRF)

Chronic kidney diseases are major causes of death worldwide with an increasing tendency. It was ranked 27th (1990) and 18th (2010) in the list of causes of total number of global deaths. Demographically, there is a wide variation between mean age for stage 3 CKD in India (51 years), China (63,6 years), African Americans (57 years), Hispanic Americans (58 years) and white Americans with 63 years of age. Furthermore, approximately 10% of the western population suffers from CKD of which between 15-20% suffer from GN (Jha et al., 2013; Kurts et al., 2013).

1.3.1 Nephrotic Syndrome

As a result of damaged glomeruli, the latter become more permeable leading to dysfunctional glomerular filtration barrier. That is the reason why leaking plasma proteins can be found in glomerular filtrate which leads to abnormal high protein concentrations (> 3,5g/d) in the urine. This symptom known as ***proteinuria*** is a principal marker for kidney damage and is therefore suitable as an indicator of renal damage severity. Proteinuria itself can cause severe injury, e.g. as a risk factor in cardio vascular disease (Culleton et al., 2000; Grimm RH Jr, 1997; Wang et al., 2017). People with CKD are three times more likely to have myocardial infarction. In addition, they suffer from elevated morbidity and higher mortality (Wang et al., 2017). CKD is also related to increased insulin resistance (Kobayashi et al., 2005; Vladu et al., 2017; Wesolowski et al., 2010).

In terms of concentration, albumin is the most common type of protein in the blood. However, in individuals with fully functional kidneys there is virtually no albumin present in the urine. In contrast, due to renal damage, this protein is detectable even in early stages of kidney diseases. Hence, proteinuria is also known as *albuminuria*. Since albumin is removed from the blood, CKD patients gets ***hypoalbuminemia***.

Creatinine as a muscle metabolite is normally released at a constant rate into the urine and acts as an indicator of the urine concentration.
To assess the albumin-to-creatinine ratio (ACR) it is therefore used to correct for the urine concentration. ACR is a very important clinical marker for different CKDs.

As a result of hypoalbuminemia, the low osmotic pressure drives water out of the blood vessels into the tissue which is called ***edema***.
In addition, loss of protein can have effects on blood- and urine levels of lipids. There are two effects: Reduction of proteins which inhibit or regulate lipid synthesis and reduction of blood albumin. Since the latter is a mediator of water-insoluble molecules (like lipids) and water itself, this leads to a fourth and fifth symptom of nephrotic syndrome, called ***hyperlipidemia*** (high lipid levels in the blood) and ***lipiduria*** (high levels of lipid in the urine).

In addition, red blood cells erythrocytes can be detected in CKD patients which is called *hematuria*. Usually, some of these cells show irregular "*mickey mouse*"-shapes (called *acanthocytes*) caused by high pressure transfer through *damaged GBM, see* **Figure 5** (Catala Lopez and Fabregas Brouard, 2002; Kohler and Wandel, 1993).

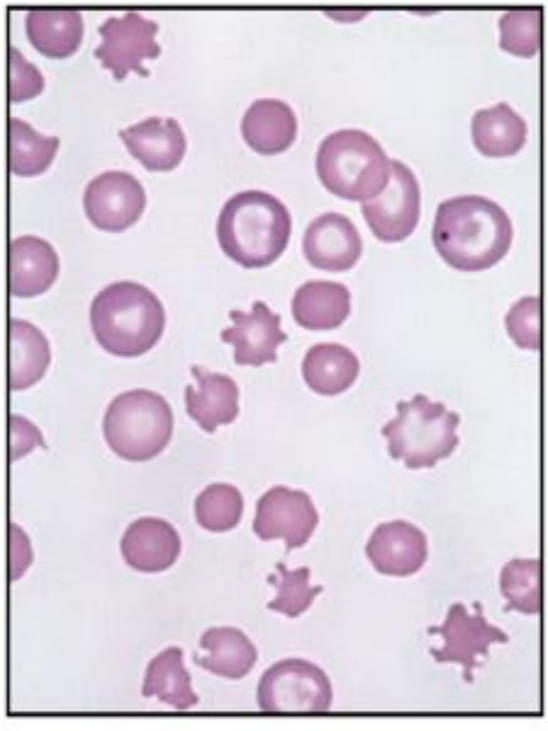

Figure 5: Acanthocytes in urine from CKD patient

Malformed (non-round-shaped) erythrocytes, so called *acanthocytes*, can often be found in urine from CKD patients. This malformation is caused by high pressure transfer from the blood through damaged GBM. (Light microscope image, Credit: eClinPath.com, Cornell University)

Dialysis

For treatment of people who suffer from CKD, dialysis is a common way to reduce uremic toxins and proteinuria This method is performed to prevent patients from described cardiovascular as well as blood pressure-related and other kidney disease-related side effects.

Urinary bioactive toxic solutes (uremic toxins) enclose a great variety of substances resulting in a great variety of chemical and biochemical properties. This fact makes it very difficult to identify and thus remove those toxins from the body during blood purification also known as dialysis (Glassock, 2008; Vanholder et al., 2008a).

One classification for uremic compounds was proposed by the European Uremic Toxin (EUTox) work group (Duranton et al., 2012; Liabeuf et al., 2011; Meijers and Evenepoel, 2011; Vanholder et al., 2008b; Yavuz et al., 2005) which is based on 85 studies published from 1968 to 2002 with an overall evaluation of 50.000 patients containing compounds which were accumulated in end-stage renal failure (ESRF) GFRs of less than 15mL/ min.

The EUTox classification separates uremic compounds in the following three groups, independent of their actual toxicity (**Table 2**).

Table 2: Classification of uremic compounds (EUTox working group)

	Low-molecular-weight and water-soluble uremic toxins	Protein-bound solutes	Middle-molecular-weight molecules
Description	▪ Molecular weight <500 Da ▪ Easily removed by dialysis ▪ 68 out of 90 compounds identified can be found in this category	▪ Molecular weight of most of most members <500 Da ▪ Difficult to remove by dialysis ▪ 25 out of 96 compounds identified can be found in this category	▪ Molecular weight >500 Da
Example compounds (excerpt)	Creatine, creatinine, hyaluronic acid, oxalate, urea, uric acid	Carboxy methyl propyl furanpropionic acid, tumor necrosis factor-α (TNF-α), cytokines, interleukins, leptin, p-cresyl glucuronide, phenol sulfate, retinol-binding protein	Adiponectin, cystatin C, a1-microglobulin, endothelin, ghrelin, prolactin, vasoactive intestinal peptide

In practice, there are two distinct forms of dialysis, peritoneal dialysis (PD) and hemodialysis (HD).

Besides advantages and disadvantages of one method over the other, they are distinguished by the location of the actual dialysis. During PD, the peritoneum is intracorporally used as natural filter to reduce uremic toxins. During PD, a dialysis fluid flows through a catheter into part of the abdomen where the peritoneum (natural dialysator) is located.

Finally, after a set time period the fluid containing the filtered waste products flows out of the abdomen and is discarded afterwards.

In contrast, HD is an extra-corporal process which takes advantage of artificially manufactured columns filled with semipermeable fiber-membranes (dialysator).

During this process blood is pumped through a cartridge in order to remove toxic waste products.

The regular number of dialysis treatments needed is about three times a week for about four hours each. Thus, the treatment remarkably reduces the general live quality of the patients. In addition, patients who undergo dialyses treatment are also more susceptible for *methicillin resistant Staphylococcus aureus* (MRSA)-related glomerulonephritis and infectious endocarditis which can itself cause acute renal failure. In general, these patients suffer from a weak immune system which makes the problem even more considerable (Karkar, 2018).

Therefore, dialysis does not represent a permanent solution but must be seen as a temporary and provisional arrangement.
Another alternative for CKD-affected patients is organ transplantation. Potential donors are healthy family members or other people with matching human leucocyte antigen (HLA)-types and other markers. However, organ transplantation leads to life-long immunosuppressive medication to prevent organ rejection, causing higher risk of infections. In 2006, there were 63.307 registered patients in Germany who undergo dialysis. Furthermore, in the same year 12.130 transplanted and dialysis patients died (*QuaSI-Niere* report*,* 2006).

These numbers stress that this problem is of tremendous significance with regard to public health and economy, not just in Germany but worldwide.

In summary, the best solution for the increasing kidney diseases is the prevention of terminal renal failure by applied research efforts.

1.3.2 Rapidly progressive GN & renal autoimmune disease

The rapid progressive glomerulonephritis (RPGN) is a very severe kidney disease. Without treatment, patients can suffer from ESRF within weeks to months due to necrotizing extracapillary proliferative crescentic glomerulonephritis (Haubitz,

2019). RPGNs are immune complex-related or anti-basal membrane glomerulonephritides. Thus, this group of kidney diseases is hallmarked by T cell infiltration into the renal tissue and renal inflammation.

Within the membranous nephropathies, there are *primary* (idiopathic) forms with unknown origin of the immune complexes which accounts for the vast majority of cases, and there are *secondary* forms, during which antibodies are formed in response to another process like medications, infections or autoimmune conditions at which auto-antibodies are formed against self-antigens. For further pathogenic mechanisms please also see **1.3.3**.

Since each cell type in the glomerulus serves distinct functions, injury to each cell type results in different clinical renal outcome and histological pattern.
However, among the RPGNs there are a number of distinctively classified diseases with different pathomechanisms involved. Except GNs with unknown underlying causes (idiopathic), RPGNs are classified into 3 main types, depicted in **Table 3** (Couser, 2012).

Table 3: Rapid progressive glomerulonephritides - Classification

	Type I	**Type II**	**Type III**
Characteristics	Antibodies against GBM	Immune complex formation	Pauci-immune ANCA[1]-association
Disease example	Anti-GBM disease, Goodpasture syndrome	Lupus erythematosus (Lupus nephritis), IgA nephropathy	Granulomatois with polyangiitis (formerly Morbus Wegener)
Known causes	Anti-GBM antibodies	Immune complexes	Associated with ANCAs, no glomerular immune depositions

[1] *ANCA* stands for **An**tineutrophil **C**ytoplasmic **A**ntibody.

1.3.3 Crescentic GN, the intestinal microbiome & the role of T_H17 cells

Anti-GBM crescentic GN (cGN) is a rare (< 1/100.000/year) but the most severe and aggressive form of autoimmune kidney diseases as mentioned earlier. This renal condition belongs to the type I, anti-GBM nephritis group within the RPGNs and is characterized by the formation of so called glomerular *crescents* (**Figure 6** and **Figure 15**). Their name originates from the characteristic shape which is visible in histological kidney sections. The number of glomerular crescents is an essential parameter to assess CKD severity.

Pathogenesis

In the course of cGN, auto- (self-directed) antibodies are created which specifically target epitopes of class IV collagen in the GBM. Those class IV collagen networks are the structural foundation for all basement membranes. They are also found in pulmonary alveoli in the lungs. In contrast to the renal situation, the pulmonary GBM-antigens are usually not accessible by these IgG′s. However, it is thought that toxins, infections and others can damage this barrier which leads to pulmonary manifestation (Pedchenko et al., 2010; Sanders et al., 2011).

This explains a syndrome in which anti-GMB antibodies are directed against the glomerular and alveolar basement membrane. This syndrome was found in 1919 by Ernest William Goodpasture and was named after him – *Goodpasture syndrome*. This lung-related effect is also known in an experimental pristane-induced lupus model (Salama et al., 2001; Self, 2009). In 1967, Lerner et al. were able to confirm the pathogenicity of human anti-GBM antibody (Lerner et al., 1967). However, the origin of the antibodies in this renal autoimmune disease is still unknown.

To investigate the plasticity of T_H17 cells in the cGN, the nephrotoxic nephritis (or *experimental glomerulonephritis*, NTN) model was used as explained in detail in **2.2.2**.

Although, the immune response in the NTN model is directed against different antigens in the GBM than in the human cGN the clinical outcome (e.g. proteinuria) as well as histological features are very similar. In addition, this model is well established since the 1960s and led to crucial contributions in the research of renal

inflammation (Chen et al., 2002; Hammer and Dixon, 1963; Unanue and Dixon, 1967).
Already in the 1960s it was defined in the NTN model that the creation of these anti-GMB antibodies leads to intraglomerular complement activation (now known via the classical pathway). In addition, chemotactic factors are released, neutrophil-mediated injury occurs and linear deposition of these IgG antibodies along the GBM takes place (Cochrane et al., 1965; Hudson et al., 1993; Hudson et al., 2003).

Furthermore, it is known that activation of pro-inflammatory signal cascade and infiltration of inflammatory cells like macrophages, IL-17-producing γδ-T cells, IFN-γ-producing T_H1 and T_H17 cells into the nephron during immune response results in gaps within the GBM. The latter causes glomerular inflammation and subsequent glomerular damage (Kurts et al., 2013; Summers et al., 2009). Since the GBM acts as a barrier, the created gaps enable blood plasma proteins and fibrin to cross this barrier.
As a consequence, this infiltration also leads to proliferation of glomerular parietal epithelial cells and formation of fibrocellular crescents (**Figure 6**). Histologically, crescents as well as glomerular hypertrophy and cell infiltrates can be observed in renal tissue sections (Krebs et al., 2016a; Riedel et al., 2016). Subsequently, glomeruli lose their function causing reduced GFR, proteinuria, hypertension, anemia etc.
With further progression, the end stage of this disease (end-stage renal disease, ESRD) is reached when kidney fibrosis and necrosis takes place resulting in loss of cellular membrane integrity.
Finally, these necrotic cells release damage-associated patterns (DAMPs) like DNA which is sensed by the macrophage *absent in melanoma 2* (AIM2) inflammasome. As a consequence, this leads to further release of pro-inflammatory cytokines like IL-18 and IL-1β (Komada et al., 2018).

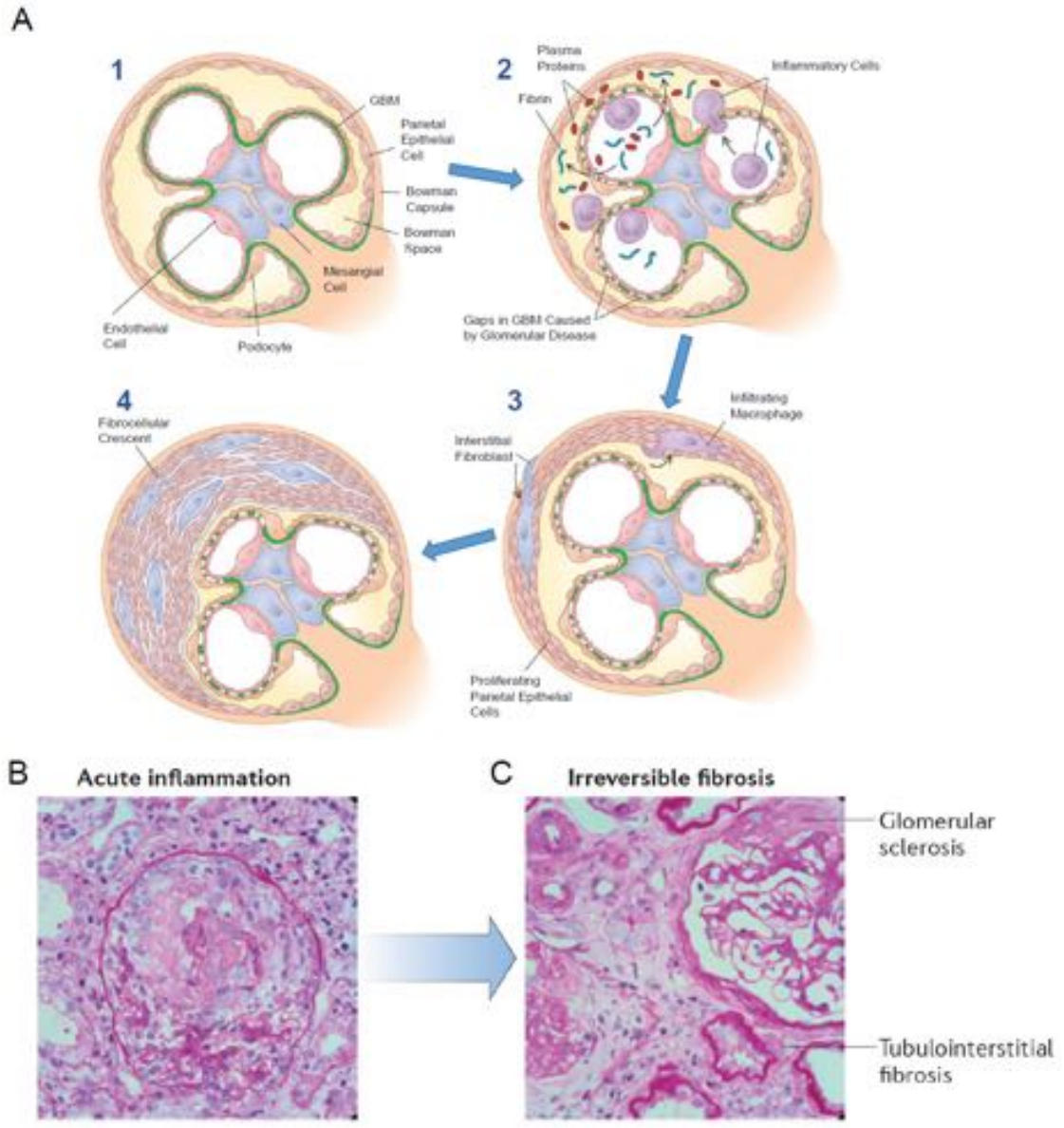

Figure 6: Pathogenesis & histology of crescentic glomerulonephritis and ESRF

(A): As explained earlier, a glomerulus consists of mesangial cells, visceral epithelial cells (also known as *podocytes*), glomerular endothelial cells and parietal cells. In the Bowman space, the primary urine (filtrate) is collected (**A, 1** - healthy glomerulus). The glomerular basal membrane (GBM) is of high importance in this disease, as the term anti-GBM nephritis implies. In cGN nephrogenic auto- (self-directed) antibodies are produced which are directed against specific epitopes of type IV collagen in the GBM. This leads to gaps within the GBM and infiltration of inflammatory cells like macrophages, IL-17-producing $\gamma\delta$-T cells, IFN-γ producing T_H1 cells as well as T_H17 cells into the nephron. This causes acute glomerular inflammation (**A, 2** and **B**). Due to the damaged barrier, blood plasma proteins and fibrin infiltrate the glomerulus as well (**A, b**). As a consequence, proliferation of parietal epithelial cells (**A, 3**) and formation of fibrocellular crescents takes place which is histologically visible as glomerular crescents (**A, 4** and **B**). This leads to overall reduced glomerular functionality, proteinuria, attenuated GFR and others. - In the end state of this disease (end-stage renal disease, ESRD), kidney fibrosis takes place in which functional nephrons are restored by fibrotic tissue (**C**). (Modified illustration depicted in (**A**) adopted from "The-Crankshaft Publishing's web site", histological pictures shown in (**B**) adopted from Kurts et al., 2013.)

As explained, among different immune cells which infiltrate the glomerulus during cGN there are clear and multiple evidence for the presence and pathogenic role of T_H17 cells (Kitching and Holdsworth, 2011; Paust et al., 2009; Riedel et al., 2016; Summers et al., 2009). Further studies in the NTN model revealed that IL-17A and IL-17F-producing T_H17 cells stimulate resident kidney cells like mesangial and tubular epithelial cell to secrete glutamate-leucine-arginine (ELR) motif chemokines, like CXCL1,2 and 5 as well as CCL20 which is a ligand for the chemokine receptor CCR6. The latter is expressed on T_H17 cells. This cascade results in the recruitment of more T_H17 cells as well as neutrophils via the chemokine receptor CXC-motif chemokine receptor 2 (CXCR2) into the renal tissue which eventually leads to renal damage (Disteldorf et al., 2015; Krebs et al., 2016a; Paust et al., 2009; Turner et al., 2010b)
The importance of the CCR6/CCL20 axis with regard to T_H17 cell recruitment was also found in other autoimmune mediated diseases like rheumatoid arthritis (Hirota et al., 2007), Psoriasis (Hedrick et al., 2009) and IgA nephropathy (Lu et al., 2017).

These findings also raised the question for the origin of recruited T_H17 cells. In recent studies it was found that the small intestine and its microbiota is of high importance in this regard.
It has long been known that the microbiota (which is the entirety of microorganisms, including bacteria, that colonize human or other living animals) plays an essential role in immune regulation of innate and adaptive immunity (Honda and Littman, 2016; Huber et al., 2012; Kato et al., 2014; Mittrucker et al., 2014; Thaiss et al., 2016). The microbiome emerged as a synergistic unit during evolution. The human intestinal tract alone harbors approximately 100 trillion (10^{14}) microbes (Whitman et al., 1998).

Among the different and rather complex mechanisms of immune regulation by the microbiota, the latter can modulate the NLRP6 inflammasome signaling via microbiota-related metabolites (Levy et al., 2015) or the production of inflammatory cytokines (Schirmer et al., 2016). In 2011, it was found that T_H17 cells are controlled in the small intestine via (1) intestinal lumen-mediated elimination and (2) simultaneous acquirement of a regulatory phenotype (Esplugues et al., 2011). Furthermore, research in our group revealed that pathogenic glomerular T_H17 cells

originated in the small intestine and migrated in a S1P receptor 1 (S1PR1)-dependent manner via the CCL20/CCR6 axis into renal tissue. The targeting of the intestinal microbiota by administration of an antibiotic resulted in reduced production of IL-1-producing $CD4^+$ T cells as well as IL-17A-producing γδ-T cells (Krebs et al., 2016a). These findings highlight the role of the microbiota in modulation of T_H17 cells in the NTN model.

CKD treatment

Treatment of patients with secondary (e.g. autoimmune-mediated) membranous glomerulonephritis usually starts by medication which treats the underlying disease. For example, by administration of antibiotics to treat infections.
In addition, the monoclonal anti-CD20 antibody *Rituximab* is clinically used to prevent antibody secretion by CD-20-expressing B cells (Iijima et al., 2017; Salles et al., 2017). Furthermore, immunosuppressive drugs like cyclophosphamide are used for treatment of autoimmune-related GN as well as steroids like glucocorticoids. The latter are also often used in primary membranous GNs. These steroid hormones are able to reduce certain immune functions like inflammation which is caused by binding of the glucocorticoid to its receptor. As a result, the expression of anti-inflammatory proteins is up-regulated and pro-inflammatory proteins are down-regulated. Not all but some immunomodulatory mechanisms of glucocorticoids are known (Rhen and Cidlowski, 2005; Rugstad, 1988).

For example, they have the ability to block several inflammatory and pain-related pathways:

- Inhibition of prostaglandin production by:
  - Induction and activation of annexin 1 (anti-inflammatory protein)
  - Induction of MAPK phosphatase I (anti-inflammatory protein)
  - Repression of transcription of cyclooxygenase 2

- Interaction with NF-κB blocks its transcriptional activity, leading to:
  - inhibition of cytokines, chemokines, complement factors

- strong reduction of T_H17 cells in cGN (unknown underlying mechanism)

The standard treatment for anti-GBM disease includes a combination of plasmapheresis to remove pathogenic antibodies as well as administration of cyclophosphamide and corticosteroids (Stephen P. McAdoo, 2017).

Subsequently, with further progressive reduction of GFR, patients often have to be dialyzed as explained earlier.

1.4 IL-27/IL-27 receptor α axis in immunity

As H. Yoshida wrote, “Interleukin-27 (IL-27) is a cytokine with strikingly diverse influences on the immune response.” (Yoshida and Hunter, 2015).
IL-27 which belongs to the IL-6/IL-17 cytokine family was first described by Pflanz et al. in 2002. Its structure is composed of p28 and *Epstein-Barr virus induced gene 3* - EBI3 (Pflanz et al., 2002). The main sources of IL-27 are myeloid cell populations which include inflammatory monocytes, microglia, macrophages and dendritic cells (DCs). In addition, endothelial and plasma cells as well as epithelial cells are able to express IL-27 (Hall et al., 2012b). In order to stimulate IL-27 production a variety of TLR-dependent microbial and immune stimuli were found including the TNF family members CD40 and CD137 (Curran et al., 2013; Dibra et al., 2012) as well as TNF Type I and Type II (Liu et al., 2007; Molle et al., 2007; Pirhonen et al., 2007; Remoli et al., 2007). Type II TNF are also known as IFN-γ (Lee and Ashkar, 2018).

In addition, soon after the 2002 Pflanz publication also structural details about the IL-27 receptor were described (Pflanz et al., 2004). According to these findings, the functional signal-transducing IL-27 receptor consist of the receptor complex WSX-1 (IL-27ra, also known as *TCCR*) and gp130 (**Figure 7**). Whereas, IL-27ra/WSX-1 is expressed in lymphocytes including naïve T cells (Chen et al., 2000; Sprecher et al., 1998), as well as in Natural killer (NK) cells (Yoshida and Hunter, 2015).
One of the regulatory phenotypes induced by activation of the IL-27 pathway is caused by inhibition of T_H17 cell differentiation and expansion of Treg cells (Wang et al., 2012a). IL-27 is also able to activate a variety of T cells like T_H1 (Yoshimura

et al., 2006). This is accomplished by induction of the essential transcription factor Tbet via p38 Map kinase, MAPK (Karpuzoglu et al., 2007; Owaki et al., 2006; Takeda et al., 2003) as well as T_H2, T_H17, Treg and Tr1 cells to produce IL-10 in infectious and autoimmune mediated conditions via STAT3 (Awasthi et al., 2007; Fitzgerald et al., 2007; Stumhofer et al., 2007). IL-10 is known for its role in limiting infection-induced inflammation (Couper et al., 2008; Kessler et al., 2017; Mosser and Zhang, 2008).
In previous experiments it was also shown that IL-$10^{-/-}$ mice developed spontaneous colitis and were more susceptible to cancer (Berg et al., 1996). Interestingly, in IL-$27^{-/-}$ or IL-$27ra^{-/-}$ mice this was not the case.

In contrast to the anti-inflammatory capabilities IL-27 is also able to promote T cell responses by its growth and survival functionalities (Kim et al., 2013).
For example, in EAE it was shown that IL-27 can suppress IL-17-producing T helper cells mediated by IL-6 and *transforming growth factor-*β -TGF-β (Batten et al., 2006; Stumhofer et al., 2006).

From pervious works it is known that IL-27 mediates its cellular function via binding of IL-27 to its receptor (IL-27ra/WSX-1 and gp130 subunit), resulting in activation of s*ignal transducer and activator of transcription* (STAT) 1 and STAT3 pathways by the *janus kinase*, former known as *just another kinase* (JAK)-STAT pathway (Stumhofer et al., 2007).

Blocking of human gp130 as part the IL-27 receptor (**Figure 7**) however was found to inhibit STAT1 and STAT3 tyrosine phosphorylation in a dose dependent manner (Pflanz et al., 2004).

JAKs are cytoplasmic tyrosine kinases which bind to specific regions in intracellular receptor domains. After binding of JAKs to these domains the kinases come in close proximity to each other which results in auto-tyrosine phosphorylation of the JAKs in a ligand-depended manner. This also increases the phosphorylation capabilities of the JAKs. Afterwards, phosphorylation of tyrosine receptor residues takes place. This leads to formation of *src homology 2* (SH2) domain- binding sites

which is of high importance for this pathway since these are structural components of STATs. As a result, STATs (-1, -2, -3, -4, -5a, -5b, and 6 in mammals) bind to these SH2 domains and will be also phosphorylated by the JAKs. This also induces the formation of SH2 domains on the STAT proteins which then causes the binding of two STAT molecules forming homo- or hetero dimers. In the further course, nuclear localization signals are accessible which results in translocation into the cellular nucleus. STAT molecules act as essential transcription factors, regulating the expression of a variety of genes (Horlad et al., 2016; Ma et al., 2019; Owaki et al., 2008; Takeda et al., 2003).

A short overview of the IL-27/IL-27 receptor pathway, including STAT activations, is illustrated in **Figure 7**.

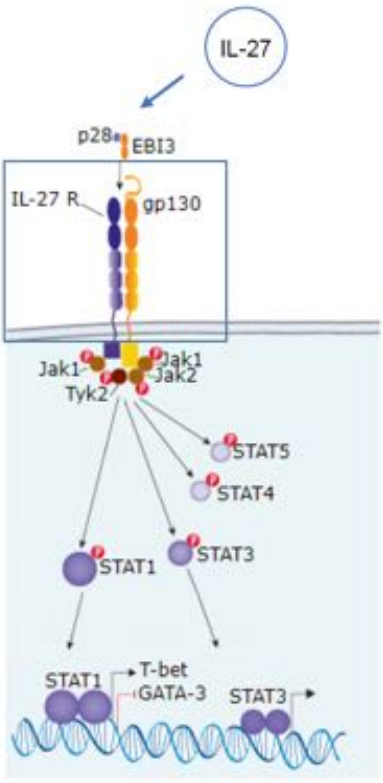

Figure 7: IL-27/IL-27 receptor-related STAT signaling pathways

After binding of IL-27 which consists of two subunits (p28 and Eps*tein-Barr virus induced gene 3* (EBI3, blue circle) to the IL-27 receptor (blue square) which consist of IL-27ra/WSX-1 (here called *IL-27R*) and gp130, JAK-STAT pathway is activated. As a result, auto-phosphorylation of JAKs takes place. After receptor formation, the latter are also phosphorylated leading to accessibility of *src homology 2* (SH2) binding sites which is essential for followed STAT binding. Afterwards, STATs are also phosphorylated (pSTATs). Subsequently, pSTAT molecules dimerize, and enter the cell nucleus via nuclear localization signals. In the nucleus pSTAT molecules act as essential transcription factors for a variety of signaling pathways. (Illustration modified after R&D Systems “IL-12 Family Signaling Pathways”.)

1.5 Hypothesis and aims

T_H17 cells are pathogenic in crescentic GN (cGN) and also show a high degree of stability. However, the molecular mechanisms underlying this T_H17 cell phenotype in GN are still elusive.

In my thesis, I hypothesized that identification of molecular targets which are responsible for the stable phenotype in NTN (cGN mouse model), can pave the way for therapeutically interventions.
This might result in reprogramming T_H17 cells into immunosuppressive phenotypes.

Therefore, with our unbiased approach, I aimed to identify potential targets which are responsible for high T_H17 cell plasticity in this work.
Further, I aimed to validate the selected target *in vivo* and to deduce underlying molecular mechanisms and pathways which are important for its role in T_H17 cells in cGN by additional experiments.

2 Material and Methods

2.1 Material

2.1.1 Mice

Internal reporter mouse name	Mutation / genetic feature	Background	Supplier / Reference
wt	-	C57BL/6	The Jackson Laboratory
IL-17A Fate Reporter	IL-17A^{CRE} x R26^{eYFP}	C57BL/6	The Jackson Laboratory donation by B. Stockinger (Hirota, 2011)
Fate^{+} Reporter	FoxP3^{RFP} IL-10^{eGFP}IL-17A^{Kat} x IL-17A^{CRE}R26^{YFP}	C57BL/6	Flavell / Gagliani (Gagliani et al., 2015)
Tbx21 (Tbet-) flox mouse	IL-17A^{CRE} x R26^{eYFP} x $_{flox}$tbx21^{flox}	C57BL/6	The Jackson Laboratory donation by B. Stockinger / UKE

2.1.2 Primer

Primer	Sequence (5'- 3')	Length (nucleotides)	Supplier
Random hexamer primer Invitrogen,	Random, mostly hexamers	-	Invitrogen Cat. No: 48190-011

2.1.3 Primer for genotyping

All primers were ordered from Invitrogen / Thermo Scientific, Waltham, Massachusetts, USA.

Primer description	**Nucleotide sequence (5' - 3')**	**Length** (nucleotides)
CD4 Cre.1	CGA GTG ATG AGG TTC GCA AG	20
CD4 cre.2	TGA GTG AAC GAA CCT GGT CG	20
17AyfpF	CAA GTG CAC CCA GCA CCA GCT GAT C	25
17AyfpRwt	CTT AGT GGG TTA GTT TCA TCA CAG C	25
17AyfpiCreR	GCA GCA GGG TGT TGT AGG CAA TGC	24
Rosa26 Seq1	AAA GTC GCT CTG AGT TGT TAT	21
Rosa26 Seq2	GCG AAG AGT TTG TCC TCA ACC	21
Rosa26 Seq3	GGA GCG GGA GAA ATG GAT ATG	21
Tbet flox A	TAT GAT TAC ACT GCA GCT GTC TTC AG	26
Tbet flox B	CAG GAA TGG GAA CAT TCG CCT GTG	24

2.1.4 qPCR probes

Nucleotide sequences were not provided by the supplier.
All probes are directed against mouse antigens, FAM labeled and ordered from *Thermo Fisher Scientific*, Waltham, Massachusetts, USA.

Target gene	Cat. No.
HPRT1 – 20x mix, 250µL (endogenous control)	Mm01545399
Il27RA	Mm00497259
Il27	Mm00461162
Tcf7	Mm00493445
Satb1	Mm1268940
FasI	Mm00438864

2.1.5 Antibodies

All used antibodies were anti-(α-) mouse directed.

Antibody	Clone	Supplier	Note
α-CD3e (Ultra-leaf purified)	145-2C11	Biolegend Cat. No. 100340	20µg per mouse
α–Albumin (Albumin ELISA)	Polyclonal	Bethyl Laboratories Inc. Cat. No. A90-134A	
α–Albumin, (HRP-conjugated)	Polyclonal	Bethyl Laboratories Inc. Cat. No. A90-134P	

2.1.6 Antibodies for FACS[2]

Antibody	Conjugate	Isotype	Clone	Supplier	Antibody dilutions
α-CD3ε	BV 450	Syrian Hamster IgG_2, κ	500A2	BD Cat. No. 560801	1:100
α-CD3	BV 510	Rat IgG2b, κ	17A2	Bio Legend Cat.No.100234	1:100
α-CD3	BV 650	Rat IgG2b, κ	17A2	Bio Legend Cat. No. 100229	1:200
α-CD3	AF 700	Rat IgG2b, κ	17A2	Bio Legend Cat. No. 100216	1:100
α-CD3	BV 785	Rat IgG2b, κ	17A2	Bio Legend Cat. No. 100232	1:100
α-CD4	APC	Rat IgG2a, κ	RM4-5	Bio Legend Cat. No. 100516	1:200
α-CD4	BV 510	Rat IgG2a, κ	RM4-5	Bio Legend Cat. No. 100559	1:100
α-CD4	BV 605	Rat IgG2a, κ	RM4-5	Bio Legend Cat. No. 100547	1:600
α-CD4	BV 650	Rat IgG2a, κ	RM4-5	Bio Legend Cat.No. 100555	1:600
α-CD4	BV 785	Rat IgG2a, κ	RM4-5	Bio Legend Cat.No. 100552	1:1000
α-CD4	PE-Cy7	Rat IgG2a, κ	RM4-5	Bio Legend Cat. No. 100528	1:200
α-CD4	PerCP	Rat DA/HA IgG2a, κ	RM4-5	BD Pharmingen Cat. No. 553052	1:100
α-CD8a	BV 785	Rat IgG2a, κ	53-6.7	Bio Legend Cat. No. 100750	1:300
α-CD11b	APC	Rat IgG2b, κ	M1/70	Bio Legend Cat. No. 101212	1:200
α-CD45.1	APC	Mouse A.SW IgG2a, κ	A20	BD Biosciences Cat. No. 558701	1:100
α-CD45	APC / Fire 750	Rat IgG2b, κ	30-F11	Bio Legend Cat. No. 103154	1:600
α-CD45	BV 785	Rat IgG2b, κ	30-F11	Bio Legend Cat. No. 103149	1:200
α-CD45	PerCP	Rat IgG2b, κ	30-F11	Bio Legend Cat. No. 103130	1:100

[2] FACS stands for: **F**luorescence-**a**ctivated **c**ell **s**orting

Antibody	Conjugate	Isotype	Clone	Supplier	Antibody dilutions
α-IL-13	eF450 / V450	Rat IgG1 κ	eBio13A	eBiosciences Cat. No. 48-7133-82	1:100
α-IL-17F	APC / AF647	Mouse IgG1, κ	9D3.1C8	Bio Legend Cat. No. 517004	1:100
α-IL-17A	eF450 / V450	Rat IgG2a, κ	eBio17B7	eBiosciences Cat. No. 48-7177-82	1:200
α-IL-17A	PE	Rat IgG1 κ	TC111810.1	Bio Legend Cat. No. 506904	1:100
α-IL-13	eF 450	Rat IgG1, κ	eBio13A	eBiosciences Cat. No. 48-7133-82	1:100
α-IL-27ra	PE	IgG2a, κ	2918	BD Cat. No. 564337	1:200
Isotype control	PE	IgG2a, κ	G155-178	BD Cat. No. 554648	1:200
α-pSTAT3 (pY705)	PE	Mouse IgG2a, κ	4/P-STAT3	BD Cat. No. 612569	1:15
α–γδ–TCR	BV 605	American Hamster IgG2, κ	GL2	BD Cat. No. 745116	1:200
α–γδ–TCR	BV 510	American Hamster IgG2, κ	GL3	Bio Legend Cat. No. 563218	1:100
α–IFN-γ	APC	Rat IgG1, κ	XMG1.2	Bio Legend Cat. No. 505810	1:200
α–IFN-γ	BV 711	Rat IgG1, κ	XMG1.2	Bio Legend Cat. No. 564336	1:100

2.1.7 Buffers, media and solutions

Buffer	Composition
Buffer A for protein isolation	7mL PBS, 1 tablet of "*Complete protease inhibitor*"
Buffer B for protein isolation	7mL PBS, 1 tablet of "*Complete protease inhibitor*", EDTA 1mM, EGTA 2mM, PMSF, NP40
Coating buffer (for albumin ELISA)	100mL aqua dest., content of one capsule carbonate-bicarbonate buffer (in 200mL cell culture flask)
Digestion medium	RPMI-1640 medium (+ Glutamine) supplemented with 1% (v/v) FCS, 1% (v/v) HEPES, 1% (v/v) Penicillin-streptomycin
Erythrocytes lysis buffer	NH_4Cl, 160mM / Tris-HCl, 170mM, pH=7,6 (9:1 v/v)
Hematoxylin solution (ready-to-use)	Components: water, ethanol, hematoxylin, sodium iodat, aluminum ammonium sulfate (Quantities not provided by the company.)
PBS, 1% FCS solution (for small intestine preparation)	PBS, 1%FCS (v/v, sterile filtered)
Percoll solution (37%, v/v)	106mL H_2O, 74mL Percoll PLUS, 20mL 10x DPBS
Paraformaldehyde (PFA) (for Histology)	22mL 37% (v/v) PFA in 178mL Sörensen buffer
Postcoat solution (for albumin ELISA)	1mL aqua dest., content of one package 50mM Tris buffered saline, pH 8,0 – 1% BSA
Re-stimulation medium	X-Vivo medium, β-Mercaptoethanol (1:1.000 v/v), Brefeldin A (1:500 v/v), PMA (1:20.000 v/v), Ionomycin (1:1.000 v/v)
Sample / conjugate diluent (for albumin ELISA)	200mL of Postcoat solution, 1mL 10% (v/v) Tween20 (in 200mL cell culture flask)
Sörensen buffer	3,03g $NaHPO_4$ + 14,14g Na_2HPO_4 add to 1L with bi dest. H_2O, pH= 7,2-7,4
Washing Buffer (for small intestine preparation)	PBS, 1% FCS (v/v, sterile filtered), 1mM EDTA
Wash solution (for albumin ELISA)	1L aqua dest., content of one package 50mM Tris buffered saline, pH 8,0 – 0,05% Tween20

2.1.8 Chemicals and consumables

Product	Supplier	Cat. No.
Agarose (*UltraPure*)	Invitrogen / Thermo Scientific, Waltham, Massachusetts, USA	16500-500
Aqua ad iniectabilia	B. Braun, Melsungen, Germany	3113087
Aqua rinse solution	B. Braun, Melsungen, Germany	0082479E
autoMACS Running Buffer	Miltenyi Biotech, Bergisch Gladbach, Germany	130-091-221
Collagenase D (*f. Clostridium histolyticum*)	F. Hoffmann-La Roche AG, Basel, Switzerland	11088866001
Complete protease inhibitor	F. Hoffmann-La Roche AG, Basel, Switzerland	05892970001
Dewar, cylindrical	KGW Isotherm, Karlsruhe, Germany	1029
Dithiothreitol (DTT), 1mM	Carl Roth, Karlsruhe, Germany	6908.1
DNase I	F. Hoffmann-La Roche AG, Basel, Switzerland	10104159001
DNA Gel Loading Dye (6x)	Thermo Fisher Scientific, Waltham, Massachusetts, USA	R0611
Dulbecco's phosphate buffered saline (DPBS resp. PBS)	Thermo Fisher Scientific, Waltham, Massachusetts, USA	14190250
Eosin solution	Carl Roth, Karlsruhe, Germany	7089
Ethylenediaminetetraacetic acid (EDTA)	Sigma Aldrich, St. Louis, Missouri USA	03690-100ML
Eukitt mounting medium	Sigma Aldrich, St. Louis, Missouri USA	03989-100ML
Fetal calf serum (FCS)	Thermo Fisher Scientific, Waltham, Massachusetts, USA	10500-064
Hank's balanced salt solution (HBSS)	Thermo Fisher Scientific, Waltham, Massachusetts, USA	14170-008
Hematoxylin solution	Carl Roth, Karlsruhe, Germany	3816
Ionomycin, Free acid, (f. *Streptomyces conglobatus*)	Sigma Aldrich, St. Louis, Missouri, USA / Merck	407950-1MG
Multistix Reagent Strips (Urea Sticks)	Siemens Healthcare GmbH, Erlangen, Germany	10SG

Product	Supplier	Cat. No.
Paraformaldehyd (PFA, 37% v/v)	Carl Roth, Karlsruhe, Germany	7392.1
Penicillin-streptomycin	Sigma Aldrich, St. Louis, Missouri USA	P4333-100ML
Percoll PLUS	Sigma Aldrich, St. Louis, Missouri, USA / Merck	GE17-5445-01
Perm Buffer III	BD (Beckton, Dickinson), Franklin Lakes, New Jersey, USA	558050
Phorbol 12-Myristate 13-Acetate (PMA)	Sigma Aldrich, St. Louis, Missouri, USA	P1585
Pristane	Sigma Aldrich, St. Louis, Missouri, USA	P2870-100
RPMI-1640 medium	Thermo Fisher Scientific, Waltham, Massachusetts, USA	21875-034
Recombinant mouse IL-27 (Stock conc.: 100mg/µL)	Biolegend Inc., San Diego, California, USA	577404
Recombinant mouse IL-6 (Stock conc.:200mg/µL)	Biolegend Inc., San Diego, California, USA	575704
TMB peroxidase substrate (for albumin ELISA)	AVIVA Systems Biology, San Diego, California, USA	OORA01684
Tris buffered saline, with BSA, pH 8,0 (for albumin ELISA	Sigma Aldrich, St. Louis, Missouri, USA	T6789
Tris buffered saline, with Tween20, pH 8,0 (for albumin ELISA	Sigma Aldrich, St. Louis, Missouri, USA	T9039
Tween20 (for albumin ELISA)	Bethyl Laboratories Inc., Montgomery, Texas, USA	E108
1kb DNA ladder	New England Biolabs (NEB), Ipswich, Massachusetts, USA	B7025

2.1.9 Equipment

Equipment	**Supplier**
BD LSR II	BD (Beckton, Dickinson), Franklin Lakes, New Jersey, USA
BD LSRFortessa	BD (Beckton, Dickinson), Franklin Lakes, New Jersey, USA
BD FACSAria IIIu	BD (Beckton, Dickinson), Franklin Lakes, New Jersey, USA
Biological safety cabinet *Nuaire KS12*	Thermo Scientific / Heraeus, Waltham, Massachusetts, USA
Centrifuge 5417R	Eppendorf, Hamburg, Germany
Centrifuge C1008-B *my Fuge* mini centrifuge	Greiner Bio-One, Kemsmünster, Austria
Citadel Tissue Processor Shandon 1000	Thermo Fisher Scientific, Waltham, Massachusetts, USA
Cooling Plate, COP 30	Medite GmbH, Burgdorf, Germany
CO_2-Incubator *HERAcell* 240	Thermo Scientific / Heraeus, Waltham, Massachusetts, USA
CO_2-Incubator, B 5042	Thermo Scientific / Heraeus, Waltham, Massachusetts, USA
Coverslips (for microscopy)	Carl Roth, Karlsruhe, Germany
Cutfix one-use scalpel	B. Braun, Melsungen, Germany
Freezer (-20°C)	Liebherr, Bulle, Switzerland
Fridge, CP 43 CPel 4313-20	Liebherr, Bulle, Switzerland

Equipment	Supplier
GentleMACS Dissociator (2 tubes)	Miltenyi Biotech, Bergisch Gladbach, Germany
Laboratory balance Navigator	OHaus, Parsippany, New Jerey, USA
Laboratory balance (fine) BP210S	Sartorius, Göttingen, Germany
Light Microscope (Zeiss *Axio Scope A1*)	Zeiss, Oberkochen, Germany
Magnetic stirrer bars	VWR International, Radnor, Pennsylvania, USA
Metal sieve (concave), 200µm pores	Linker, Kassel, Germany
Microtome RM2255	Leica Biosystems, Wetzlar, Germany
Multichannel pipette, 12 channels, 20-200 µL	VWR International, Radnor, Pennsylvania, USA
Multifuge 1S-R	Thermo Scientific / Heraeus, Waltham, Massachusetts, USA
Multifuge X3R	Thermo Scientific / Heraeus, Waltham, Massachusetts, USA
Neubauer counting slide	Carl Roth, Karlsruhe, Germany
pH-Meter, *FiveEasy*	Carl Roth, Karlsruhe, Germany
Pipettes (*PIPETMAN classic*)	Gilson Inc., Middleton, Wisconsin, USA
Pipet Boy	INTEGRA Biosciences AG, Zizers, Switzerland
Qubit 2.0 Fluorometer	Invitrogen / Thermo Scientific, Waltham, Massachusetts, USA
QuantStudio 3 Real-Time PCR System, 96-well, 0.3mL	Applied Biosystems / Thermo Scientific, Waltham, Massachusetts, USA
Qubit 4 Florometer	Thermo Scientific / Heraeus, Waltham, Massachusetts, USA
Syringe *Omnifix-F*	B. Braun, Melsungen, Germany
Syringe *Injekt-F*	B. Braun, Melsungen, Germany
Syringe needle, Sterican 23G	B. Braun, Melsungen, Germany
Syringe needle, Sterican G20	B. Braun, Melsungen, Germany
Spectrophotometer DS11	DeNovix Inc., Wilmington, USA
Surgical instruments (Scissors, clambs, tweezers, sharp spoon)	Carl Roth, Karlsruhe, Germany

Equipment	Supplier
TC20 Automated cell counter	Laboratories Inc.
Thermal Cycler C1000 Touch	Bio-Rad Laboratories Inc., Hercules, California, USA
Thermocycler T3	Biometra GmbH, Göttingen, Germany
T Professional Trio Thermocler	Biometra GmbH, Göttingen, Germany
TissueLyser II	Qiagen, Hilden, Germany
Tungsten carbide beads	Qiagen, Hilden, Germany
Tube magnet (*The big easy EasySep*)	Stemcell Technologies, Vancouver, Canada
Ultra-low freezer (-80°C), TSX70086V	Thermo Scientific, Waltham, Massachusetts, USA
Vortexer V1 S000	IKA, Staufen, Breisgau, Germany
Zeiss light microscope IM35	Carl Zeiss AG, Jena/ Oberkochen, Germany
Water bath incubator, Typ 1012	Gesellschaft für Labortechnik, GFL, Burgwedel, Germany

2.1.10 Plasticware

Product	Supplier	Cat. No.
C tube (for GentleMACS Dissociator)	Miltenyi Biotech, Bergisch Gladbach, Germany	130-093-37
Cell culture micro plate, 96-well, u-bottom	Greiner Bio-One Holding, Kremsmünster, Austria	650180
Cell culture micro plate, 96-well, v-bottom	Greiner Bio-One Holding, Kremsmünster, Austria	651160
Cell counting slides	Bio-Rad Laboratories Inc., Hercules, California, USA	145.0015
CryoPure cryo tubes	Sarstedt, Nümbrecht/Rommelsdorf Germany	72.380.992

Product	Supplier	Cat. No.
Disposable pipetting reservoirs	VWR International, Radnor, Pennsylvania, USA	89094-662
Falcon Round-Bottom Polypropylene tubes, 5ML (FACS tubes), with caps	Stemcell Technologies, Vancouver, Canada	38057
Falcon Round-Bottom Polypropylene tubes, 5ML (FACS tubes), without caps	Stemcell Technologies, Vancouver, Canada	38056
Falcon tubes 15mL	Greiner Bio-One Holding, Kremsmünster, Austria	188271
Falcon tubes 50mL	Greiner Bio-One Holding, Kremsmünster, Austria	227261
Filter Tip, 10µL	Sarstedt, Nümbrecht/Rommelsdorf Germany	70.1130.410
Filter Tip, 100µL	Sarstedt, Nümbrecht/Rommelsdorf Germany	70.760.12
Filter Tip, 200µL	Sarstedt, Nümbrecht/Rommelsdorf Germany	70.760.211
Filter Tip, 1000µL	Sarstedt, Nümbrecht/Rommelsdorf Germany	70.762.411
Micro tube, 1,5mL	Sarstedt, Nümbrecht/Rommelsdorf Germany	72.690.001
Micro tubes, 1,5mL (screw cap)	Sarstedt, Nümbrecht/Rommelsdorf Germany	72.692
Micro tube, 1,3mL (filled with K3 EDTA)	Sarstedt, Nümbrecht/Rommelsdorf Germany	41.1504.015
Petri dish (92x16mm)	Sarstedt, Nümbrecht/Rommelsdorf Germany	82.1473
Pipette Tip (w/o filter), 10µL	Sarstedt, Nümbrecht/Rommelsdorf Germany	70.1130.460
Pipette Tip (w/o filter), 200µL	Sarstedt, Nümbrecht/Rommelsdorf Germany	70.760.502
Serological pipettes, 25mL	Sarstedt, Nümbrecht/Rommelsdorf Germany	86.1685.001
Serological pipettes, 10mL	Sarstedt, Nümbrecht/Rommelsdorf Germany	86.1254.001
Serological pipettes, 5mL	Sarstedt, Nümbrecht/Rommelsdorf Germany	86.1253.001
T175 Cell culture flask	Sarstedt, Nümbrecht/Rommelsdorf Germany	83.3912

2.1.11 Kits

Product	Supplier	Cat. No.
LEGENDplex bead-based immunoassay (Cytometric Bead Array), Mouse T Helper Cytokine Panel	Biolegend Inc., San Diego, California, USA	740749
LEGENDplex bead-based immunoassay (Cytometric Bead Array), Mouse Inflammation Panel	Biolegend Inc., San Diego, California, USA	740446
$CD4^+$ T Cell Isolation Kit (anti-mouse)	Miltenyi Biotech, Bergisch Gladbach, Germany	130-104-454
DC Protein Assay	BIO-RAD Laboratories Ltd., Hertfordshire, United Kingdom	5000112
EasySep Mouse CD4+ T Cell Isolation Kit	Stemcell Technologies, Vancouver, Canada	19852A
LIVE/DEAD Fixable Near-IR Dead cell staining Kit	Thermo Fisher Scientific, Waltham, Massachusetts, USA	L34975
Qubit dsDNA HS Assay Kit	Thermo Fisher Scientific, Waltham, Massachusetts, USA	Q32854
RNeasy Plus Micro Kit (50)	Qiagen, Hilden, Germany	74034
XNAT2 Extract-N-Amp Tissue PCR Kit	Sigma Aldrich, St. Louis, Missouri USA	XNAT2

2.1.12 Software

Software	Developer
Adobe Illustrator CS6; version 16.0.0	Adobe Inc., San José, California, USA
BD FACS Diva software; version 8.0.1	BD Biosciences, Franklin Lakes, New Jersey, USA
EndNote; version X9.1	Clarivate Analytics, Spring Garden, Philadelphia, USA
FlowJo; version 10.5.3	Tree Star, Ashland, Oregon, USA
GraphPad Prism; versions 6, 7 and 8	GraphPad Software Inc., La Jolla, California, USA
LEGENDplex Data Analysis Software; version 7.0	Biolegend Inc., San Diego, California, USA
Microsoft Office Professional Plus 2013; version 15.0.5127.1000	Microsoft, Redmond, Washington, USA
Sequencing Software (STAR and other self-programmed codes/ programs)	Reference: (Dobin, 2013)
T-Base; version 14.3	4D SAS, 60 Rue d`Alsace, 92110 Clichy, France

2.2 Methods

All mouse experiments were performed in accordance with the latest national guidelines and according to the German Animal Welfare Act (*Tierschutzgesetz*) and approved by local health authorities.

Mice were housed under specific-pathogen-free (SPF) hygiene measures. Mice treated with staphylococcus aureus (*S.aureus*) were housed under SPF conditions in individually ventilated cages (IVCs). All mice were fed with standard food and water *ad libitum*.
Animals in experiment were evaluated daily for: General appearance like skin, movement, nose hairs, tails, social behavior etc. and special parameters were checked according to the individual experimental requirements like: Bodyweight, EAE scoring (**2.2.13**), proteinuria etc.

Before organ extractions, if not other noticed, the animals were first anaesthetized with an 4% (v/v) isoflurane/ oxygen mixture in a chamber under a fume hood in the animal facility. The reflexes were checked in the lower murine leg for proper and sufficient anesthesia. Afterwards, mice were sacrificed by cervical dislocation and organs were removed from the murine body.

2.2.1 Genotyping of trans genic mice

To determine and validate the genotype of the used transgenic mice (**2.1.1**) a PCR-based approach was used.
Genotyping was initiated by DNA extraction and amplification from mice biopsies (mice tails). For this purpose the *XNAT2 Extract-N-Amp Tissue PCR kit* was used according to the manufacturers recommendations and protocol.

In the first step of the process, a *PCR mix* of 100µL *Extraction Solution* and 25µL of *Tissue Preparation Solution* (TP) was mixed and added to the mice tail. The DNA was then released from the biopsy by incubation at 55°C for 10min in a thermal cycler. The DNA extraction was stopped by adding 100µL of

Neutralizing Solution. After this step, the DNA was ready for further PCR amplification. To do so, a PCR mix was prepared according to **Table 4** and **Table 5** (for 1x approach). Primer (stock concentration of 100µM, if not other depicted) were used depending on the gene of interest, see **2.1.3**.

Table 4: PCR mix for CD4 cre-, IL17A cre- and Rosa26 (YFP) genotyping

Reagent/ Primer	Volume
Extract PCR Reaction Mix	10µL
Primer 1	1µL
Primer 2	1µL
(Primer 3 - if necessary, see **2.1.3**)	1µL
Nuclease free H_2O	Ad 16µL

Here, the PCR Reaction Mix included all reagents important for PCR amplification of target genes (buffer, salts, dNTPs, *Taq* polymerase).
In addition, 4µL of the extracted DNA was added for CD4 *cre*-, *Il17A cre*-, and *Rosa26* (YFP) genotyping.

Table 5: PCR mix for Tbx21 flox genotyping of transgenic mice

Reagent/ Primer	Volume
Tbx21 flox A primer (10µM)	1µL
Tbx21 flox B primer (10µM)	1µL
dNTPs (10mM)	0,4µL
10x *Dream Taq* buffer	2µL
Dream Taq	0,1µL
Nuclease free H_2O	14,5µL

For *Tbx21* (Tbet-) flox genotyping, 1µL of the extracted DNA was added to the PCR reaction mix. The thermocycler program was set according to the gene of interest (**Table 6**) caused by different annealing temperatures of the used primers due to different nucleotide lengths and sequences.

Table 6: Thermocycler programs for genotyping of transgenic mice

Gene of interest	Temperature	Duration	Note
CD4 cre	***95°C***	5min	
	95°C	30sec	
	62°C	20sec	
	72°C	30sec	No. of cycles: 2x33
	72°C	3min	
	4°C	∞	Band at 390bp
Il17A cre	**94°C**	90sec	
	94°C	30sec	
	61°C	40sec	
	72°C	50sec	No. of cycles: 2x31
	72°C	3min	
	4°C	∞	Mutant band at 597bp, Wt band at 304bp
Rosa26 **(YFP)**	**94°C**	5min	
	94°C	30sec	
	51°C	30sec	
	72°C	30sec	No. of cycles: 2x33
	72°C	5min	
	4°C	∞	Band at 600bp
Tbx21 **flox**	**94°C**	5min	Band at 600bp
	94°C	30sec	Band at 600bp
	60°C	30sec	Band at 600bp
	72°C	1min	
	72°C	5min	
	4°C	∞	Wt band at 298bp, *Tbx21* null at 400bp, *Tbx21* flox at 440bp

During DNA amplification, a 200mL and 1,5% agarose gel was prepared for gel electrophoresis.
During this molecular biological process, the electrical charge of nucleic acids strains (which is caused by the negatively charged phosphate residues) is used to separate them by size and charge in an electrical field. Other substances like proteins can be separated with this method as well.
While gel electrophoresis, the negatively charged nucleic acids (DNA/ RNA) migrate to the positive charge through a matrix of agarose or other substances. Shorter molecules migrate more easily through the pores of the agarose matrix than longer ones.

After the PCR reaction was finished and the prepared gel was ready to use, 4µL of ethidium bromide (EtBr) and DNA gel loading dye was mixed with the PCR amplification product. Finally, the gel pockets were loaded with these samples (including one pocket filled with a 1000bp DNA ladder) and the voltage was set to 120v and 400mA. The run was finished after the visible blue band reached the lower end of the gel. Afterwards, the gel was analyzed by the DNA ladder and according to the gel band pattern.

2.2.2 Induction of nephrotoxic nephritis (NTN)

In order to induce a nephrotoxic nephritis (cGN, NTN) in mice, anti-murine glomerular basement membrane (GBM) sheep antiserum was applied to healthy animals (female, 10-14 weeks old). Although the immune response in the human cGN is directed against different antigens compared to NTN the clinical outcome (e.g. proteinuria) and histology in the experimental mouse model shows very similar pathological features compared to the human situation in cGN as depicted in **Figure 8** (Unanue and Dixon, 1967). The antiserum was applied i.p. into the animals. Due to the different specificities of the antiserum the injected volumes and the pathogenic potential to induce the NTN and an immune response differed from batch to batch.

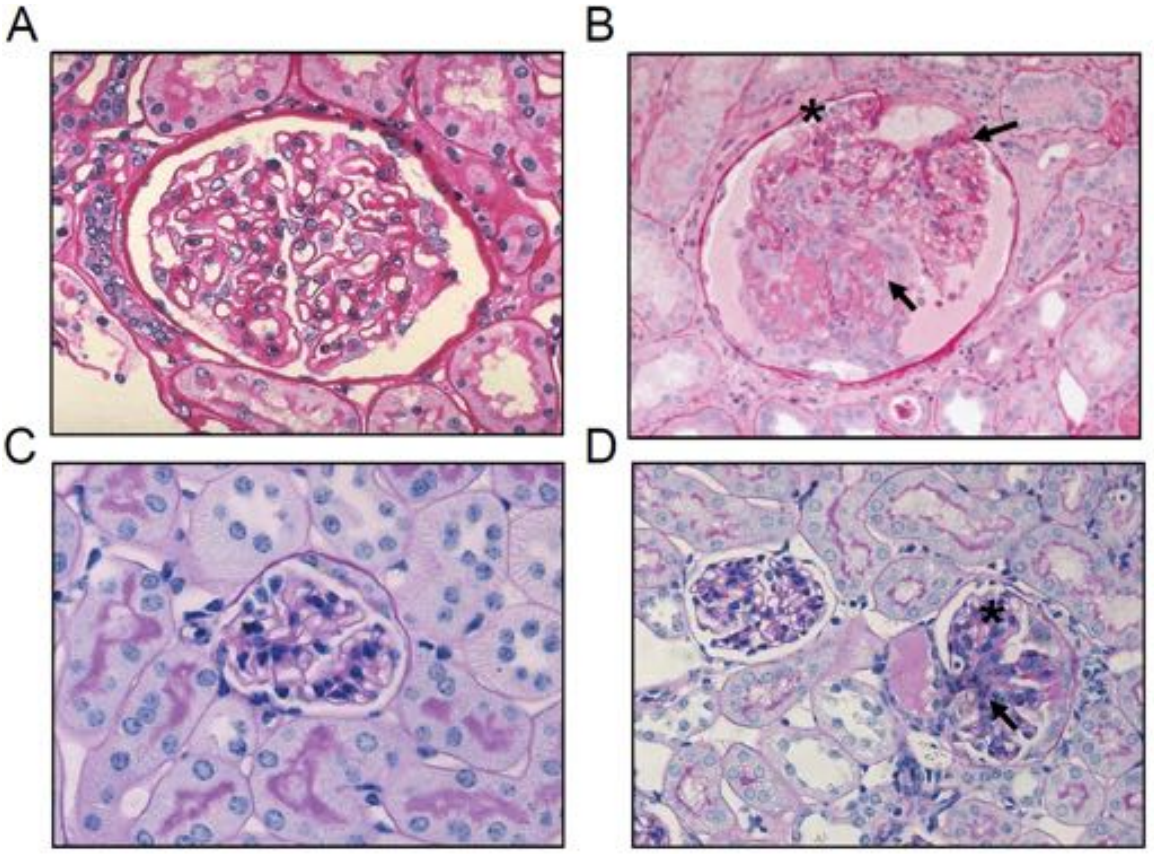

Figure 8: Histology of human & murine PAS-stained kidney sections

Periodic acid-Schiff (PAS) staining of kidney sections: **A**: Healthy and **B** cGN glomerulus. The nephritis-damaged glomerulus shows typical structural features which are also seen in cGN mice samples **D** but not in the healthy murine glomerulus **C**. As a result of autoimmune-mediated kidney inflammation, the damaged glomeruli exhibit cellular infiltrates (**arrow**) and necrotic tissue (**asterisk**), shown in **B** and **D**, so called *crescents*. The progression of the kidney disease finally leads to reduced glomerular filtration rate (GFR) and renal failure. (Image **A** and **B**: Courtesy of Prof. Dr. med. Thorsten Wiech, Institute of pathology, University Medical Center Hamburg-Eppendorf, Hamburg, Germany)

Ten days after NTN induction, organs were extracted (**3.3**) and analysis was performed in all NTN experiments.

2.2.3 Induction of Lupus Nephritis (Pristane model)

As a second glomerulonephritis model, the pristane-induced lupus nephritis has been chosen. From previous work it is known that in this systemic disorder is also dependent on a T_H17 cell-mediated immune response and exhibit a relatively high

T_H17 cell stability, similar to the NTN model (Krebs et al., 2016b). Also see results, **3.1.5**. The exact causes for this complex disease are still unknown.

Pristane is a natural occurring colorless oil. Chemically, it is a C19 branched alkane with the molecular formula $C_{19}H_{40}$ (**Figure 9**). The IUPAC (*International Union of Pure and Applied Chemistry*) name is 2,6,10,14-tetramethylpentadecane.

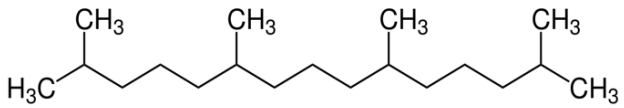

Figure 9: Structural formula of Pristane (2,6,10,14-tetramethylpentadecane)

To induced lupus nephritis via pristane, 0,5mL of this oil were injected into 4-month-old female IL-17A reporter mice.
It is known that about 8-10 days after pristane injection, the mice suffer from effects that could affect the animal lungs. Hence, in this time period, the mice were checked daily for abnormalities in behavior and appearance.

As a long-term experiment with slow progression, the mice were housed in mice cages for 52 weeks with food and water *ad libitum*, as described earlier.
In between, every 3-4 weeks urine samples were collected and proteinuria was measured using urea sticks.

2.2.4 Urinary sample collection and urinary proteinuria determination

The murine urinary samples were collected in a metabolic cage (**Figure 10**) within approximately four hours.

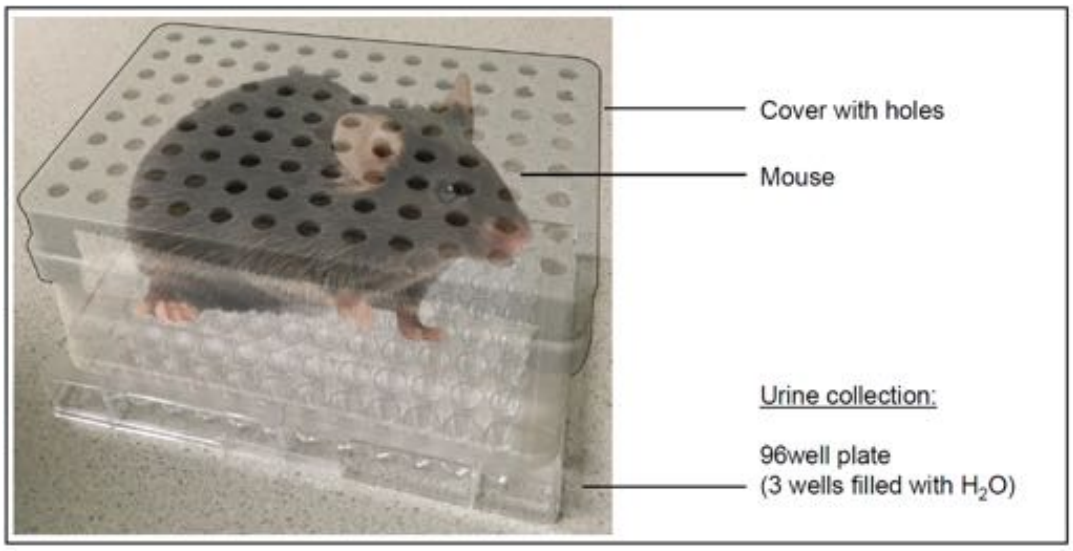

Figure 10: Metabolic cage for murine urine collection (scheme)

The mouse from which the urine was collected was placed inside the metabolic cage, sitting on top of a 96well plate. Three wells were filled with water. The lid was made from a pipet tip box. Holes were present for sufficient air supply. The whole cage was connected with adhesive tape. The collection procedure took about four hours. Afterwards, the mouse was released into normal cage. (Credit: Jacqueline Zimmerling / own photographs.)

The urinary protein content was determined by urea sticks. To do so, multiple parameter sticks were covered with 10µL urine from murine samples. Depending on the protein concentration, the color of the stick changed to yellow (negative/ no detectable urinary protein, "-" symbol), green (low proteinuria/ traces, "+/-" symbol) or to dark blue (high urinary protein, four "+" symbols), correlating with protein concentrations ranging as follows (**Table 7**).

Table 7: Determination of urinary protein by urea sticks

Symbol (on stick)	Color	Urinary protein content [mg/dL]
-	Increasing color: from yellow (negative, no protein) to dark blue (++++, high protein)	0 (negative)
+/-		>0 / <30 (traces)
+		30
++		100
+++		300
++++		≥ 2000

2.2.5 Histological renal tissue preparation

2.2.5.1 Preparation of tissue slices for PAS staining

To determine the histological renal damage, murine kidneys were extracted as described previously (**2.2.6**). Afterwards, slices of kidney tissue were stored in 4% v/v paraformaldehyde (PFA) overnight at 4°C. Then, the tissue slides were washed three times with phosphate buffered saline (PBS) for five minutes (min) each on the shaker. In order to reduce the water content and to prepare the tissue samples for paraffin embedding, tissue samples were first treated in a solution of 50% (v/v) ethanol (EtOH) for two hours at room temperature (RT).
Afterwards, the tissues were processed in a histological citadel, pre-filled with ethanol (EtOH, 60%, 70%, 96%, 100% v/v), paraffin and xylol in differently temperatured baths for 15 hours. After paraffin-embedding, the tissue was cooled down to -15°C and sliced with a microtome to a thickness of 0,5-1,0µm for periodic acid-schiff (PAS) staining.

After slicing, the tissue samples were de-paraffinized and hydrated again in order to prepare the tissue for PAS staining (**2.2.5.2**) according to **Table 8**.

Table 8: Sample treatment for preparation of PAS staining

Step	Component	Content (vol-%)	Duration (min)
1	Xylol	100	5
2	Xylol	100	5
3	Xylol	100	5
4	EtOH	100	5
5	EtOH	100	5
6	EtOH	100	5
7	EtOH	96	5
8	EtOH	96	5
9	EtOH	96	5
10	EtOH	70	5
11	EtOH	70	5
12	EtOH	70	5
13	Aqua dest.	100	5
14	Aqua dest.	100	5
15	Aqua dest.	100	5

2.2.5.2 PAS staining

This dye was used for staining of kidney tissue sections.

After re-hydration and de-paraffinination, the tissue samples were oxidized with periodic acid solution (0,5% v/v) for 15min at RT. Then, the samples were washed first with running tap water for 2-3min followed by washing with aqua dest. The slices were treated with RT-preheated *Schiff`s reagent* for 40min at RT, followed by washing with warm running tap water for 7min and then with aqua dest. During the incubation with *Schiff`s reagent*, the sections became a light pink color.
The actual staining of cell nuclei, mitochondria, elastin, myelin and collagen fibers was accomplished by incubation of the tissue slices with RT-warm ready-to-use hematoxylin solution (Böhmer, 1865) for 1-2min. Here, the sections immediately became dark pink. After PAS staining, the histological samples were checked for proper staining and may be repeated afterwards for appropriate time. Then, all samples were washed with warm running tap water for 2-3min and were then very

shortly treated with hydrochloric acid (HCl)/EtOH by shortly dipping each sample into the solution 2-3 times.
The samples were washed again under cold running water for 2min, followed by aqua dest.-washing. Finally, the PAS-stained tissue slices were dehydrated and coversliped using a mounting medium (*Eukitt*).

2.2.5.3 Hematoxylin-Eosin (HE) staining

During this procedure, hematoxylin is oxidized to haematein. Here, the alkaline haemalum dye is used to stain acidic or basophile structures blue. These structures include the ribosome-enriched endoplasmic reticulum and the cell nuclei-containing DNA. This dye was used for staining of small intestinal tissue samples.

After re-hydration and de-paraffinination, the tissue samples were incubated with haemalum for 2min. Afterwards, the samples were washed for 8min under running tap water and aqua dest. Next, tissue was incubated in eosin (0,5% v/v) for 15sec and were washed with aqua dest. After this step, tissues were washed first with 96% EtOH and then twice with 100% EtOH. Finally, tissue samples were washed twice with xylol and were then embedded with *Eukitt*.

2.2.5.4 Light microscopic crescent counting

Then, the slices were transferred onto a microscope slide holder for following microscopic investigation and crescent counting.
In order to determine the renal damage according to the microscopic tissue slices, 30 glomeruli in total were counted (**Figure 10**) and the ratio of pathogenic glomeruli was calculated. For this purpose, an objective with 20-fold magnification was used, leading to a total microscopic magnification of 200-fold.

2.2.6 Preparation of leukocytes from murine kidneys

After extraction of murine kidneys, the kidney capsule was gently removed in order to optimize later tissue digestion. Then, the organ was transferred onto a petri dish. A small piece of the kidney pole was removed for RNA isolation and a middle slice was cut with a scalpel for histological investigations (**2.2.5**). The rest of the organ was cut with a scalpel into very small pieces. Afterwards, the tissue was transferred into a “C tube” (for GentleMACS dissociator), prefilled with 5mL RPMI-digestion medium (**2.1.7**). For tissue digestion 20µL Collagenase D and 10µL of DNase I was added to the cell suspension and was incubated after gentle mixing at 37°C in a water bath for 40min.
After digestion, the cell suspension was treated twice in a GentleMACS (standard programs: “mSpleen 1.01” and then “mLung 2.01”). Then, the suspension was centrifuged at 300g for 8min and 4°C and the supernatant was removed. For leukocyte enrichment, the cell suspension was centrifuged for 15min at 500g and RT in density gradient (using a 5mL of a 37% colloidal silica particle suspension - “Percoll”, see **2.1.7**).

This step was done in a 15mL tube. After the centrifugation, the tube was placed upside down in a tube stand and the remaining cells were transferred into a 1,5mL micro tube for later treatments like $CD4^+$ enrichment (**2.2.17**), re-stimulation and/or FACS staining.

2.2.7 Isolation of cells from murine spleens

The previously extracted spleen was removed from fatty tissue and then transferred into 50mL tubes, pre-filled with 10mL Hank′s balanced salt solution (HBSS). Then, the organ was mashed through a 70µm cell strainer in order to homogenize the cells. Afterwards, the strainer was washed three times with 10mL ice cold HBSS each. Eventually, the cell suspension was centrifuged at 300g at 4°C for 7min followed by removal of the supernatant.

To remove fatty tissue residues and not to clog the FACS device, the cell suspension was filtered a second time using a 40µm cell strainer. Again, the strainer was washed with ice cold HBSS (three times with 5mL each).
The final volume of 15mL was used for cell number quantification (**2.2.9**).

2.2.8 Erythrocyte lysis of spleen cells

Efficient FACS detection of lymphocytes depends on the elimination of interfering cells. Therefore, spleen cells were prepared as described in **2.2.7**.
Red blood cells (erythrocytes) were lysed by addition of a two-component solution made of NH_4Cl, and Tris(hydroxymethyl)aminomethane hydrochlorid (Tris-HCl) in a ratio of 9:1 v/v (**2.1.7**). 1mL of this solution was added to the cell pellet. Then, the suspension was incubated at RT for 5min. The lysis was stopped by addition of 5mL of ice cold PBS or HBSS. Eventually, the cells were centrifuged at 350g for 5min at 4°C and finally washed two times with 2mL of cold PBS.

2.2.9 Automated and manual cell count

For automated cell counting, an 10µL aliquot was used. This cell suspension was diluted with 10µL of trypan blue (TB) staining dye. The suspension was incubated for about one min at RT. If a cell is dead the dye will migrate through the porous cell membrane and therefore stains dead cells blue.

However, living cells with an intact cell membrane are not stained which is visible under the light microscope. Afterwards, this suspension was added onto a cell counting slide and inserted into the automated cell counter (**2.1.9**). Finally, a size selection (4-12µm) was set and the counter displayed the living and dead cell number.

Manual cell counting is (if executed carefully) more precise in terms of the actual cell number compared to the automated cell counting (see above), but takes significantly longer. In order to manually determine the cell number, a microscopic

glass slide with embedded gridlines (Hemacytometer, Neubauer cell chamber) was used (**Figure 11**).

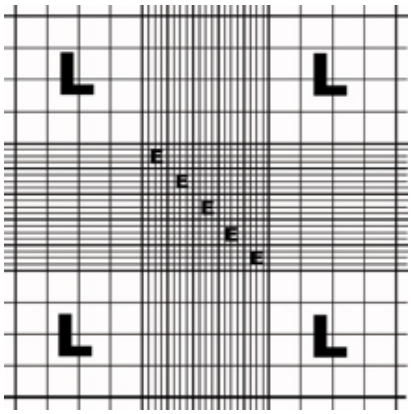

Figure 11: Neubauer cell counting chamber

Hemocytometer used for manual cell counting. Four squares (indicated by the letter **L**) were counted. Then, the mean cell count was calculated. The cell number was subsequently calculated by multiplication of the mean sum, the dilution factor and the chamber factor.

First, the hemocytometer was cleaned with alcohol and water. Then, a 5µL aliquot of the well homogenized and mixed harvested cells was removed and 5µL of PBS was added. Next, 10µL of TB was added to the cell suspension and the suspension was incubated for 1min at RT.
Afterwards, four corner squares (see **Figure 11**, marked with **L**) were counted using a microscope with 20-fold magnification and the mean cell count was determined.
Finally, the cell number was calculated (mean sum of counted cells **x** dilution factors **x** 10.000, for the *chamber factor* of the hemocytometer).

2.2.10 Enzyme-linked immunosorbent assay (ELISA) of renal albumin

The principals of the *enzyme-linked immunosorbent assay* (ELISA) are the same as the *cytometric bead array* (CBA) or vice versa (**2.2.31**). In contrast, the used sandwich ELISA reaction takes place not on a bead but on the surface of a 96-well plate coated with an anti-murine, anti-albumin antibody.

The detection reaction is also different to that of the CBA. In the ELISA, a horseradish peroxidase (HRP-) coupled detection antibody is used. In the process, the HRP reacts with the 3, 3', 5, 5'–tetramethylbenzidine (TMB) substrate solution. During this chemical reaction, the peroxide (H_2O_2) is being reduced to water (H_2O) and the TMBE is oxidized (

Figure 12). As a result, the color of the solution gets blue (at an absorption maximum at 650nm). In the course of the reaction, more and more oxidized TMB is formed which tends to precipitate from the solution. In order to get accurate measurements, the reaction is stopped by addition of sulfuric acid (H_2SO_4). After this step, the solution gets yellow at a wavelength of 450nm (Martin et al., 1984).

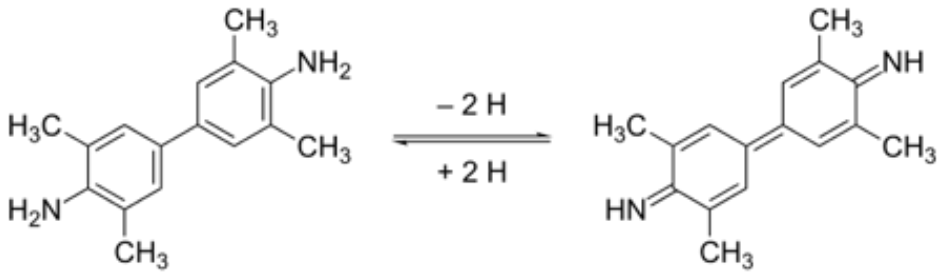

Figure 12: Oxidation of TMB by horseradish peroxidase

In the course of the ELISA detection reaction 3', 5, 5'–tetramethylbenzidine (TMB) is being oxidized by the horseradish peroxidase (HRP), coupled to the detection antibody. During this reaction, the peroxidase (H_2O_2) is reduced into water (H_2O). As a result, the solution color gets blue at 650nm. After this step the stop solution (sulfuric acid, H_2SO_4) prevents precipitation of the oxidized TMB and the color gets yellow du to elector shifts.

In order to perform the albumin ELISA from collected murine urine samples (**2.2.4**), the following buffer and solutions were prepared one day in advance (**Table** 9 and **2.1.7**).

Table 9: Buffers and solutions for albumin ELISA

Buffer / solution
Coating buffer
Wash solution
Postcoat solution
Sample / Conjugate diluent

One day before the actual albumin quantification, a high-binding 96well-plate was coated with anti-murine albumin antibody (**2.1.5**). To do so, 100µL of the well mixed antibody was diluted into 9900µL of prepared coating buffer in a 50mL tube. Then, 100µL of the 1:100 antibody dilution was transferred into the plate via a multichannel pipette. The plate was covered and coated over night at 4°C.
The next day, the plate was washed three times with 200µL washing buffer per well. After each washing step, the plate was tapped onto the laboratory bench covered with paper tissues. After the last washing step, it was very important to remove any residual liquid from the wells to ensure proper pre- sample dilutions (see below).

After plate washing 200µL of postcoat solution per well were transferred into the plate, followed by 30min of incubation time at RT in order to block unspecific binding sites. Meanwhile, sample and standard dilutions were prepared (see below). Afterwards, the plate was washed three times with 200µL washing buffer per well, according to previous washing steps.

To quantify albumin in murine urine samples via ELISA, serial sample dilutions were prepared according to their proteinuria level (by urine sticks, **2.2.4**). As shown in **Table 10**, dilutions are depicted according to their proteinuria level.

Table 10: Pre- sample dilutions for albumin ELISA

Level of proteinuria (according to urea stick, by symbols)	**Urinary protein content [mg/dL]**	**Pre-dilution of urine samples for albumin ELISA**
-	0 (negative)	**No ELISA**
+/-	>0 / <30 (traces)	1:1000 / 1:500
+	30	1:1000
++	100	1:20.000
+++	300	1:50.000
++++	≥ 2000	1:100.000

After preparation of all sample pre-dilutions with sample / conjugate diluent solution in 1,5mL tubes, albumin standards were prepared from mouse-albumin 1mg/mL according to **Table 11**.

Table 11: Albumin standard dilutions for ELISA

Standard No.	**Standard concentration [ng/mL]**
S0	10.000
S1	1.000
S2	500
S3	250
S4	125
S5	62,5
S6	31,25
S7	15,63
S8	7,8

In the next step of the albumin ELISA, 100µL of sample or standard dilution were pipetted into the appropriate wells. The plate was then incubated with sample- and standard dilutions for 1h at RT. Again, the wells were washed five times with 200µL

washing buffer per well. For Incubation with the HRP-coupled detection antibody, the well mixed secondary antibody (**2.1.5**) was diluted 1:50.000 in 50mL of sample diluent. Then, 100µL of the detection antibody per well was transferred and then incubated for 1h at RT and covered. Afterwards, the plate was again washed 5 times and the substrate reaction followed by addition of 100µL of ready-to-use TMBE substrate solution to each well. The plate was incubated in the dark for 15min at RT. Meanwhile, the photometer was switched on the plate layout was set in order to ensure fast sample measurement. The substrate reaction was stopped by addition of 100µL 2M H_2SO_4 per well under the fume hood. Immediately after the reaction was stopped, the plate was measured via a photometer at 450nm and the albumin was quantitatively determined in the murine samples.

2.2.11 Quantification of other parameters in murine blood and urine

Quantification of creatinine, urea, triglycerides and cholesterol from murine blood and urine samples were performed in the central laboratory facility (*Zentrallabor*) of the UKE.

2.2.12 Induction of experimental autoimmune encephalomyelitis (EAE)

EAE is one of the most common animal model for MS which shares many pathophysiological and clinical features (Constantinescu et al., 2011; Robinson et al., 2014). In this model, the disease is caused by immunization of the mice with peptides of myelin proteins (Aharoni et al., 1997; Althaus, 2004; Arnon and Aharoni, 2009). The latter is a glycoprotein which forms an insulation layer around the axons of nerve cells in the central nervous system (CNS). The myelin facilities higher nerve conduction velocity at relatively small axon diameter by the salutatory excitation conduction (Campbell et al., 2015).
Due to the relatively low immunogenic potential of the myelin peptides, strong adjuvants (like complete Freund`s adjuvant, CFA) are used.

EAE induction was performed on day 0 of the experiment by injection of 2x100µg of myelin oligodendrocyte glycoprotein (MOG_{35-55}) into the tail roots of the anaesthetized animals (male mice, 12 weeks old). The immunogenic epitope MOG_{35-55} was suspended in CFA prior to immunization.
On day 0 and 2 days later, 100µL of a solution containing 200ng pertussistoxin (PTx) was injected retrobulbary using a fine insulin needle (Bittner et al., 2014).
In the course of the disease, mice develop a self-limiting monophasic EAE with ascending paralysis within 8-14 days after immunization starting from the tail. After EAE induction, the mice were evaluated daily until the end of the experiment (**chapter 2** and **2.2.13**). In addition, mice were provided with liquefied normal dry food directly after the first signs for tail paralysis and until the end of the experiment.

2.2.13 Mice evaluation during EAE experiments (EAE scoring)

To evaluate the disease severity, mice were clinically checked in respect to general conditions like body weight, skin-, eye-, after-, tail- and hair- appearance and social behavior (aggressive, lethargic etc.).
Also, grid tests were performed in order to determine the degree of paralysis of the extremities according to **Table 12** (Brooks and Dunnett, 2009).
Therefore, mice were put on a cage grid and then the grid was turned over to check the grip of the tail and the legs of the animal.
Mice with EAE scores above 3,5 were sacrificed to according by the guidelines of the animal protocol.

Table 12: Evaluated Features and scoring points during EAE scoring

Disease severity	EAE Score	Grid test	Walk	Additional Scoring points
-	0	Secure grip, tail used for climbing	Normal	**+0,5** Weak tail, loss of contact during climbing
Low	1	Secure grip, feet put sequentially	Normal	**+0,25** One criteria from “1,5” fulfilled
Moderate	1,5	Feed slip off *AND* feed were put simultaneously	Slight waddling	**+0,25** Both feed put simultaneously
	2	Loss of both feed during climbing, can be restored	Waddling (good to overserve)	**+0,25** Longer loss of contact
High	2,5	Loss of both feed during climbing, can *NOT* be restored	Clear waddling	**+0,25** Feed seem to be stiff (heavy waddling)
Very high	3,0		Partial paralysis of one or both legs	**+0,25** One leg completely paralyzed
End-stage disease (mice were sacrificed)	3,5		Complete paralysis of both legs	**-0,25** Only one leg is completely paralyzed

2.2.14 Preparation of leukocytes from murine brains

On day 14 after EAE induction (**2.2.12**) and appropriate EAE score (at least 1,5 of 3,5), the experiment was finished by extraction and analysis of immunological cells from the murine brain.
The animals were continuously anesthetized (**2.2**). For the following coronae perfusion, 600µL of the analectic burprenorphin (0,1µg/g body weight) was injected subcutaneous into the mice. Then, the mice were placed in position to open the abdomen. The lungs were cut and 5mL of perfusion solution (PBS or NaCl) was slowly injected into the heart of the animals. During this procedure, the liver turned from red to whitish. To ensure death of the animals, the heart was cut in two after perfusion.

For brain extraction, the mice were fixed on a cork plate and the skin was opened from the back to the nose of the animal. Then, the skull and the intramedullary canal was carefully opened with a small sharp scissor and the brain was completely and very carefully removed from the inner scull via a sharp small spoon, including olfactory bulb, cortex, midbrain, cerebellum and a short part (ca. 1cm) of the medulla/ spinal cord.
After organ extraction, the fine-sheared brain tissue was transferred into a C tube containing 5mL of digestion medium, 50µL Collagenase D and 25µL DNase I. The cell suspension was incubated in a water bath for 40min at 37°C. Afterwards, the suspension was further shredded in a gentleMACS (1^{st} pre-set program: “Brain 3.0”, 2^{nd} pre-set program “spleen 2.0”). The tube was then centrifuged at 350g for 6min at RT and the supernatant was removed. The pellet was washed two times with 5mL of PBS each. To homogenize the cells, the suspension was mashed through a 40µm strainer and was washed twice again (see above). Afterwards, 5mL of percoll was added and resuspended for density gradient centrifugation (15min at 500g and RT, break 4 of 9). The supernatant was removed carefully and 1mL of PBS was used to resuspend the cell pellet.

2.2.15 Induction of anti-CD3 mediated duodenitis

In order to induce anti-CD3 duodenitis, a sepsis model, mice were i.p.-injected with 20µg of anti-mouse anti-CD3ε antibody/ PBS solution on day 0 using a 1mL syringe. On day 2, the procedure was repeated a second time, four hours before extraction of the small intestine.

2.2.16 Isolation of murine mononuclear cells from small intestine

First, the organ was extracted from mice to prepare cells from the small intestine (si), located between stomach and cecum. The organ was transferred to a PBS soaked paper towel and fatty tissue and Peyer`s patches were removed. After this, a ring of the small intestine was cut for histology and the organ was cut open longitudinally. The latter was put into a well of a 6well plate, filled with 6mL of washing buffer. The feces were removed by shaking around the tissue in washing buffer with forceps. The step was repeated in fresh buffer and the tissue was transferred into a petri dished filled with washing buffer. After this step, the tissue was cut into pieces one cm in length in a 50mL tube, pre-filled with 20mL of pre-warmed (37°C water bath) washing buffer and a magnetic stirring bar. 10µL of dithiothreitol (DDT) was added to a final concentration of 1mM and the tube was put on top of a magnetic stirrer in an incubator for 7min at 37°C. Then, the suspension was poured through a concave metal sieve (200µm) and the remaining tissue was washed by rinsing with cold washing buffer. Thereafter, the tissue was transferred with forceps into a 50mL tube containing 20mL of pre-warmed washing buffer and a magnetic stirring bar. Again, the suspension was incubated for 7min on top of a magnetic stirrer and in a 37°C incubator but this time without DDT.
Afterwards, the suspension was again poured through a concave metal sieve and the remaining tissue was washed twice by shaking around with forceps in a petri dish, containing 6mL of PBS, 1% FCS solution (**2.1.7**). The tissue was cut in very small pieces with a scissor and the remaining cell mash was transferred to a 50mL tube filled with 10mL digestion medium using a truncated pipet tip.

The tip was washed two times with liquid from the top of the tube. Then, 40µL of Collagenase D and 20µL of DNase I was added and the suspension was incubated for 30min at 37°C.
After this incubation, a 70µm nylon mesh (cell strainer) was placed into a 50mL tube and the cells were mashed through the mesh for homogenization. The strainer was then washed two times with 10mL of washing buffer and the tube was centrifuged at 360g for 7min at 4°C.

The supernatant was removed by tube inversion and 5mL of a 37% percoll solution was added for density gradient centrifugation at 500g (with reduced break 4 of 9 to sustain the formed gradient) for 15min at RT. Again, the supernatant was carefully removed and the cells were transferred into a FACS tube. Finally, cells were washed with 2mL of MACS buffer.

2.2.17 Enrichment of $CD4^+$ T cells from cell suspension

All antibodies used for $CD4^+$ enrichment were directed against anti-mouse antigens.

2.2.17.1 $CD4^+$ T cell isolation kit (Miltenyi Biotec)

The kit was used according to the manufacturers recommendations and protocol.

Before the actual $CD4^+$ enrichment of the separated cells (as described in **2.2.6**, **2.2.7** and **2.2.14**), the cell suspension was centrifuged at 360g for 7min at 4°C.
Next, 400µL of MACS buffer was added and the mixtures was vortexed gently to detach the cell pellet and to homogenize the cells. Then, 100µL of the well mixed Biotin antibody cocktail was added and the cells were incubated in the fridge (4°C) for 5min. 300µL of MACS buffer was added. Afterwards, 200µL of the very well (for at least 60sec) vortexed anti-biotin Microbeads was added and the mixture was incubated for another 10min at 4°C. In the meantime, in order to prepare the columns for the next step, the latter were placed in a magnetic column holder and were first flushed with 1mL of MACS buffer three times each.

Also, a 30µm filter was put on top of the column to prevent cells from clogging in the FACS device. To optimize flow-through, the filter was also flushed with 500µL of MACS buffer. Eventually, a 15mL tube was placed beneath the column to collect the $CD4^+$ enriched cellular flow-trough.
After incubation, the cell suspension was added on top of the filter.
Finally, the column was washed three times with 1mL MACS to recover as much $CD4^+$-enriched cells as possible. The cell suspension was washed one time with MACS buffer by centrifugation at 360g, 4°C.

2.2.17.2 EasySep Mouse $CD4^+$ T cell isolation kit (Stemmcell)

In later experiments, a different CD^+ T cell isolation kit (*Stemmcell*) was used, because of practical advantages over the *Miltenyi* kit (faster procedure, no column needed).

The kit was used according to the manufacturers recommendations and protocol. The cell concentration was set to $1x10^8$ cells/mL in a volume range of 0,25-2mL, as proposed by the manufacturer.
In order to fulfill the manufacturers requirements for this kit, the cells were counted prior, as described in **2.2.9**. In case of variations in cell number, the volumes were adjusted accordingly.

Again, as explained for the Miltenyi $CD4^+$ separation, before the actual $CD4^+$ enrichment of the separated cells (as described in **2.2.6**, **2.2.7** and **2.2.14**), the cell suspension was centrifuged in a 5mL FCAS tube at 360g for 7min at 4°C.
Then, 50µL of rat serum per mL sample was added and the suspension was carefully mixed. Next, 50µL of isolation cocktail per sample was added and the cells were gently mixed and incubated for 10min at RT. During incubation time, the magnetic beads (*RapidSpheres*) were well vortexed for at least 60sec.
After incubation, 75µL of the magnetic beads per mL of sample were added and the cell suspension was gently mixed and 2.5min of incubation time at RT followed. Then, the suspension was filled to 2.5mL with PBS.

Finally, the tube containing the cell suspension was placed in a single tube magnetic holder for 2.5min. Then, the supernatant was filled into a 5mL tube.
These cells were enriched $CD4^+$ T cells. The cells were washed one time with PBS and stored at 4°C as described earlier.

2.2.18 *Ex vivo* re-stimulation of cells from spleen and kidney

PMA (Phorbol 12-Myristate 13-Acetate) and Ionomycin (from the bacterium *Streptomyces conglobatus*) are commonly used in combination to stimulate T cells and hence promote the intracellular production of Ca^{2+} and cytokines in different cytokines (Ai et al., 2013; Elzi et al., 2001).
For *ex vivo* re-stimulation, organs (spleen, kidneys) were extracted and a homogenous cell suspension was prepared (see **2.2.7** and **2.2.6**). Then, the cell suspension was centrifuged in a FACS tube at 360g and 4°C for 5min. Next, the stimulation medium was prepared according to **2.1.7**.
For re-stimulation, 1mL of this freshly prepared medium was added to each sample. After gentle mixing, the samples were incubated in a 37°C incubator without CO_2 for 3,5h. Afterwards, the samples were washed two times each with 2mL of MACS buffer for further FACS staining.

2.2.19 Cellular surface- and intracellular staining for FACS analysis

This chapter describes the cellular surface- and intracellular staining for FACS analysis in a 96well plate format.

For cell surface staining, cells were first centrifuged at 350g and 4°C for 6min. After homogenization and detachment of the cell pellet by gentle vortexing, the appropriate cell surface marker was selected and added according to **2.1.6.**
Cells were incubated in the fridge for 30min at 4°C to prevent bleaching of the fluorescent conjugates. Two times washing with 2mL PBS each and centrifugation as mentioned followed. Then, the cells were carefully transferred into a

96-well plate. For cell fixation, 200µL of freshly prepared 3,7% (v/v) PFA was added by gentle resuspension.
After incubation in the fridge for 17min, cells were centrifuged at 350g and 4°C for 2min. In order to gently permeabilize the cells, 200µL of the nonionic, non-denaturing detergent octylphenoxy poly(ethyleneoxy)ethanol (IGEPAL CA-630, NP-40, 0,1% (v/v) final concentration) was added and incubated in the fridge for 5min. Afterwards, the sample was centrifuged at 350g and 4°C for 2min. Finally, 100µL of a dilution of the appropriate intracellular antibody (**2.1.6**) was added and the cell suspension was incubated in the fridge for 30min.
Before FACS measurement, the sample was washed two times with 200µL MACS buffer and live/dead staining was performed by addition of 500µL of a 1:1000 dilution (v/v) of Near-IR (NIR) dead cell stain reagent (**2.1.11**) and incubation for 25min at 4°C in the dark. For FACS measurement, cells were washed with 200µL of PBS.

2.2.20 Induction of *staphylococcus aureus* infection

All Staphylococcus aureus (*S.aureus*) experiments were performed with the *SH1000* bacterial strain.
In order to prepare a bacteria suspension from *one* colony, stock bacteria suspension was plated on a ready-to-use blood agar-based nutrient medium in a petri dish and in a pathogen free area. Therefore, a glass inoculating loop was cleaned and partly sterilized with ethanol. Then, the loop was burned over a Bunsen burner flame. After short cool down of the loop, it was inserted into a stock *SH1000* bacteria culture and was then streaked over the medium in the petri dish. To get well separated single-bacterial colonies, the bacteria mixture was spread over the surface of the agar medium that fewer and fewer bacteria were deposited at widely separated points over the surface of the medium (streak-plate procedure). After the first bacteria streak over the medium, a second and then a third sterilized loop was plated crossing the previous streaks.
After incubation at 37°C and 5% CO_2 (v/v) for two to three days, petri dishes with bacteria colonies were removed from the incubator. Then, 10mL PBS was filled into a 15mL tube. One bacteria colony was carefully replaced into the

PBS-pre-filled tube via a sterilized inoculation loop. *SH 1000 S.aureus* bacteria tend to stick to each other. To separate and homogenize the bacteria suspension, a *sonicator* (ultrasonic probe) was used. Therefore, the probe was first sterilized with ethanol. Then, the probe was inserted into the center of the 15mL tube which was put into an ice-filled bucket to reduce heat formation during the sonication process.
The *sonicator* was set to 20sec and 70% of the maximal sonication amplitude. Afterwards, 700µL of the bacteria suspension and 700µL of PBS were mixed and transferred into a photo spectrometer cuvette. The optical density at 600nm (OD_{600}) was measured and dilutions were prepared. Mice (males, 10 weeks old) received $1x10^7$ staphylococci in 200µL sterile PBS via the lateral tail vein.
In addition, bacteria inocula were controlled by planting serial dilutions onto blood agar plates. On day 14 after infection with *S.aureus*, mice were sacrificed and organs were analyzed.

2.2.21 Flow cytometric cell sort and bulk sequencing

All cell sorts were performed with the BD *FACSAria IIIu* according to the manufacturer. Cell sorts were performed by the UKE FACS Core Facility.

Cells for further RNA isolation and RNA sequencing were sorted directly into refrigerated 1,5mL micro tubes containing 350µL of RLT lysis buffer (*RNeasy Plus Micro* kit, see **2.1.11**), supplemented with 1:1000 (v/v) ß-mercaptoethanol.

For RNA sequencing, at least 20.000 cells were sorted each to ensure sufficient cell number and RNA content. Three independent experimental samples were send for sequencing per disease model and YFP status (**Table 20**).

RNA sequencing was performed by *Novogene* genome sequencing company in Beijing, China.

2.2.22 RNA isolation from cell suspension for sequencing

For isolation of RNA the *RNeasy Plus Micro* kit from Qiagen was used and handled according to the manufacturers recommendations and protocol.

Other cells which were not sorted by flow cytometry (**2.2.21**) were stored at -20°C/ -80°C and thawed before RNA isolation. Then, 350µL of RTL lysis buffer was isolated and were incubated for 2min at RT.

First, the cell lysate was loaded onto an gDNA eliminator column in order to remove genomic DNA. During centrifugation at 8000g for 30s, the flow-through containing RNA was kept for next steps in the procedure. The genomic DNA was absorbed to the gDNA eliminator column and was disposed. Then, the flow-through was loaded onto a RNA-isolation column. During the next steps, buffer conditions enabled RNA-specific adsorption to the column silica membrane and removal of impurities and other contaminants. By repeated buffer washing and centrifugation steps, contaminants passed through the membrane while the RNA was bound to the silica membrane. Finally, the purified RNA was eluted in water. The elution was then repeated a second time to ensure maximal RNA yield. Then, RNA was quantified with via a spectrophotometer (**chapter 2.2.23**).

2.2.23 DNA and RNA quantification

To quantify nucleic acids in solutions, a fluorometer (*Qubit*) and a micro volume UV-/Vis spectrophotometer (DeNovix-*DS11*).
In general, the fluorometer is more accurate for measuring small amount of nucleic acids in solution, but is also more time consuming.
In order to approximately determine the amount of RNA for cDNA synthesis, the spectrophotometer (*DeNovix-DS11)* was used.

Quantification with fluorometer

The Qubit HS (High sensitivity) kit was used according to the manufacturer's recommendations and protocol.

First, a 1:200 dsDNA HS reagent dilution in dsDNA HS buffer was prepared (1µL reagent and 199µL buffer). Then, 190µL (for two standards) and 198µL (for the samples) of this dilution were pipetted into a Qubit tube. Next, 10µL (standards) or 2µL (sample solution) were added to the previously pipetted dilutions, respectively. The tubes were incubated for 2min at RT. Afterwards, one tube after the other was inserted into the fluorometer and the DNA concentration was measured.

In the next step, the *RIN* value (RNA integrity number) which is an algorithm for assessing integrity of RNA, evaluated from the 28S to 18S RNA, was determined. In all cases the RIN was in the range of 8,5 to 9,9 from 10 for best RNA integrity.

Quantification with spectrophotometer

To quantify nucleic acids, the device was turned on and the samples type (DNA/RNA) was set in the software main menu. Then, the photometer was washed three times with water by adding 2µL of liquid, followed my clean-wiping with tissue paper to ensure no contamination with other samples measured in the device. Eventually, 1µL of the sample diluent (mostly RNase-/ DNase free purified water) was added to the sample pedestal. The pedestal arm was closed and the sample free fluid was measured and set to zero (*blank*). Now, the pedestal was cleaned with a paper tissue and the rest of the samples were measured accordingly. Finally, the pedestal was washed again with water and dry cleaned with paper tissue.

2.2.24 Complementary DNA (cDNA) transcription *in vitro*

In order to perform qPCR measurements/ analysis, the previously isolated RNA needed to be transcribed into complementary DNA (cDNA). Therefore, first Master Mix 1 was prepared according to **Table 13** into 250µL PCR sample tube stripes. The used random hexamer primer stock solution was diluted 30-fold with H_2O.

Table 13: Composition of Master Mix 1 for cDNA synthesis

Reagent for each well / tube	Concentration	Comment
2µL Random hexamer primer	Stock: 3µg/µL	Diluted 1:30 (H_2O)
2µL dNTP`s	5µmol/L	
Add 16µL ddH_2O per Tube		

Then, 4µL each of RNA sample solution with a concentration of 100ng/µL was added to Master Mix 1. The resulting 20µL of solution per sample was incubated in a thermal cycler at 65°C for 5 min.
The sample tube stripes were centrifuged shortly with a table centrifuge to remove condensate water from the tubes which were caused during thermal cycling. Next, 16µL of Master Mix 1 (**Table 14**) was added to Master Mix 2, per sample.

Table 14: Composition of Master Mix 2 for cDNA synthesis

For each well/ Tube	Comment
8µL reaction buffer (5x)	5x reaction buffer
4µL H_2O	
2µL revert Aid Reverse Transcriptase	
2µL RNase Out	Recombinant Ribonuclease Inhibitor

Finally, sample tubes were removed from the thermal cycler and centrifuged again. Then, the sample tubes were inserted into a thermal cycler. The applied thermal program is depicted in **Table 15**.

Table 15: Thermal cycler program used for cDNA synthesis

Temperature	Duration
25°C	10min
42°C	1h
70°C	15min
4°C	∞

After cDNA synthesis, the generated cDNA was stored at -20°C for further use.

2.2.25 Quantitative real-time PCR (qPCR) analysis

In the first step of this real-time PCR method, the temperature is increased (95°C) in order to denature the double stranded cDNA. During this step, the 5'-end bound FAM fluorophore signal is restrained by a 3'-quencher molecule (dual-labeled probe). Afterwards, the temperature is decreased (60°C) allow specific hybridization of primer and probe. As the *Taq*-DNA-polymerase thermostable DNA polymerase from ***T****hermus* ***aq****uaticus*) extends the primer and synthesizes complementary DNA strands by non-labled primers and the templates, the 5' to 3' exonuclease activity of the *Taq* polymerase degrades the probe that has annealed to the template (Chien et al., 1976). This leads to the release of the fluorophore (here FAM) from the probe and thereby from the close proximity to the quencher. With each PCR cycle, more fluorescent labels are released which cause an increased fluorescent signal proportional to the amount of amplification products (Holland et al., 1991). For qPCR analysis, all samples were measured in duplicates.

After cDNA synthesis of isolated RNA (**2.2.24**), qPCR master mix was prepared as seen according to **Table 16**.

Table 16: qPCR master mix composition

Component	Volume
qPCR Primer (FAM-labeled target-probe, e.g. IL-27ra)	0,5µL
Fast Universal PCR Master Mix (2x)	5,0µL
H_2O	2,5µL

Then, in a qPCR 96well-plate, 1µL of sample was added to 9µL of the qPCR master mix each. In addition, 2 wells were loaded with 9µL qPCR master mix and 1µL water.

The plate was sealed with an adherent foil, followed by centrifugation at 1000rpm for 1min. Finally, the qPCR plate was inserted and the qPCR Thermo cycler was stared with pre-set sample plate layout and thermocycler program according to **Table 17**.

Table 17: qPCR cycler program

Temperature	Duration
95°C	20sec (1x)
95°C	1sec
60°C	20sec
	(Number of cycles: 45)

Determination of n-fold relative gene expression via ΔΔCt method

To determine the relative gene expression, the gene expression of a gene of interest (GOI) is normalized to a non-regulated Housekeeping gene (HKG).

Here, the expression of the GOI is referred to a ubiquitously and homogenously expressed gene (HKG). All qPCR`s were performed with the widely used

*HPRT1 (*hypoxanthine–guanine phosphoribosyltransferase), EC 2.4.2.8., ENSEMBL ENSG00000165704) as a HKG (Baddela et al., 2014; Tan et al., 2012). In the first step, the differences of the Ct values of the GOI and the HKG was calculated:

$$\Delta Ct = Ct(GOI) - Ct(HKG)$$

After this normalization, if there was an external control vs. and a treated sample the ΔΔCt was calculated by:

$$\Delta\Delta Ct = \Delta Ct(treatment) - \Delta Ct(control)$$

The relative difference in gene expression (expression fold change) of a sample between treatment and control (*ratio*), normalized to the reference gene (*HPRT1*) and related to a standard sample is given by:

$$ratio = 2^{-\Delta\Delta Ct}$$

(All calculations are in logarithm base 2 (log2). Since, every time there is twice as much of DNA the values for Ct decrease by one.)
An average (mean) of three separate qPCR experiments was calculated.

The ΔΔCt method is based on the assumption of optimal PCR efficiency during real-time analysis which means doubling of the DNA amount (number of DNA strands) after each PCR cycle. However, this is not true in practice. Therefore, this method is only a quantitative approximation (Pabinger et al., 2014; Pfaffl, 2004).

2.2.26 Flow cytometric measurements and analysis

All FACS analysis were performed according to the experiments using either the *BD LSR II* or *BD LSRFortessa* instrument with installed *BD Diva* software (**2.1.12**) and according to the manufacturer.

Before FACS measurements, cells were checked for cellular conglomerates and impurities which could potentially clog and damage the FACS device. If minor conglomerates were visible by eye, cells were homogenized using a 30µm cell strainer.

FACS data analysis were performed via the *FlowJo* and *Graphpad Prism* software (**2.1.12**).

2.2.27 IL-27 treatment of NTN-mice

In order to investigate the effect of IL-27 application in NTN-mice, NTN was induced as described in **2.2.2**. On day 5 after induction recombinant mouse IL-27 was daily injected i.p. in NTN and non-NTN mice for 5 days. As a control, PBS was injected in control mice as well.
To test the effect of cytokine injection, experiments were performed with different amounts of cytokine, ranging from 1µg, 3µg and 5µg per mouse (data not shown). The appropriate amount of cytokine was diluted and prepared in a final volume of 200µL using sterile PBS. Finally, 5µg of IL-27 was used per mouse for further experiments.

2.2.28 *In vitro* IL-27/ IL-6 stimulation and pSTAT3 staining

In order to investigate the effect of stimulation with IL-27 and IL-6 (Stumhofer et al., 2007) with regard to STAT3 activation, organs (spleens and kidneys) of NTN mice (NTN induction see **2.2.2**) or non-NTN mice were extracted and a homogenous cell suspension was prepared (**2.2.7** and **2.2.6**).
Before the actual stimulation of the cells, $CD4^+$ enrichment was performed (**2.2.17.2**).
Afterwards, cells were transferred in 1mL of digestion medium (**2.1.7**).
Since pSTAT3 and other STAT members easily get activated (/phosphorylated) by extracellular and intracellular stimuli, cells were incubated in FACS tubes for 2,5 hours at 37°C and 5% CO_2 to slow down metabolic processes and pSTAT3

formation. In order to prevent further cellular stress responses which could also result in STAT activation, during all processes high temperature shifts were tried to keep at a minimum until cell fixation. The cell suspension was then centrifuged at 350g and RT for 5min.
For preparation of cell surface staining, blocking of unspecific targets was performed by addition of 50µL PBS and 10µL mouse serum and incubation for 5min at RT. Cell surfaces were stained according to **2.2.19**.

Since the cell fixation potentially denature the epitope of surface marker, resulting in non-binding antibodies, it was important to perform cell surface staining before subsequent cell fixation.

After washing of the stained cells with PBS, cytokine dilutions were prepared in digestion medium and from stock solutions as depicted in **Table 18.**
To determine effective cytokine working concentrations, research in the literature was conducted (Owaki et al., 2008) and built the basis for our working concentrations.
Eventually, after centrifugation 1mL of each stimulation approach was added to the cells in the FACS tubes and they were incubated in a water bath (37°C) for indicated times.

Table 18: In vitro cytokine stimulation approaches

No. of approach for spleens	No. of approach for kidneys	Cytokine	Final conc. [ng/mL]	Duration of stimulation [min]
1	1	IL-6	20	15
2	2	IL-6	10	15
3	3	**IL-27**	10	10
4	4	**IL-27**	10	20
5	5	PBS	---	15
	6	**IL-27**	10	Over night
	7	PBS	---	Over night

To prevent further cell stimulation, 1mL of MACS buffer (RT) was added and the cells were immediately centrifuged at 350g for 5min at RT. Then, the supernatant was removed and cells were fixed by addition of 800µL of a solution of 2% (v/v) PFA in MACS buffer for 35min at RT. Next, cells were centrifuged at 600g for 7min at RT.
For preparation of subsequent permeabilization of the cells, a sample tube holder was placed and covered in ice to ensure fast sample cooling and gentle permeabilization conditions after addition of 1mL of freezing cold (-20°C) BD *Perm Buffer III* (**2.1.8**) to the cells. This was done under constant stirring.
The process was stopped after 30min at 4°C by addition of 3mL MACS buffer and centrifugation at 600g for 7min at 4°C. Washing steps were repeated two more times to ensure sufficient permeabilization buffer removal.
For the final intranuclear pSTAT3 staining, cells were centrifuged again at 600g for 7min at RT and 15µL of anti-mouse anti-STAT3 PE-conjugated antibody was added to the permeabilized and fixed cells. Incubation for 1h at RT and in the dark followed. After washing with 3mL PBS, cells were analyzed via FACS.

2.2.29 Protein isolation from renal tissue

To quantify cytokines in the kidney via Cytometric Bead Array (CBA), it was first important to inhibit proteases by addition of 300µL of an inhibitory protease cocktail ("*buffer A*", **2.1.7**) to ½ of a murine kidney in a 2mL tube. The cocktail was prepared shortly in advance from 7mL of PBS and one tablet of "*complete protease inhibitor*". Then, 300µL of a mixture from PBS, *complete protease inhibitor*, ethylenediaminetetraacetic acid (EDTA), ethylene glycol-bis(β-aminoethyl ether)-N,N,N′,N′-tetraacetic acid (EGTA), phenylmethylsulfonyl fluorid (PMSF), *NP40* ("*buffer B*") and a small metal sphere (**2.1.9**) was added . For cell lysis and homogenization, the tube was inserted into a shaker (*TissueLyser*) for 1min at 30Hz. Then, the lysate was checked for homogeneity and was then centrifuged at 4000g and 4°C for 10min. The supernatant was aliquoted and transferred into a new 1,5mL tube. The protein lysate was stored at -20°C until CBA analysis.

2.2.30 Protein quantification via *DC Protein Assay*

To quantify total protein in solution, the *DC Protein Assay* from BIO-RAD was used according to the manufacturer's instructions and protocol. The method is based on Lowry's folin phenol reagent reaction (Lowry, 1951).
The assay was performed on a 96well-plate and in duplicates. First, Bovine serum albumin (BSA) standards were prepared by serial dilutions according to **Table 19**.

Table 19: BSA standard concentrations for protein quantification

Standard No.	BSA standard concentration [ng/mL]
S1	10
S2	5
S3	2,5
S4	1,25
S5	0,625
S6	0,313

Then, 5µL of sample dilution (supernatant after protein isolation, see **2.2.29**) or standard solution were pipetted into two wells, followed by addition of 25µL "reagent 1" per well each and then 200µL per well of "reagent 2" (see referred method after Lowry et al., above). The well mixed reagents were incubated for 15min at RT. Eventually, the samples and standards were measured via Photometer at 630nm.

2.2.31 Cytometric bead array (CBA)

The Cytometric Bead Array (CBA) is a very sensitive multiplexed bead-based immunoassay using fluorescence-encoded beads suitable for use in flow cytometry to quantify e.g. chemokines, growth factors, cytokines and others.

This soluble protein assay was used according to the manufacturer's instructions and protocol.

The CBA kit was used for quantification of IL-27, IL-10 and IFN-γ in supernatants of kidney cells from IL-27-treated mice (**3.6.6**). For this purpose, the BD *LEGENDplex* mouse "*T Helper Cytokine Panel*" and the mouse "*Inflammation Panel*" was used (**2.1.11**).

Before the CBA could be performed, total protein of cellular supernatant was isolated from IL-27-treated animals (**2.2.29**) and total protein was quantified (**2.2.30**).

The principle of the assay (**Figure 13**) is the same as sandwich immunoassays (ELISA), where each bead set is conjugated with a specific antibody on its surface and serves as the capture beads for the particular analyte of interest in the supernatant. After several washing steps a biotinylated detection antibody cocktail was added, where each detection antibody in this cocktail bound to its specific analyte which were bound on the capture beads. Here, the components formed capture bead-analyte-detection antibody sandwiches. After addition of Streptavidin-phycoerythrin (SA-PE), the latter bound to the biotinylated detection antibodies which provided fluorescent signal intensities in proportion of the amount of bound analytes according to a pre-prepared analyte standard curves. Flow cytometric data were then analyzed by the Biolegend "*LEGENDplex Data Analysis Software*".

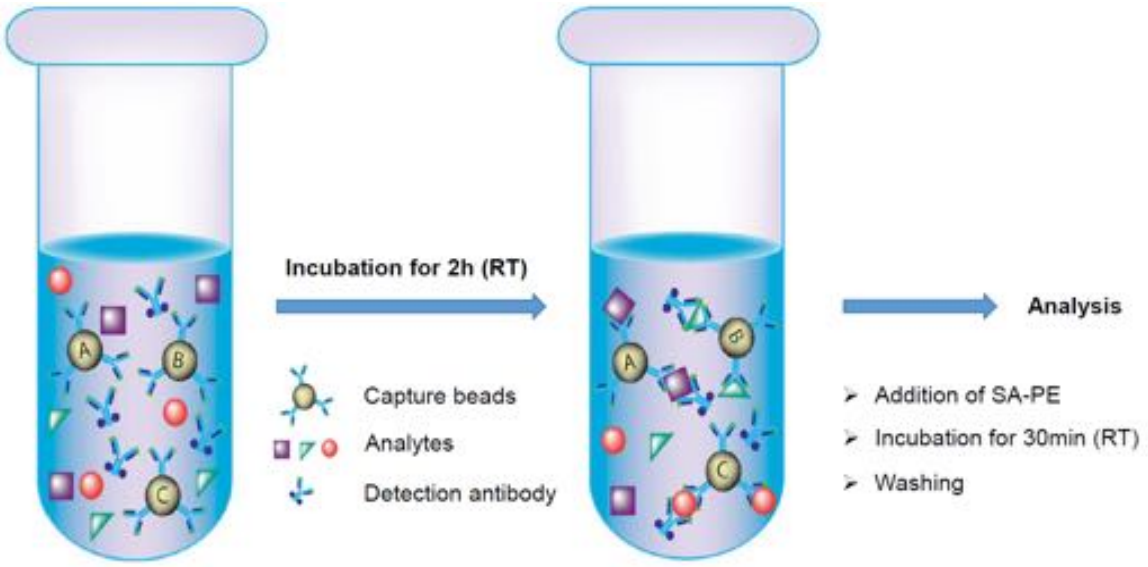

Figure 13: Principle of cytometric bead array (CBA)

A complex is formed from analyte, capture beads and detection antibody. After addition of Streptavidin-phycoerythrin (SE-PE), incubation and washing steps, the amount of analytes is measured by flow cytometry in proportion to fluorescent signal intensities according to a standard curve. (Adopted and modified after: Biolegend® *LEGENDplex*™ protocol 77677_V02.)

3 Results

To provide an overview of the performed processes, the subsequent outline will guide through the experimental results.

In order to prove proper and functional disease induction with regard to pathogenic markers in NTN, glomerular histology and crescent counting as well as marker for proteinuria like BUN and albumin-to-creatinine ration (ACR) were assessed.
In anti-CD3-induced duodenitis, a common model for sepsis, histological investigations were performed which was also the case for *S.aureus*-infected mice.
To assess the clinical outcome during EAE, mice were scored according to motor phenotype assessment. Here, all models, except the Pristane-induced lupus nephritis, showed positive disease onset (**3.1**).
Next, T_H17 cell plasticity was analyzed via flow cytometry (**3.2**). In summary, T_H17 plasticity was found to increase from the NTN model (stable T_H17 cells, limited cell plasticity) to anti-CD3-induced duodenitis and *S.aureus*-infected mice. The highest T_H17 cell plasticity was found in EAE, as expected.
In the next chapters, flow cytometric plots from $T_H17^{+/-}$ ($YFP^{+/-}$) cell sort (**3.3**), prior to bulk sequencing data analysis, raw data quality checks and data procession (**3.4**) are provided. The latter analysis implied sufficient T cell sorting efficacy in FACS plots as well as in analysis of T_H17 signature genes and others.
Further, T_H17 cell plasticity-related target gene selection is explained in terms of gene selection criteria and differential gene expression analysis (**3.5**). Here, IL-27 receptor α (IL-27ra) as well as the important T_H1 transcription factor Tbet were selected and sequencing data were validated. Furthermore, functional *in vivo* as well as *in vitro* experiments were conducted to analyze the role of these proteins in the experimental nephrotoxic nephritis (NTN) model (**3.6.1** - **3.6.6**). As a result, IL-27 intervention showed a protective effect with regard to renal damage in NTN-mice. Experiments with conditional Tbet-floxed NTN-mice however did not show significant differences neither in renal damage nor in T_H17 cell plasticity, compared to control mice (**3.7**).

3.1 Disease induction & check for pathogenic features

From previous research, it was known that T_H17 cells play a pivotal role not just in experimental glomerulonephritis but also for example in MS (EAE), lupus nephritis (SLE), rheumatoid arthritis, psoriasis and others (Gaffen et al., 2014).
While it has been shown that T_H17 cells display a high degree of plasticity in models of autoimmune inflammation of the brain and intestine (EAE, anti-CD3 duodenitis), our group has shown that renal T_H17 cells show a limited cell plasticity.
Based on these observations, it was the aim to understand the molecular differences between T_H17 cell plasticity in selected models (EAE, *S.aureus* infection, α-CD3 duodenitis) compared to T_H17 cells with a stable phenotype in GN (NTN).

We hypothesized that by comparing transcriptional differences between stable and plastic T_H17 cells, we can understand the molecular mechanisms of this phenomenon.
For T_H17 cell sort by FACS and subsequent comparative gene expression analysis based on bulk sequencing data, it was necessary to proof successful disease induction in the different used models which is shown in this chapter.

3.1.1 NTN induction

3.1.1.1 Infiltrating T cells during NTN

As part of the immune response in kidney inflammation among innate immune mechanisms, e.g. by macrophages and mast cells, T_H17 as well as IL-17-producing $\gamma\delta$-T cells and IFN-γ-producing T_H1 cells play a pivotal role in the pathogenesis of NTN, as described in the introduction in **1.3.3** (Cornelissen et al., 2009; Summers et al., 2009; Turner et al., 2012; Turner et al., 2010a; Turner et al., 2010b).
Six days after experimental nephrotoxic nephritis (NTN) induction, kidney infiltrating T_H17 cells which eventually mediate kidney damage by $\gamma\delta$-T cell

mediated-activated neutrophil recruitment display the majority of immune cells in the kidneys (Kurts et al., 2013; Paust et al., 2009; Summers et al., 2009).
After about 21 days, the peak of T_H1 cells is reached. Treg cells however evolve slowly after 10 days into the disease, depicted in **Figure 14** (Krebs and Panzer, 2018). Hence, in order to investigate T_H17 cells and their role in the pathogenesis of NTN, day 6 has been chosen for analysis of T_H17 cell plasticity.

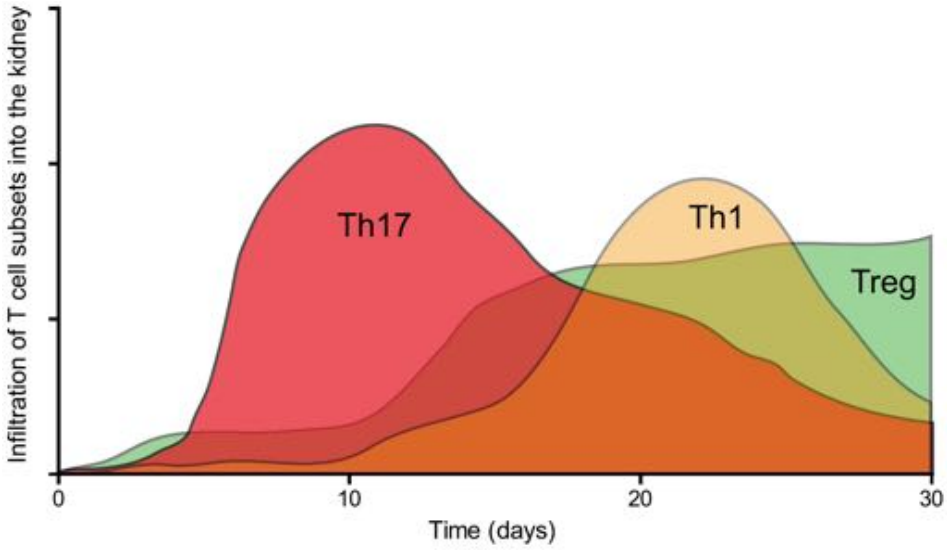

Figure 14: Kidney infiltrating T cell subsets during NTN

The first days after sheep antibody injection are highlighted by the presence of innate immune cells like mast cells, neutrophils and IL-17-producing γδ-T cells which cause first renal damage. Approximately 4 days after NTN initiation, first T_H17 cells can be found in the renal tissue. Ten days after NTN induction, the amount of T_H17 infiltrating T cells is the highest, followed by T_H1 cells, approximately on day 21, followed by monocytes and fibrocytes. The population of T regulatory cells (Tregs) evolves slowly in the course of the disease (Krebs and Panzer, 2018).

3.1.1.2 Renal histology of NTN mice

In the course of the NTN, glomerular damage caused by infiltrating leucocytes and subsequent formation of necrotic renal tissue is responsible for strongly reduced glomerular filtration rate (GFR) and overall kidney damage.

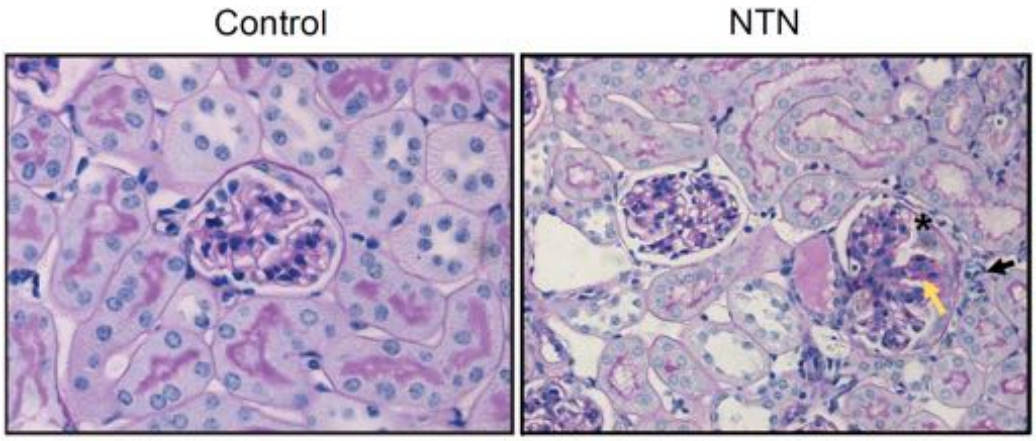

Figure 15: Renal histology of healthy and NTN mice (PAS-stained)

Ten days after NTN induction, mice were sacrificed and kidney sections were PAS-stained for histological analysis. **Left:** PBS only treated control mouse glomerulus. In contrast, **right** histological picture of NTN tissue section shows characteristic glomerular and periglomerular infiltrates (**black arrow**) and necrotic tissue formation (**yellow arrow**). Also visible: Glomerular crescent formation (*****).

3.1.1.3 Proteinuria, crescents, BUN, albumin-to-creatinine ratio

As a result of damaged glomerular filtration barrier, leaking protein can be found in glomerular filtrate which leads to abnormal high protein concentrations in the urine. As a clinical marker, the albumin-to-creatinine ratio (ACR) was calculated by division of albumin by creatinine-values, as explained in **1.3.1**.

In addition to albumin-to-creatinine ratio (ACR) and blood urea nitrogen (BUN), proteinuria was measured via urine sticks on day 3 after NTN induction as an indicator of renal damage severity (**Figure 16**).
Only mice with successful disease induction were chosen for further analysis.

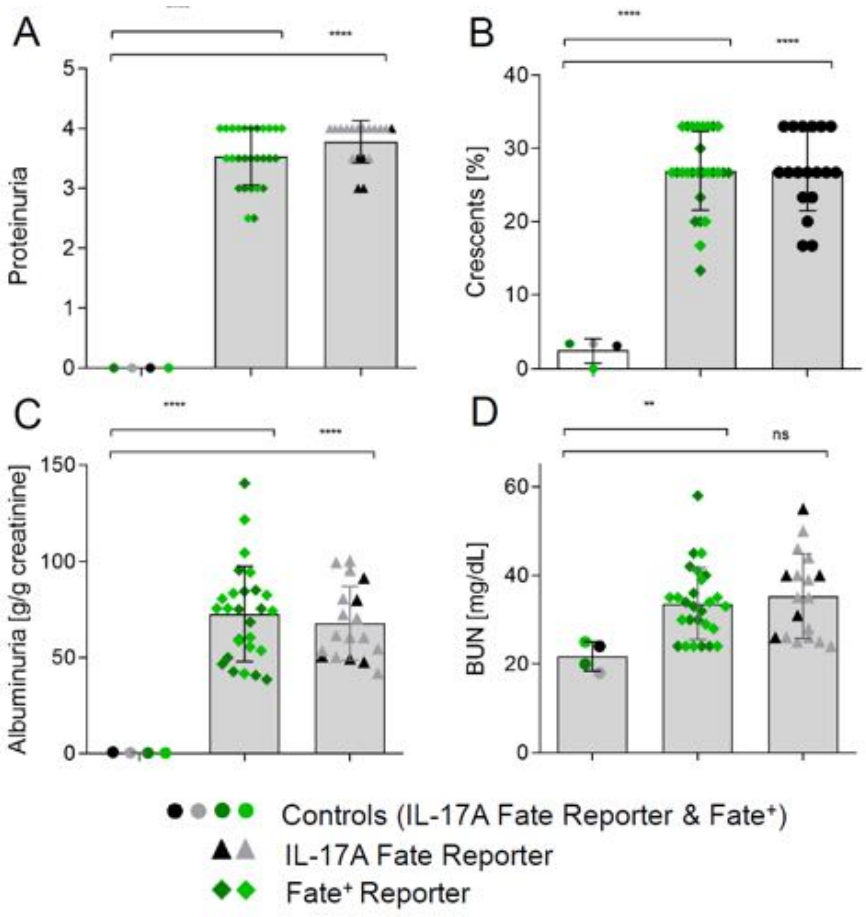

Figure 16: Assessment of proteinuria in NTN-mice

To determine the renal damage during NTN experiments using IL-17A Fate Reporter and Fate$^+$ reporter mice compared to healthy control mice, proteinuria was measured via: **(A)** urea sticks on day 3 after NTN induction for rough valuation. In addition, glomerular crescents were counted and percentage of glomerular crescents per 30 glomeruli was calculated **(B)**. Furthermore, albumin-to-creatinine ratio - ACR **(C)** and **(D)** blood urea nitrogen (BUN) was determined. (For determination of proteinuria (A), average was calculated for samples with uncertain results, e.g. ++/+++ = 2,5)

As a result, all NTN-mice used for T_H17 cell sort (**3.3**) and subsequent sequencing exhibited a robust renal damage, as indicated by renal histology (**Figure 15)** and proteinuria (**Figure 16**).

3.1.2 α-CD3 duodenitis

Injection of hamster anti-murine CD3ε monoclonal antibody that specifically recognized the ε chain of the murine CD3 molecule was found to suppress T cell function as shown for example in skin (Hirsch et al., 1988) and kidney with induction of an immunomodulatory phenotype in T_H17 cells marked by high expression of IL-10 and attenuated kidney damage (Krebs et al., 2016b). Furthermore, as mentioned in **1.2.4,** it was shown that T_H17 cells express IL-10 receptor α (IL-10rα) in this model and that both $FoxP3^+$ Treg cells as well as $FoxP3^-$ Tr1 cells were able to attenuate T_H17 as well as T_H17/T_H1 cells in a IL-10-dependend manner (Huber, 2011).

In contrast, it was shown that *in vivo* administration of this monoclonal antibody induces potent but also transient T cell activation (Chatenoud et al., 1989; Ferran et al., 1991; Ferran et al., 1990; Leo et al., 1987).

To investigate T_H17 cell plasticity in this model by RNA bulk sequencing, anti-CD3-mediated duodenitis was induced in IL-17A Fate Reporter mice, as described in **2.2.15**.

3.1.2.1 Small intestinal histology

Two days after monoclonal antibody administration, mice were sacrificed and small intestinal (si) hematoxylin (HE)-stained sections were analyzed. Results depicted in **Figure 17** positively show a high degree of small intestinal inflammation, indicated by tissue hypertrophy and cell infiltration, compared to PBS-treated mice.

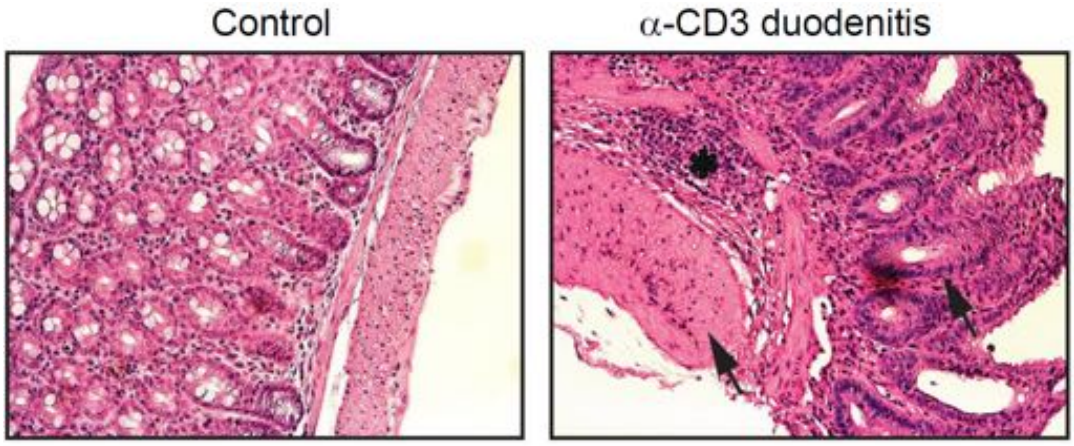

Figure 17: Histological analysis of α-CD3-induced duodenitis (HE)

On day 2 after initial α-CD3 treatment, mice were sacrificed and sections of the small intestine (si) were hematoxylin-eosin (HE)-stained for histological analysis. **Left:** Si of PBS only treated control mouse. **Right:** Section of HE-stained si from α-CD3-treted animals shows hypertrophy (**arrows**) and cell infiltration (**asterisk**) by intestinal inflammation.

3.1.3 EAE

Experimental autoimmune encephalomyelitis (EAE) as a model for multiple sclerosis (MS) is a complex immunopathological and neuropathological condition which leads to an approximation to the human MS model in terms of inflammation, demyelination and subsequent axonal loss (Aharoni et al., 1997; Althaus, 2004; Arnon and Aharoni, 2009; Zhao et al., 2008).

3.1.3.1 Clinical EAE score

As a result of this neurological disorder model, clinical symptoms of EAE-mice manifest in progressive ascending paralysis within 8-14 days after immunization, starting from the animal's tail which affects climbing-, balancing- and walking capabilities of the animals. The entirety of those symptoms was clinically determined as the *EAE score* (**2.2.13**). Results from bodyweight- and EAE score progression from two independent EAE experiments are depicted in **Figure 18**.

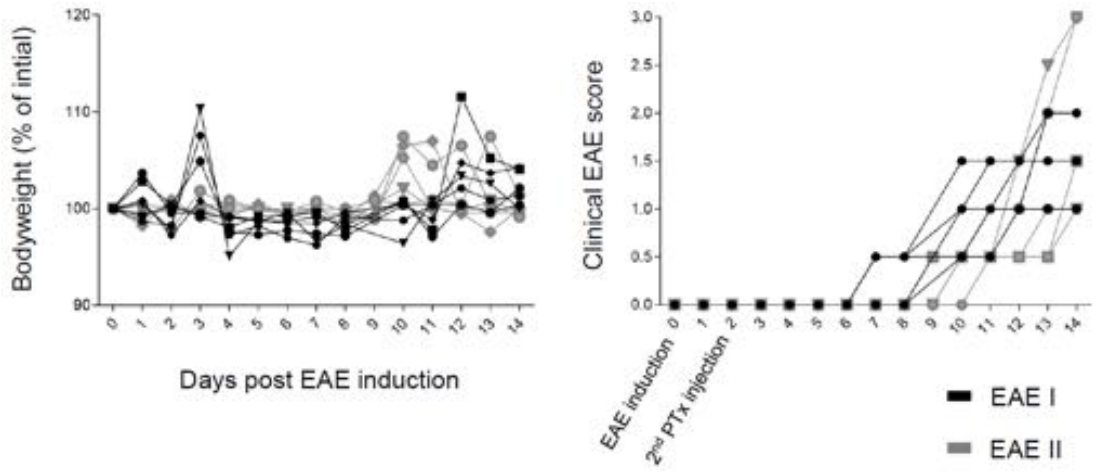

Figure 18: Mice bodyweights and Clinical EAE scores

EAE-mice intended for bulk sequencing of brains were daily checked for (**left**) bodyweight over the entire duration of this model (14 days). In addition, the clinical EAE score (**right**) was determined from a number of clinical markers, including climbing-, balancing- and walking- capabilities of the animals. (Data from 2 independent EAE experiments depicted black and grey).

It was shown that, beside minor variations, no changes in bodyweight (in % of initial) during EAE progression occurred. In contrast, clinical onset of EAE was detectable from day 6 (minor symptoms for partial tail paralysis) and partially progressed until end of the experiments on day 14. Most mice however did not show continuous EAE score progression over this period.

3.1.4 *S.aureus* infection

Many pathogens, including bacteria, are thought to be involved in the development and progression of CKD. Among the wealth of bacteria, *S.aureus* is one of the known bacteria which can cause GN, called *staphylococcus-associated glomerulonephritis* (Mahmood et al., 2018).
Furthermore, the infection with ubiquitous *S.aureus* is the main cause of infectious morbidity and mortality in hemodialysis patients (Vandecasteele et al., 2009).

However, the precise underlying mechanisms are not understood in detail, but with regard to immunity it was found that many bacteria are capable to induce T_H17 cells

in certain limits and with varying potential (Tan et al., 2016). Therefore, this model was also used to investigate T_H17 cell plasticity.

3.1.4.1 Renal histology of S.aureus infected mice

To asses kidney damage in *S.aureus* (*SH 1000 strain*) infected animals, PAS staining of renal sections and analysis was performed (**Figure 19**).
In addition, bacterial smears from pure *S.aureus* strains and electron microscopic investigations were carried out in collaboration with the microbiology department (data not shown), to confidently identify *S.aureus* bacteria in the performed experiments.

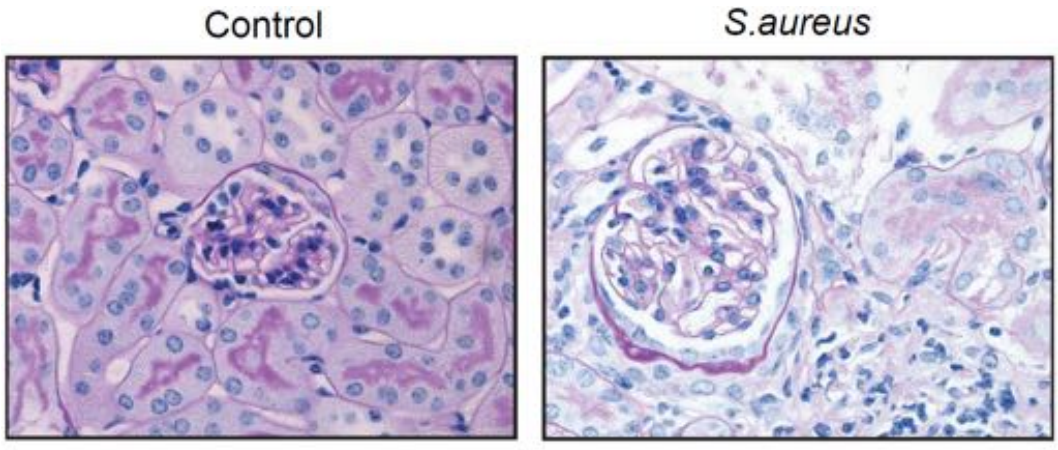

Figure 19: Renal histology (PAS) of S.aureus infected mice

10 days after *S.aureus* infection, mice were sacrificed and kidney sections were PAS-stained for histological analysis. **Left:** PBS only treated control mouse glomerulus. **Right:** histological PAS-stained section shows no glomerular defects.

The results from renal histological sections from *S.aureus* infected mice show no glomerular defects in terms of formation of glomerular crescents or massive leukocyte tissue infiltration whatsoever. However, it was shown in our group that infection with *S.aureus* leads to formation of abscesses (data not shown) mediated by a strong immune response including T_H17 cells. The formation of these abscesses are the main cause of death among experimental animals in this disease model.

3.1.5 Pristane-induced lupus nephritis

Systemic lupus erythematosus (SLE) is a chronic disorder which is characterized by over-production of nuclear autoantibodies which results in immune-complex formations. In addition, it was found that the experimental approach of pristane-induced lupus nephritis also depends on a T_H17 immune response (Summers et al., 2014).
Subsequently, the formation of these complexes leads to an immune response and tissue inflammation which further causes destruction of multiple organs, including the kidneys (Li et al., 2017; Pons-Estel et al., 2010).

For RNA sequencing and gene expression analysis, it was intended to add another model of glomerulonephritis to the nephrotoxic sheep serum-induced nephrotoxic nephritis (NTN). From previous experiments (Krebs et al., 2016b), it was known that pristane-induced lupus nephritis also shows a similar high degree of T_H17 cell stability like NTN.

However, 52 weeks after pristane injection into the animals, no signs of successful disease onset by BUN or albumin-to-creatinine ratio (ACR) were present. As shown in **Figure 21** although, a high degree of T_H17 cell stability in pristane-treated mice were found (**Figure 20**) which is comparable to NTN mice (**Figure 23**). Furthermore, during regular check via urine sticks, no significant proteinuria was detectable in pristane-treated mice.

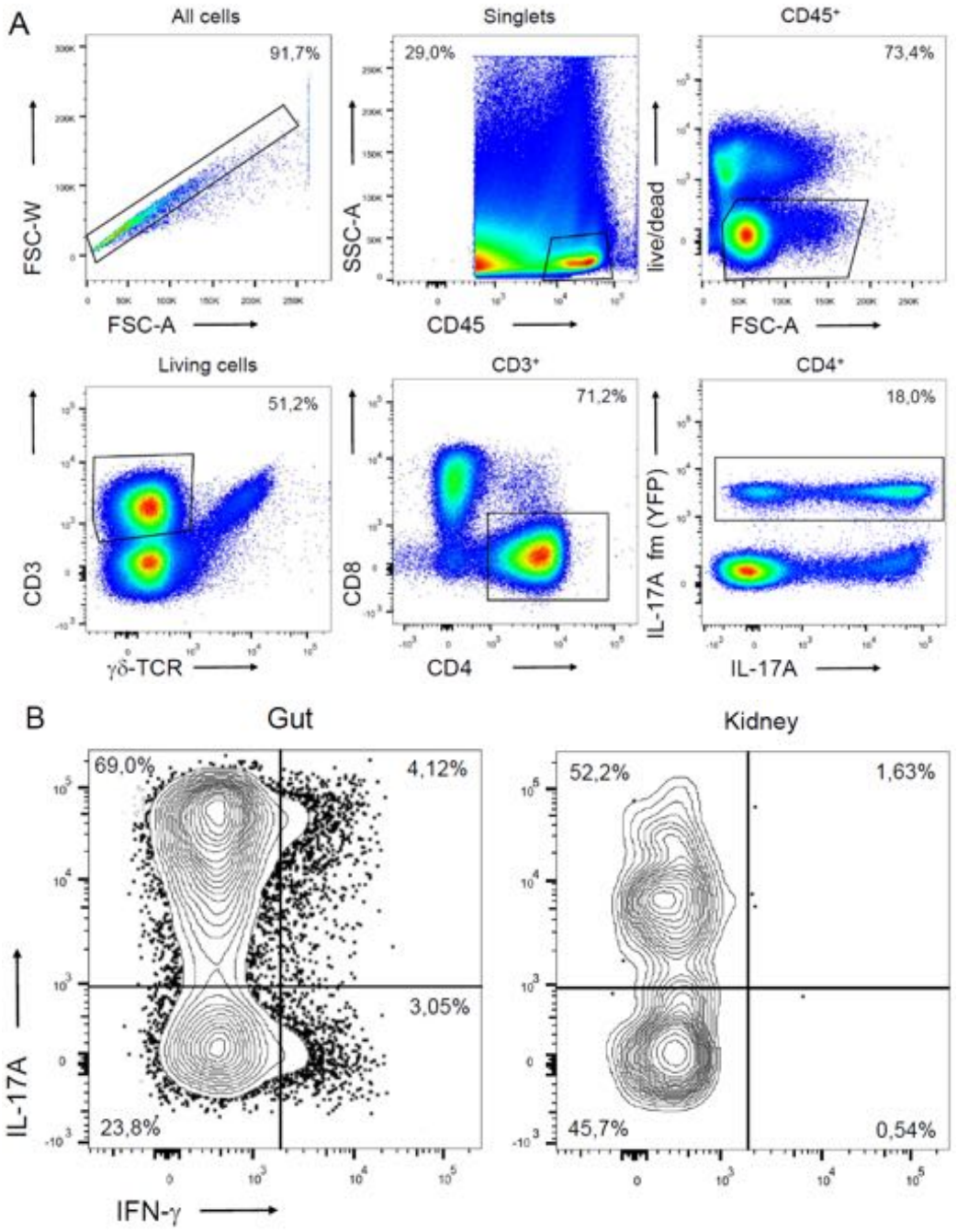

Figure 20: FACS analysis of T_H17 cell plasticity in pristane-treated mice

Pristane-treated female IL-17A Fate Reporter mice were sacrificed 52 weeks after disease induction and organs (lungs, kidneys and guts) were FACS-analyzed for T_H17 cell plasticity. Gating was performed as followed: **A** singlet, $CD45^+$, living, $CD3^+$ $\gamma\delta$-TCR^- $CD4^+$ $CD8^-$ cells. Then, cells were gated for IL-17 fm^+ (YFP^+). Finally, **B** T_H17 cell plasticity (IL17A/ IFN-γ) was analyzed. (**B, left**): Gut, (**B, right**): kidney. (Depicted FACS gating **A** performed from gut of pristane-treated mice.)

During organ extraction however, white granules were visible all-over distributed in the murine abdomen (**Figure 21**). Due to time constrains, the granules were not further analyzed.

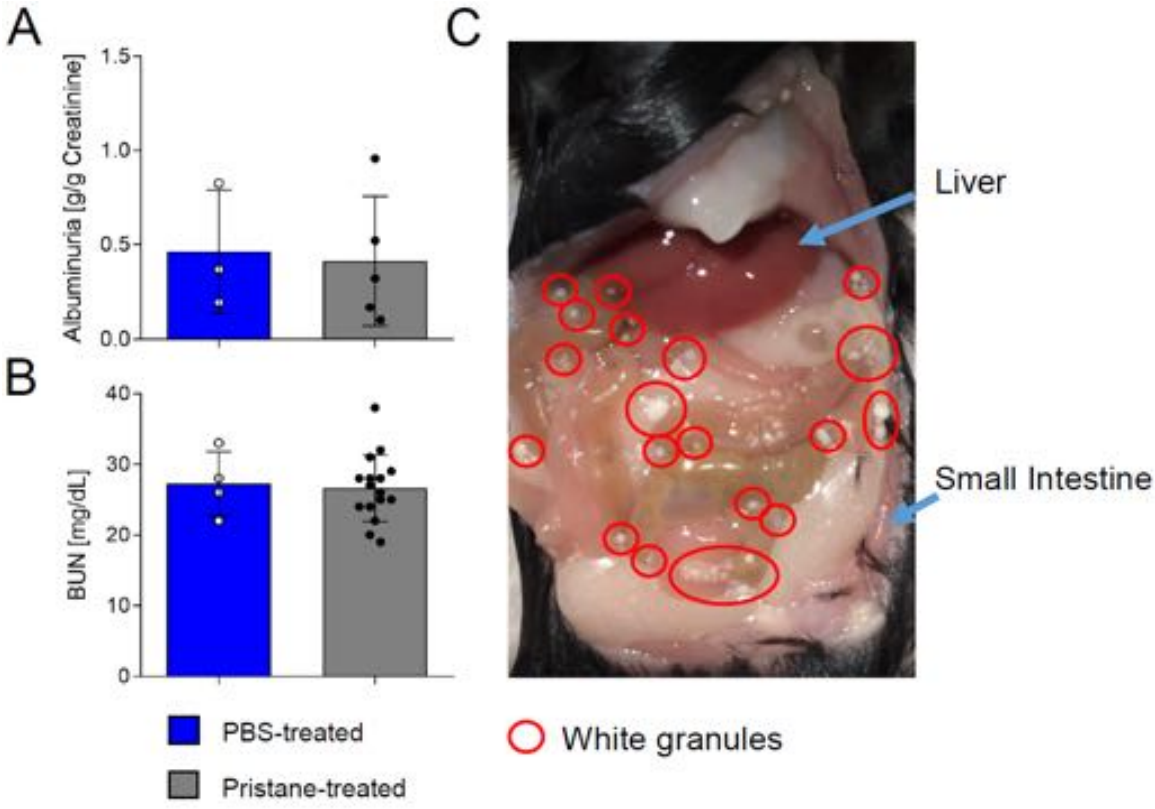

Figure 21: Analysis of pristane-induced lupus nephritis mice

52 weeks after pristane injection into IL-17A Fate Reporter, mice were sacrificed and kidneys were analyzed. In addition, the degree of proteinuria was measured by **A** albumin-to-creatinine ratio (ACR) and **B** blood urea nitrogen (BUN). During organ extraction, white granules (red circles) were found unevenly distributed in the murine abdomen, **C**.

Therefore, it was decided not to include samples from pristane-treated mice into the sequencing samples. RNA bulk sequencing was not performed. Because of the duration of this experiment and due to the fact that there were already numerous samples for T_H17 cell comparison and gene expression analysis, it was decided not to repeat these experiments.

According to the depicted results, it could be shown that all models (NTN, EAE, anti-CD3 duodenitis and *S.aureus* infection), except the pristane-induced lupus

nephritis model, were successfully performed and all animals were sick and exhibited specific disease symptoms, as expected.

This is of high importance and the basis for followed T_H17 cell plasticity comparison between different disease models.

3.2 T_H17 cell plasticity in different disease models

To show the degree of T_H17 cell plasticity in all used disease models as a basis for RNA sequencing data comparison, cells from kidneys (NTN and *S.aureus* infection), brain (EAE) and small intestine (anti-CD3 duodenitis) of $IL17A^{cre}$ $R26^{YFP}$ Fate Reporter mice were isolated. Cells were re-stimulated with PMA/Ionomycin (**2.2.18**) and stained for IL-17A, IFN-γ and other surface markers (**Figure 22**). Finally, cells were analyzed by FACS and IL-17A/IFN-γ expression was evaluated.

Results from FACS gating to determine the degree of T_H17 cell plasticity and stability are depicted in **Figure 22** and **Figure 23**.

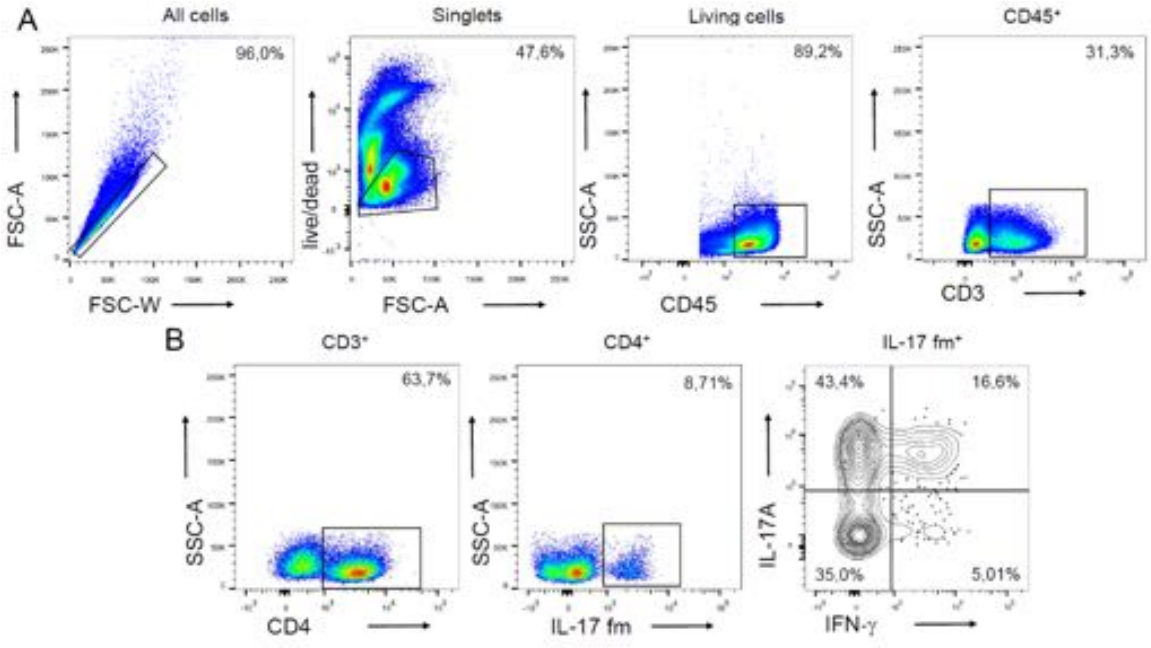

Figure 22: FACS gating for T_H17 cell plasticity and stability analysis

To assess T_H17 cell plasticity, FACS sorted cells were gated as follows: **A**, **top** singlets, living, $CD45^+$, (**middle**) $CD3^+$, $CD4^+$, IL-17 fm^+ ($eYFP^+$) cells. **B,** further analysis was performed for IL-17A and IFN-γ (n=3). (Examples from re-stimulated small intestinal cells in anti-CD3 duodenitis.)

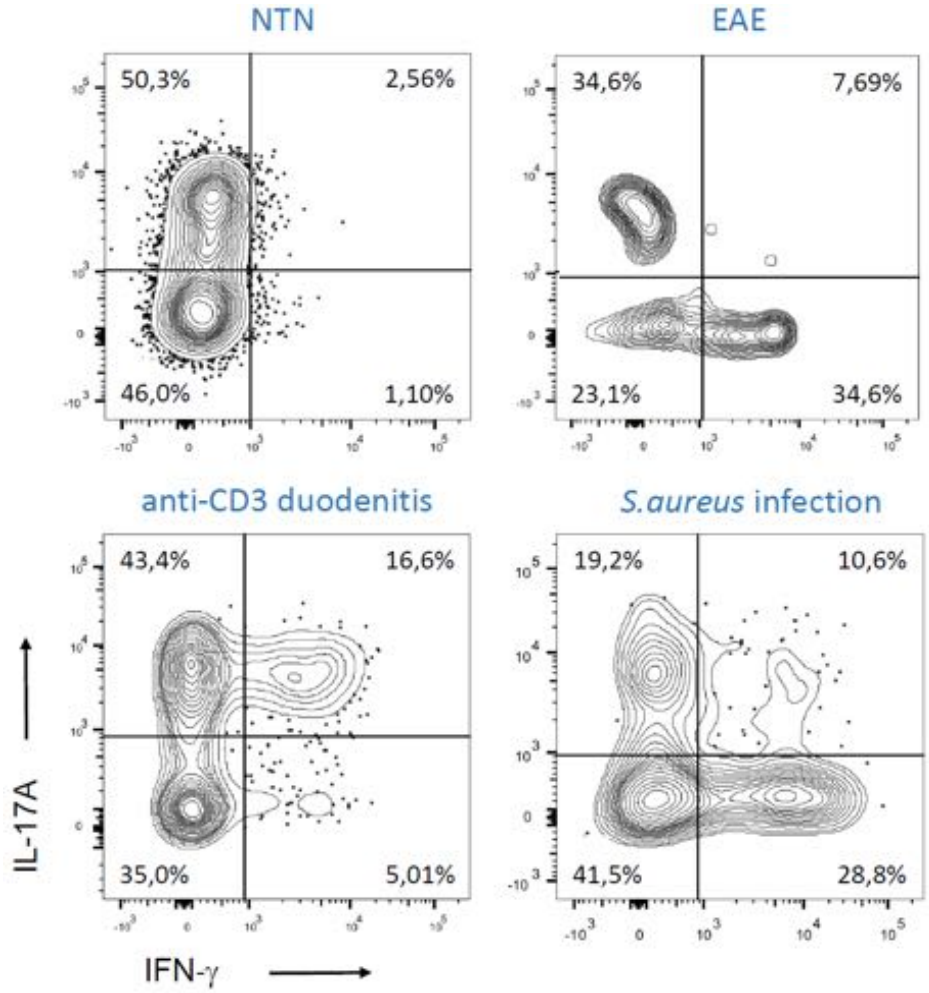

Figure 23: Assessment of T_H17 cell plasticity in different disease models

After disease induction and FACS gating for singlets, living cells, $CD45^+$ $CD3^+$ $CD4^+$ IL-17 fm^+ ($eYFP^+$) cells, T_H17 cell plasticity was analyzed from: NTN, EAE, anti-CD3 duodenitis and *S.aureus* infection samples as depicted.

As a result, it was found that T_H17 cell plasticity is the highest in EAE and *S.aureus*-infected mice followed by anti-CD3-induced duodenitis and NTN exhibiting a high degree of T_H17 cell stability as expected.

3.3 FACS sort of T_H17 and non-T_H17 cells for RNA sequencing

To identify genes which could play a role in T_H17 cell stability in the kidney, it was aimed to compare transcriptional profiles of T_H17 cells in NTN with T_H17 cells from models with a stable T_H17 phenotype. Here, IL-17 Fate Reporter mice (IL-17A^{Cre} x R26^{eYFP}, **2.1.1**) were used. If in a cell the IL-17A promotor is activated in these mice, a cre (from *Cyclization recombinase*) recombinase is expressed. After sensing of specific recognition sites (locus of X-over P1 (loxP) sites, from bacteriophage P1) cre is then able to perform recombination of these specific sites. For its mode of operation, the method is called *Cre-Lox recombination* (Abremski et al., 1986; Missirlis et al., 2006).
The cre recombination leads to excision of a floxed stop codon upstream of eYFP protein under the control of a ubiquitously active promoter (*Rosa26* in this case) and thus marks the cell with this fluorescent label regardless of its actual cytokine production status at the time of analysis (**Figure 24** ,**A**).

In addition, so called *Fate*$^+$ reporter mice (a combination of IL-17A Fate Reporter and Acute Reporter) were used which combine IL-17A Fate Reporter and Acute Reporter properties to mark IL-17A$^+$, FoxP3$^+$ and IFN-γ^+ and IL-17 fm$^+$ cells without the need of cell re-stimulation (Gagliani et al., 2015). The transgenic construct of the Fate$^+$ mouse is illustrated in **Figure 24**, **B**.

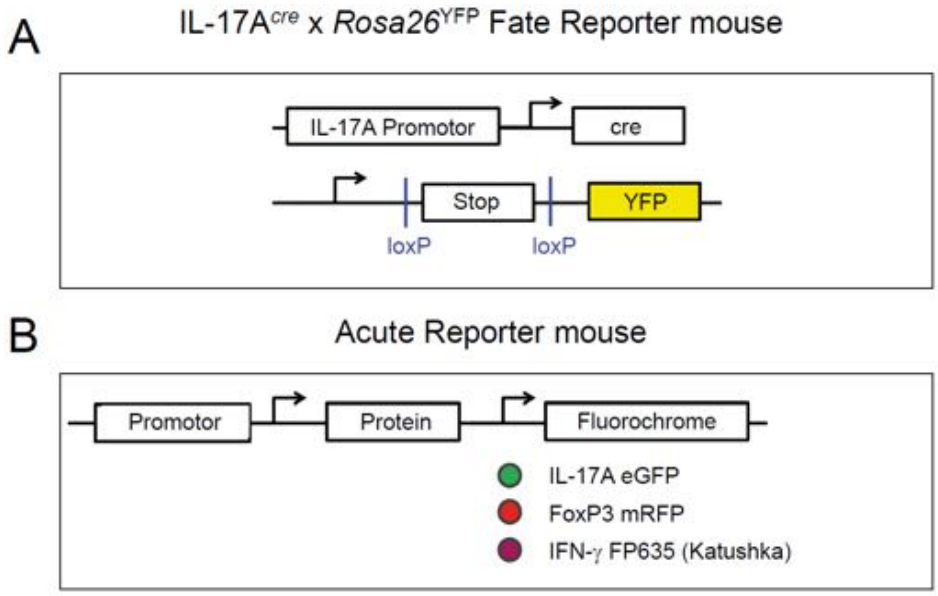

Figure 24: IL-17A Fate Reporter & Fate$^+$ Reporter mouse constructs

A: IL-17A Fate Reporter mouse: After activation of the IL-17A promoter, cre recombinase expression leads to excision of a floxed stop codon upstream of fluorescent eYFP protein under the control of *Rosa26* promoter. The cell with activated IL-17A promoter is therefore permanently eYFP marked regardless of its actual IL-17A production. **B:** Acute reporter mouse: This reporter mouse is independent of cre expression. Here, IL-17A, FoxP3 as well as IFN-γ are fluorescently marked. The Fate$^+$ Reporter mouse combines IL-17A Fate Reporter and Acute Reporter properties. Here, IL-17A, FoxP3 and IFN-γ as well as IL-17 fm$^+$ are fluorescently labeled.

As a consequence, these reporter mice allow reliable conclusions in regard to the fate and origin of IL-17-producing cells (T_H17 cells).

For flow cytometric cell sorting, CD4$^+$ CD3$^+$ YFP$^+$ T_H17 cells, so called T_H17 *fate-mapped* (fm) cells, (and non-T_H17 cells) could be identified and FACS sorted by their permanent eYFP signal (**Figure 25** and **Figure 26**), as well as IL-17A$^+$ and IL-17A$^-$ cells.

As a result it was feasible to compare gene expression profiles of kidneys from NTN-mice featuring high T_H17 cell stability with other models with high T_H17 cell plasticity (EAE, anti-CD3 duodenitis and *S.aureus* infection) by RNA bulk sequencing.

To analyze YFP$^+$ T_H17 and non-T_H17 (YFP$^-$) cells, cell populations were gated for living, singlets, CD45$^+$ CD4$^+$ CD3$^+$ cells as seen in **Figure 25**.

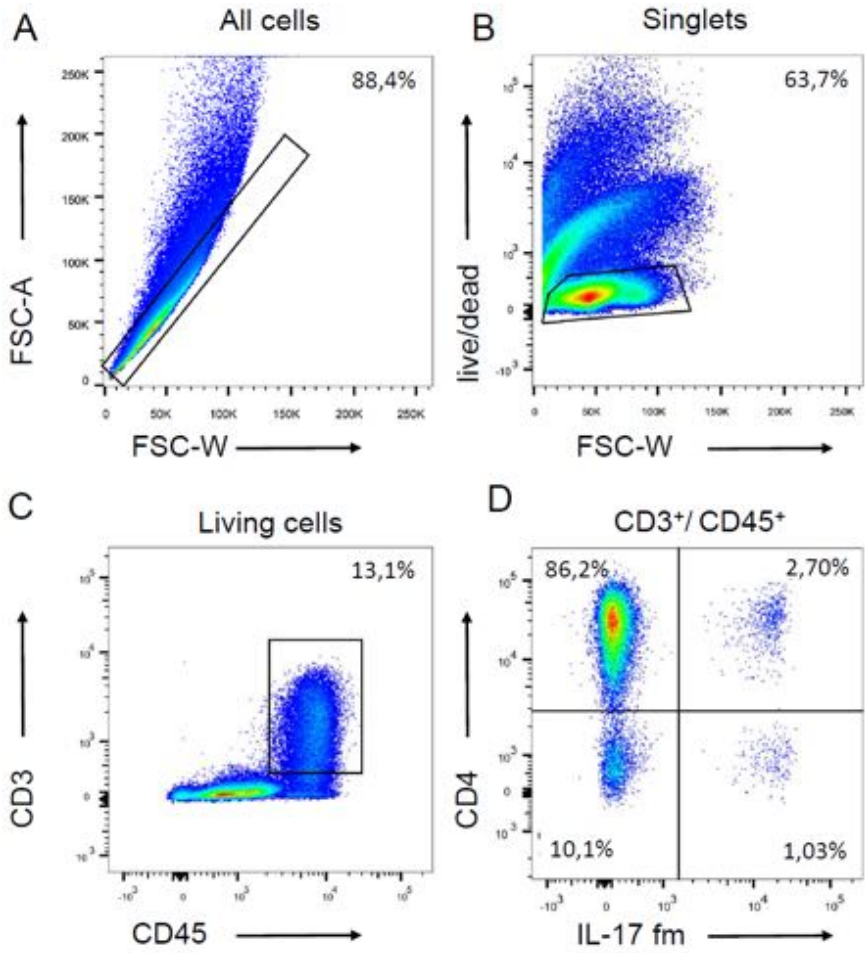

Figure 25: FACS gating for singlet CD45$^+$ CD4$^+$ CD3$^+$ YFP$^{+/-}$ cells

To separate T_H17^+ (IL-17 fm$^+$) cells for FACS sort, cell populations were gate as follows. **A**: singlet cells, **B**: living cells, **C**: CD3$^+$ CD45$^+$, **D**: CD4$^+$ IL-17 fm$^+$ (eYFP$^+$) and CD4$^+$ IL-17 fm$^-$ (eYFP$^-$).

In order to compare and analyze CD4$^+$CD3$^+$ T_H17 (YFP$^+$) and non-T_H17 (YFP$^-$) cells with cells of organs from other disease models, the same gating strategy was applied for FACS sorting of those cells depicted in **Figure 26**.

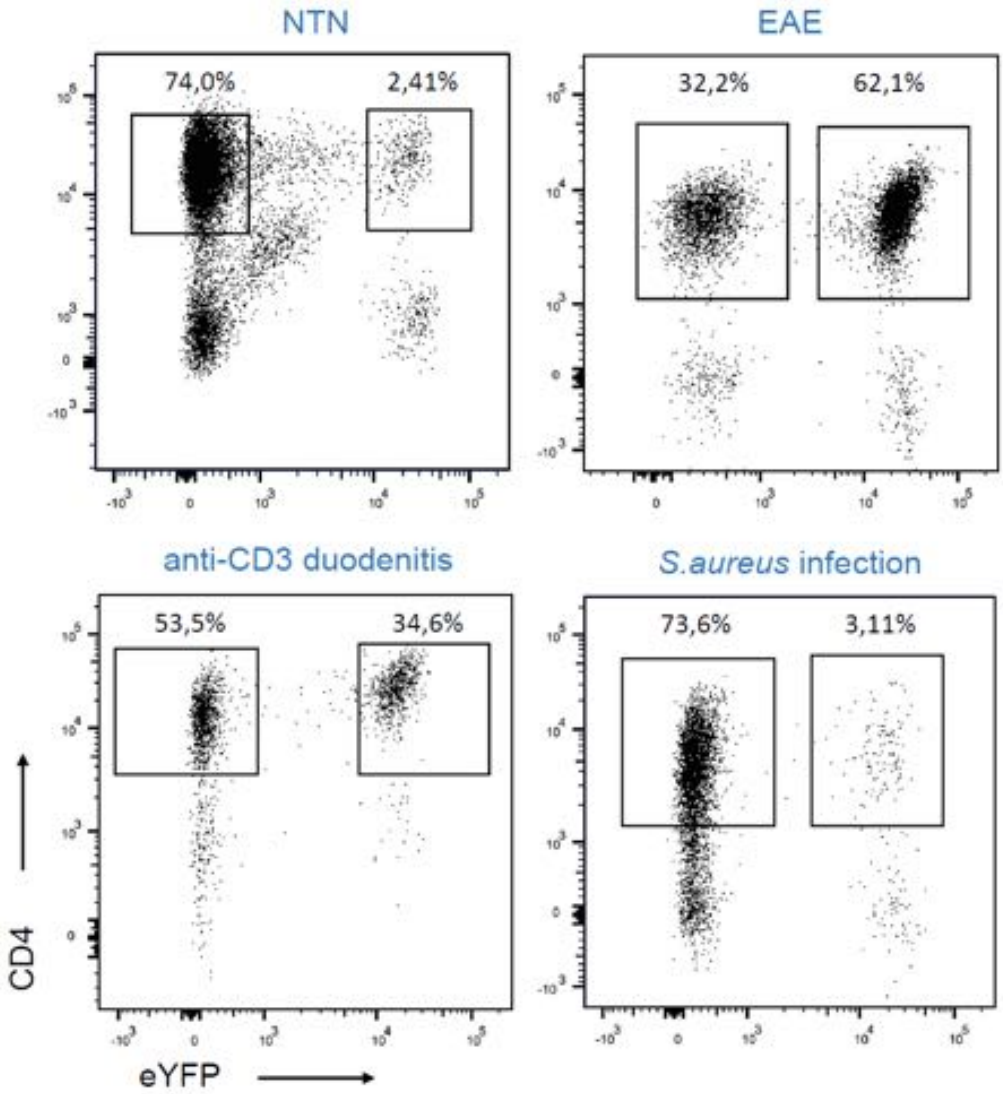

Figure 26: FACS sort of YFP$^+$ (T_H17^+) and YFP$^-$ (T_H17^-) cells

Due to the eYFP labeling of cells in which the IL-17A promoter was activated, it was possible to FACS sort these cells by their permanent fluorescent label. To compare differential gene expressions in NTN (kidney) with other disease models, $CD4^+$ $CD3^+$ T_H17^+ and T_H17^- cells from brains (EAE), intestine (anti-CD3 duodenitis) and kidney (*S.aureus* infection) were sorted by flow cytometry.

3.4 Bulk sequencing data analysis

For the investigation of T_H17 cell plasticity and the high degree of T_H17 cell stability in the NTN model, RNA bulk sequencing was performed.
RNA “bulk” sequencing means the analysis of RNA expression from a large cell population. This procedure, like microarray, is often used as a standard method for analysis of large cell populations.
Therefore, RNA bulk sequencing is a suitable technique to get a very detailed overview of gene expression profiles between samples from different cell populations. In addition, it is an unbiased approach which does not rely on detailed knowledge about potential target genes and is not supervised by the investigator. For this purpose, another advantage to the newer *next-generation sequencing* (NGS) techniques is the reduced amount of generated data. This leads to faster, less complex data analysis.
In contrast to single cell sequencing, a disadvantage of bulk sequencing is the lack of information about very small and mixed cell populations and cell heterogeneity.

In a first approach, sequencing was performed to compare NTN vs. anti-CD3 duodenitis with regard to differential gene expression. Therefore, three samples per organ and model from sort of YFP^+ (T_H17^+) cells, one spleen sample from healthy mice (as a sample reference for sequencing) and three samples per organ and model from sort of YFP^- (T_H17^-) cells were sequenced.

Hence, for the NTN experiments, samples of YFP^+ and YFP^- cells (S1+S8, S2+S9 and S3+S10) were pooled from one experiment, each with the same sheep serum used for NTN induction. The same is true for α-CD3 experiments: YFP^+/YFP^- cells from S4+S11, S5+S12 and S6+S13.
For sample details, like disease model and organ, YFP status of sorted cells and cell number of sequenced cells see **Table 20**.

Table 20: RNA sequencing sample details: NTN vs. anti-CD3 duodenitis

Sample No.	Disease model/ organ	YFP status	Cell number	Used sheep serum / clone
S1	NTN, kidney	+	2421	SS14-7
S2	NTN, kidney	+	1499	SS14-7
S3	NTN, kidney	+	5676	SS14-7
S4	α-CD3 duodenitis, small intestine	+	20.000	145-2C11
S5	α-CD3 duodenitis, small intestine	+	8354	145-2C11
S6	α-CD3 duodenitis, small intestine	+	20.000	145-2C11
S7	Healthy, spleen	+ and -	20.000	
S8	NTN, kidney	-	37.860	SS14-7
S9	NTN, kidney	-	20.000	SS14-7
S10	NTN, kidney	-	20.000	SS14-7
S11	α-CD3 duodenitis, small intestine	-	9544	145-2C11
S12	α-CD3 duodenitis, small intestine	-	15.124	145-2C11
S13	α-CD3 duodenitis, small intestine	-	20.000	145-2C11

3.4.1 Principal component analysis - PCA

For quality control of the sequencing data obtained from FACS sort of $CD45^+$ $CD4^+$ $CD3^+$ $YFP^{+/-}$ T cells and $Fate^+$ mice, principal component analysis (PCA) was performed. PCA is a statistical method used to structure, simplify and visualize complex data sets. This procedure is an approximation of a number of possibly correlating statistical variables by a relatively low number of linear combinations (*principal components*) by orthogonal transformations. Thereby, PCA reduces high-dimensional data into fewer dimensions (Jackson, 1991; Jake Lever, 2017). Thus, it is possible to estimate the group cohesiveness of data sets.

NTN vs. anti-CD3 duodenitis

PCA analysis of the obtained sequencing data from kidney, gut and spleen with $YFP^{+/-}$ status (**Figure 27**) revealed a relatively high cohesion of YFP^{+} and YFP^{-} sorted cells from gut (small intestine) and from YFP^{-} kidney cells as well.

Results from PCA analysis showed differences between cells from kidney vs. small intestine. Moreover, is was found that YFP^{+} and YFP^{-} cells from kidneys reduced group cohesiveness. In contrast, YFP^{+} and YFP^{-} cells from small intestinal samples showed only reduced grouping in the PCA analysis. Importantly, PCA analysis also revealed significant differences in group cohesiveness in samples from kidney vs. small intestine

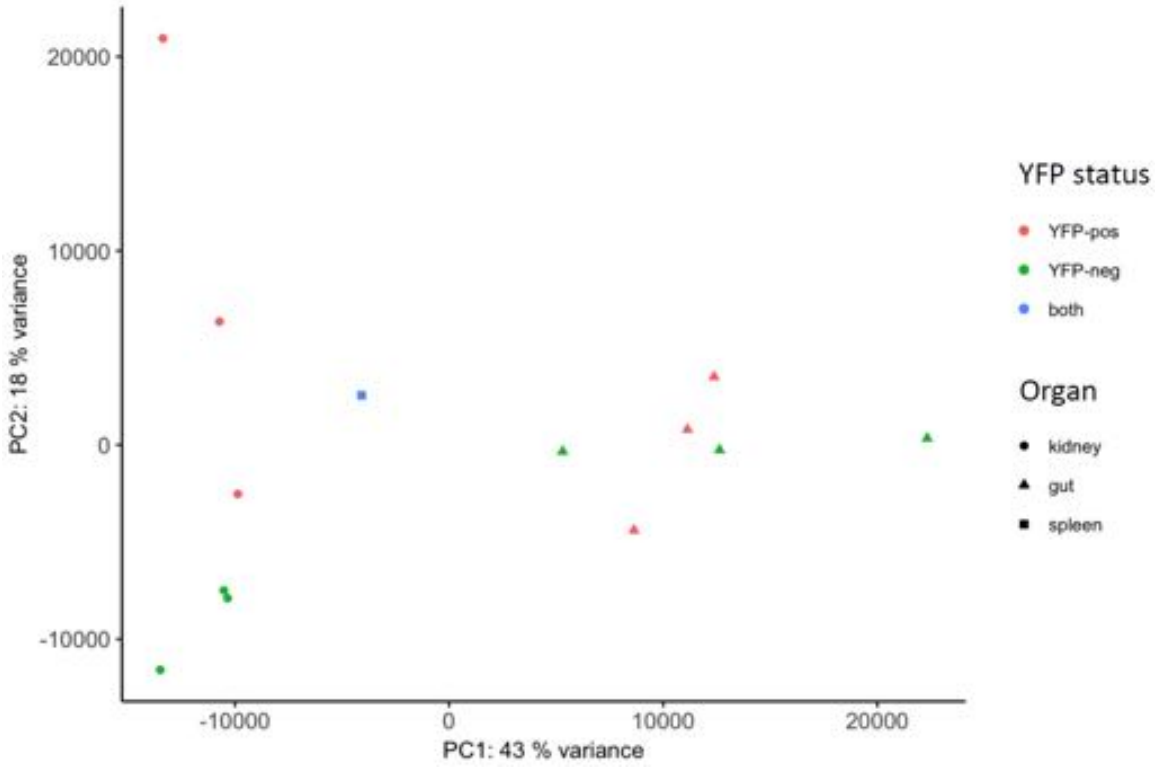

Figure 27: Bulk sequencing data sanity check in IL-17A Fate Reporter: PCA

Principal component analysis (PCA) of tpm normalized reads from kidneys (NTN), gut (small intestine, anti-CD3) and healthy spleens with different YFP status (indicated by color: red, green and blue).

NTN YFP$^+$ IL-17A$^+$ vs. YFP$^+$ IL-17A$^-$

In PCA analysis, a high group cohesiveness of the data sets from both YFP$^+$ / IL-17$^+$ and YFP$^+$ / IL-17$^-$ cells from kidneys of NTN-mice was found. Furthermore, PCA data revealed significant differences between samples from YFP$^+$ / IL-17$^+$ cells vs. YFP$^+$ / IL-17$^-$ cells as shown in **Figure 28**.

Table 21: RNA sequencing sample details: YFP$^+$ IL-17A$^+$ vs. YFP$^+$ IL-17A$^-$

Sample No.	Disease model/ organ	YFP status	IL-17A status	Cell number	Used sheep serum
S1	NTN, kidney	+	-	2940	SS14-8
S2	NTN, kidney	+	+	10.133	SS14-8
S3	NTN, kidney	+	-	7113	SS14-8
S4	NTN, kidney	+	+	1809	SS14-8
S5	Healthy, spleen	+ and -		20.000	-

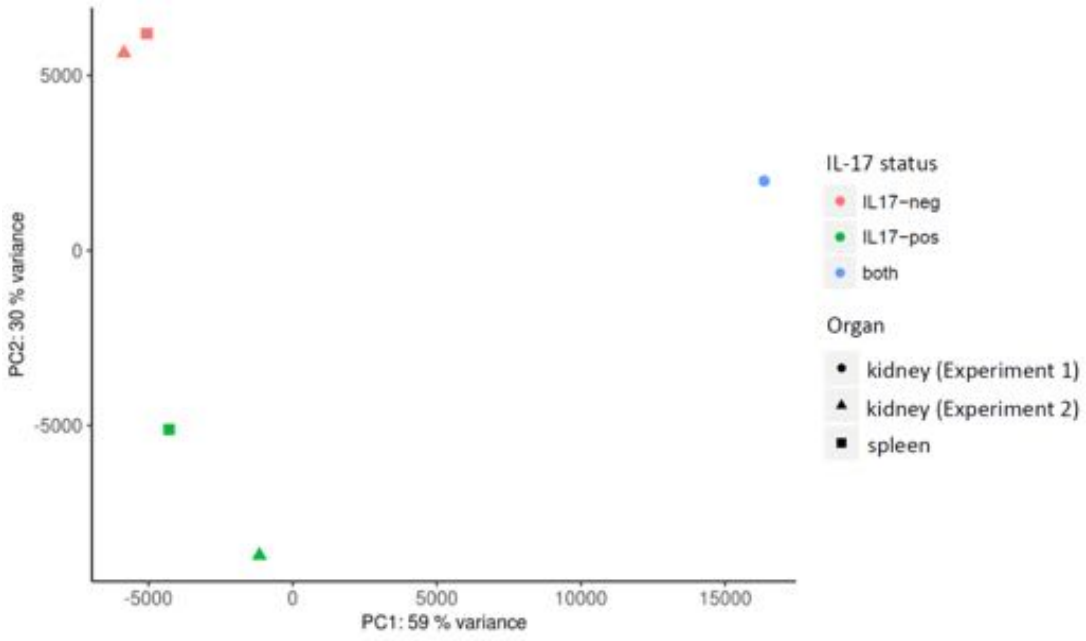

Figure 28: Bulk sequencing data sanity check in Fate$^+$ reporter: PCA

Principal component analysis (PCA) of tpm normalized reads from NTN-mice: YFP$^+$ / IL-17$^+$ (red) and YFP$^+$ / IL-17$^-$ (green) or both (blue) in healthy spleen cells. Sequencing data were acquired from sampled of 2 separated NTN-experiments.

3.4.2 Sanity check of sequencing data – eYFP and *cre* expression

Results for IL-17A Fate Reporter sanity checks are depicted below. Sanity checks were also performed for Fate$^+$ sequencing data sets (data not shown).

To assess the FACS sorting-efficiency to select T_H17^+ (eYFP$^+$) / T_H17^- (eYFP$^-$) only cells, the expression of cre recombinase and eYFP was evaluated as displayed in **Figure 29** where tpm (transcripts per million) is normalized for gene length (longer genes have more reads mapping to them) and sequencing depth (sequencing runs with higher depth have more reads mapping to each gene).

The data show that YFP$^+$ cells have a significantly high *cre* expression, as expected while YFP$^-$ cells have no significant *cre* expression which is true for samples of all organs. However, the gene expression of eYFP was also significantly high in YFP$^+$ cells and absent in YFP$^-$ sorted cells, as expected. Furthermore, expression of *cre* and eYFP was significantly higher in samples from gut compared to kidney samples. In addition, cells from healthy spleen (YFP$^+$ and YFP$^-$ cells) showed no *cre* or eYFP expression whatsoever.
As a result, these data suggest an effective FACS separation of cells which produced IL-17 and those who never expressed IL-17.

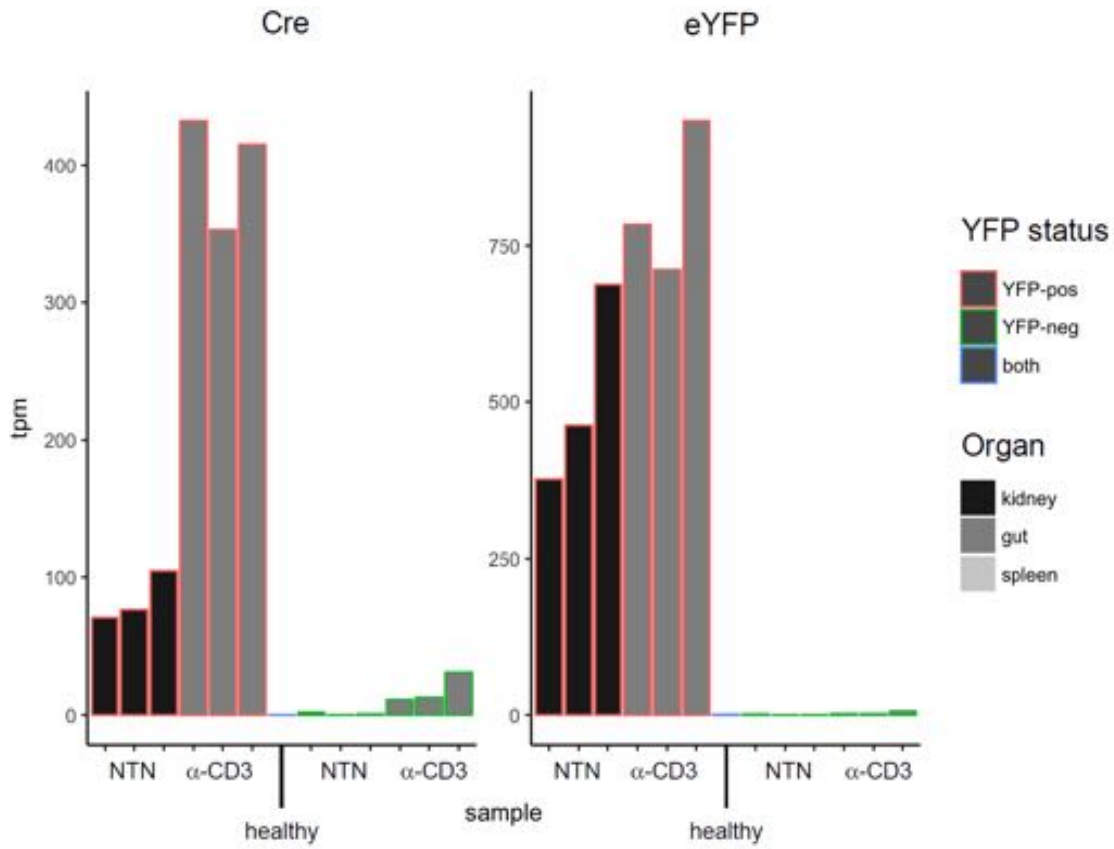

Figure 29: Bulk sequencing data sanity check: eYFP and cre expression

For quality of sequencing data and assessment of FACS cell sort, expression of *cre* (left) and eYFP (right) was analyzed in cells from of tpm normalized reads from kidney (NTN), gut (small intestine, anti-CD3 duodenitis) and spleen as a reference. As expected, YFP^+ sorted cells (red frame) are indicated by a high *cre* and eYFP expression, whereas YFP^- sorted cells (green frame) show no or just minimal *cre* and eYFP expression.

3.4.3 Analysis of bulk sequencing data – T_H17 signature genes

After assessment of RNA sequencing data in regard to FACS sorting effectivity by *cre*- and eYFP expression (**Figure 29**), T_H17 signature genes (*Il17a*, *Il17f* and *Rorc*) were analyzed for further sequencing data quality control (**Figure 30**).

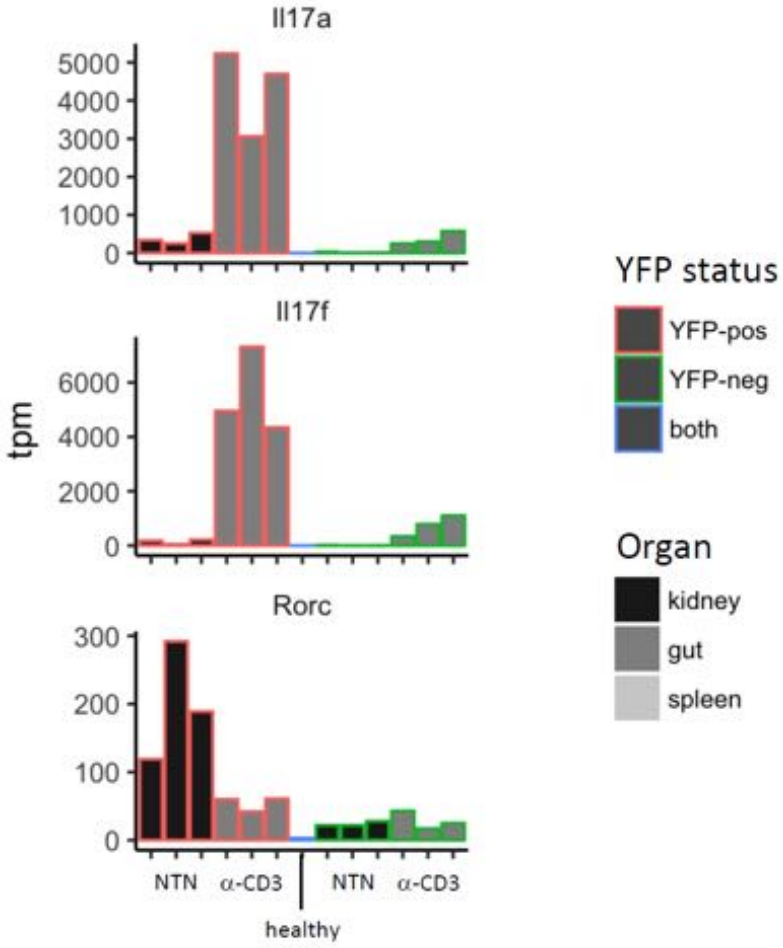

Figure 30: Bulk sequencing data sanity check: IL-17 signature genes

For sanity check of sequencing data and assessment of FACS cell sort, *Il17a* (**top**), *Il17f* (**middle**) and *Rorc* (**bottom**) gene expression was analyzed in cells from of tpm normalized reads from kidney (NTN), gut (small intestine, anti-CD3 duodenitis) and healthy spleen.

As expected, YFP^+ sorted gut cells from anti-CD3 treatment show a high expression of *Il17a* and *Il17f*. Whereas the expression of these genes was reduced in YFP^- gut samples and YFP^+ cells from kidney samples. The expression of these genes in healthy spleen samples and in YFP^- cells from kidney was not significantly

detected. However, the expression of *Rorc* was highest in YFP$^+$ cells from NTN-kidneys. Furthermore, significant but lower expression of this gene was detected in YFP$^+$ cells from α-CD3 gut, as well as in YFP$^-$ cells from anti-CD3-treated- and NTN-mice.

3.4.4 Sanity check of sequencing data – Other genes

To check for other (T_H17-related) genes, more sanity checks were performed, depicted in **Figure 31**.

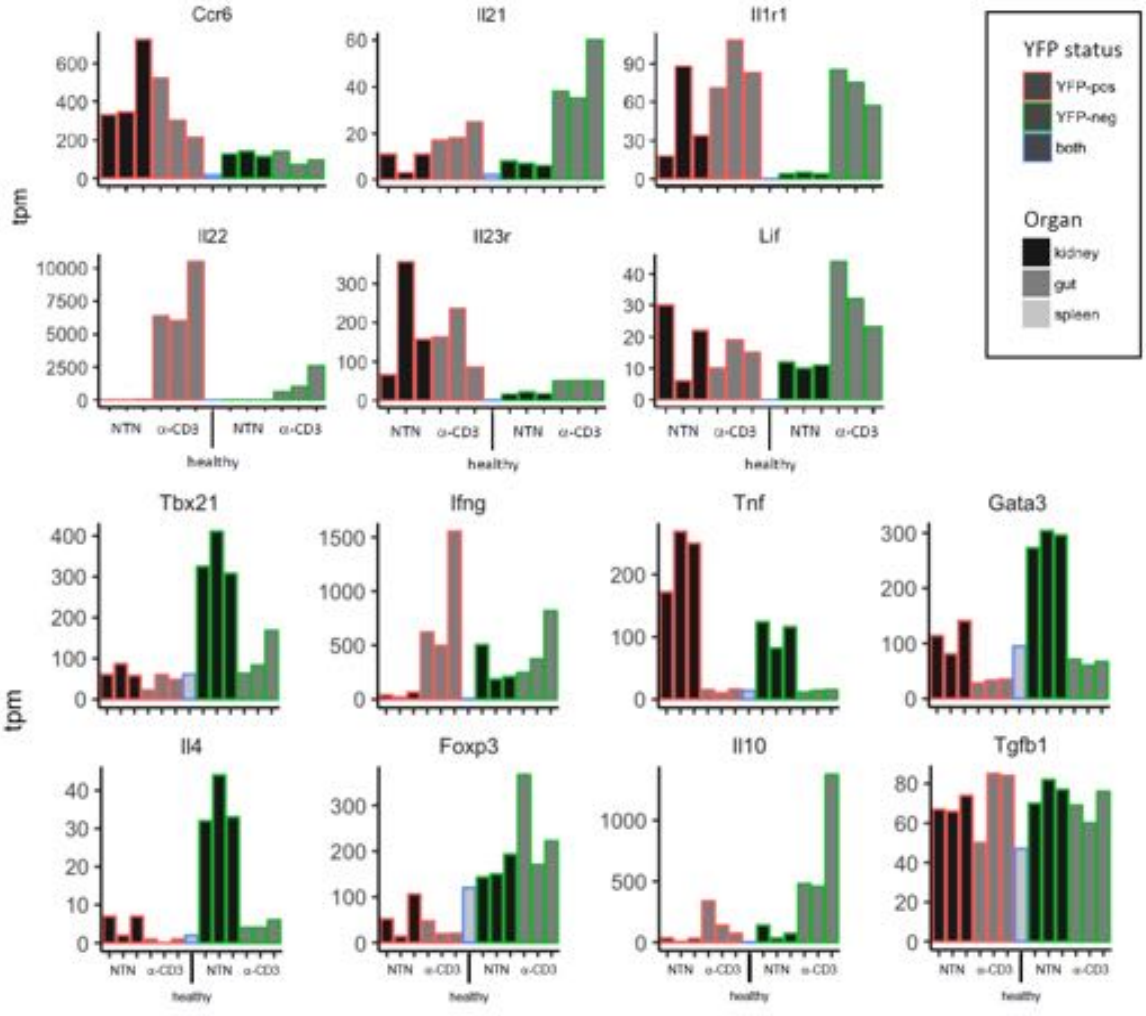

Figure 31: Sequencing data analysis of other relevant genes

For plausibility assessment further sequencing data, quality checks were performed. Among others, the gene expression of different receptors like *Crr6*, *Il1r1*, *Ifng*, *Il10* and *Il23r* were checked, as well as gene expression of essential cytokines and transcription factors like *Tbx21*, *FoxP3, Gata3* and others.

3.4.5 Gene expression analysis of RNA bulk sequencing data

As described earlier (**3.4** and **Table 20**), YFP^+ ($IL\text{-}17^+$) and YFP^- ($IL\text{-}17^-$) cells from IL-17A Fate Reporter mice were sorted by flow cytometry. Afterwards, RNA bulk sequencing was performed and gene expression profiles from *both*, YFP^+ *and* YFP^- cells were analyzed and depicted in a *vulcano plot* (**Figure 32**). In addition, a statistical significance-threshold was set by bioinformatical data processing in order to exclude non-significant sequencing data from analysis.

Vu*lcano plot*s are a common method to visualize sequencing data. The y-axis shows the adjusted p-value (*padj*) and the x-axis the log2 fold change in gene expression of one condition, compared to another (left/right). Non-differentially expressed genes are depicted in the center of the plot.

The adjusted p-value is the smallest significance level (familywise) at which a particular comparison will be declared as statistically significant, as part of the multiple comparison testing (Jafari and Ansari-Pour, 2019).

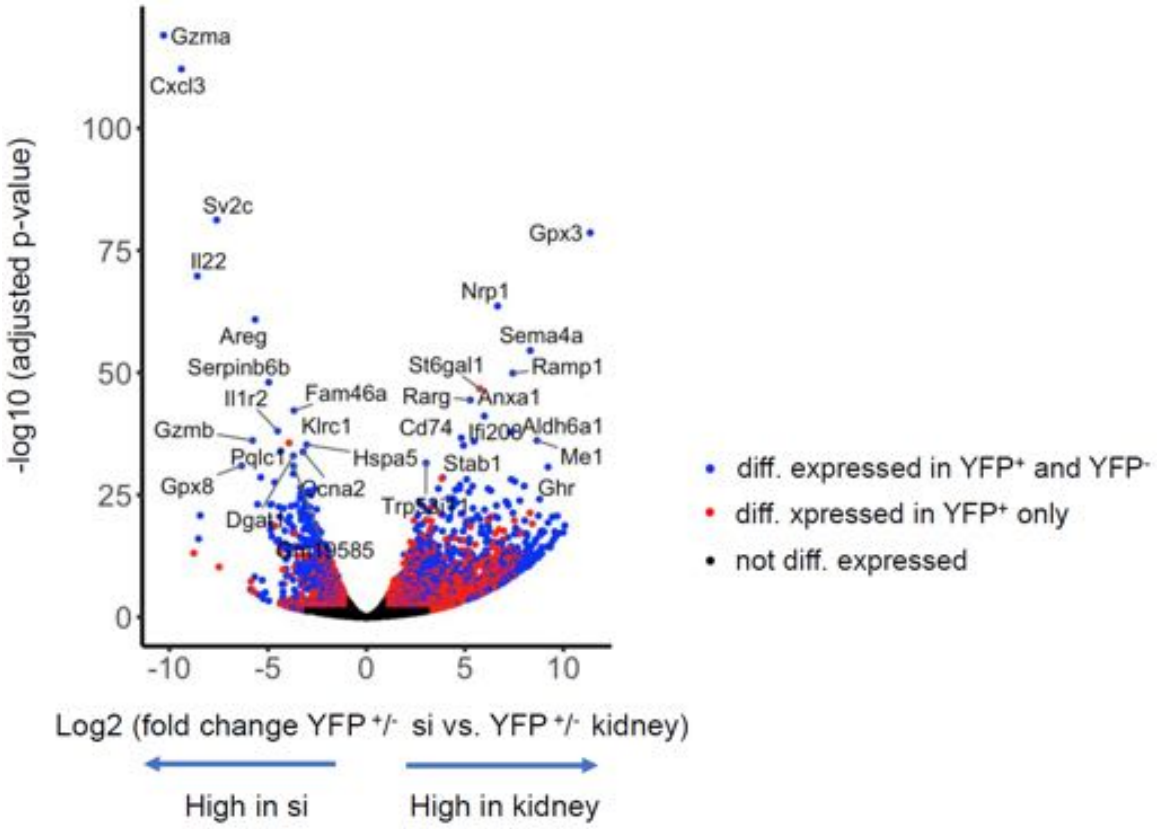

Figure 32: Vulcano plot: YFP$^+$ & YFP$^-$ cells from NTN vs. α-CD3 duodenitis samples

For sequencing data comparison and to visualize bulk sequencing data sets from NTN and anti-CD3 duodenitis, differential gene expression (log2 fold change, x-axis) data were plotted against adjusted p-value (y-axis) in a *vulcano plot*. Non-differentially expressed genes in NTN vs. α-CD3 duodenitis are depicted in the center of the plot (black). Depicted are data from genes differentially expressed in *both* YFP$^+$ *and* YFP$^-$ T_H17 cells (blue) as well as genes differentially expressed only in YFP$^+$ T_H17 cells (red). Genes, highly expressed in YFP$^+$/YFP$^-$ and YFP$^+$ only in kidneys are shown on the right side of the vulcano plot. And vice versa for genes high in small intestine, shown left.

In order to investigate gene expression profiles of genes from cells which are or has been IL-17A-producing T_H17 cells (IL-17A fm^+ / YFP^+ cells), bulk sequencing data were bioinformatically processed as illustrated in **Figure 33**.

To find genes which are differentially expressed specifically only in YFP^+ (NTN) vs. YFP^+ (in other models), genes from the former comparison of the two populations (**Figure 32**) were removed which were lower or higher expressed in YFP^- (NTN) vs. YFP^- in other models.

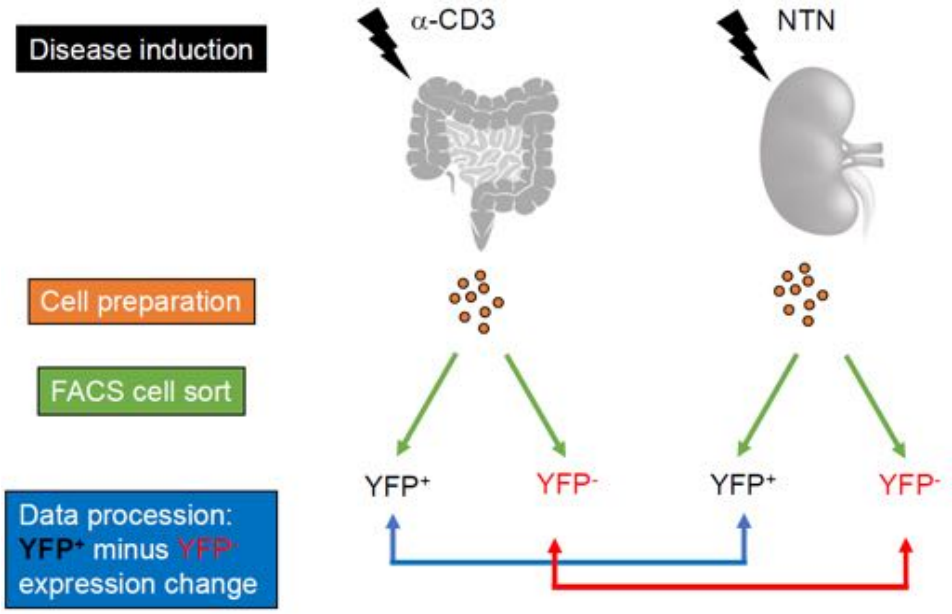

Figure 33: Bulk sequencing data procession: gene expression in YFP^+/ cells

After disease induction, cell preparation and flow cytometric sort of IL-17A fm^+ (YFP^+) and IL-17A fm^- (YFP^-) cells, bulk sequencing data were processed to identify differentially expressed genes from IL-17A fm^+ (YFP^+) in NTN vs. other models only. Therefore, genes from the previous comparison of the two populations were removed which were lower or higher expressed in IL-17A fm^- (YFP^-) in NTN vs. YFP^- in other models.

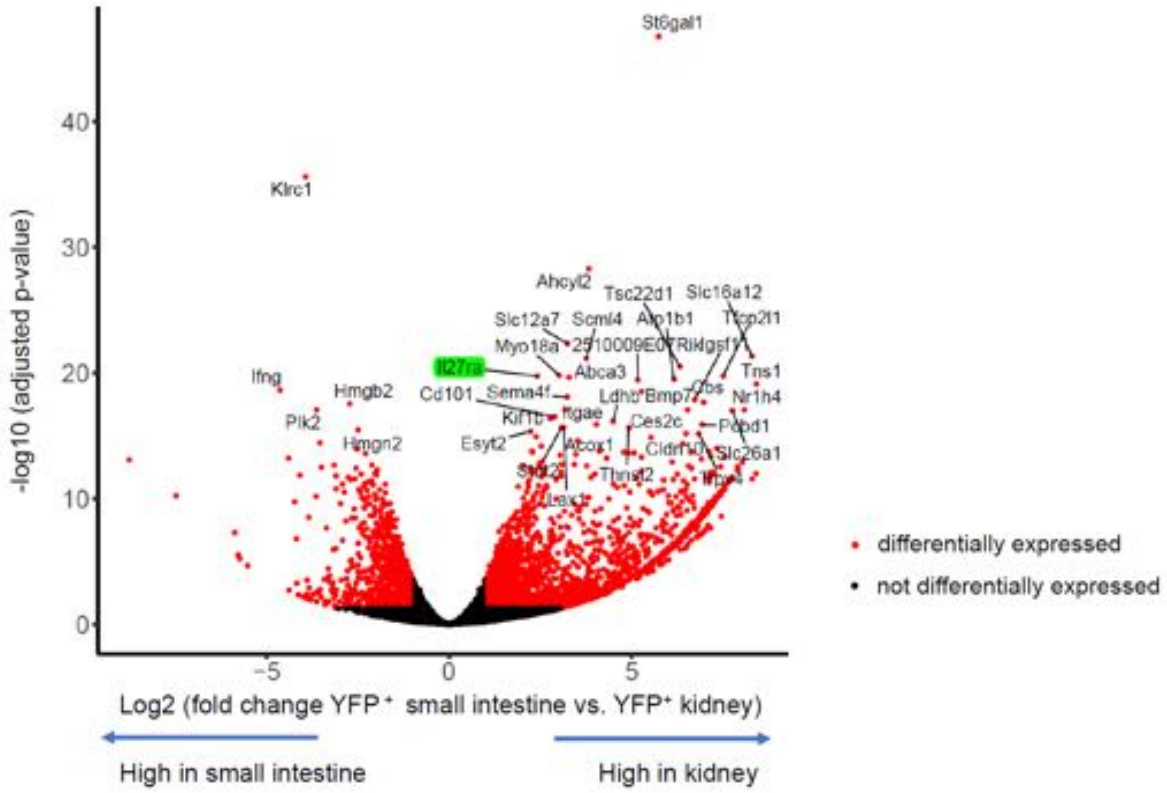

Figure 34: Vulcano plot from NTN and α-CD3-treated IL17A Fate Reporter sequencing data

To compare and visualize sequencing data from NTN and anti-CD3 duodenitis, differential gene expression (log2 fold change, x-axis) data was plotted against adjusted p-value (y-axis). Genes which were not differentially expressed in NTN vs. α-CD3 duodenitis are depicted in the center of the plot (black). Depicted are data after data procession from genes differentially expressed in YFP^+ only. Genes, highly expressed in YFP^+ T_H17 cells in kidneys are shown on the right side of the vulcano plot and vice versa for genes high in small intestine shown left. Il27ra as a potential target gene is marked green.

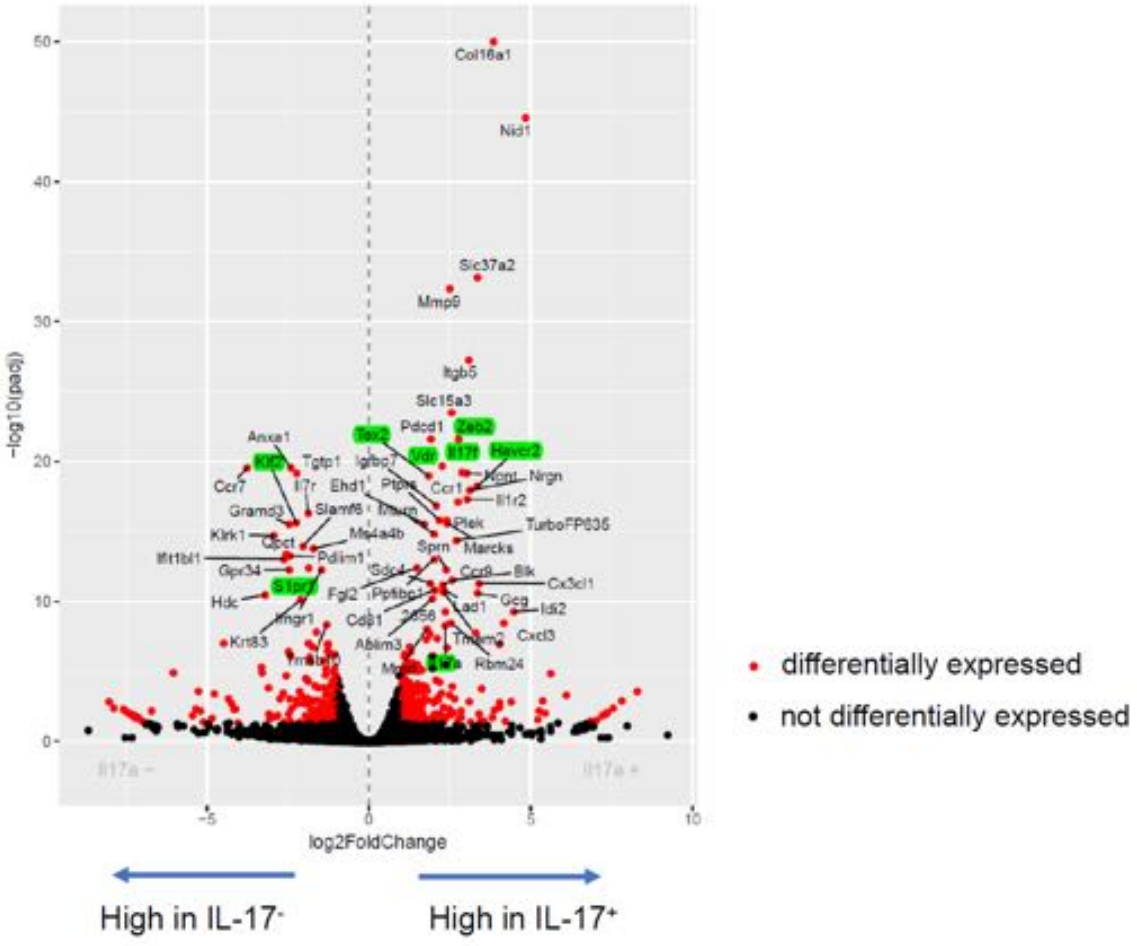

Figure 35: Vulcano plot from NTN-treated Fate^{+} sequencing data

For comparison and visualization sequencing data from NTN Fate^{+} mice, differential gene expression (log2 fold change, x-axis) data were plotted against adjusted p-value (y-axis) in a *vulcano plot*. Genes which were not differentially expressed in YFP^{+} **IL-17A^{+}** vs. YFP^{+} **IL-17A^{-}** are depicted in the center of the plot (black). Some potential target genes are marked green.

3.5 T_H17 cell plasticity: Target gene selection from sequencing data

To structure, manage and simplify the high amount of potentially interesting target genes, the latter were bionomically sorted according to their GO (*Gene Ontology*) classifications. The international bioinformatics GO classification is based on the functional mode of operation of a distinct gene. Therefore, multifunctional genes or their corresponding translational products can be classified into not only one but several different GO terms. Genes with already known functions were sorted into: Transcription factors, cytokines/ chemokines, cytokine-/ chemokine- receptors and genes involved in intracellular signaling (**Table 22**).

Table 22: Initial number of genes in different GO term classifications

Pathway involvement	GO term	Number of sequenced genes with sufficient significance
Chemokine and cytokine activity (up)	0008009/ 0005125	15
Chemokine and cytokine activity (down)		7
Cytokine receptors (up)	0004896	14
Cytokine receptors (down)		2
Chemokine receptors (up)	0042379	1
Chemokine receptors (down)		1
Transcription factors (up)	0008134	131
Transcription factors (down)		36
Intracellular signal transduction (up)	0007165	351
Intracellular signal transduction (down)		75

To further separate and identify possibly interesting gene targets with regard to T_H17 cell plasticity, a combined approach of literature- and data bank research was performed. (For applied Data banks please refer to the *References* at the end of this thesis.)

The following criteria were set and applied to the sequencing results in order to find potential target genes related to T_H17 cell stability in experimental nephrotoxic nephritis (NTN). Notably, not all of these *criteria* had to apply to all potential target genes. Those were only considered for further target gene selection.

General criteria of target gene choice:

- Already known mutations in humans and relation to (auto-) immunity
- Experimental accessibility, e.g. targeting of receptors, knockout mice available (for first trial experiments)
- Already mentioned in literature with regard to immunomodulatory functions and/ or T_H17 cell plasticity etc.

Sequencing data requirements and criteria:

- Statistically significance in differential gene expression
- n-fold gene expression change in NTN compared to other models with higher T_H17 cell plasticity
- Adoption: genes active in T_H17^+ cells important with regard to T_H17 cell stability in NTN but not in T_H17^- cells (see data procession, **Figure 33**)

After target gene selection, heat maps with corresponding z scores from IL-17A Fate Reporter (**Figure 36**) and $Fate^+$ mice (**Figure 37**) were generated.
Here, the z score of a gene indicates the number of standard deviations away from the mean expression in the (spleen-) reference (Chris Cheadle, 2003). Genes indicated in red are differentially higher expressed in NTN kidneys than in other models.

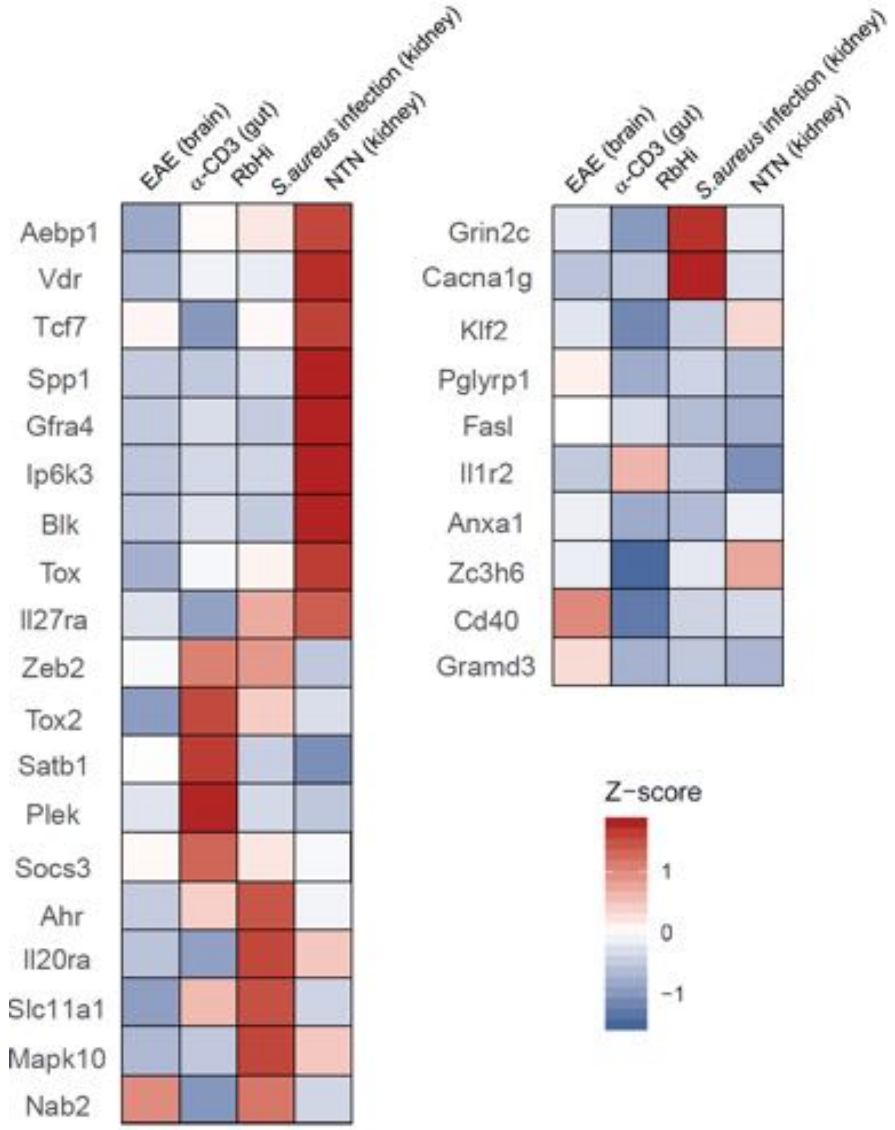

Figure 36: Selected genes & z scores in different conditions (IL-17A Fate Reporter)

Depicted are the heat maps of selected target genes from bulk sequencing data of NTN IL-17A Fate Reporter mice compared to other models (and analyzed organs) which are EAE (brain), anti-CD3 duodenitis (gut, small intestine) and *S.aureus* infection (kidney).

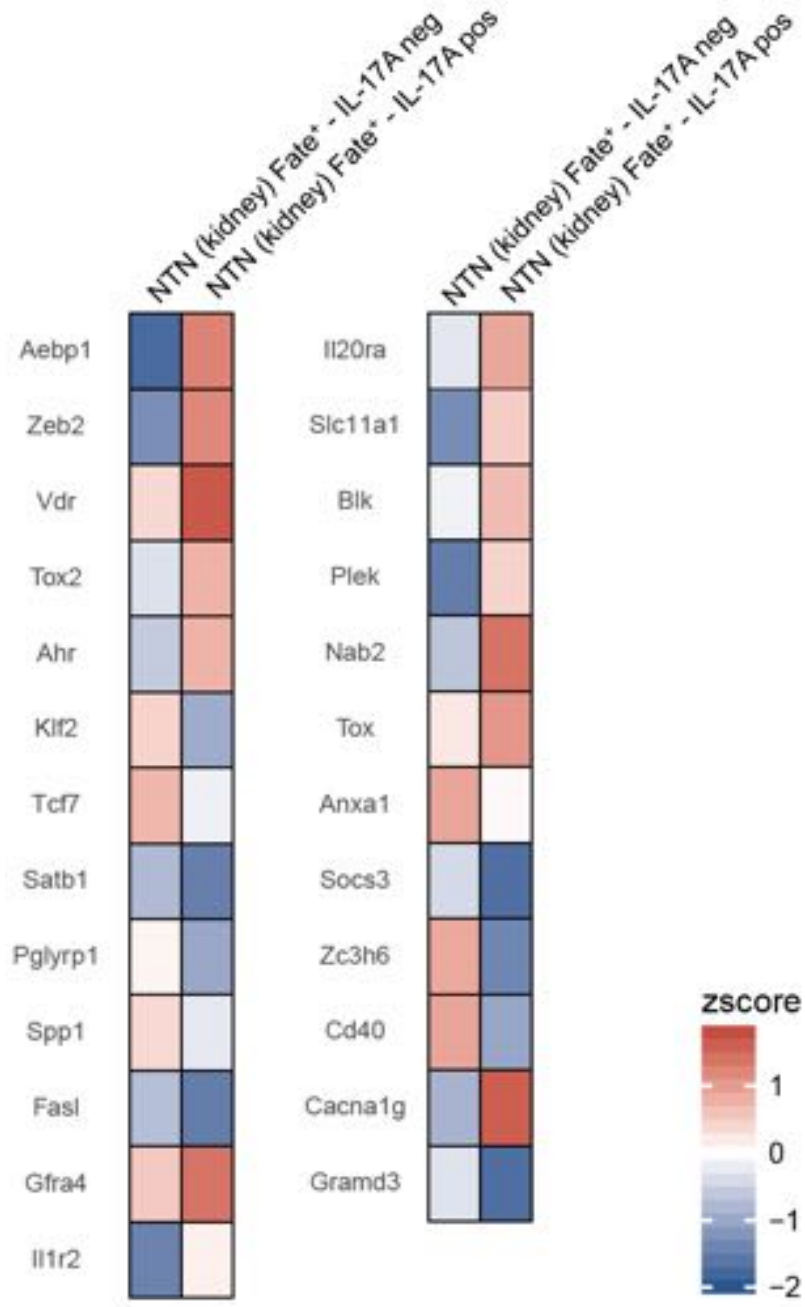

Figure 37: Selected genes & z scores in different conditions (Fate^{+} Reporter)

Depicted are the heat maps of selected target genes from bulk sequencing data of NTN Fate^{+} mice. Data shown from NTN-mice, YFP^{+} **IL-17A^{+}** compared to YFP^{+} **IL-17A^{-}** sorted cells from kidneys.

Of note, not all initially selected target genes (like *Il27ra*) were found in IL-17A Fate Reporter and Fate^{+} mice.

Based on (optional) gene selection criteria and combined literature- and data bank research, the IL-27ra (Interleukin-27 receptor subunit a)/IL-27-axis was found to be a very interesting and promising first target gene candidate for further investigations of its role in T_H17 cell stability in NTN. *IL-27ra* was found to be differentially higher expressed in NTN kidneys vs. small intestine in anti-CD3 duodenitis.

Among Interleukin 27-related pathways, it was also decided to investigate the role of Tbet (encoded by the gene *Tbx21*) in NTN mice and its potential relation to T_H17 cell stability in NTN.

Detailed reasons for these two selected target genes for experimental analysis are explained below, see **3.6** (IL-27ra/IL-27-axis) and **3.7** (Tbet/ *Tbx21*).

3.6 IL-27/ IL-27ra and its role in NTN and T_H17 cell stability/ plasticity

By comparative gene expression analysis of bulk sequencing data from NTN and α-CD3-treated IL-17A Fate Reporter mice, among others, IL-27/IL-27ra axis was found to be an interesting pathway, possibly involved in T_H17 cell stability in NTN. This was the first experimentally investigated pathway in NTN.

In bulk sequencing data, Interleukin-27 receptor subunit alpha (IL-27ra, gene name *Il27RA,* also known as *WSX-1 or TCRR*) was found to be significantly higher expressed in T_H17 cells in NTN-mice than in all other disease models with higher T cell plasticity (**Figure 36, left heat map, 9th gene from top**).

In addition, from comparison of NTN vs. α-CD3-induced duodenitis in IL-17A Fate Reporter mice IL27RA was differentially higher expressed in (**Figure 34, marked in green**).
Also in terms of significance this gene showed a low adjusted p-value (padj), as seen below.

Ensembl gene ID	Gene	Log2 fold change (differential gene expression)	Adjusted p-value (padj)
NSMUSG00000005465	*Il27RA*	2,42	$1{,}71 \times 10^{-20}$

Furthermore, as part of a cellular receptor, this protein is rather suitable for investigation by overexpression, blocking, ligand-mediated stimulation etc.

In addition, literature research indicated interesting IL-27/IL-27ra pathway related features with regard to immune regulatory functions, as explained in detail in **1.4**.

3.6.1 IL-27ra expression in NTN and anti-CD3 duodenitis

IL-27ra protein expression in NTN and anti-CD3 duodenitis (FACS)

To validate the RNA sequencing data, first the IL-27ra protein level was analyzed via flow cytometry (FACS).

To do so, cells from kidneys (NTN) and intestine (anti-CD3 duodenitis) were extracted and subsequently stained and FACS gated for living, $CD45^+$, $CD4^+$, $CD3^+$ cells, as well as IL-27ra and a corresponding IgG isotype control (see **2.1.6** and **Figure 38**).

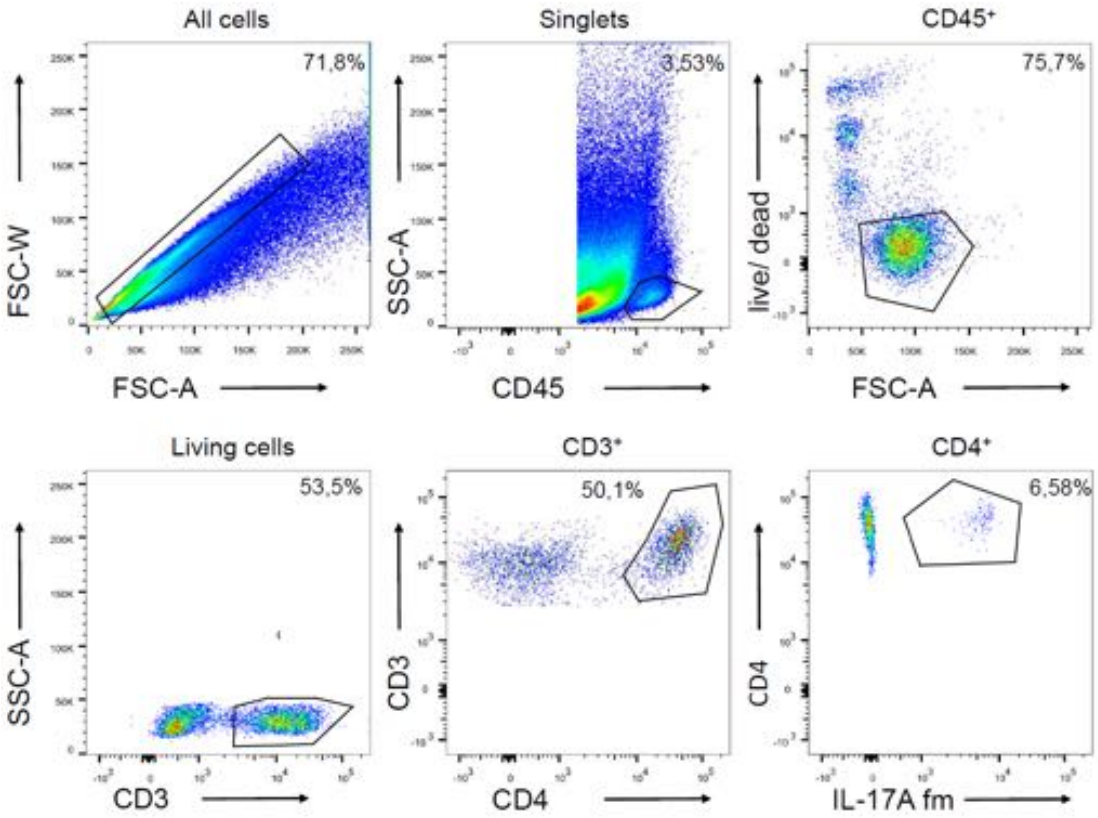

Figure 38: IL-27ra protein expression - FACS gating

To validate bulk sequencing data with regard to IL-27ra protein expression via flow cytometry, renal (NTN) and small intestinal (α-CD3 duodenitis) cells were FACS-stained for live/dead cells, CD45, CD3, CD4, IL-27ra and the corresponding IgG isotype control. To analyze IL-27ra in T_H17 cells, cell populations were gate as follows: (**Top, left to right**) singlet cells, $CD45^+$, living cells and (**bottom, left to right**): $CD3^+$, $CD4^+$, IL-17 fm^+ ($eYFP^+$). Depicted are results from FACS analysis of NTN samples only.

Flow cytometric analysis of IL-27ra protein expression in NTN and anti-CD3 duodenitis are shown in **Figure 39** and **Figure 40**.

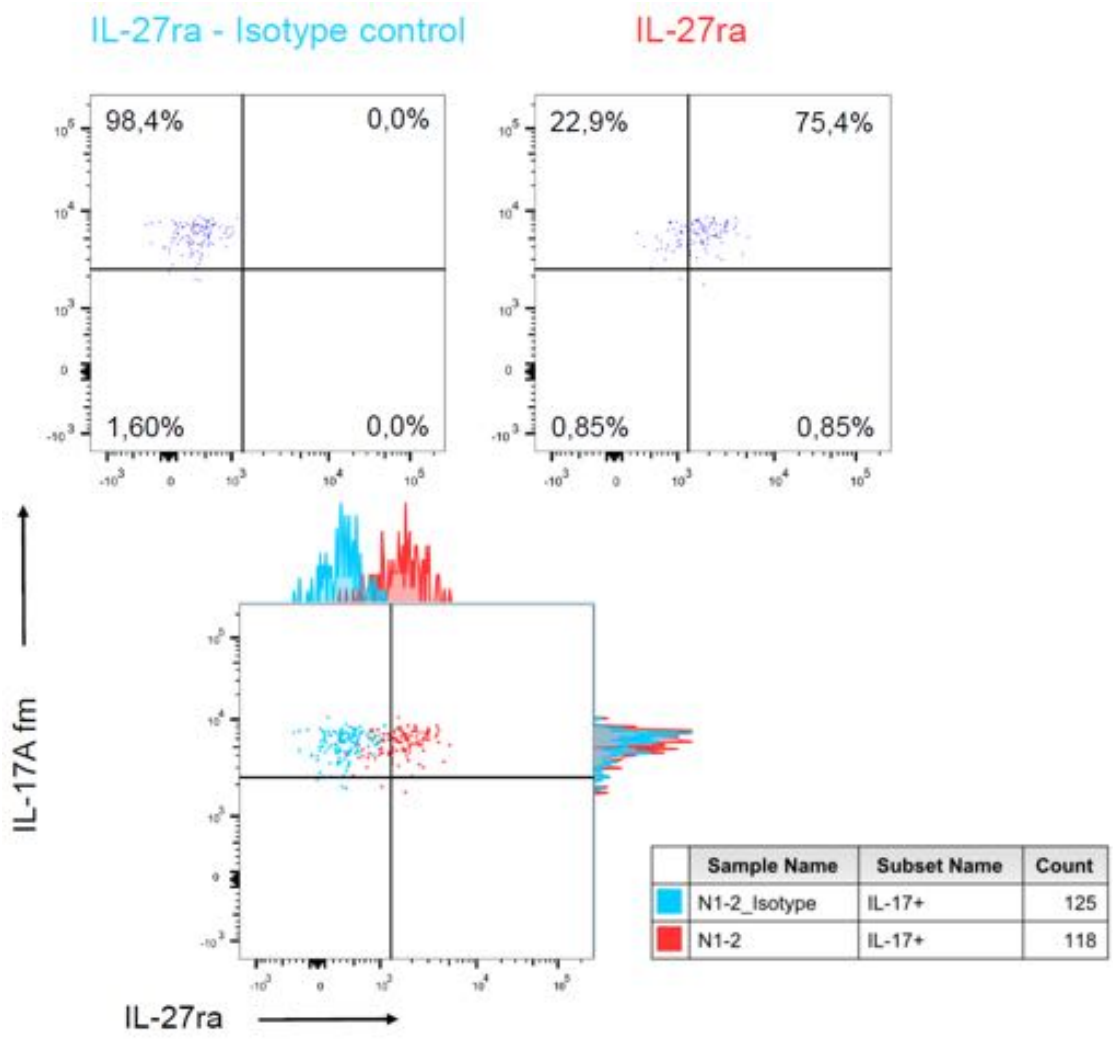

Figure 39: IL-27ra protein expression in in renal T_H17 cells in NTN-mice

To validate bulk sequencing data, IL-27ra protein expression was determined in T_H17 cells from NTN- and α-CD3 treated mice via flow cytometry (FACS). Therefore, renal (NTN) and small intestinal (α-CD3 duodenitis) cells were FACS-stained and gated as depicted including staining for IL-27ra (top right) and IgG isotype control (top left), also shown as an overlap of both (bottom), IgG isotype control (blue) and IL-27ra (red). Depicted are results from FACS analysis of NTN samples only.

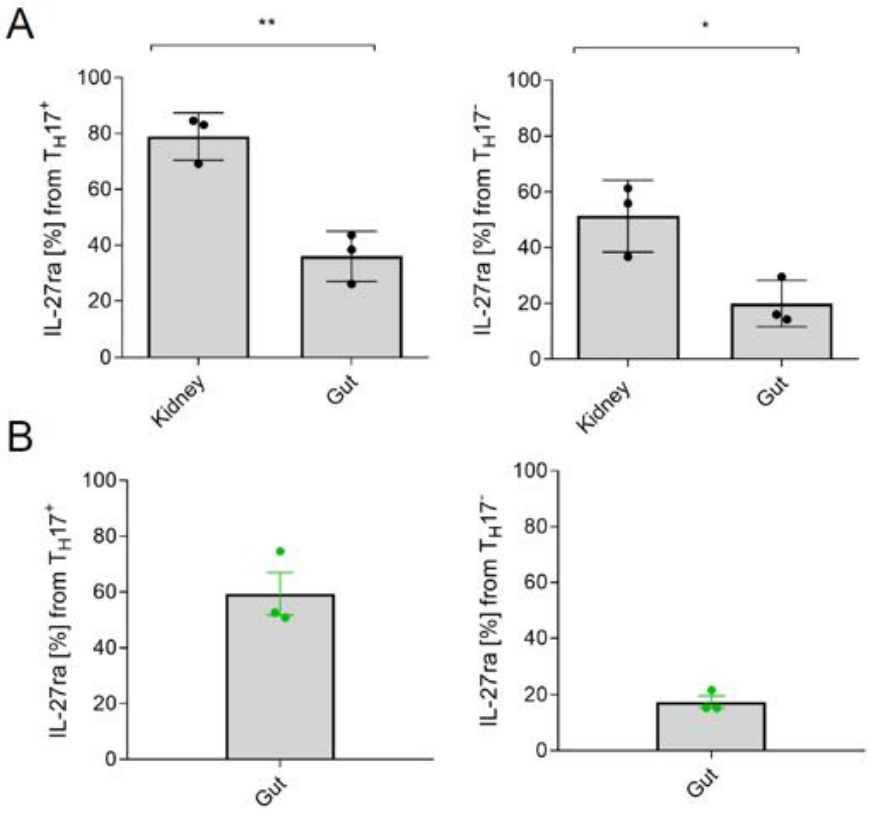

Figure 40: FACS analysis of IL-27ra in NTN & α-CD3 mice in kidney and gut

A: Ten days after NTN induction, IL-27ra protein proportion of IL-17A fm$^+$ (YFP$^+$) and IL-17A fm$^-$ (YFP$^-$) cells from renal and small intestinal samples were measured in IL-17A Fate Reporter mice via flow cytometry in kidney (left) and gut (right). **B**: In addition, two days after initial anti-CD3-treatment, IL-27ra protein proportion of IL-17A fm$^+$ (YFP$^+$) and IL-17A fm$^-$ (YFP$^-$) cells was measured in samples from small intestine in IL-17A Fate Reporter mice via flow cytometry.

As a result, high *Il27RA* gene expression found in bulk sequencing data (NTN vs. α-CD3 duodenitis) could be positively verified in IL-17A fm$^+$ (eYFP$^+$) cells compared to IL-17A fm$^-$ (eYFP$^-$) cells as well as by comparison of kidney versus gut by protein expression analysis via flow cytometry.

3.6.2 IL-27 gene expression in the course of NTN

In the course of further analysis, an elevated IL-27ra protein expression level was measured via flow cytometry. Hence, it was feasible to analyze gene expression of the IL-27ra ligand (IL-27) in the course of NTN in a time-depended manner.
Here, all *TaqMan* qPCR experiments were performed using the hypoxanthine phosphoribosyltransferase 1 (*HPRT1*) as a housekeeping gene reference (**2.2.26**).

To do so, after NTN induction, at different time points (24h, d3, d5, d7, d10, d14 and d21), kidneys from NTN-treated and non-NTN-treated (control-) animals were extracted and RNA was isolated (**2.2.22**). Finally, RNA was transcribed into cDNA (**2.2.24**).

Of note: Two independent time-kinetic experiments were performed and all NTN experiments were performed using *C57BL/6* wild-type (wt) mice.

Results from IL-27-NTN time-kinetic qPCR experiments (**Figure 41**) show increased *Il27* gene expression over time in the course of NTN.
Il27 gene expression was found to increase from day 7, where also T_H17 cells are generated in the kidney.

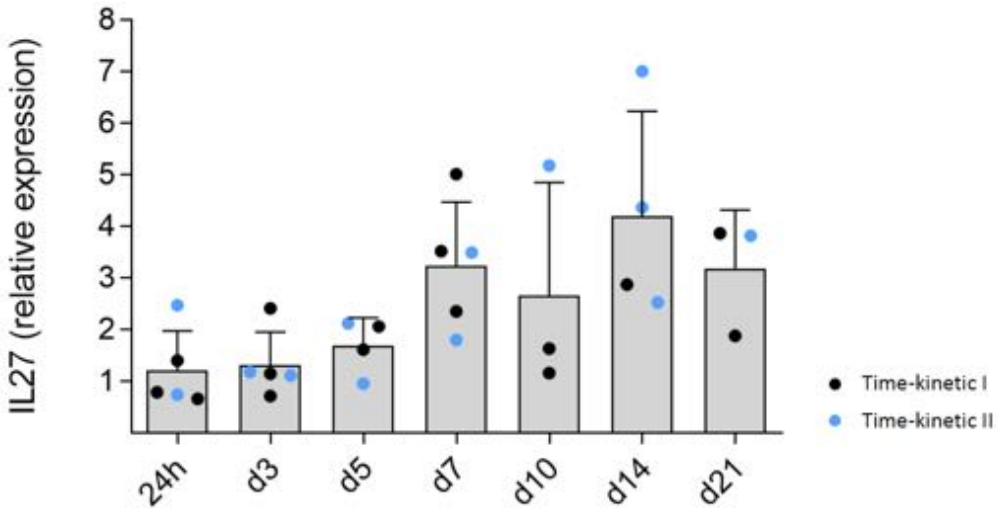

Figure 41: Relative gene expression of IL27 in the course of NTN (PCR)

To assess the gene expression of *Il27* in the course of NTN relative to a house keeping gene (*HPRT1*), *TaqMan* qPCR was performed from NTN time-kinetic experiments in *C57BL/6* wild-type mice. RNA samples were provided by the *Panzer lab*, UKE, Hamburg, Germany.

3.6.3 IL-27 intervention in NTN-mice

After analysis of obtained sequencing data and identification of the IL-27ra as an interesting target gene, it was feasible to validate these data in protein expression by flow cytometry (**Figure 40**). The results revealed a higher abundance and differential gene expression of IL-27ra in renal NTN-samples compared to small intestinal samples from α-CD3-treated mice which validated the sequencing data. Furthermore, gene expression analysis via qPCR revealed increased IL-27 cytokine transcript levels over time, starting from day 7, in the course of NTN. This time point represents also the occurrence of first kidney infiltrating T_H17 cells in NTN (Krebs and Panzer, 2018). Hence, it is feasible to assume that IL-27 will have an effect on these cells at this time point.

To further investigate the effect of the IL-27/ IL-27ra axis *in vivo*, an experiment was conducted to functionally test the effect of recombinant mouse IL-27 cytokine in NTN-mice, as schematically seen in **Figure 42**.

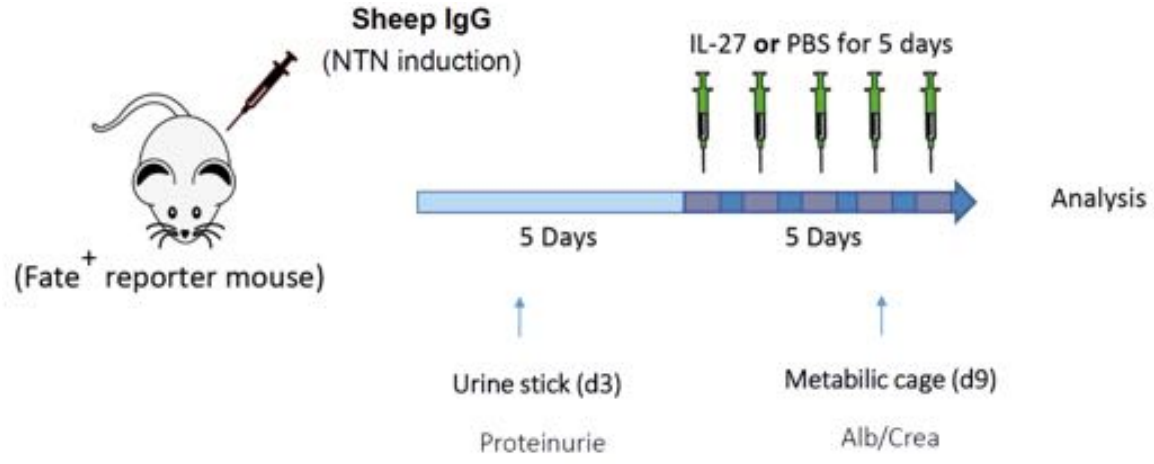

Figure 42: Experimental approach to investigate the role of IL-27 in NTN-mice

On day 0, NTN was induced in female mice (10-12 weeks old) via i.p. injection of 450µL sheep IgG per animal directed against mice GBM. In the course of the disease, the animals developed proteinuria caused by damaged glomeruli, determined by urine sticks on day three. Five days after NTN induction, daily treatment with IL-27 by i.p. administration or PBS started and last for 5 days in total. On day 9, urine was collected in metabolic cages and renal albumin and creatinine was quantified. On day 10 after NTN induction animals were sacrificed and samples were analyzed.

Therefore, NTN was induced in female Fate$^+$ reporter mice via sheep IgG administration (**2.2.2**). Furthermore, non-NTN control animals received the same volume of PBS compared to the volume of NTN-positive sheep IgG-administered mice.

In order to get a proper T_H17-related immune response (description in **3.3** and **Figure 14**), the daily i.p. administration of recombinant IL-27 cytokine (and PBS-treatment as control) started on day 5 after NTN induction.
To assess the severity of kidney damage during NTN, proteinuria was measured via urine sticks on day 3 post NTN induction (data not shown). In addition, glomerular crescents were counted (**Figure 44**) in histological kidney sections from d10 after NTN-induction (**Figure 43**) and albumin-to-creatinine ratio was analyzed (**Figure 44**) from urine samples collected in metabolic cages on day 9.

In addition, supernatants of homogenized kidney tissue were collected for further IL-27 cytokine quantification via *cytometric bead array* (CBA) as described in **2.2.31** and **3.6.6**.

Subsequent experiments were performed with 5µg of recombinant mouse IL-27 per animal in the range according to previous works of others (Owaki et al., 2008).

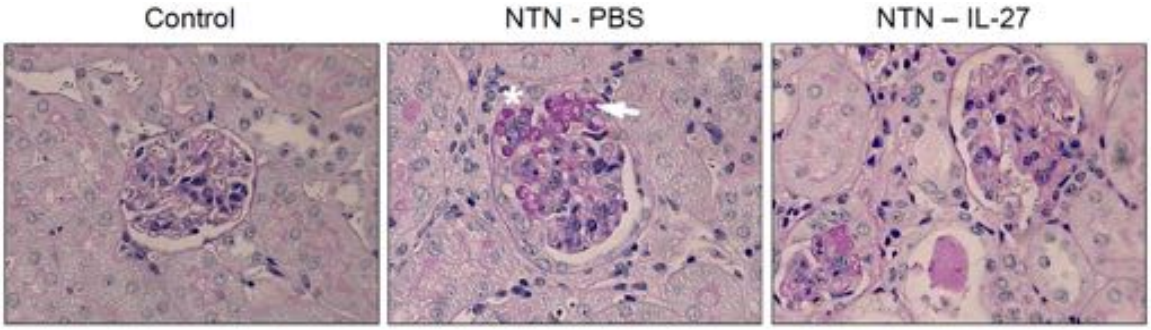

Figure 43: Histology of IL-27- treatment NTN-mice vs. PBS-treated NTN-mice

To functionally study the role of IL-27 application *in vivo*, NTN Fate^{+} mice were treated with PBS (**middle**) or with 5µg recombinant mouse IL-27 cytokine per mouse (**right**) for 5 days starting from day 5 after NTN induction. In control mice (**left**) no NTN was induced. 10 days post NTN disease induction, histological kidney sections were PAS-stained and glomerular crescents were counted in order to assess the kidney damage. In kidney sections of PBS-treated NTN mice high leukocyte cell infiltration and necrotic glomerular tissue was found (**white arrow**), as well as glomerular crescent formation (**white asterisk**) which were significantly reduced in IL-27-treated NTN-mice (**right**). However, non-NTN mice did not show glomerular damage.

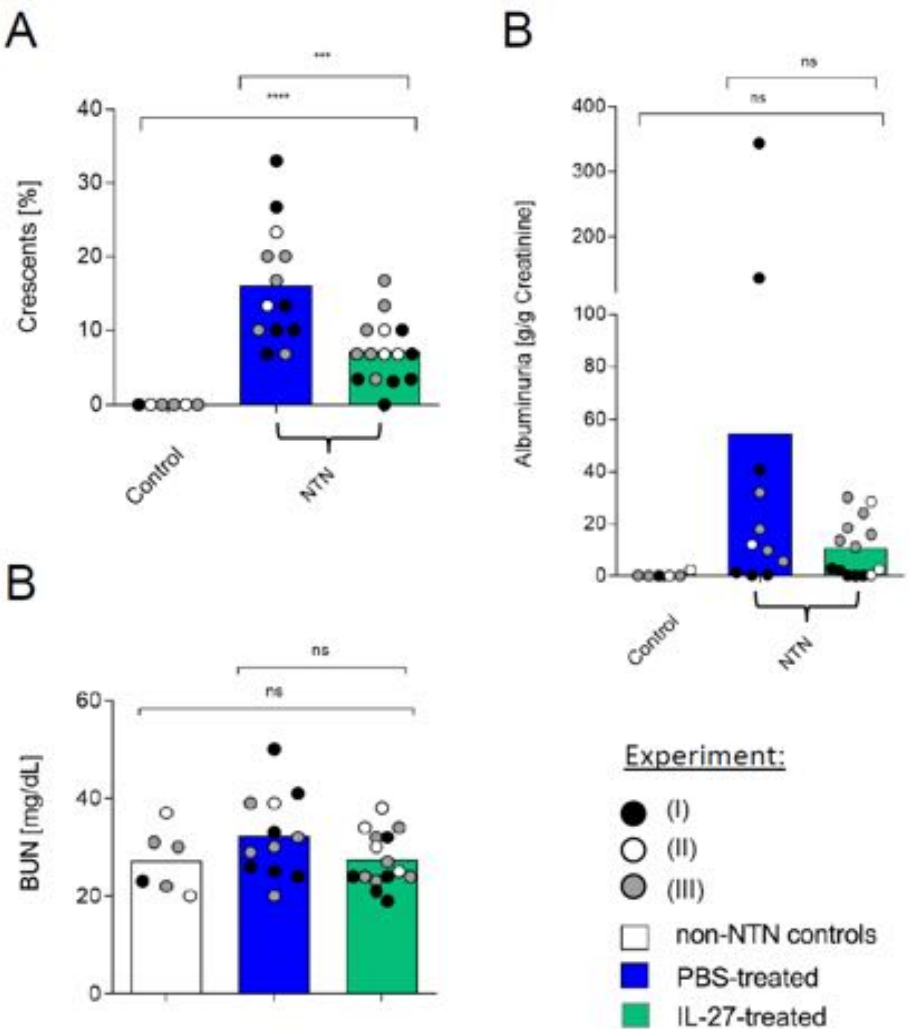

Figure 44: Renal damage in IL-27 treated NTN-mice

Ten days after initial NTN induction and 5 days of daily IL-27- (green bar) or PBS- (blue bar) treatment, renal damage was significantly reduced in IL-27-treated NTN-animals according to **A** glomerular crescents, **B**: albuminuria and **C** blood urine nitrogen (BUN, both on day 9) compared to PBS-treated NTN-mice. Non-NTN mice (white bar) exhibited no crescent formation or high albumin/ creatinine ratios and low BUN levels. Depicted plots had been generated from three independent experiments, coded by white-, grey- and black color code. (Results from 3 independent experiments.)

Histologically kidney sections from PBS-treated NTN-mice indicated a high degree of kidney damage by formation of glomerular crescents as well as cell infiltration into the glomeruli and necrotic tissue formation. In contrast, NTN-mice treated with recombinant mouse IL-27 cytokine exhibited significantly reduced histological damage. Non-NTN mice did not show glomerular damage as expected (**Figure 43** and **Figure 44**).

The same tendency was found in regard to proteinuria (BUN and ACR) which showed significantly less proteinuria in IL-27-treated NTN-mice compared to PBS-treated control NTN-mice. Non-NTN mice did not indicate elevated protein levels in the urine or blood (**Figure 44**).

Summarizing, these *in vivo* results indicate that IL-27-treatment in NTN compared to PBS-treated NTN-mice exhibit a significantly protective effect related to kidney damage.

3.6.4 IL-17 / IL-10 in IL-27 intervention in NTN (FACS)

From literature, it is known that the IL-27/IL-27ra axis is capable to exhibit pro- and anti-inflammatory properties for example by activation of IL-10 expression or by inhibition of T_H17 cell differentiation depending on experimental or clinical circumstances as explained in **3.6**.

Therefore, the aim of further experiments was the elucidation of the underlying molecular mechanisms for the significantly reduced renal damage in NTN-mice treated with recombinant mouse IL-27 cytokine.

Based on findings from literature (**3.6**.), it was hypothesized that the observed NTN-protective phenotype in IL-27-treated animals is caused by reduced amount of T_H17 cells by inhibited T_H17 cell differentiation and elevated expression of IL-10 in the kidney of mice with induced NTN. To proof this hypothesis, IL-17A and IL-10 protein levels were analyzed in $Fate^+$ mice by via flow cytometry.

IL-17 / IL-10 in IL-27 intervention in NTN – FACS gating strategy

Flow cytometric gating for analysis of IL-17A and IL-10 in NTN-mice with injected IL-27 or PBS (control) is shown in **Figure 45**.

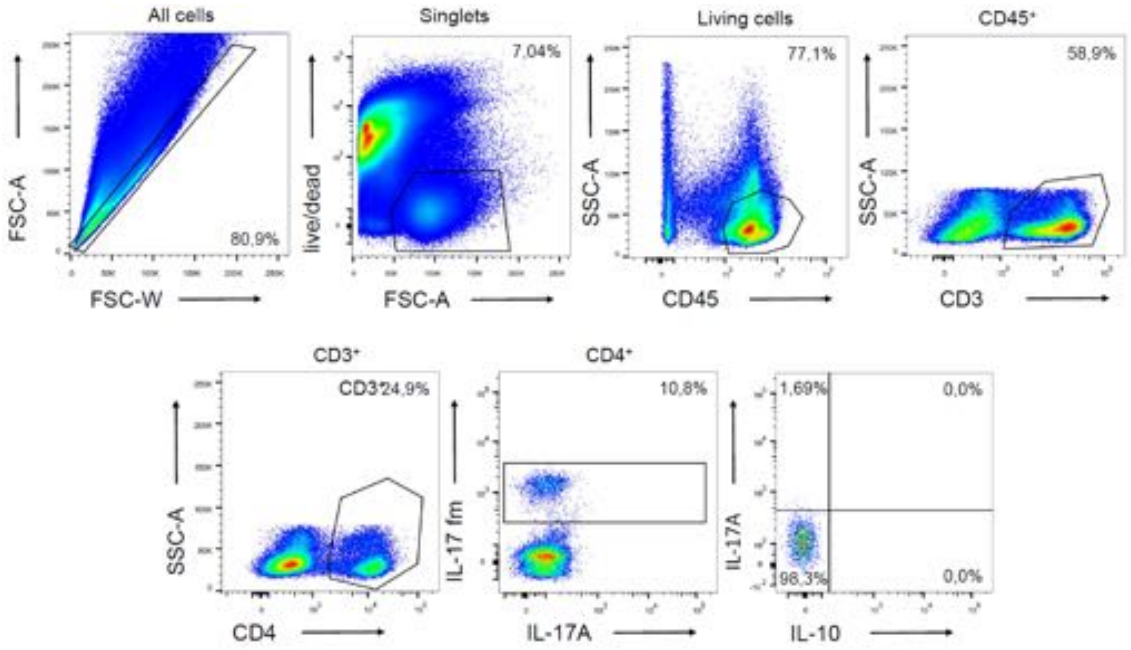

Figure 45: IL-17A & IL-10 analysis in IL-27-treated NTN-mice - FACS gating

For analysis of IL-17A and IL-10 in NTN-mice after IL-27 recombinant mouse cytokine intervention, cell populations were gated for living, singlet $CD45^+CD3^+$ cells (**top row**). Furthermore, $CD4^+$ IL-17 fm^+ ($eYFP^+$) cells were selected (**lower row**). Finally, the proportion of IL-17A and IL-10 producing cells was determined. (Example gating strategy from NTN-mice with IL-27 intervention.)

Proportion of IL-17 fm$^+$ (eYFP$^+$) cells in non-NTN and NTN (PBS/ IL-27) mice.

Figure 46 show flow cytometric analysis of IL-17 fm$^+$ (eYFP$^+$) cells among non-NTN mice and NTN mice treated with PBS or IL-27 cytokine.

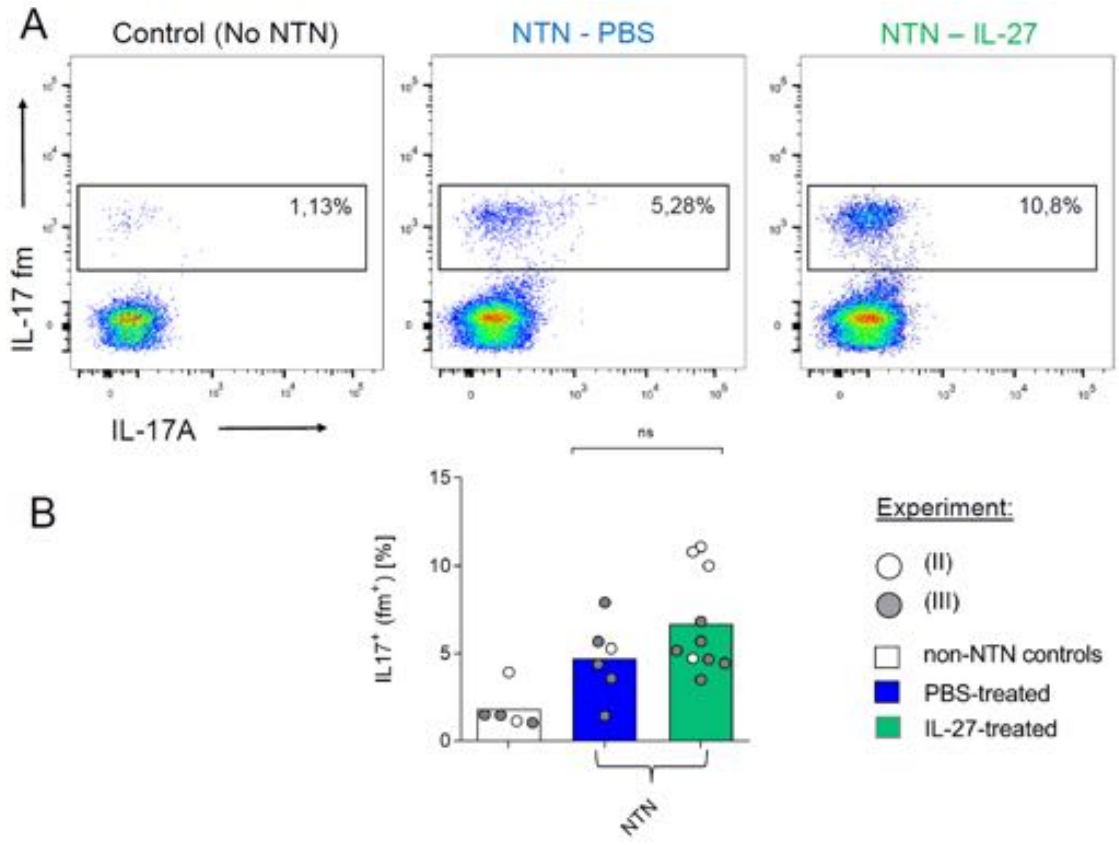

Figure 46: Analysis of IL-17 fm$^+$ (eYFP$^+$) cell populations IL-27-treated NTN-mice

For further analysis, IL-17 fm$^+$ (eYFP$^+$) cell populations were studied in **A, from left to right**: Non-NTN control mice (white bar) and NTN-induced mice, treated with PBS (blue bar) or IL-27 recombinant mouse cytokine (green bar) via flow cytometry. Quantified FACS results are depicted in **B**. Results from two independent experiments indicated by grey and white circles.

Interestingly, results from analysis of proportion of IL-17 fm$^+$ (eYFP$^+$) cells showed smaller population of cells which produced IL-17A (IL-17 fm$^+$) in PBS-treated NTN-mice compared to mice with IL-27 intervention (**Figure 46** ,**A** and **B**) in two separate experiments. However, a brought distribution of FACS-readings was observed. In non-NTN induced mice however, the percentage of IL-17 fm$^+$ cells was very low as expected.

Analysis of IL-17A / IL-10 producing T cells in IL-17 fm$^+$ (eYFP$^+$) cells populations in PBS/ IL-27-treated NTN-mice

Afterwards, the percentage of IL-17A and IL-10 producing cell populations within IL-17 fm$^+$ cells was further analyzed by FACS, as shown in (**Figure 47**).

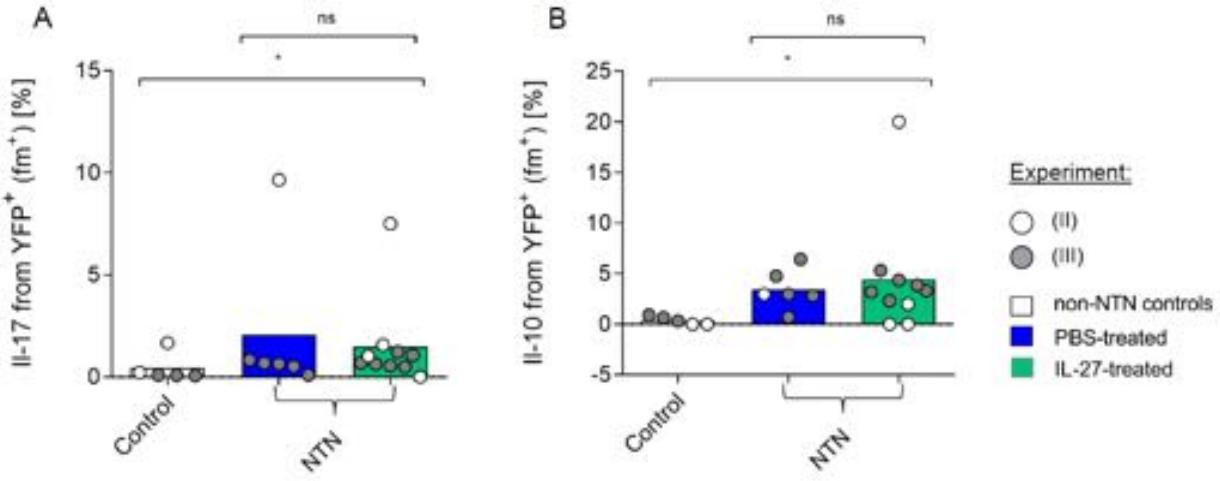

Figure 47: Analysis of IL-17A & IL-10 in IL-27/PBS-treated NTN-mice (FACS)

Depicted are the quantifications of IL-17A and IL-10 producing cells in IL-17 fm$^+$ cell populations based on previous flow cytometric results. **A**: IL-17A and **B**: IL-10 in IL-17 fm$^+$ (eYFP$^+$) cells.

With regard to the previous hypothesis, no significant increase in IL-10 nor reduced levels of IL-17A-producing cells was found in IL-27-treated NTN-mice compared to PBS-NTN-mice in IL-17 fm$^+$ populations.

3.6.5 STAT3 activation after *in vitro* IL-27-stimulation in CD4$^+$ cells

In previously performed experiments, it was found that IL-27-treated NTN-mice showed significantly reduced kidney damage compared to PBS-treated NTN-mice.

This result raised the question for the underlying molecular pathways for this protective IL-27-mediated phenotype. To investigate a potential role of IL-17A and IL-10 in T_H17 cells during experiments with IL-27 intervention in NTN-mice, these cytokines were analyzed via flow cytometry. However, no increase in IL-10

nor reduction in IL-17A in IL-17 fm^+ cell population was found contrary to the set hypothesized.

To find hints for underlying molecular pathways for the protective effect of IL-27 in NTN-mice, it was therefore aimed to test activation of the STAT3 pathway by analysis of pSTAT3 formation *in vitro* in IL-27-stimulated cells from healthy spleens. Caused by the predicted small amount of cells and for precise and sensitive pSTAT3 quantification, flow cytometry was chosen for analysis over western blot.
To do so, spleens of healthy mice were extracted. Afterwards, $CD4^+$ cells were enriched (**2.2.17**), stimulated, fixed and FACS-stained (**2.2.19**).

Since STAT pathways are involved in many pathways, after $CD4^+$ enrichment cells were placed in a 37°C-incubator for 2,5h for cellular rest.
Then, cells were placed into a 6-well plate and finally stimulated with IL-6 as a positive control for STAT3 (Owaki et al., 2008; Stumhofer et al., 2007), IL-27 or PBS. For detailed procedure please refer to **2.2.28**.
To additionally test different cytokine concentrations (IL-6) and varying durations for *in vitro* stimulation (IL-27), a set of experiments were conducted. For details please refer to **Table 18**.

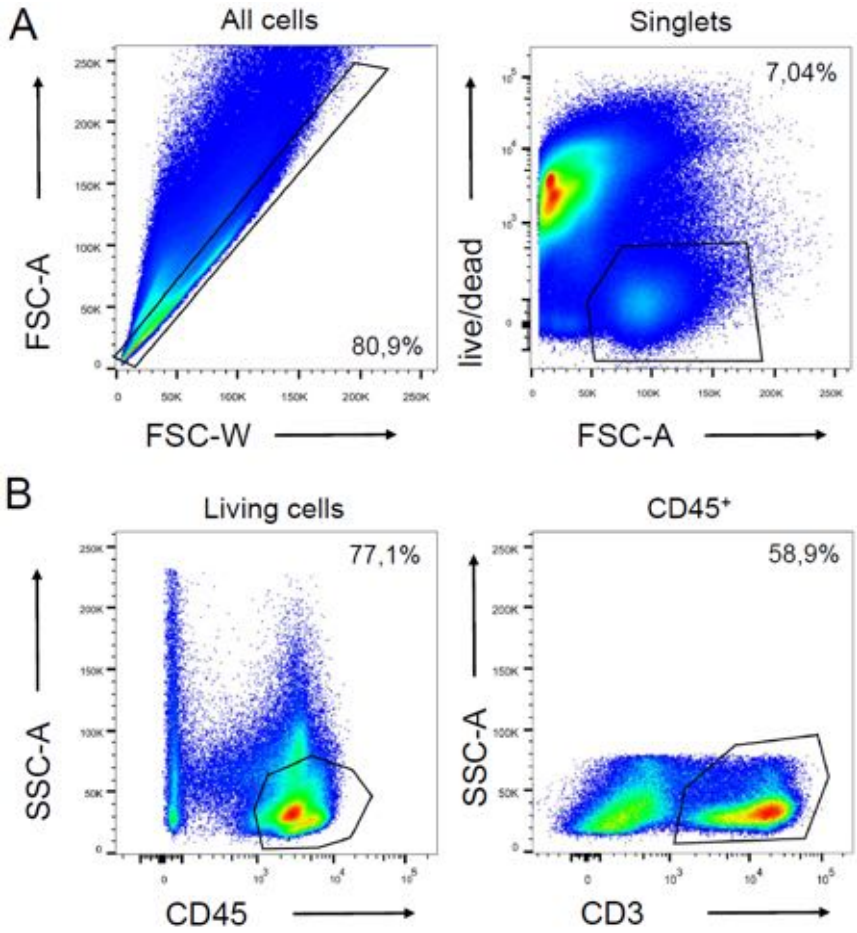

Figure 48: STAT3 activation in IL-27 / IL-6-stimulated CD4$^+$ cells – FACS gating

After extraction of and enrichment of CD4$^+$ cells from healthy spleen, cells were incubated for 2,5h for cell rest. Afterwards, CD4$^+$ enriched cells were stimulated with IL-6 (positive control), IL-27 or PBS (negative control). Cells were immediately fixed with para formaldehyde (PFA), stained for flow cytometric pSTAT3 analysis and gated for **A**: singlet, living, **B**: CD45$^+$ CD3$^+$ cells. (Example from IL-6 (10ng/ml)-stimulated spleen sample 1 of 2.)

To determine STAT3 activation via IL-6 and IL-27 *in vitro* stimulated CD4$^+$ enriched healthy spleen samples, pSTAT3 molecules were FACS-stained and the quantitative shift of STAT3 unstimulated (basal) molecules towards pSTAT3 molecules was quantified via for flow cytometry as shown in **Figure 49**.

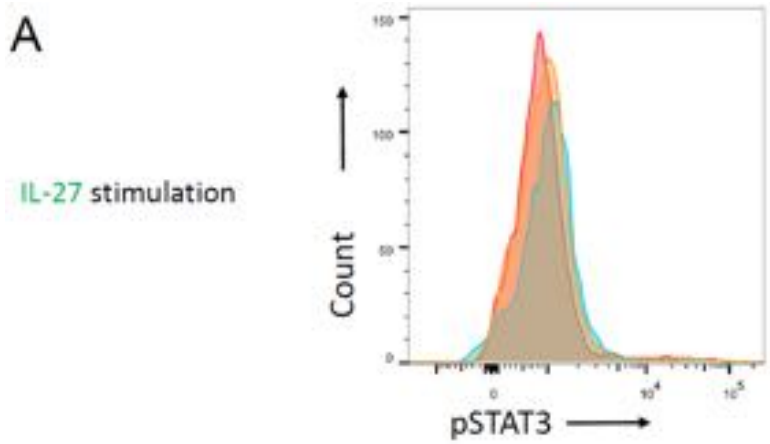

	Sample Name	Subset Name	Count
	_M2_Il-27_10 ng_ mL_10 min	pSTAT3, IL-17 rep subset-1	5614
	_M2_Il-27_10 ng_ mL_20 min_	pSTAT3, IL-17 rep subset-1	4668
	_M2_basal	pSTAT3, IL-17 rep subset-1	5231

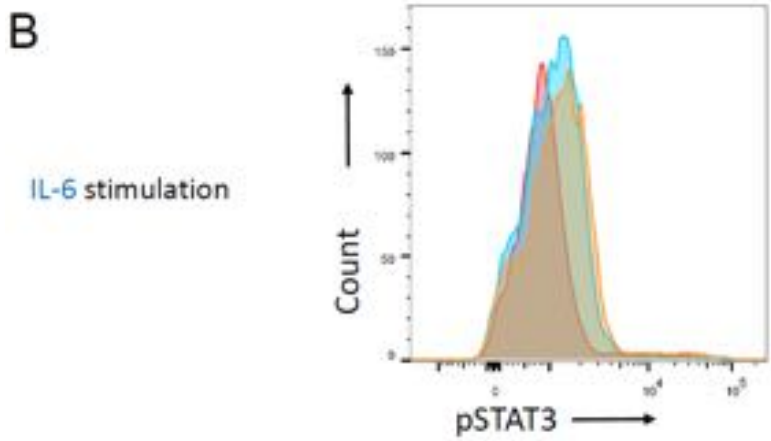

	Sample Name	Subset Name	Count
	_M2_Il-6_10 ng_ mL	pSTAT3, IL-17 rep subset-1	7286
	_M2_Il-6_20 ng_ mL	pSTAT3, IL-17 rep subset-1	7962
	_M2_basal	pSTAT3, IL-17 rep subset-1	5231

Figure 49: Analysis of STAT3 activation in IL-27 / IL-6-stimulated CD4$^+$ cells

After previous FACS gating, cell populations were analyzed for pSTAT3 formation, indicating STAT3 pathway activation. **A** shows an overlay of flow cytometric pSTAT3 results from CD4$^+$ enriched cells after in vitro IL-27 stimulation with: 10ng/ml for 10min (orange curve), 10ng/ml for 20min (blue curve) as well as non-stimulated (basal) cells (red curve). **B**: cells after IL-6 stimulation with: 10ng/ml for 15min (orange curve), 20ng/ml for 15min (blue curve) as well as non-stimulated (basal) cells (red curve). Data for long-term (overnight) stimulation are not shown.

Although, a moderate increase of pSTAT3 formation was found in IL-6 stimulating conditions (10ng/mL and 20ng/mL) compared to non-stimulated (basal) spleen

samples, flow cytometric quantitative and comparative analysis of pSTAT3 formation did not exhibit a significant shift of STAT3 molecules towards pSTAT3 in IL-27 stimulating conditions. This was also true for long-term (overnight) cytokine stimulation *in vitro* (data not shown).

In conclusion, it was experimentally not possible to clearly verify STAT3 activation by IL-27 *in vitro* in CD4+ enriched spleen cells.

3.6.6 IL-27 cytokine quantification in IL-27 treated kidneys (CBA)

Since, from the experimental analysis it was not possible to clearly verify the activation of the STAT3 pathway in a IL-27 ligand depended manner, it was also unclear, if IL-27 cytokine is responsible for its protective effect in NTN-mice by mediation of immune responses directly in the renal tissue.

For direct quantification of IL-27 cytokine in renal tissue, half of a kidney from IL-27-treated NTN-mice was homogenized and total protein was extracted and quantified as described in **2.2.29** and **2.2.30**. Then, cytometry bead array (CBA) was performed as described in **2.2.31**. Results are depicted in **Figure 50**.

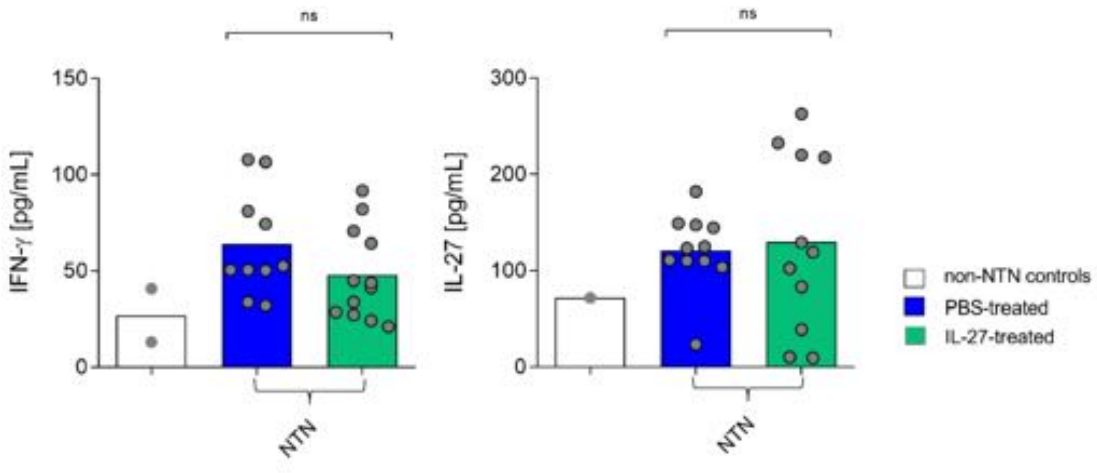

Figure 50: IL-27 cytokine quantification in IL-27-treated NTN-mice via CBA

After treatment with IL-27 and PBS, total protein form kidney supernatant was isolated from NTN-mice. Afterwards, IFN-γ (**left**) and IL-27 (**right**) were quantified via cytometric bead array (CBA). The latter were also analyzed in non-NTN control mice.

In conclusion, CBA results did not show increased IL-27 levels in NTN-mice after IL-27 injection in total renal protein samples.

3.7 Tbet and its role in NTN-pathogenesis and T_H17 cell stability

As explained before in **1.2.1** Tbet (encoded by the gene *Tbx21*) is the master transcription factor in T_H1 cells. Among other functions, it is crucial for the production of the pro-inflammatory cytokine IFN-γ (Djuretic et al., 2007).

To analyze the role of Tbet in NTN-induced mice with regard to T_H17 cell plasticity and NTN pathogenesis, transgenic mice from crossing of IL-17A Fate Reporter mice with *Tbx21* floxed mice were generated, as illustrated in **Figure 51**.

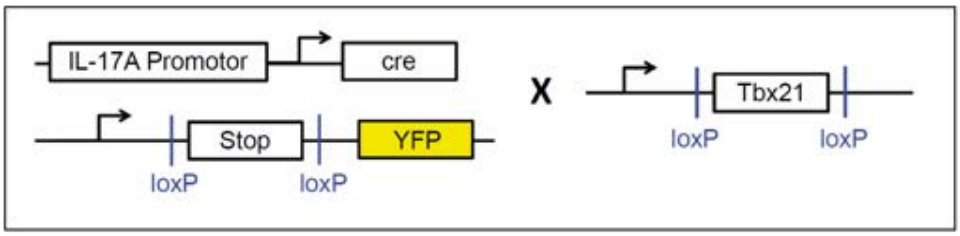

Figure 51: Generation of Tbx21-floxed IL-17A Fate Reporter mouse

To get *Tbx21*-floxed transgenic mice, IL-17A Fate Reporter were crossed with *Tbx21* floxed mice. The resulting trans genic mice were used for all Tbet knockout (*Tbx21*-floxed) experiments. If in a cell the IL-17A promotor is activated, a cre recombinase is expressed, leading to excision of the floxed Tbx21 gene and permanent mark of these cells with fluorescent YFP.

Therefore, NTN was induced in female *Tbx21*-floxed- and IL-17A Fate Reporter mice (**2.2.2**) and proteinuria (via BUN and ACR) was checked as well as glomerular damage (via histological, PAS-stained tissue section). Results are depicted in **Figure 52**.

To analyze the percentage of IL-17fm$^+$ cells (**Figure 54**), IFN-γ producing IL-17fm$^-$ (**Figure 55**) and IL-17fm$^+$ cells and T_H17 cell plasticity (**Figure 56**) in these mice, kidneys were extracted and stained for flow cytometry as depicted in **Figure 53**, **Figure 55** and **Figure 56**.

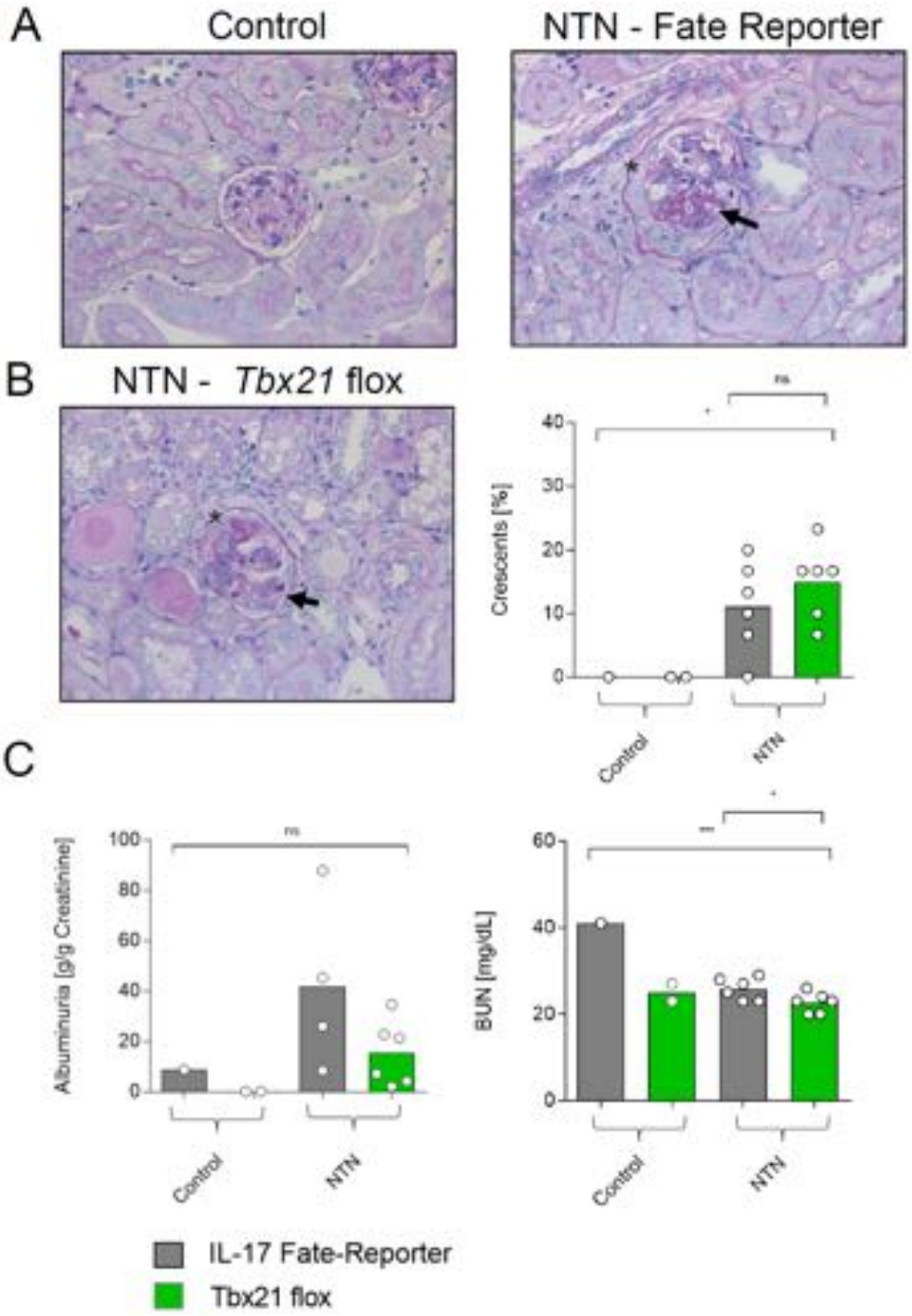

Figure 52: Renal damage in IL-17 Fate Reporter & Tbx21-floxed NTN-mice

After induction of NTN in female IL-17A Fate Reporter and *Tbx21*-floxed mice, kidney sections were PAS-stained (**A and B, left**) and glomerular damage was determined in terms of glomerular crescents: (**B, right**) and album-to-creatinine ratio (ACR) as well as blood urea nitrogen (BUN), as shown in **C**. All parameters were determined from NTN and non-NTN *Tbx21* floxed (green bars) and IL-17A Fate Reporter (grey bars) mice. In histological picture, glomerular damage in terms of hypercellularity and formation of necrotic glomerular tissue is shown by **arrows**. Formation of glomerular crescents is marked by **asterisks**. Albumin readings were obtained from 3 independent ELISA experiments. BUN was measured on day 9 post-NTN induction.

With regard to renal damage, non-NTN *Tbx21* floxed control mice showed no glomerular damage and no tubulointerstitial cell infiltration whatsoever. Same was true for IL-17 Fate Reporter (Histology not shown). In contrast, both, IL-17A Fate Reporter and *Tbx21* floxed NTN-mice showed glomerular damage in terms of hypercellularity and formation of necrotic glomerular tissue as well as formation of glomerular crescents. Mean number of crescents was slightly higher in *Tbx21*-floxed NTN-mice compared to IL-17 Fate Reporter mice with induced NTN. With regard to ACR, higher readings were found in IL-17 Fate Reporter NTN-mice compared to *Tbx21* floxed NTN-mice. In addition, BUN analysis exhibited slightly but insignificantly higher readings obtained from IL-17 Fate Reporter mice with induced NTN. Non-NTN control mice exhibited no significant ACR, as expected. Unexpectedly, high BUN readings were obtained from control mice.

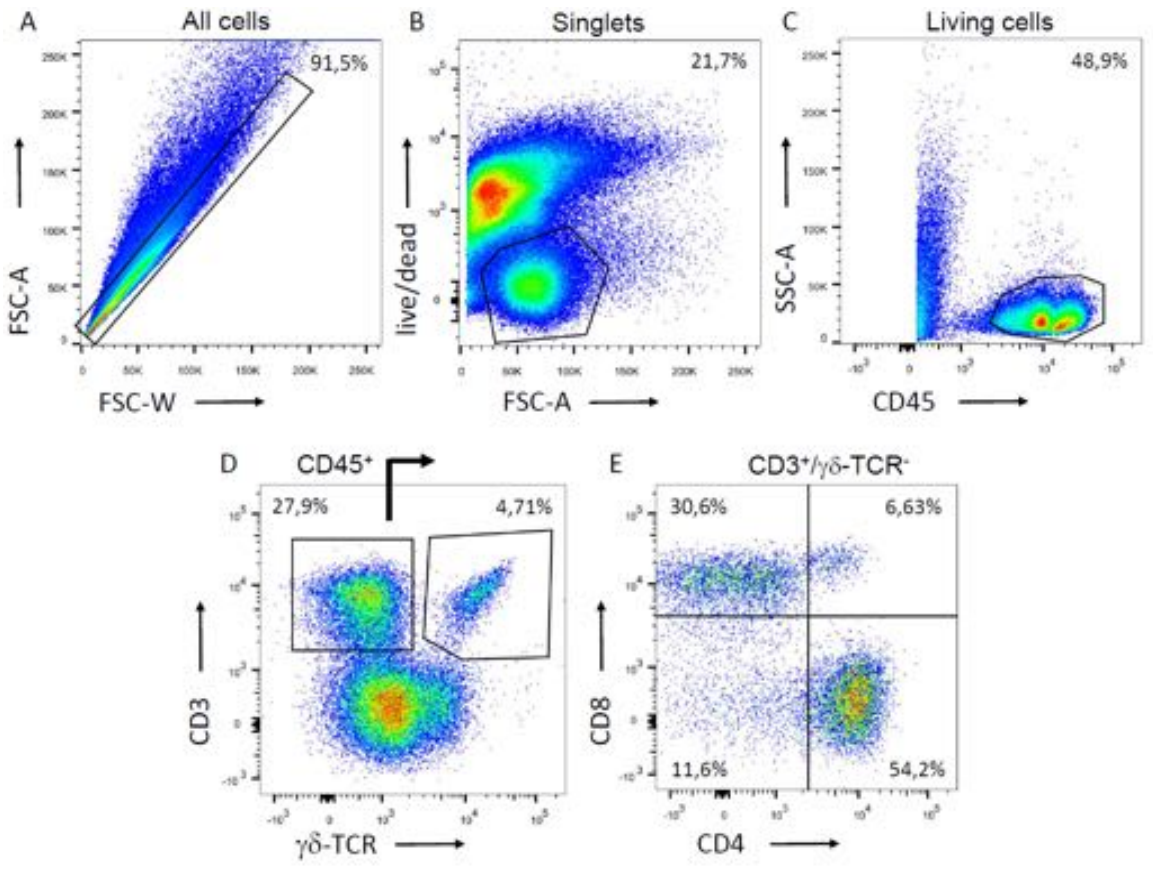

Figure 53: Analysis of Tbx21-floxed mice – FACS gating strategy

In order to analyze T_H17 cell plasticity, FACS-stained cells from kidney preparation of IL-17A Fate Reporter- and *Tbx21*-floxed NTN-mice kidneys were gated as follows. **A**: singlet, **B**: living, **C**: $CD45^+$, **D**: $CD3^+ \gamma\delta\text{-TCR}^-$, **E**: $CD8^- CD4^+$

Quantitative analysis of flow cytometric results from **Figure 53** are depicted in **Figure 54**.

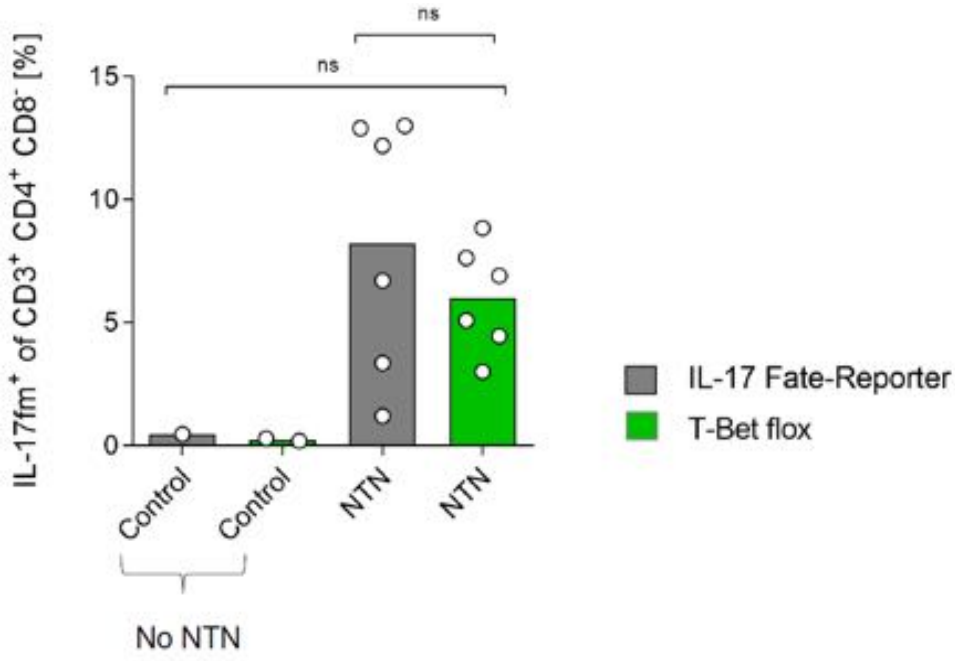

Figure 54: IL-17 fm$^+$ populations in IL-17 Fate Reporter and Tbx21-floxed NTN-mice

After FACS gating as shown before, *Tbx21(Tbet)*-floxed mice (green bars) and IL-17A Fate Reporter mice (grey bars) with induced NTN were compared with regard to their ability to activate the IL-17A promotor, leading to IL-17A production. Depicted are percentages of IL-17 fm$^+$ cells from IL-17A Fate Reporter an Tbx21-floxed mice. In addition, IL-17fm$^+$ cells were quantified in non-NTN induced control mice as well.

The comparison *Tbx21*-floxed and IL-17A Fate Reporter NTN-mice revealed no significant difference in the percentage of IL-17fm$^+$ (eYFP$^+$) cells in the CD3$^+$ CD8$^+$ CD4$^+$ T cell subpopulation as shown in **Figure 54**.

Next, IL-17fm$^-$, IFN-γ producing cell populations were compared in both transgenic mice in the NTN model.

As a result, the percentage of IFN-γ producing cells was reduced in cell populations from *Tbx21*-floxed NTN-mice compared to IL-17A Fate Reporter mice (**Figure 55**).

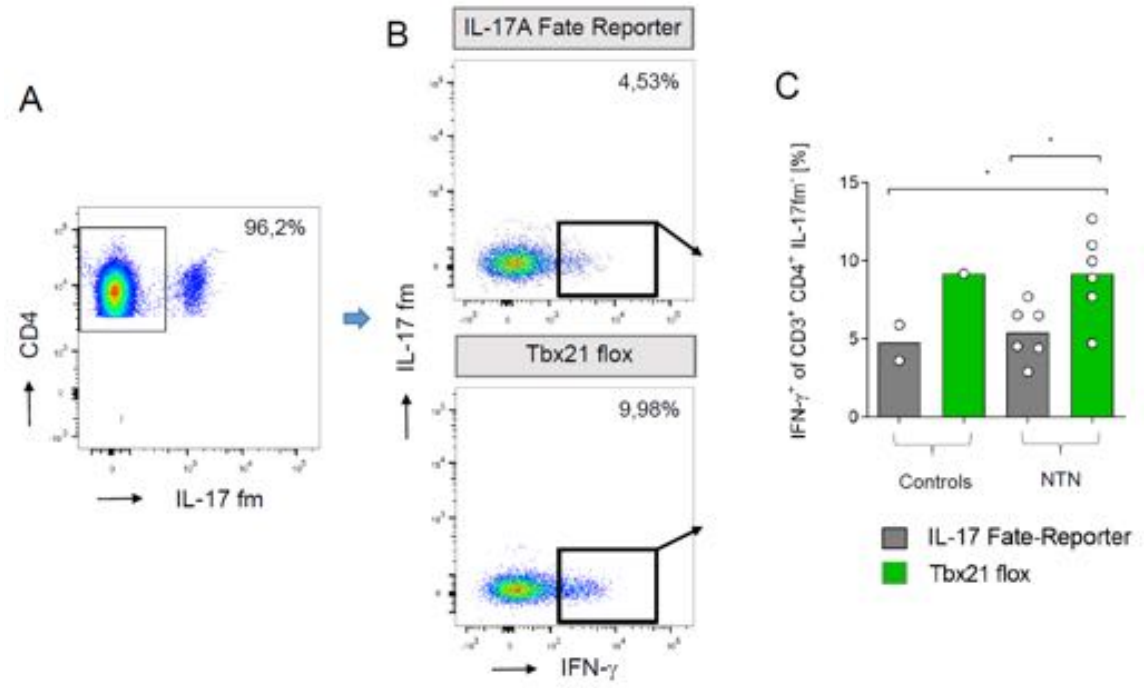

Figure 55: IFN-γ in IL-17A Fate Reporter and Tbx21-floxed mice

To determine percentage of IFN-γ producing cells in $CD4^+CD8^-CD3^+$ IL-$17fm^-$ cell populations, the previous FACS gating strategy was extended for $CD4^+$IL-$17fm^-$ cells as shown in **A**. Next, IFN-γ-producing cell populations from IL-17A Fate Reporter (**B, top**) and *Tbx21*-floxed mice (**B, bottom**) were selected. **C**: Results from *Tbx21*-floxed mice are shown in green, IL-17A Fate Reporter in grey. Control mice did not get NTN sheep serum.

Since cre recombinase was only expressed after activation of IL-17A promoter, *Tbx21* was only floxed in IL-17 fm^+, IL-17A-producing (T_H17) cells and subsequently did not lead to suppressed IFN-γ production in IL-17 fm^- cell populations.

Form literature it is know that Tbet (and *Runx3*) is essential for IFN-γ production in T_H1 cells (Djuretic et al., 2007).

In order to validate *Tbx21* conditional knockout and T_H17 cell plasticity in NTN-mice, IFNγ- and IL-17A production of $CD4^+$ IL-$17fm^+$ cell populations were analyzed in *Tbx21* floxed and IL-17A Fate Reporter mice, as shown in **Figure 56**.

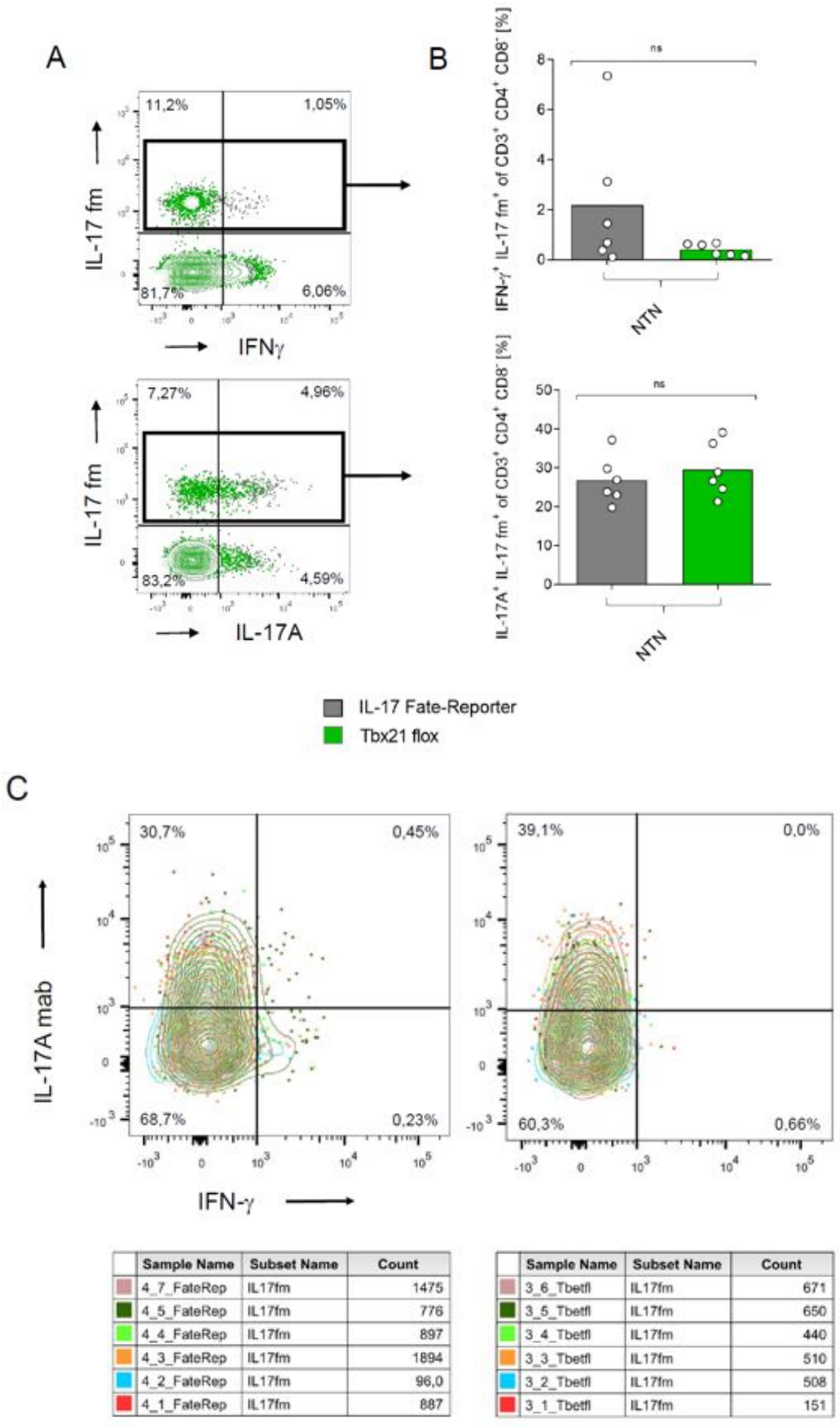

	Sample Name	Subset Name	Count
	4_7_FateRep	IL17fm	1475
	4_5_FateRep	IL17fm	776
	4_4_FateRep	IL17fm	897
	4_3_FateRep	IL17fm	1894
	4_2_FateRep	IL17fm	96,0
	4_1_FateRep	IL17fm	887

	Sample Name	Subset Name	Count
	3_6_Tbetfl	IL17fm	671
	3_5_Tbetfl	IL17fm	650
	3_4_Tbetfl	IL17fm	440
	3_3_Tbetfl	IL17fm	510
	3_2_Tbetfl	IL17fm	508
	3_1_Tbetfl	IL17fm	151

Figure 56: T_H17 cell plasticity in IL-17A Fate Reporter and Tbx21-floxed NTN-mice

Cells from NTN-induced IL-17A Fate Reporter (grey dots and bars) and *Tbx21*-floxed (green dots and bars) NTN-mice were gated as shown before for $CD4^+$ $CD8^-$ $\gamma\delta$-TCR^- $CD3^+$ cell populations. **A**: cells were further gated for IL-17 fm^+ ($eYFP^+$) cells and IFN-γ (**A, Top**) and IL-17A-producing (**A, bottom**) cells. Furthermore, **A** show an overlay of IFN-γ (**top**) and IL-17A-producing (**bottom**) *Tbx21*-floxed and IL-17A Fate Reporter NTN-mice. **B**: Quantifications of FACS results are shown from NTN-induced mice only. T_H17 cell plasticity in both transgenic NTN-mice is shown in **C** as an overlay of all analyzed samples from IL-17A Fate Reporter ("FateRep", left) and *Tbx21*-floxed ("Tbetfl") mice (right).

In summary, the comparison of IL-17A Fate Reporter and *Tbx21*-floxed NTN-mice revealed no significant difference with regard to NTN severity, nor to T_H17 cell plasticity in the nephrotoxic nephritis (NTN) model. Both transgenic mice in this model exhibited a high degree of T_H17 cell stability.

4 Discussion

Since Mosmann, Coffman and colleagues identified “two types of murine helper T cell clones” in 1986 and classified them according into T helper cells (T_H)1 and 2. This model helped to make new contributions into the field of immunology (Mosmann et al., 1986; Mosmann and Coffman, 1989).

However, provided with explanations for previously unknown immunological mechanisms, over time this applied model has been offended since not all immunological responses fit the T_H1/T_H2 paradigm. In fact, Mosmann and Sad stated in the 1990s, some time before the discovery of the now known T_H17 and T follicular helper (Tfh) cells or ILC`s that the classification into T_H1 and T_H2 cells “[…]may underestimate the full complexity of some responses.” (Mosmann and Sad, 1996).

Paradoxically, cytokine research was one of the key elements, not only as the basis for the existence of this paradigm but also one of the key aspects for overwhelming immune responses and termination of inflammatory reactions. T_H1/T_H2 classification was scientifically introduced based on the observation that these cells expressed different cytokines leading to different effector functions. For example, among others T_H1 cells produce IFN-γ, IL-2 while T_H2 cells produce IL-4, IL-5, IL-6 and others. On the other hand, cytokines were found which could not be explained neither by T_H1 nor by T_H2 cells.

In addition, it was found that late T helper cell fate decisions were also not as strict as assumed. In fact, studies have shown that T cells are not static but that they can provide the ability to adapt to immunological conditions and requirements. In general, the ability to adapt to a changing micro-environment is of fundamental importance on a small scale (cells plasticity) as well on large scales (human evolution).

In contrast, the lost ability to adapt to changing circumstances often results in dysfunctional biological systems.

Accordingly, T_H17 cell plasticity is one possibility to adapt to immunological conditions since T_H17 cells can produce pro-inflammatory cytokines like IL-17.

However, they are also capable to transdifferentiate into other cell types like T_H1 or more protective Tr1 cells which express immune-suppressive IL-10 (Gagliani et al., 2015; Huber et al., 2011).
Nowadays, many studies provided evidence that T_H17 cells act as main driver of many autoimmune-mediated diseases like rheumatoid arthritis, psoriasis, multiple sclerosis or chronic kidney diseases (Gaffen et al., 2014). Although, many animal studies were conducted key molecular mechanisms are still elusive, for example regarding T_H17 cell plasticity. If it was possible, to develop drug-mediated intervention toward regulatory, immuno-protective phenotypes could potentially be prevented.
Therefore, this thesis aimed to better understand molecular mechanisms of T_H17 cell plasticity/stability in organ-specific autoimmunity.

In the early phase of chronic autoimmune kidney disease, the therapeutical approach is based on administration of immune-suppressive drugs, as described in **1.3.3**. Since glomerular injury caused by inflammatory reactions are partly inhibited or attenuated by this therapy, patients who undergo the medical drug treatment often show reduced renal symptoms and therefore provide an overall beneficial clinical outcome in an early phase. However, therapies are unspecific and can have severe side effects.
In many patients, disease progression continues despite treatment, often leading to end-stage renal disease (ESRD) and requirement of renal replacement / dialysis (Kurts et al., 2013). Furthermore, due to unspecific immunosuppression, patients get more susceptible for infections and secondary diseases like cardio vascular defects (McIntyre et al., 2011; Wouters et al., 2015).
In summary, the current CKD treatments are rather unspecific and partly ineffective. Individual and more specific therapies are needed which also consider individual immunological conditions.
Here, one conceivable clinical approach not only for autoimmune kidney disease but also for other T_H17-mediated autoimmune disorders could be provided by the modulation of pro-inflammatory T_H17 cells towards a more regulatory and protective T cell phenotype.

Therefore, in this thesis mechanisms of T_H17 cell stability in the kidney were investigated by generation and comparative analysis of gene expression profiles in murine autoimmune-mediated disease models with high (EAE, anti-CD3 duodenitis) and low (NTN) T_H17 cell plasticity.

To compare gene expression profiles, these models were chosen since they are well established disease models with relatively high T_H17 cell plasticity. For comparative analysis, it is very important to validate successful disease onset in all models.
The results for clinical disease-related outcomes provided evidence for successful disease onset in all models, except in the pristane-induced lupus nephritis model which was chosen as an alternative renal disease model for stable T_H17 cells (Krebs and Panzer, 2018).
With regard to proteinuria and glomerular damage, the latter showed no evidence of renal or other organ-specific pathogenicity. However, abnormal formation of white granules was observed in the abdomen of pristane-treated mice 52 weeks after administration (**Figure 21**) which were not further analyzed. But since these encapsulations were not observed in non-pristane treated animals, these findings imply a (immunological) protective reaction against the injected oil.
This hypothesis is supported by Chowdhary et al. which described “lipid granules in macrophages” in pristane-induced lupus nephritis *in vivo* (Chowdhary et al., 2007). In fact, T_H17 cells did show a high degree of stability similar to renal T_H17 cells in experimental nephrotoxic nephritis as shown earlier (**Figure 20**). Previously, this was already shown by Krebs et al. 2016. But since no clear disease onset was found, this experimental mouse model for systemic lupus erythematosus was not implemented for further comparative gene expression analysis.

By usage of RNA bulk sequencing, our unbiased approach delivered a cross section of differential gene expressions of T_H17 cells in the inflamed tissue in models of autoimmune disease. This provided the basis for comparative gene expression analysis.

It was decided to do RNA sequencing of IL-17 Fate Reporter and Fate$^+$ reporter which was performed for two main reasons. IL-17 Fate Reporter mice are a good tool for analysis of T_H17 cell fate status. Via their YFP status cells can be separated into populations which activated IL-17A promotor and became what is known as T_H17 *cells* and populations who didn`t activated this promotor at the time of analysis. So, the analysis is independent of the current IL-17 status. On the other hand, Fate$^+$ reporter mice provide insights into the current status of cell populations with regard to IL-17A, FoxP3 and IFN-γ production (**Figure 24**) which allows T cell classification. Furthermore, by using Fate$^+$ for RNA sequencing, biases caused by individual and organ-related gene expression patterns in the NTN model are excluded.

Based on sequencing results and data quality checks from IL-17 Fate Reporter as well as from Fate$^+$ reporter (data not shown), *IL17A* and *cre* gene expression analysis implied successful and efficient flow cytometric sorting of cells with activated IL-17A promotor (YFP$^+$) and never activated IL-17A promotor (YFP$^-$).

In addition, principal component analysis (PCA) indicated a rather high group cohesiveness among different samples with regard to gene expression profiles in YFP$^+$ vs. YFP$^-$ cells (IL-17A Fate Reporter, see **Figure 27**) as well as YFP$^+$ IL-17$^+$ vs. YFP$^+$ IL-17$^-$ cells (Fate$^+$ Reporter, see **Figure 28**). The group cohesiveness in Fate$^+$ samples however was higher in kidney samples compared to YFP$^+$ renal samples from NTN-induced IL-17 Fate Reporter mice. Since the latter does not give information about the current status of IL-17A reporter, as it is the case in acute and Fate$^+$ reporter mice, it is feasible to assume that these cells did not necessarily evolved in a common manner, subsequently leading to activation of different genes which would explain different gene expression pattern and reduced PCA group cohesiveness.
In summary, these results supported evidence for successful flow cytometric cell sort of these cell populations as a basis for comparative gene expression analysis.

Target gene selection

After application of selection criteria as described in **3.5**, a list of potential target genes were selected from the comparative analysis of IL-17 Fate Reporter (**Figure** 36) and Fate$^+$ Reporter mice (**Figure 37**). These genes were significantly up- or down regulated in models for higher T_H17 cell plasticity vs. NTN as a model for rather stable T_H17 cells. Also see vulcano plots (**Figure 34** and **Figure 35**).

Based on gene ontology (GO) classifications (**3.5**), the selected target genes can be sorted in the following main subclasses according to their known effector functions or to the known effector functions of the proteins they encode respectively.

- Cytokine receptors (Il27ra, Il1r2, Il20ra)
- Transcription factors (Zeb2, TOX2, Klf2 etc.)
- Chromatin remodeling factors (Tcf7, TOX, TOX2, Satb1 etc.)
- Other intracellular signaling (Aebp1, Vdr, Ahr, Fasl etc.)

IL-27/IL-27ra axis as target selected

As a first target gene from comparative gene expression analysis from anti-CD3 duodenitis vs. NTN the IL-27 receptor α (encoded by *Il27RA*) was chosen.

The sequencing data revealed a significant overexpression of *Il27ra* in NTN-treated IL-17 Fate Reporter mice compared to anti-CD3ε-treated IL-17 Fate Reporter mice which led to T cell stimulation. Subsequently the small intestinal inflammation caused sepsis.

IL-27ra sequencing data validation & IL-27 time-kinetic analysis in NTN

Since the IL-27/IL-27ra axis is known for its bifunctional roles as a pro- and anti-inflammatory effector pathway (Owaki et al., 2006; Stumhofer et al., 2006; Yoshida and Hunter, 2015), it was decided to validate the *IL27RA* sequencing data and to functionally analyze the role of this pathway in the experimental nephrotoxic nephritis mouse model.

In order to validate the RNA sequencing data, protein expression of IL-27ra analyzed via flow cytometry (**3.6.1**).

These data validated the sequencing data on protein level since they showed significantly higher IL-27ra expression in renal samples from NTN-mice compared to samples from α-CD3-treated mice in small intestine (**Figure 40**). Overall, significantly more renal cells expressed the IL-27 receptor α in IL-17 fm^+ (YFP^+) compared to IL-17 fm^- (YFP^-) cells in the NTN model. We therefore hypnotize that IL-17 fm^+ cells with higher IL-27 receptor expression would also perform more IL-27-related signaling.

To test this, the relative IL-27 gene expression was analyzed via qPCR in the course of the disease from day 0 to day 20 (**3.6.2**).

The results from these analyses revealed an increase in *Il27* RNA-transcripts over time with a first peak on day 7 which coincide with the appearance of first kidney-infiltrating T_H17 cells. However, 14 days after NTN induction, the amount of *IL27* appears to decrease as shown in **Figure 41**. This raises the question for the cellular source of IL-27 during NTN.

IL-27 is not known to be produced by T_H17 cells but rather by antigen presenting cells (APCs) like dendritic cells, epithelial cell and macrophages as well (Villarino et al., 2005; Yoshida and Miyazaki, 2008). Since the latter migrate into the kidney during NTN (Kurts et al., 2013), it is likely that these cells are one of the main source of IL-27 here.

IL-27 intervention in NTN

In summary, the results showed the existence of IL-27ra-expressing T_H17 cells in the NTN-kidney. Furthermore, the results implied increase of IL-27 in the course of the NTN. Therefore, it was suggested that these T_H17 cells would be able to signal upon IL-27 secretion.

Since the population of T_H17 increases in the course of the NTN model (**Figure** 14), the results suggested that IL-27-depenend T_H17 signaling would be effective within 10 days after NTN induction. Hence, at this time point there were many IL-27ra-expressing T_H17 cells as well as (potentially) IL-27 secreting macrophages present in the kidney.

Based on published data, it is known that IL-27 mediates pro-inflammatory immune responses like Tbet-induced T_H1 differentiation (Owaki et al., 2006) via STAT1 (Takeda et al., 2003) as well as inhibition of Treg differentiation via STAT3 (Huber et al., 2008) and others as well as anti-inflammatory immune responses like suppression of IL-17 production (Batten et al., 2006), promotion of IL-10 production (Fitzgerald et al., 2007; Freitas do Rosario et al., 2012; Stumhofer et al., 2007) or promotion of “distinct Treg populations” (Hall et al., 2012a).

In order to assess the role of IL-27-intervention during NTN and its consequences for renal pathogenesis, an experiment was conducted in which NTN-mice were treated with recombinant mouse IL-27 cytokine 5 days after disease induction. Further treatment by i.p. injection was performed by daily application for 5 days. Subsequently, kidney injury was analyzed at day 10 after NTN-induction as described in **3.6.3**. Interestingly, it was found that on day 10 after NTN-induction all clinical markers for kidney damage were significantly reduced. This included the degree of proteinuria (BUN, ACR) as well crescent formation (**Figure 43** and **Figure 44**). Importantly, on day 3 prior to PBS- and IL-27-treament all NTN-induced animals showed high proteinuria (measured via urine sticks) indicating successful disease induction.

This protective effect of IL-27-intervention in NTN supports the idea that the renal IL-27, suppresses overwhelming inflammatory reactions in order to prevent further tissue damage in the kidney, caused by T_H17 cells.

Analysis of underlying mechanism for protective IL-27 effect during NTN

The significantly protective effect caused my IL-27 administration in NTN raised the question for the underlying molecular mechanisms.

Since kidney damage is mediated by renal inflammation, an anti-inflammatory IL-27 mechanism was suggested. Furthermore, one of the anti-inflammatory effector functions of IL-27 is based on the suppression of IL-17 production (Batten et al., 2006) and promotion of IL-10 production, as mentioned before (Fitzgerald et al., 2007; Freitas do Rosario et al., 2012; Stumhofer et al., 2007).

Hence, renal samples from NTN-mice were flow cytometrically checked for IL-17 and IL-10.
Interestingly, neither a decrease in IL-17 nor an increase in the immune-regulatory cytokine IL-10 was observed (see **Figure 45** and **Figure 47**). As expected, only a small fraction of IL-17 fm^+ cells was observed in non-NTN mice. But surprisingly the percentage of actually IL-17-producing IL-17 fm^+ cells was slightly higher in the IL-17 fm^+ fraction in IL-27-treated animals than in the PBS group as depicted in **Figure 46**.

In addition, it was found that the percentage of IL-17 fm^+ cell populations which actually produced IL-17A was overall very low at approximately 2,5% of IL-17fm^+ cells (**Figure 47**, **A**) compared to previous NTN-experiments conducted in our group (data not shown). This could potentially be explained either by methodical/ experimental insufficiencies or by insufficient initial immune response caused by this distinct anti-GBM sheep serum which was used for NTN-induction. Furthermore, the fact that both groups, PBS- and IL-27-treated NTN-mice showed almost similar and rather high IL-10 expression among IL-17 fm^+ cell populations (approximately 4-5% of these cells, see **Figure 47**, **B**), questions these results. Therefore, these experiments need to be repeated to better understand the role of IL-27 in T_H17 cell plasticity and IL-10 induction. Moreover, to check the IL-27-related expression of IL-10 and IL-17 it would be possible to do initial *in vitro* experiments of renal samples from NTN-mice and to perform IL-27 stimulation and FACS analysis.

Although, no evidence could be provided that this protective IL-27-effect is mediated by increased secretion of IL-10 and/or attenuated secretion of IL-17, it is feasible to assume that T_H17 cells are involved in the mechanism which protects glomeruli from glomerular damage in the NTN model. This assumption is reasonable since T_H17 cells are the main population of kidney infiltrating cells at this time point, illustrated in **Figure 14** (Kurts et al., 2013).
The fact that these T_H17 cells in the NTN are able to express the IL-27 receptor α (as shown in the bulk sequencing data and flow cytometry), an intervention was performed by administration of its ligand (IL-27) which leads to the assumption that

the cells will perform IL-27 signaling. In addition, it was found that also kidney infiltrating mast cells can express IL-27ra also known as WSX-1 (Pflanz et al., 2004). However, using WSX-1$^{-/-}$ mice it was found *in vivo* that this receptor showed no effect on mast cell activity, since the mean number of mast cells didn`t change in these mice (Artis et al., 2004).

Since it is known that IL-27 mediates its immunological functions via STAT1 and STAT3 (Yoshida and Hunter, 2015), also see **chapter 1.4**, **Figure 7**, it was feasible to check for upstream IL-27 pathway activation via STAT3 by flow cytometry (see **chapter 3.6.5** ,**Figure 49**). In addition, recent studies showed that STAT3 is able to control glomerulonephritis by regulatory T cells in a T_H17-specific manner (Kluger et al., 2014).

As a positive control for *in vitro* the STAT3 activation which finally leads to formation of phospho (p)STAT3 (described in **chapter 1.4**, see **Figure** 7), the cytokine IL-6 was used (Stumhofer et al., 2006; Stumhofer et al., 2007).

Although, a moderate increase towards pSTAT3 formation was observed during IL-6 stimulation, no clear and significant evidence was found for STAT3 activation by IL-27 (**Figure 50**). Most probably these results are inapplicable since many studies could clearly show an activation of the STAT3 pathway by IL-27 as well as IL-6 (Hall et al., 2012b; Horlad et al., 2016; Huber et al., 2008; Owaki et al., 2008). Since STAT3 pathways are involved in many pathways as explained earlier (**1.4**), there is a rather high basal level of both STAT3 and pSTAT3. For example, STAT3 activation is also essential for differentiation of T_H17 cells as mentioned in **chapter 1.2.4.1**.

In addition, unless $CD4^+$ cells were enriched, it is reasonable to assume that in the process of cell preparation from kidney samples not only T cells were isolated but also other renal cells. As explained in **chapter 1.3**, the kidney is also important for EPO-mediated blood formation. EPO also mediates receptor signaling via STAT3 (Cao et al., 2010).

As a result, it is challenging to perform experiments to analyze differences in STAT3 activation of stimulated and unstimulated cell populations. However, this does not explain why even with IL-6 which is a strong STAT3 activator, there is only a moderate shift toward pSTAT3 formation.

From other studies it is known that the differentiation of T_H17 is suppressed by activation of STAT1 (Peters et al., 2015). Thus, as an alternative experiment, it would be reasonable to check for IL-27-mediated STAT1 activation instead of STAT3.
In addition, it would be interesting to analyze the expression of the T_H17-essential transcription factor RORγt via flow cytometry. The latter is known to suppress IL-10 production in T_H17 cells in intestinal inflammation (Sun et al., 2019). Assuming a IL-10-dependend regulatory function, one reason for the protective effect of IL-27 in NTN-mice could be explained by potential decrease of RORγt expression by IL-27 which can also be determined by flow cytometry.
Another experimental approach to assess the function of IL-27 in NTN would be the blocking of IL-27 via antibody binding in $Fate^+$ mice which would hypothetically deteriorate the clinical outcome caused by non-suppressive IL-27 effector function. Furthermore, it would be possible to analyze the current expression of IFN-γ, FoxP3 and IL-17A.

To check whether the injected recombinant IL-27 cytokine can be detected in renal sample, total protein from renal samples of NTN- and IL-27-treated mice were isolated. Afterwards, a cytometric bead array (CBA), a rather sensitive ELISA-based FACS method to quantify cytokine, hormones and others was performed. However, no differences in IL-27 or IFN-γ could be detected in IL-27- vs. PBS-treated NTN mice, as depicted in **Figure 50** in **chapter 3.6.6**. which is most probably caused by experimental limitations, since all measured cytokine amounts were within the lower limit of the standard curve. Results obtained from this region of the standard curve does not allow sufficient and accurate cytokine analysis.

Other possibilities for the overall low cytokine amount could be caused by a potentially (1) rapid decomposition of the cytokines in the protein supernatant or by (2) lack of CBA IL-27-antigen/epitope detection caused by usage of recombinant mouse IL-27 cytokine compared to non-recombinant protein. Furthermore, higher protein input and/or higher protein sample concentration would may cause more accurate cytokine quantification.

Moreover, it is also reasonable that the kidney-protective effect of IL-27 in NTN-mice is not caused or mediated by T_H17 cells and related T_H17-effector functions but by other (immune) cells.
As mentioned, it was found that T_H17 cells are partly controlled in the small intestine (Esplugues et al., 2011). Furthermore, it was found that T_H17 cells from the small intestine can migrate to the kidney causing renal damage during experimental crescentic glomerulonephritis (Krebs et al., 2016a). Hence, IL-27 could potentially effect T_H17 cells in the small intestine leading to higher IL-27 cytokine levels in the small intestine which could be analyzed by CBA as well or by *Meso Scale* analysis which is another immunoassay.

Quality assessment of identified candidate genes and further remarks
In summary, experiments conducted during my thesis provided a number of potential interesting target genes with regard to T_H17 cell stability/plasticity in autoimmune-mediated renal disease.

Recent studies found evidence for pivotal T_H17 cell plasticity-related roles of some of our selected target genes which were published after we obtained RNA bulk sequencing data. These include for example *transcription factor 1* (TCF-1) encoded by *Tcf7* (Johnson et al., 2018) and *fas ligand* (Fasl) encoded by *Fasl (Meyer Zu Horste et al., 2018)*. This supports the notion that the genes identified in this thesis are of high relevance in T_H17 cell biology.

TCF-1 has long been known for its essential role in early T_H17 cell differentiation (Danilo et al., 2018; Yang et al., 2019). However, underlying mechanisms were elusive. In 2018, Johnson et al. found that T cell fate commitment is depended on chromatin accessibility. If chromatin is in closed conformation, several essential differential genes are inaccessible leading to suppressed cell differentiation. As the authors claim, this could potentially be also interesting in later T cell linage commitment.
Therefore, also genes with chromatin remodeling functionalities were selected (see above, **chapter 4** "**Target gene selection"**, **Figure 36** and **Figure 37**.). Some of them like *Satb1*, *Tcf7*, *Tox* and *Fasl* were also validated by qPCR (data not shown.)

Fasl was previously mainly known for its apoptotic effector functions by interaction with the “death receptor” Fas (Waring and Mullbacher, 1999). However, in 2018 zu Horste et al. published a paper in which they show that Fasl not only promotes T_H17 cell differentiation but also that this ligand has the ability to prevent T_H17 cell transdifferentiation into T_H1 cells (Meyer Zu Horste et al., 2018).

Since we also found these genes before the T_H17 cell plasticity-related function was published, it is reasonable to assume the selected gene targets are of high relevance with regard to functionality in T_H17 cell stability.
Additionally, although IL-27 experiments could not clearly find evidence for shifted T_H17 cell stability in NTN, results indicated a significantly protective effect of IL-27 during intervention in NTN-mice, potentially mediated by modified T_H17 cell plasticity.

Although, most of the experiments were conducted *in vivo*, the obtained results might not directly translate into the human situation in renal autoimmune disease. However, they are essential for research and potentially for clinical applications. Thus, also data from human renal biopsies were acquired and single cell sequencing was performed in our lab to additionally map (1) differential gene expression profiles in small cell populations and (2) to take cell heterogeneity into account. However, data from renal biopsies are biased, since patients diagnosed with CKD are immediately treaded, mostly with steroids which is feasible for ethical reasons.
These drugs have been shown to have some beneficial clinical effects, but the underlying reasons are still elusive. As a result, statements and implications gathered from human biopsies should be treated with care.

Conditional *Tbx21*(*Tbet*-) flox experiments

As mentioned earlier in **chapter 1.2.1** Tbet is an essential transcription factor for IFN-γ production in T cells and in T_H1 cells Tbet (encoded by the *Tbx21* gene) is the main transcription factor (Singh et al., 2017).
During T helper cell differentiation, the function of Tbet is suppressed in T_H2, T follicular helper (Tfh) and T_H17 cells (Zhu and Paul, 2010). In contrast,

RUNX1 and RUNX3 function as co-factors which promote the production of IFN-γ by Tbet in $CD4^+$ T cells. Hence, *Tbx21* is one of the factors which are controlled by T_H17 cells and are involved in T cell fate commitments. Interestingly, IL-$17A^+$/IFN-γ^+-producing (T_H17/T_H1) cells, so called *double producers,* express both, RORγt as well as *Tbx21* which derived from T_H17 cell precursors (Chen et al., 2017). In this case, however RORγt seems not to suppress *Tbx21* expression.

Therefore, and independently from the list of potential target genes, which was obtained from RNA bulk sequencing (**Figure 36** and **Figure 37**), it was the aim of further experiments to investigate the effect of *Tbx21* in conditional knockout NTN-mice.
In order to generated conditional *Tbx21*-knockout mice, IL-17A Fate Reporter were crossed with *Tbx21* floxed mice as illustrated in **Figure 51**. As a result, IL-17A-activated promotor leads to expression of cre recombinase which leads to excision of the floxed *Tbx21* gene and permanent eYFP-mark of these cells.

As a result of these experiments, no evidence was shown for changed glomerular damage in terms of proteinuria or number of formed crescents (**Figure 52**) in *Tbx21*-floxed vs. IL-27A Fate Reporter NTN-mice.

Since $CD4^+$ IL-17 fm^- ($eYFP^-$) cells do not activate IL-17A promotor and subsequent cre expression in *Tbx21*-floxed NTN-mice, IFN-γ was not suppressed in this cell population (**Figure 55**).
In contrast, $CD4^+$ IL-17 fm^+ ($eYFP^+$) cell populations showed significantly reduced IFN-γ production in flow cytometry as expected (**Figure 56** ,**B**, **top**). Beside *Tbx21*-genotyping, this was an additional proof of functional *Tbx21*-conditional knockout.

With respect to T_H17 cell plasticity in these NTN mice, no differences were observed IL-17A Fate Reporter compared to *Tbx21*-floxed animals in flow cytometry, as depicted in **Figure 56** ,**C**.
These results are consistent with previous studies which found that Tbet-expressing T_H1 cells seem not play a significant role in the pathogenesis of NTN within 10 days after disease induction as illustrated in **Figure 14**

(Krebs and Panzer, 2018; Riedel et al., 2016; Turner et al., 2012). This early time point in the pathogenesis is rather dominated by glomeruli-infiltrating IL-17A and IL-17F-producing T cells like T_H17- and γδ-T cells (Krebs and Panzer, 2018; Riedel et al., 2016). Therefore, it was not expected to find significant differences in T_H17 cell plasticity by conditional *Tbx21*-knockout mice 10 days after NTN induction. At a later time point however, the effector functions mediated by Tbet-expressing cells increases. Thus, it would be interesting to repeat these experiments and investigate disease outcome at later time points to assess the role of Tbet in TH17 cells at later stages of the disease. However, beside T_H1 cells, Tbet is also important in a T regulatory population called *Treg1* cells. Nosko et al. found in their studies, in which they used FoxP3^{cre}xTbet$^{fl/fl}$ mice, that Tbet is essential for this Treg subtype. Furthermore, they found that Tbet enhances the ability of these cells to suppress inflammatory T_H1 cells in NTN (Nosko et al., 2017).

In summary, a number of potential candidate genes were identified which might play important functional roles in the stability of T_H17 cells in organ-specific autoimmune diseases.
Experiments investigated the IL-27/IL-27ra axis to target T cell plasticity in a therapeutic approach show a protective effect mediated by IL-27 in a model of renal autoimmunity. Importantly, IL-27 administration led to significantly reduced kidney injury after induction of NTN which is important for potential clinical applications.

Since some of the genes selected based on the analysis of expression profiles of T_H17 cells in different models of autoimmune diseases in this thesis were also identified by other labs to contribute to T_H17 cell stability and plasticity, we think that our experimental approach will indeed result in a better understanding of the molecular mechanisms that drive T_H17 cell immune response specifically in the kidney. Therefore, the results of this thesis might build the basis for the identification of novel therapeutic targets. This ultimately result in new targeted therapies that push pathogenic T_H17 cells into immuneregulatory T cell phenotypes in the kidney in renal autoimmunity. Potentially, these results could also be translated into the treatment of autoimmune diseases in other organs.

References

1. Abremski, K., Wierzbicki, A., Frommer, B., and Hoess, R.H. (1986). Bacteriophage P1 Cre-loxP site-specific recombination. Site-specific DNA topoisomerase activity of the Cre recombination protein. J Biol Chem *261*, 391-396.

2. Acosta-Rodriguez, E.V., Rivino, L., Geginat, J., Jarrossay, D., Gattorno, M., Lanzavecchia, A., Sallusto, F., and Napolitani, G. (2007). Surface phenotype and antigenic specificity of human interleukin 17-producing T helper memory cells. Nat Immunol *8*, 639-646.

3. Ada, G. (2008). The enunciation and impact of Macfarlane Burnet's clonal selection theory of acquired immunity. Immunol Cell Biol *86*, 116-118.

4. Aggarwal, S., Ghilardi, N., Xie, M.H., de Sauvage, F.J., and Gurney, A.L. (2003). Interleukin-23 promotes a distinct CD4 T cell activation state characterized by the production of interleukin-17. J Biol Chem *278*, 1910-1914.

5. Aharoni, R., Teitelbaum, D., Sela, M., and Arnon, R. (1997). Copolymer 1 induces T cells of the T helper type 2 that crossreact with myelin basic protein and suppress experimental autoimmune encephalomyelitis. Proc Natl Acad Sci U S A *94*, 10821-10826.

6. Ai, W., Li, H., Song, N., Li, L., and Chen, H. (2013). Optimal method to stimulate cytokine production and its use in immunotoxicity assessment. Int J Environ Res Public Health *10*, 3834-3842.

7. Althaus, H.H. (2004). Remyelination in multiple sclerosis: a new role for neurotrophins? Prog Brain Res *146*, 415-432.

8. Amatya, N., Garg, A.V., and Gaffen, S.L. (2017). IL-17 Signaling: The Yin and the Yang. Trends Immunol *38*, 310-322.

9. Arnon, R., and Aharoni, R. (2009). Neuroprotection and neurogeneration in MS and its animal model EAE effected by glatiramer acetate. J Neural Transm (Vienna) *116*, 1443-1449.

10. Artis, D., Villarino, A., Silverman, M., He, W., Thornton, E.M., Mu, S., Summer, S., Covey, T.M., Huang, E., Yoshida, H.*, et al.* (2004). The IL-27

receptor (WSX-1) is an inhibitor of innate and adaptive elements of type 2 immunity. J Immunol *173*, 5626-5634.

11. Awasthi, A., Carrier, Y., Peron, J.P., Bettelli, E., Kamanaka, M., Flavell, R.A., Kuchroo, V.K., Oukka, M., and Weiner, H.L. (2007). A dominant function for interleukin 27 in generating interleukin 10-producing anti-inflammatory T cells. Nat Immunol *8*, 1380-1389.

12. Baddela, V.S., Baufeld, A., Yenuganti, V.R., Vanselow, J., and Singh, D. (2014). Suitable housekeeping genes for normalization of transcript abundance analysis by real-time RT-PCR in cultured bovine granulosa cells during hypoxia and differential cell plating density. Reprod Biol Endocrinol *12*, 118.

13. Batten, M., Li, J., Yi, S., Kljavin, N.M., Danilenko, D.M., Lucas, S., Lee, J., de Sauvage, F.J., and Ghilardi, N. (2006). Interleukin 27 limits autoimmune encephalomyelitis by suppressing the development of interleukin 17-producing T cells. Nat Immunol *7*, 929-936.

14. Bending, D., De la Pena, H., Veldhoen, M., Phillips, J.M., Uyttenhove, C., Stockinger, B., and Cooke, A. (2009). Highly purified Th17 cells from BDC2.5NOD mice convert into Th1-like cells in NOD/SCID recipient mice. J Clin Invest *119*, 565-572.

15. Berg, D.J., Davidson, N., Kuhn, R., Muller, W., Menon, S., Holland, G., Thompson-Snipes, L., Leach, M.W., and Rennick, D. (1996). Enterocolitis and colon cancer in interleukin-10-deficient mice are associated with aberrant cytokine production and CD4(+) TH1-like responses. J Clin Invest *98*, 1010-1020.

16. Bettelli, E., Carrier, Y., Gao, W., Korn, T., Strom, T.B., Oukka, M., Weiner, H.L., and Kuchroo, V.K. (2006). Reciprocal developmental pathways for the generation of pathogenic effector TH17 and regulatory T cells. Nature *441*, 235-238.

17. Bie, Q., Zhang, B., Sun, C., Ji, X., Barnie, P.A., Qi, C., Peng, J., Zhang, D., Zheng, D., Su, Z.*, et al.* (2017). IL-17B activated mesenchymal stem cells enhance proliferation and migration of gastric cancer cells. Oncotarget *8*, 18914-18923.

18. Bittner, S., Afzali, A.M., Wiendl, H., and Meuth, S.G. (2014). Myelin oligodendrocyte glycoprotein (MOG35-55) induced experimental autoimmune encephalomyelitis (EAE) in C57BL/6 mice. J Vis Exp.

19. Böhmer, F. (1865). Zur pathologischen, Anatomie der Meningitis cerebromedularis epidemia. Ärztliches Intelligenz-Blatt *12*, 539-550.

20. Brand, S. (2009). Crohn's disease: Th1, Th17 or both? The change of a paradigm: new immunological and genetic insights implicate Th17 cells in the pathogenesis of Crohn's disease. Gut *58*, 1152-1167.

21. Brinkmann, V., Reichard, U., Goosmann, C., Fauler, B., Uhlemann, Y., Weiss, D.S., Weinrauch, Y., and Zychlinsky, A. (2004). Neutrophil extracellular traps kill bacteria. Science *303*, 1532-1535.

22. Brooks, S.P., and Dunnett, S.B. (2009). Tests to assess motor phenotype in mice: a user's guide. Nat Rev Neurosci *10*, 519-529.

23. Burnet, F.M. (1957). A modification of Jerne's theory of antibody production using the concept of clonal selection. Australian Journal Science., 67-69.

24. Campbell, N.A., Reece, J.B., and Urry, L.A. (2015). Campbell Biologie, Vol 10 (Pearson Studium).

25. Cao, Y., Lathia, J.D., Eyler, C.E., Wu, Q., Li, Z., Wang, H., McLendon, R.E., Hjelmeland, A.B., and Rich, J.N. (2010). Erythropoietin Receptor Signaling Through STAT3 Is Required For Glioma Stem Cell Maintenance. Genes Cancer *1*, 50-61.

26. Catala Lopez, J.L., and Fabregas Brouard, M. (2002). [Acanthocyturia is more efficient in to differentiate glomerular from non-glomerular hematuria then dysmorphic erythrocytes]. Arch Esp Urol *55*, 164-166.

27. Chatenoud, L., Ferran, C., Reuter, A., Legendre, C., Gevaert, Y., Kreis, H., Franchimont, P., and Bach, J.F. (1989). Systemic reaction to the anti-T-cell monoclonal antibody OKT3 in relation to serum levels of tumor necrosis factor and interferon-gamma [corrected]. N Engl J Med *320*, 1420-1421.

28. Chen, Q., Ghilardi, N., Wang, H., Baker, T., Xie, M.H., Gurney, A., Grewal, I.S., and de Sauvage, F.J. (2000). Development of Th1-type immune responses requires the type I cytokine receptor TCCR. Nature *407*, 916-920.

29. Chen, S.M., Mukoyama, T., Sato, N., Yamagata, S., Arai, Y., Satoh, N., and Ueda, S. (2002). Induction of nephrotoxic serum nephritis in inbred mice and suppressive effect of colchicine on the development of this nephritis. Pharmacol Res *45*, 319-324.

30. Chen, Y., Chauhan, S.K., Shao, C., Omoto, M., Inomata, T., and Dana, R. (2017). IFN-gamma-Expressing Th17 Cells Are Required for Development of Severe Ocular Surface Autoimmunity. J Immunol *199*, 1163-1169.

31. Chien, A., Edgar, D.B., and Trela, J.M. (1976). Deoxyribonucleic acid polymerase from the extreme thermophile Thermus aquaticus. J Bacteriol *127*, 1550-1557.

32. Chowdhary, V.R., Grande, J.P., Luthra, H.S., and David, C.S. (2007). Characterization of haemorrhagic pulmonary capillaritis: another manifestation of Pristane-induced lupus. Rheumatology (Oxford) *46*, 1405-1410.

33. Chris Cheadle, M.P.V., William J. Freed, Kevin G. Becker (2003). Analysis of Microarray Data Using Z Score Transformation. J Mol Diagn. *5*.

34. Ciofani, M., Madar, A., Galan, C., Sellars, M., Mace, K., Pauli, F., Agarwal, A., Huang, W., Parkhurst, C.N., Muratet, M.*, et al.* (2012). A validated regulatory network for Th17 cell specification. Cell *151*, 289-303.

35. Cochrane, C.G., Unanue, E.R., and Dixon, F.J. (1965). A Role of Polymorphonuclear Leukocytes and Complement in Nephrotoxic Nephritis. J Exp Med *122*, 99-116.

36. Constantinescu, C.S., Farooqi, N., O'Brien, K., and Gran, B. (2011). Experimental autoimmune encephalomyelitis (EAE) as a model for multiple sclerosis (MS). Br J Pharmacol *164*, 1079-1106.

37. Cornelissen, F., van Hamburg, J.P., and Lubberts, E. (2009). The IL-12/IL-23 axis and its role in Th17 cell development, pathology and plasticity in arthritis. Curr Opin Investig Drugs *10*, 452-462.

38. Couper, K.N., Blount, D.G., and Riley, E.M. (2008). IL-10: the master regulator of immunity to infection. J Immunol *180*, 5771-5777.

39. Couser, W.G. (2012). Basic and translational concepts of immune-mediated glomerular diseases. J Am Soc Nephrol *23*, 381-399.

40. Cua, D.J., Sherlock, J., Chen, Y., Murphy, C.A., Joyce, B., Seymour, B., Lucian, L., To, W., Kwan, S., Churakova, T.*, et al.* (2003). Interleukin-23 rather than interleukin-12 is the critical cytokine for autoimmune inflammation of the brain. Nature *421*, 744-748.

41. Cua, D.J., and Tato, C.M. (2010). Innate IL-17-producing cells: the sentinels of the immune system. Nat Rev Immunol *10*, 479-489.

42. Culleton, B.F., Larson, M.G., Parfrey, P.S., Kannel, W.B., and Levy, D. (2000). Proteinuria as a risk factor for cardiovascular disease and mortality in older people: a prospective study. Am J Med *109*, 1-8.

43. Curran, M.A., Geiger, T.L., Montalvo, W., Kim, M., Reiner, S.L., Al-Shamkhani, A., Sun, J.C., and Allison, J.P. (2013). Systemic 4-1BB activation induces a novel T cell phenotype driven by high expression of Eomesodermin. J Exp Med *210*, 743-755.

44. Danilo, M., Chennupati, V., Silva, J.G., Siegert, S., and Held, W. (2018). Suppression of Tcf1 by Inflammatory Cytokines Facilitates Effector CD8 T Cell Differentiation. Cell Rep *22*, 2107-2117.

45. Daugirdas, J.T. (2011). Handbook of CKD Management.

46. Delerive, P., Monte, D., Dubois, G., Trottein, F., Fruchart-Najib, J., Mariani, J., Fruchart, J.C., and Staels, B. (2001). The orphan nuclear receptor ROR alpha is a negative regulator of the inflammatory response. EMBO Rep *2*, 42-48.

47. Dibra, D., Cutrera, J.J., and Li, S. (2012). Coordination between TLR9 signaling in macrophages and CD3 signaling in T cells induces robust expression of IL-30. J Immunol *188*, 3709-3715.

48. Diller, M.L., Kudchadkar, R.R., Delman, K.A., Lawson, D.H., and Ford, M.L. (2016). Balancing Inflammation: The Link between Th17 and Regulatory T Cells. Mediators Inflamm *2016*, 6309219.

49. Disteldorf, E.M., Krebs, C.F., Paust, H.J., Turner, J.E., Nouailles, G., Tittel, A., Meyer-Schwesinger, C., Stege, G., Brix, S., Velden, J.*, et al.* (2015). CXCL5 drives neutrophil recruitment in TH17-mediated GN. J Am Soc Nephrol *26*, 55-66.

50. Djuretic, I.M., Levanon, D., Negreanu, V., Groner, Y., Rao, A., and Ansel, K.M. (2007). Transcription factors T-bet and Runx3 cooperate to activate Ifng and silence Il4 in T helper type 1 cells. Nat Immunol *8*, 145-153.

51. Dobin (2013). STAR: ultrafast universal RNA-seq aligner. Bioinformatics *29*, 15-21.

52. Dolff, S., Witzke, O., and Wilde, B. (2019). Th17 cells in renal inflammation and autoimmunity. Autoimmun Rev *18*, 129-136.

53. Duranton, F., Cohen, G., De Smet, R., Rodriguez, M., Jankowski, J., Vanholder, R., Argiles, A., and European Uremic Toxin Work, G. (2012). Normal and pathologic concentrations of uremic toxins. J Am Soc Nephrol *23*, 1258-1270.

54. Dzhagalov, I., Giguere, V., and He, Y.W. (2004a). Lymphocyte development and function in the absence of retinoic acid-related orphan receptor alpha. J Immunol *173*, 2952-2959.

55. Dzhagalov, I., Zhang, N., and He, Y.W. (2004b). The roles of orphan nuclear receptors in the development and function of the immune system. Cell Mol Immunol *1*, 401-407.

56. Elzi, D.J., Bjornsen, A.J., MacKenzie, T., Wyman, T.H., and Silliman, C.C. (2001). Ionomycin causes activation of p38 and p42/44 mitogen-activated protein kinases in human neutrophils. Am J Physiol Cell Physiol *281*, C350-360.

57. Esplugues, E., Huber, S., Gagliani, N., Hauser, A.E., Town, T., Wan, Y.Y., O'Connor, W., Jr., Rongvaux, A., Van Rooijen, N., Haberman, A.M.*, et al.* (2011). Control of TH17 cells occurs in the small intestine. Nature *475*, 514-518.

58. Ferran, C., Dy, M., Sheehan, K., Merite, S., Schreiber, R., Landais, P., Grau, G., Bluestone, J., Bach, J.F., and Chatenoud, L. (1991). Inter-mouse strain differences in the in vivo anti-CD3 induced cytokine release. Clin Exp Immunol *86*, 537-543.

59. Ferran, C., Sheehan, K., Dy, M., Schreiber, R., Merite, S., Landais, P., Noel, L.H., Grau, G., Bluestone, J., Bach, J.F., and et al. (1990). Cytokine-related syndrome following injection of anti-CD3 monoclonal antibody:

further evidence for transient in vivo T cell activation. Eur J Immunol *20*, 509-515.

60. Fitzgerald, D.C., Zhang, G.X., El-Behi, M., Fonseca-Kelly, Z., Li, H., Yu, S., Saris, C.J., Gran, B., Ciric, B., and Rostami, A. (2007). Suppression of autoimmune inflammation of the central nervous system by interleukin 10 secreted by interleukin 27-stimulated T cells. Nat Immunol *8*, 1372-1379.

61. Fort, M.M., Cheung, J., Yen, D., Li, J., Zurawski, S.M., Lo, S., Menon, S., Clifford, T., Hunte, B., Lesley, R.*, et al.* (2001). IL-25 induces IL-4, IL-5, and IL-13 and Th2-associated pathologies in vivo. Immunity *15*, 985-995.

62. Freitas do Rosario, A.P., Lamb, T., Spence, P., Stephens, R., Lang, A., Roers, A., Muller, W., O'Garra, A., and Langhorne, J. (2012). IL-27 promotes IL-10 production by effector Th1 CD4+ T cells: a critical mechanism for protection from severe immunopathology during malaria infection. J Immunol *188*, 1178-1190.

63. Gaffen, S.L., Jain, R., Garg, A.V., and Cua, D.J. (2014). The IL-23-IL-17 immune axis: from mechanisms to therapeutic testing. Nat Rev Immunol *14*, 585-600.

64. Gagliani, N., Amezcua Vesely, M.C., Iseppon, A., Brockmann, L., Xu, H., Palm, N.W., de Zoete, M.R., Licona-Limon, P., Paiva, R.S., Ching, T.*, et al.* (2015). Th17 cells transdifferentiate into regulatory T cells during resolution of inflammation. Nature *523*, 221-225.

65. Glassock, R.J. (2008). Uremic toxins: what are they? An integrated overview of pathobiology and classification. J Ren Nutr *18*, 2-6.

66. Gooderham, M., Posso-De Los Rios, C.J., Rubio-Gomez, G.A., and Papp, K. (2015). Interleukin-17 (IL-17) inhibitors in the treatment of plaque psoriasis: a review. Skin Therapy Lett *20*, 1-5.

67. Grimm RH Jr, S.K., Kasiske B, Keane WF, Wahi MM. (1997). Proteinuria is a risk factor for mortality over 10 years of follow-up. MRFIT Research Group. Multiple Risk Factor Intervention Trial. Kidney Int Suppl. *63*, 10-14.

68. Gupta, S., and Kaplan, M.J. (2016). The role of neutrophils and NETosis in autoimmune and renal diseases. Nat Rev Nephrol *12*, 402-413.

69. Hall, A.O., Beiting, D.P., Tato, C., John, B., Oldenhove, G., Lombana, C.G., Pritchard, G.H., Silver, J.S., Bouladoux, N., Stumhofer, J.S*., et al.* (2012a). The cytokines interleukin 27 and interferon-gamma promote distinct Treg cell populations required to limit infection-induced pathology. Immunity *37*, 511-523.

70. Hall, A.O., Silver, J.S., and Hunter, C.A. (2012b). The immunobiology of IL-27. Adv Immunol *115*, 1-44.

71. Hammer, D.K., and Dixon, F.J. (1963). Experimental glomerulonephritis. II. Immunologic events in the pathogenesis of nephrotoxic serum nephritis in the rat. J Exp Med *117*, 1019-1034.

72. Harrington, L.E., Hatton, R.D., Mangan, P.R., Turner, H., Murphy, T.L., Murphy, K.M., and Weaver, C.T. (2005). Interleukin 17-producing CD4+ effector T cells develop via a lineage distinct from the T helper type 1 and 2 lineages. Nat Immunol *6*, 1123-1132.

73. Haubitz, M. (2019). [Rapid progressive glomerulonephritis]. Internist (Berl) *60*, 478-484.

74. Hedrick, M.N., Lonsdorf, A.S., Shirakawa, A.K., Richard Lee, C.C., Liao, F., Singh, S.P., Zhang, H.H., Grinberg, A., Love, P.E., Hwang, S.T., and Farber, J.M. (2009). CCR6 is required for IL-23-induced psoriasis-like inflammation in mice. J Clin Invest *119*, 2317-2329.

75. Hirota, K. (2011). Fate mapping of IL-17-producing T cells in inflammatory responses. Nat. Immunol. *12, (255-263)*.

76. Hirota, K., Turner, J.E., Villa, M., Duarte, J.H., Demengeot, J., Steinmetz, O.M., and Stockinger, B. (2013). Plasticity of Th17 cells in Peyer's patches is responsible for the induction of T cell-dependent IgA responses. Nat Immunol *14*, 372-379.

77. Hirota, K., Yoshitomi, H., Hashimoto, M., Maeda, S., Teradaira, S., Sugimoto, N., Yamaguchi, T., Nomura, T., Ito, H., Nakamura, T*., et al.* (2007). Preferential recruitment of CCR6-expressing Th17 cells to inflamed joints via CCL20 in rheumatoid arthritis and its animal model. J Exp Med *204*, 2803-2812.

78. Hirsch, R., Eckhaus, M., Auchincloss, H., Jr., Sachs, D.H., and Bluestone, J.A. (1988). Effects of in vivo administration of anti-T3 monoclonal

antibody on T cell function in mice. I. Immunosuppression of transplantation responses. J Immunol *140*, 3766-3772.

79. Holland, P.M., Abramson, R.D., Watson, R., and Gelfand, D.H. (1991). Detection of specific polymerase chain reaction product by utilizing the 5'----3' exonuclease activity of Thermus aquaticus DNA polymerase. Proc Natl Acad Sci U S A *88*, 7276-7280.

80. Honda, K., and Littman, D.R. (2016). The microbiota in adaptive immune homeostasis and disease. Nature *535*, 75-84.

81. Hoppenbrouwers, T., Autar, A.S.A., Sultan, A.R., Abraham, T.E., van Cappellen, W.A., Houtsmuller, A.B., van Wamel, W.J.B., van Beusekom, H.M.M., van Neck, J.W., and de Maat, M.P.M. (2017). In vitro induction of NETosis: Comprehensive live imaging comparison and systematic review. PLoS One *12*, e0176472.

82. Hori, S., Nomura, T., and Sakaguchi, S. (2003). Control of regulatory T cell development by the transcription factor Foxp3. Science *299*, 1057-1061.

83. Horlad, H., Ma, C., Yano, H., Pan, C., Ohnishi, K., Fujiwara, Y., Endo, S., Kikukawa, Y., Okuno, Y., Matsuoka, M.*, et al.* (2016). An IL-27/Stat3 axis induces expression of programmed cell death 1 ligands (PD-L1/2) on infiltrating macrophages in lymphoma. Cancer Sci *107*, 1696-1704.

84. Hu, G., Cui, K., Fang, D., Hirose, S., Wang, X., Wangsa, D., Jin, W., Ried, T., Liu, P., Zhu, J.*, et al.* (2018). Transformation of Accessible Chromatin and 3D Nucleome Underlies Lineage Commitment of Early T Cells. Immunity *48*, 227-242 e228.

85. Huber, M., Steinwald, V., Guralnik, A., Brustle, A., Kleemann, P., Rosenplanter, C., Decker, T., and Lohoff, M. (2008). IL-27 inhibits the development of regulatory T cells via STAT3. Int Immunol *20*, 223-234.

86. Huber, S., Gagliani, N., Esplugues, E., O'Connor, W., Jr., Huber, F.J., Chaudhry, A., Kamanaka, M., Kobayashi, Y., Booth, C.J., Rudensky, A.Y.*, et al.* (2011). Th17 cells express interleukin-10 receptor and are controlled by Foxp3(-) and Foxp3+ regulatory CD4+ T cells in an interleukin-10-dependent manner. Immunity *34*, 554-565.

87. Huber, S., Gagliani, N., and Flavell, R.A. (2012). Life, death, and miracles: Th17 cells in the intestine. Eur J Immunol *42*, 2238-2245.

88. Hudson, B.G., Reeders, S.T., and Tryggvason, K. (1993). Type IV collagen: structure, gene organization, and role in human diseases. Molecular basis of Goodpasture and Alport syndromes and diffuse leiomyomatosis. J Biol Chem *268*, 26033-26036.

89. Hudson, B.G., Tryggvason, K., Sundaramoorthy, M., and Neilson, E.G. (2003). Alport's syndrome, Goodpasture's syndrome, and type IV collagen. N Engl J Med *348*, 2543-2556.

90. Iijima, K., Sako, M., and Nozu, K. (2017). Rituximab for nephrotic syndrome in children. Clin Exp Nephrol *21*, 193-202.

91. Ishigame, H., Kakuta, S., Nagai, T., Kadoki, M., Nambu, A., Komiyama, Y., Fujikado, N., Tanahashi, Y., Akitsu, A., Kotaki, H.*, et al.* (2009). Differential roles of interleukin-17A and -17F in host defense against mucoepithelial bacterial infection and allergic responses. Immunity *30*, 108-119.

92. Ivanov, II, McKenzie, B.S., Zhou, L., Tadokoro, C.E., Lepelley, A., Lafaille, J.J., Cua, D.J., and Littman, D.R. (2006). The orphan nuclear receptor RORgammat directs the differentiation program of proinflammatory IL-17+ T helper cells. Cell *126*, 1121-1133.

93. Jackson, J.E. (1991). A User's Guide to Principal Components (John Wiley & Sons).

94. Jafari, M., and Ansari-Pour, N. (2019). Why, When and How to Adjust Your P Values? Cell J *20*, 604-607.

95. Jake Lever, M.K., Naomi Altman (2017). Points of Significance - Principal component analysis. Nature Methods *14*, 641-642.

96. James, M.T., Hemmelgarn, B.R., and Tonelli, M. (2010). Early recognition and prevention of chronic kidney disease. Lancet *375*, 1296-1309.

97. Jha, V., Garcia-Garcia, G., Iseki, K., Li, Z., Naicker, S., Plattner, B., Saran, R., Wang, A.Y., and Yang, C.W. (2013). Chronic kidney disease: global dimension and perspectives. Lancet *382*, 260-272.

98. Johnson, J.L., Georgakilas, G., Petrovic, J., Kurachi, M., Cai, S., Harly, C., Pear, W.S., Bhandoola, A., Wherry, E.J., and Vahedi, G. (2018). Lineage-Determining Transcription Factor TCF-1 Initiates the Epigenetic Identity of T Cells. Immunity *48*, 243-257 e210.

99. Jones-Burton, C., Mishra, S.I., Fink, J.C., Brown, J., Gossa, W., Bakris, G.L., and Weir, M.R. (2006). An in-depth review of the evidence linking dietary salt intake and progression of chronic kidney disease. Am J Nephrol *26*, 268-275.

100. Karkar, A. (2018). Infection control guidelines in hemodialysis facilities. Kidney Res Clin Pract *37*, 1-3.

101. Karpuzoglu, E., Phillips, R.A., Gogal, R.M., Jr., and Ansar Ahmed, S. (2007). IFN-gamma-inducing transcription factor, T-bet is upregulated by estrogen in murine splenocytes: role of IL-27 but not IL-12. Mol Immunol *44*, 1808-1814.

102. Kastelein, R.A., Hunter, C.A., and Cua, D.J. (2007). Discovery and biology of IL-23 and IL-27: related but functionally distinct regulators of inflammation. Annu Rev Immunol *25*, 221-242.

103. Kato, L.M., Kawamoto, S., Maruya, M., and Fagarasan, S. (2014). The role of the adaptive immune system in regulation of gut microbiota. Immunol Rev *260*, 67-75.

104. Kessler, B., Rinchai, D., Kewcharoenwong, C., Nithichanon, A., Biggart, R., Hawrylowicz, C.M., Bancroft, G.J., and Lertmemongkolchai, G. (2017). Interleukin 10 inhibits pro-inflammatory cytokine responses and killing of Burkholderia pseudomallei. Sci Rep *7*, 42791.

105. Kim, B.S., Lu, H., Ichiyama, K., Chen, X., Zhang, Y.B., Mistry, N.A., Tanaka, K., Lee, Y.H., Nurieva, R., Zhang, L.*, et al.* (2017). Generation of RORgammat(+) Antigen-Specific T Regulatory 17 Cells from Foxp3(+) Precursors in Autoimmunity. Cell Rep *21*, 195-207.

106. Kim, G., Shinnakasu, R., Saris, C.J., Cheroutre, H., and Kronenberg, M. (2013). A novel role for IL-27 in mediating the survival of activated mouse CD4 T lymphocytes. J Immunol *190*, 1510-1518.

107. Kitching, A.R., and Holdsworth, S.R. (2011). The emergence of TH17 cells as effectors of renal injury. J Am Soc Nephrol *22*, 235-238.

108. Kluger, M.A., Luig, M., Wegscheid, C., Goerke, B., Paust, H.J., Brix, S.R., Yan, I., Mittrucker, H.W., Hagl, B., Renner, E.D.*, et al.* (2014). Stat3 programs Th17-specific regulatory T cells to control GN. J Am Soc Nephrol *25*, 1291-1302.

109. Kobayashi, S., Maesato, K., Moriya, H., Ohtake, T., and Ikeda, T. (2005). Insulin resistance in patients with chronic kidney disease. Am J Kidney Dis *45*, 275-280.

110. Koch, U., and Radtke, F. (2011). Mechanisms of T cell development and transformation. Annu Rev Cell Dev Biol *27*, 539-562.

111. Kohler, H., and Wandel, E. (1993). Acanthocyturia detects glomerular bleeding. Nephrol Dial Transplant *8*, 879.

112. Komada, T., Chung, H., Lau, A., Platnich, J.M., Beck, P.L., Benediktsson, H., Duff, H.J., Jenne, C.N., and Muruve, D.A. (2018). Macrophage Uptake of Necrotic Cell DNA Activates the AIM2 Inflammasome to Regulate a Proinflammatory Phenotype in CKD. J Am Soc Nephrol *29*, 1165-1181.

113. Krebs, C.F., and Panzer, U. (2018). Plasticity and heterogeneity of Th17 in immune-mediated kidney diseases. J Autoimmun *87*, 61-68.

114. Krebs, C.F., Paust, H.J., Krohn, S., Koyro, T., Brix, S.R., Riedel, J.H., Bartsch, P., Wiech, T., Meyer-Schwesinger, C., Huang, J.*, et al.* (2016a). Autoimmune Renal Disease Is Exacerbated by S1P-Receptor-1-Dependent Intestinal Th17 Cell Migration to the Kidney. Immunity *45*, 1078-1092.

115. Krebs, C.F., Schmidt, T., Riedel, J.H., and Panzer, U. (2017). T helper type 17 cells in immune-mediated glomerular disease. Nat Rev Nephrol *13*, 647-659.

116. Krebs, C.F., Turner, J.E., Paust, H.J., Kapffer, S., Koyro, T., Krohn, S., Ufer, F., Friese, M.A., Flavell, R.A., Stockinger, B.*, et al.* (2016b). Plasticity of Th17 Cells in Autoimmune Kidney Diseases. J Immunol *197*, 449-457.

117. Krohn, S., Nies, J.F., Kapffer, S., Schmidt, T., Riedel, J.H., Kaffke, A., Peters, A., Borchers, A., Steinmetz, O.M., Krebs, C.F.*, et al.* (2018). IL-17C/IL-17 Receptor E Signaling in CD4(+) T Cells Promotes TH17 Cell-Driven Glomerular Inflammation. J Am Soc Nephrol *29*, 1210-1222.

118. Kurts, C., Panzer, U., Anders, H.J., and Rees, A.J. (2013). The immune system and kidney disease: basic concepts and clinical implications. Nat Rev Immunol *13*, 738-753.

119. Langrish, C.L., Chen, Y., Blumenschein, W.M., Mattson, J., Basham, B., Sedgwick, J.D., McClanahan, T., Kastelein, R.A., and Cua, D.J. (2005). IL-23 drives a pathogenic T cell population that induces autoimmune inflammation. J Exp Med *201*, 233-240.

120. Laprevotte, E., Cochaud, S., du Manoir, S., Lapierre, M., Dejou, C., Philippe, M., Giustiniani, J., Frewer, K.A., Sanders, A.J., Jiang, W.G.*, et al.* (2017). The IL-17B-IL-17 receptor B pathway promotes resistance to paclitaxel in breast tumors through activation of the ERK1/2 pathway. Oncotarget *8*, 113360-113372.

121. Lawand, M., Dechanet-Merville, J., and Dieu-Nosjean, M.C. (2017). Key Features of Gamma-Delta T-Cell Subsets in Human Diseases and Their Immunotherapeutic Implications. Front Immunol *8*, 761.

122. Lee, A.J., and Ashkar, A.A. (2018). The Dual Nature of Type I and Type II Interferons. Front Immunol *9*, 2061.

123. Leo, O., Foo, M., Sachs, D.H., Samelson, L.E., and Bluestone, J.A. (1987). Identification of a monoclonal antibody specific for a murine T3 polypeptide. Proc Natl Acad Sci U S A *84*, 1374-1378.

124. Lerner, R.A., Glassock, R.J., and Dixon, F.J. (1967). The role of anti-glomerular basement membrane antibody in the pathogenesis of human glomerulonephritis. J Exp Med *126*, 989-1004.

125. Levy, M., Thaiss, C.A., Zeevi, D., Dohnalova, L., Zilberman-Schapira, G., Mahdi, J.A., David, E., Savidor, A., Korem, T., Herzig, Y.*, et al.* (2015). Microbiota-Modulated Metabolites Shape the Intestinal Microenvironment by Regulating NLRP6 Inflammasome Signaling. Cell *163*, 1428-1443.

126. Li, P., Spolski, R., Liao, W., Wang, L., Murphy, T.L., Murphy, K.M., and Leonard, W.J. (2012). BATF-JUN is critical for IRF4-mediated transcription in T cells. Nature *490*, 543-546.

127. Li, W., Titov, A.A., and Morel, L. (2017). An update on lupus animal models. Curr Opin Rheumatol *29*, 434-441.

128. Liabeuf, S., Drueke, T.B., and Massy, Z.A. (2011). Protein-bound uremic toxins: new insight from clinical studies. Toxins (Basel) *3*, 911-919.

129. Liu, J., Guan, X., and Ma, X. (2007). Regulation of IL-27 p28 gene expression in macrophages through MyD88- and interferon-gamma-mediated pathways. J Exp Med *204*, 141-152.

130. Lowry, O.H. (1951). Preotein Measurement ith the Folin Phenol Reagent. The Journal of Biological Chemistry *193, 265-275*.

131. Lu, G., Zhang, X., Shen, L., Qiao, Q., Li, Y., Sun, J., and Zhang, J. (2017). CCL20 secreted from IgA1-stimulated human mesangial cells recruits inflammatory Th17 cells in IgA nephropathy. PLoS One *12*, e0178352.

132. Ma, N., Fang, Y., Xu, R., Zhai, B., Hou, C., Wang, X., Jiang, Z., Wang, L., Liu, Q., Han, G., and Wang, R. (2019). Ebi3 promotes T- and B-cell division and differentiation via STAT3. Mol Immunol *107*, 61-70.

133. Mahmood, T., Puckrin, R., Sugar, L., and Naimark, D. (2018). Staphylococcus-Associated Glomerulonephritis Mimicking Henoch-Schonlein Purpura and Cryoglobulinemic Vasculitis in a Patient With an Epidural Abscess: A Case Report and Brief Review of the Literature. Can J Kidney Health Dis *5*, 2054358118776325.

134. Mangan, P.R., Harrington, L.E., O'Quinn, D.B., Helms, W.S., Bullard, D.C., Elson, C.O., Hatton, R.D., Wahl, S.M., Schoeb, T.R., and Weaver, C.T. (2006). Transforming growth factor-beta induces development of the T(H)17 lineage. Nature *441*, 231-234.

135. Martin, T.L., Mufson, E.J., and Mesulam, M.M. (1984). The light side of horseradish peroxidase histochemistry. J Histochem Cytochem *32*, 793.

136. Matysiak-Scholze, U., and Nehls, M. (1997). The structural integrity of ROR alpha isoforms is mutated in staggerer mice: cerebellar coexpression of ROR alpha1 and ROR alpha4. Genomics *43*, 78-84.

137. McGeachy, M.J., Bak-Jensen, K.S., Chen, Y., Tato, C.M., Blumenschein, W., McClanahan, T., and Cua, D.J. (2007). TGF-beta and IL-6 drive the production of IL-17 and IL-10 by T cells and restrain T(H)-17 cell-mediated pathology. Nat Immunol *8*, 1390-1397.

138. McIntyre, C.W., Harrison, L.E., Eldehni, M.T., Jefferies, H.J., Szeto, C.C., John, S.G., Sigrist, M.K., Burton, J.O., Hothi, D., Korsheed, S.*, et al.* (2011). Circulating endotoxemia: a novel factor in systemic inflammation

and cardiovascular disease in chronic kidney disease. Clin J Am Soc Nephrol *6*, 133-141.

139. McMahon, E.J., Bauer, J.D., Hawley, C.M., Isbel, N.M., Stowasser, M., Johnson, D.W., and Campbell, K.L. (2013). A randomized trial of dietary sodium restriction in CKD. J Am Soc Nephrol *24*, 2096-2103.

140. Meijers, B.K., and Evenepoel, P. (2011). The gut-kidney axis: indoxyl sulfate, p-cresyl sulfate and CKD progression. Nephrol Dial Transplant *26*, 759-761.

141. Meyer Zu Horste, G., Przybylski, D., Schramm, M.A., Wang, C., Schnell, A., Lee, Y., Sobel, R., Regev, A., and Kuchroo, V.K. (2018). Fas Promotes T Helper 17 Cell Differentiation and Inhibits T Helper 1 Cell Development by Binding and Sequestering Transcription Factor STAT1. Immunity *48*, 556-569 e557.

142. Missirlis, P.I., Smailus, D.E., and Holt, R.A. (2006). A high-throughput screen identifying sequence and promiscuity characteristics of the loxP spacer region in Cre-mediated recombination. BMC Genomics *7*, 73.

143. Mittrucker, H.W., Seidel, D., Bland, P.W., Zarzycka, A., Kaufmann, S.H., Visekruna, A., and Steinhoff, U. (2014). Lack of microbiota reduces innate responses and enhances adaptive immunity against Listeria monocytogenes infection. Eur J Immunol *44*, 1710-1715.

144. Molle, C., Nguyen, M., Flamand, V., Renneson, J., Trottein, F., De Wit, D., Willems, F., Goldman, M., and Goriely, S. (2007). IL-27 synthesis induced by TLR ligation critically depends on IFN regulatory factor 3. J Immunol *178*, 7607-7615.

145. Mosmann, T.R., Cherwinski, H., Bond, M.W., Giedlin, M.A., and Coffman, R.L. (1986). Two types of murine helper T cell clone. I. Definition according to profiles of lymphokine activities and secreted proteins. J Immunol *136*, 2348-2357.

146. Mosmann, T.R., and Coffman, R.L. (1989). TH1 and TH2 cells: different patterns of lymphokine secretion lead to different functional properties. Annu Rev Immunol *7*, 145-173.

147. Mosmann, T.R., and Sad, S. (1996). The expanding universe of T-cell subsets: Th1, Th2 and more. Immunol Today *17*, 138-146.

148. Mosser, D.M., and Zhang, X. (2008). Interleukin-10: new perspectives on an old cytokine. Immunol Rev *226*, 205-218.

149. Murphy, C.A., Langrish, C.L., Chen, Y., Blumenschein, W., McClanahan, T., Kastelein, R.A., Sedgwick, J.D., and Cua, D.J. (2003). Divergent pro- and antiinflammatory roles for IL-23 and IL-12 in joint autoimmune inflammation. J Exp Med *198*, 1951-1957.

150. Nakae, S., Nambu, A., Sudo, K., and Iwakura, Y. (2003). Suppression of immune induction of collagen-induced arthritis in IL-17-deficient mice. J Immunol *171*, 6173-6177.

151. Nosko, A., Kluger, M.A., Diefenhardt, P., Melderis, S., Wegscheid, C., Tiegs, G., Stahl, R.A., Panzer, U., and Steinmetz, O.M. (2017). T-Bet Enhances Regulatory T Cell Fitness and Directs Control of Th1 Responses in Crescentic GN. J Am Soc Nephrol *28*, 185-196.

152. Owaki, T., Asakawa, M., Fukai, F., Mizuguchi, J., and Yoshimoto, T. (2006). IL-27 induces Th1 differentiation via p38 MAPK/T-bet- and intercellular adhesion molecule-1/LFA-1/ERK1/2-dependent pathways. J Immunol *177*, 7579-7587.

153. Owaki, T., Asakawa, M., Morishima, N., Mizoguchi, I., Fukai, F., Takeda, K., Mizuguchi, J., and Yoshimoto, T. (2008). STAT3 is indispensable to IL-27-mediated cell proliferation but not to IL-27-induced Th1 differentiation and suppression of proinflammatory cytokine production. J Immunol *180*, 2903-2911.

154. Owyang, A.M., Zaph, C., Wilson, E.H., Guild, K.J., McClanahan, T., Miller, H.R., Cua, D.J., Goldschmidt, M., Hunter, C.A., Kastelein, R.A., and Artis, D. (2006). Interleukin 25 regulates type 2 cytokine-dependent immunity and limits chronic inflammation in the gastrointestinal tract. J Exp Med *203*, 843-849.

155. Pabinger, S., Rodiger, S., Kriegner, A., Vierlinger, K., and Weinhausel, A. (2014). A survey of tools for the analysis of quantitative PCR (qPCR) data. Biomol Detect Quantif *1*, 23-33.

156. Parham, C., Chirica, M., Timans, J., Vaisberg, E., Travis, M., Cheung, J., Pflanz, S., Zhang, R., Singh, K.P., Vega, F.*, et al.* (2002). A receptor for the heterodimeric cytokine IL-23 is composed of IL-12Rbeta1 and a novel cytokine receptor subunit, IL-23R. J Immunol *168*, 5699-5708.

157. Park, H., Li, Z., Yang, X.O., Chang, S.H., Nurieva, R., Wang, Y.H., Wang, Y., Hood, L., Zhu, Z., Tian, Q., and Dong, C. (2005). A distinct lineage of CD4 T cells regulates tissue inflammation by producing interleukin 17. Nat Immunol *6*, 1133-1141.

158. Paust, H.J., Turner, J.E., Steinmetz, O.M., Peters, A., Heymann, F., Holscher, C., Wolf, G., Kurts, C., Mittrucker, H.W., Stahl, R.A., and Panzer, U. (2009). The IL-23/Th17 axis contributes to renal injury in experimental glomerulonephritis. J Am Soc Nephrol *20*, 969-979.

159. Pedchenko, V., Bondar, O., Fogo, A.B., Vanacore, R., Voziyan, P., Kitching, A.R., Wieslander, J., Kashtan, C., Borza, D.B., Neilson, E.G.*, et al.* (2010). Molecular architecture of the Goodpasture autoantigen in anti-GBM nephritis. N Engl J Med *363*, 343-354.

160. Peters, A., Fowler, K.D., Chalmin, F., Merkler, D., Kuchroo, V.K., and Pot, C. (2015). IL-27 Induces Th17 Differentiation in the Absence of STAT1 Signaling. J Immunol *195*, 4144-4153.

161. Pfaffl, M.W. (2004). Real-time RT-PCR: Neue Ansätze zur exakten mRNA Quantifizierung. BIOspektrum *10. Jahrgang*.

162. Pflanz, S., Hibbert, L., Mattson, J., Rosales, R., Vaisberg, E., Bazan, J.F., Phillips, J.H., McClanahan, T.K., de Waal Malefyt, R., and Kastelein, R.A. (2004). WSX-1 and glycoprotein 130 constitute a signal-transducing receptor for IL-27. J Immunol *172*, 2225-2231.

163. Pflanz, S., Timans, J.C., Cheung, J., Rosales, R., Kanzler, H., Gilbert, J., Hibbert, L., Churakova, T., Travis, M., Vaisberg, E.*, et al.* (2002). IL-27, a heterodimeric cytokine composed of EBI3 and p28 protein, induces proliferation of naive CD4+ T cells. Immunity *16*, 779-790.

164. Pirhonen, J., Siren, J., Julkunen, I., and Matikainen, S. (2007). IFN-alpha regulates Toll-like receptor-mediated IL-27 gene expression in human macrophages. J Leukoc Biol *82*, 1185-1192.

165. Pons-Estel, G.J., Alarcon, G.S., Scofield, L., Reinlib, L., and Cooper, G.S. (2010). Understanding the epidemiology and progression of systemic lupus erythematosus. Semin Arthritis Rheum *39*, 257-268.

166. Remijsen, Q., Kuijpers, T.W., Wirawan, E., Lippens, S., Vandenabeele, P., and Vanden Berghe, T. (2011). Dying for a cause: NETosis, mechanisms behind an antimicrobial cell death modality. Cell Death Differ *18*, 581-588.

167. Remoli, M.E., Gafa, V., Giacomini, E., Severa, M., Lande, R., and Coccia, E.M. (2007). IFN-beta modulates the response to TLR stimulation in human DC: involvement of IFN regulatory factor-1 (IRF-1) in IL-27 gene expression. Eur J Immunol *37*, 3499-3508.

168. Reynolds, J.M., Lee, Y.H., Shi, Y., Wang, X., Angkasekwinai, P., Nallaparaju, K.C., Flaherty, S., Chang, S.H., Watarai, H., and Dong, C. (2015). Interleukin-17B Antagonizes Interleukin-25-Mediated Mucosal Inflammation. Immunity *42*, 692-703.

169. Rhen, T., and Cidlowski, J.A. (2005). Antiinflammatory action of glucocorticoids--new mechanisms for old drugs. N Engl J Med *353*, 1711-1723.

170. Riedel, J.H., Paust, H.J., Krohn, S., Turner, J.E., Kluger, M.A., Steinmetz, O.M., Krebs, C.F., Stahl, R.A., and Panzer, U. (2016). IL-17F Promotes Tissue Injury in Autoimmune Kidney Diseases. J Am Soc Nephrol *27*, 3666-3677.

171. Robinson, A.P., Harp, C.T., Noronha, A., and Miller, S.D. (2014). The experimental autoimmune encephalomyelitis (EAE) model of MS: utility for understanding disease pathophysiology and treatment. Handb Clin Neurol *122*, 173-189.

172. Rouvier, E., Luciani, M.F., Mattei, M.G., Denizot, F., and Golstein, P. (1993). CTLA-8, cloned from an activated T cell, bearing AU-rich messenger RNA instability sequences, and homologous to a herpesvirus saimiri gene. J Immunol *150*, 5445-5456.

173. Rugstad, H.E. (1988). Antiinflammatory and immunoregulatory effects of glucocorticoids: mode of action. Scand J Rheumatol Suppl *76*, 257-264.

174. Sakaguchi, S., Sakaguchi, N., Asano, M., Itoh, M., and Toda, M. (1995). Immunologic self-tolerance maintained by activated T cells expressing IL-2 receptor alpha-chains (CD25). Breakdown of a single mechanism of self-tolerance causes various autoimmune diseases. J Immunol *155*, 1151-1164.

175. Salama, A.D., Levy, J.B., Lightstone, L., and Pusey, C.D. (2001). Goodpasture's disease. Lancet *358*, 917-920.

176. Salles, G., Barrett, M., Foa, R., Maurer, J., O'Brien, S., Valente, N., Wenger, M., and Maloney, D.G. (2017). Rituximab in B-Cell Hematologic Malignancies: A Review of 20 Years of Clinical Experience. Adv Ther *34*, 2232-2273.

177. Samoilova, E.B., Horton, J.L., Hilliard, B., Liu, T.S., and Chen, Y. (1998). IL-6-deficient mice are resistant to experimental autoimmune encephalomyelitis: roles of IL-6 in the activation and differentiation of autoreactive T cells. J Immunol *161*, 6480-6486.

178. Sanders, J.S., Rutgers, A., Stegeman, C.A., and Kallenberg, C.G. (2011). Pulmonary: renal syndrome with a focus on anti-GBM disease. Semin Respir Crit Care Med *32*, 328-334.

179. Saran, R., Padilla, R.L., Gillespie, B.W., Heung, M., Hummel, S.L., Derebail, V.K., Pitt, B., Levin, N.W., Zhu, F., Abbas, S.R.*, et al.* (2017). A Randomized Crossover Trial of Dietary Sodium Restriction in Stage 3-4 CKD. Clin J Am Soc Nephrol *12*, 399-407.

180. Schirmer, M., Smeekens, S.P., Vlamakis, H., Jaeger, M., Oosting, M., Franzosa, E.A., Horst, R.T., Jansen, T., Jacobs, L., Bonder, M.J.*, et al.* (2016). Linking the Human Gut Microbiome to Inflammatory Cytokine Production Capacity. Cell *167*, 1897.

181. Self, S. (2009). Goodpasture's 1919 article on the etiology of influenza-the historical road to what we now call Goodpasture Syndrome. Am J Med Sci *338*, 154.

182. Singh, R., Miao, T., Symonds, A.L.J., Omodho, B., Li, S., and Wang, P. (2017). Egr2 and 3 Inhibit T-bet-Mediated IFN-gamma Production in T Cells. J Immunol *198*, 4394-4402.

183. Sprecher, C.A., Grant, F.J., Baumgartner, J.W., Presnell, S.R., Schrader, S.K., Yamagiwa, T., Whitmore, T.E., O'Hara, P.J., and Foster, D.F. (1998). Cloning and characterization of a novel class I cytokine receptor. Biochem Biophys Res Commun *246*, 82-90.

184. Stephen P. McAdoo, C.D.P. (2017). Anti-Glomerular Basement Membrane Disease. *12*, 1162-1172.

185. Stumhofer, J.S., Laurence, A., Wilson, E.H., Huang, E., Tato, C.M., Johnson, L.M., Villarino, A.V., Huang, Q., Yoshimura, A., Sehy, D.*, et al.* (2006). Interleukin 27 negatively regulates the development of interleukin 17-producing T helper cells during chronic inflammation of the central nervous system. Nat Immunol *7*, 937-945.

186. Stumhofer, J.S., Silver, J.S., Laurence, A., Porrett, P.M., Harris, T.H., Turka, L.A., Ernst, M., Saris, C.J., O'Shea, J.J., and Hunter, C.A. (2007). Interleukins 27 and 6 induce STAT3-mediated T cell production of interleukin 10. Nat Immunol *8*, 1363-1371.

187. Summers, S.A., Odobasic, D., Khouri, M.B., Steinmetz, O.M., Yang, Y., Holdsworth, S.R., and Kitching, A.R. (2014). Endogenous interleukin (IL)-17A promotes pristane-induced systemic autoimmunity and lupus nephritis induced by pristane. Clin Exp Immunol *176*, 341-350.

188. Summers, S.A., Steinmetz, O.M., Li, M., Kausman, J.Y., Semple, T., Edgtton, K.L., Borza, D.B., Braley, H., Holdsworth, S.R., and Kitching, A.R. (2009). Th1 and Th17 cells induce proliferative glomerulonephritis. J Am Soc Nephrol *20*, 2518-2524.

189. Sun, M., He, C., Chen, L., Yang, W., Wu, W., Chen, F., Cao, A.T., Yao, S., Dann, S.M., Dhar, T.G.M.*, et al.* (2019). RORgammat Represses IL-10 Production in Th17 Cells To Maintain Their Pathogenicity in Inducing Intestinal Inflammation. J Immunol *202*, 79-92.

190. Takeda, A., Hamano, S., Yamanaka, A., Hanada, T., Ishibashi, T., Mak, T.W., Yoshimura, A., and Yoshida, H. (2003). Cutting edge: role of IL-27/WSX-1 signaling for induction of T-bet through activation of STAT1 during initial Th1 commitment. J Immunol *170*, 4886-4890.

191. Tan, S.C., Carr, C.A., Yeoh, K.K., Schofield, C.J., Davies, K.E., and Clarke, K. (2012). Identification of valid housekeeping genes for quantitative RT-PCR analysis of cardiosphere-derived cells preconditioned

under hypoxia or with prolyl-4-hydroxylase inhibitors. Mol Biol Rep *39*, 4857-4867.

192. Tan, T.G., Sefik, E., Geva-Zatorsky, N., Kua, L., Naskar, D., Teng, F., Pasman, L., Ortiz-Lopez, A., Jupp, R., Wu, H.J.*, et al.* (2016). Identifying species of symbiont bacteria from the human gut that, alone, can induce intestinal Th17 cells in mice. Proc Natl Acad Sci U S A *113*, E8141-E8150.

193. Thaiss, C.A., Zmora, N., Levy, M., and Elinav, E. (2016). The microbiome and innate immunity. Nature *535*, 65-74.

194. Trinchieri, G. (2003). Interleukin-12 and the regulation of innate resistance and adaptive immunity. Nat Rev Immunol *3*, 133-146.

195. Turner, J.E., Krebs, C., Tittel, A.P., Paust, H.J., Meyer-Schwesinger, C., Bennstein, S.B., Steinmetz, O.M., Prinz, I., Magnus, T., Korn, T.*, et al.* (2012). IL-17A production by renal gammadelta T cells promotes kidney injury in crescentic GN. J Am Soc Nephrol *23*, 1486-1495.

196. Turner, J.E., Paust, H.J., Steinmetz, O.M., and Panzer, U. (2010a). The Th17 immune response in renal inflammation. Kidney Int *77*, 1070-1075.

197. Turner, J.E., Paust, H.J., Steinmetz, O.M., Peters, A., Riedel, J.H., Erhardt, A., Wegscheid, C., Velden, J., Fehr, S., Mittrucker, H.W.*, et al.* (2010b). CCR6 recruits regulatory T cells and Th17 cells to the kidney in glomerulonephritis. J Am Soc Nephrol *21*, 974-985.

198. Unanue, E.R., and Dixon, F.J. (1967). Experimental glomerulonephritis: immunological events and pathogenetic mechanisms. Adv Immunol *6*, 1-90.

199. van der Fits, L., Mourits, S., Voerman, J.S., Kant, M., Boon, L., Laman, J.D., Cornelissen, F., Mus, A.M., Florencia, E., Prens, E.P., and Lubberts, E. (2009). Imiquimod-induced psoriasis-like skin inflammation in mice is mediated via the IL-23/IL-17 axis. J Immunol *182*, 5836-5845.

200. Vandecasteele, S.J., Boelaert, J.R., and De Vriese, A.S. (2009). Staphylococcus aureus infections in hemodialysis: what a nephrologist should know. Clin J Am Soc Nephrol *4*, 1388-1400.

201. Vanholder, R., Meert, N., Schepers, E., and Glorieux, G. (2008a). Uremic toxins: do we know enough to explain uremia? Blood Purif *26*, 77-81.

202. Vanholder, R., Van Laecke, S., and Glorieux, G. (2008b). What is new in uremic toxicity? Pediatr Nephrol *23*, 1211-1221.

203. Veldhoen, M., Hocking, R.J., Atkins, C.J., Locksley, R.M., and Stockinger, B. (2006). TGFbeta in the context of an inflammatory cytokine milieu supports de novo differentiation of IL-17-producing T cells. Immunity *24*, 179-189.

204. Villarino, A.V., Larkin, J., 3rd, Saris, C.J., Caton, A.J., Lucas, S., Wong, T., de Sauvage, F.J., and Hunter, C.A. (2005). Positive and negative regulation of the IL-27 receptor during lymphoid cell activation. J Immunol *174*, 7684-7691.

205. Villey, I., de Chasseval, R., and de Villartay, J.P. (1999). RORgammaT, a thymus-specific isoform of the orphan nuclear receptor RORgamma / TOR, is up-regulated by signaling through the pre-T cell receptor and binds to the TEA promoter. Eur J Immunol *29*, 4072-4080.

206. Vladu, M., Clenciu, D., Efrem, I.C., Fortofoiu, M.C., Amzolini, A., Micu, S.T., Mota, M., and Fortofoiu, M. (2017). Insulin Resistance and Chronic Kidney Disease in Patients with Type 1 Diabetes Mellitus. J Nutr Metab *2017*, 6425359.

207. Wang, A., Sun, Y., Liu, X., Su, Z., Li, J., Luo, Y., Chen, S., Wang, J., Li, X., Zhao, Z*., et al.* (2017). Changes in proteinuria and the risk of myocardial infarction in people with diabetes or pre-diabetes: a prospective cohort study. Cardiovasc Diabetol *16*, 104.

208. Wang, R.X., Yu, C.R., Mahdi, R.M., and Egwuagu, C.E. (2012a). Novel IL27p28/IL12p40 cytokine suppressed experimental autoimmune uveitis by inhibiting autoreactive Th1/Th17 cells and promoting expansion of regulatory T cells. J Biol Chem *287*, 36012-36021.

209. Wang, X., Zhang, Y., Yang, X.O., Nurieva, R.I., Chang, S.H., Ojeda, S.S., Kang, H.S., Schluns, K.S., Gui, J., Jetten, A.M., and Dong, C. (2012b). Transcription of Il17 and Il17f is controlled by conserved noncoding sequence 2. Immunity *36*, 23-31.

210. Waring, P., and Mullbacher, A. (1999). Cell death induced by the Fas/Fas ligand pathway and its role in pathology. Immunol Cell Biol *77*, 312-317.

211. Weaver, K.M.C. (2018). Janeway Immunology, Vol 9 (Springer Spektrum).

212. Wesolowski, P., Saracyn, M., Nowak, Z., and Wankowicz, Z. (2010). Insulin resistance as a novel therapeutic target in patients with chronic kidney disease treated with dialysis. Pol Arch Med Wewn *120*, 54-57.

213. Whitman, W.B., Coleman, D.C., and Wiebe, W.J. (1998). Prokaryotes: the unseen majority. Proc Natl Acad Sci U S A *95*, 6578-6583.

214. Wouters, O.J., O'Donoghue, D.J., Ritchie, J., Kanavos, P.G., and Narva, A.S. (2015). Early chronic kidney disease: diagnosis, management and models of care. Nat Rev Nephrol *11*, 491-502.

215. Wu, H.H., Hwang-Verslues, W.W., Lee, W.H., Huang, C.K., Wei, P.C., Chen, C.L., Shew, J.Y., Lee, E.Y., Jeng, Y.M., Tien, Y.W.*, et al.* (2015). Targeting IL-17B-IL-17RB signaling with an anti-IL-17RB antibody blocks pancreatic cancer metastasis by silencing multiple chemokines. J Exp Med *212*, 333-349.

216. Yang, B.H., Wang, K., Wan, S., Liang, Y., Yuan, X., Dong, Y., Cho, S., Xu, W., Jepsen, K., Feng, G.S.*, et al.* (2019). TCF1 and LEF1 Control Treg Competitive Survival and Tfr Development to Prevent Autoimmune Diseases. Cell Rep *27*, 3629-3645 e3626.

217. Yang, X.O., Panopoulos, A.D., Nurieva, R., Chang, S.H., Wang, D., Watowich, S.S., and Dong, C. (2007). STAT3 regulates cytokine-mediated generation of inflammatory helper T cells. J Biol Chem *282*, 9358-9363.

218. Yang, Y.F., Lee, Y.C., Lo, S., Chung, Y.N., Hsieh, Y.C., Chiu, W.C., and Yuan, S.F. (2018). A positive feedback loop of IL-17B-IL-17RB activates ERK/beta-catenin to promote lung cancer metastasis. Cancer Lett *422*, 44-55.

219. Yao, Z., Fanslow, W.C., Seldin, M.F., Rousseau, A.M., Painter, S.L., Comeau, M.R., Cohen, J.I., and Spriggs, M.K. (1995a). Herpesvirus

Saimiri encodes a new cytokine, IL-17, which binds to a novel cytokine receptor. Immunity *3*, 811-821.

220. Yao, Z., Painter, S.L., Fanslow, W.C., Ulrich, D., Macduff, B.M., Spriggs, M.K., and Armitage, R.J. (1995b). Human IL-17: a novel cytokine derived from T cells. J Immunol *155*, 5483-5486.

221. Yasuda, K., Takeuchi, Y., and Hirota, K. (2019). The pathogenicity of Th17 cells in autoimmune diseases. Semin Immunopathol *41*, 283-297.

222. Yavuz, A., Tetta, C., Ersoy, F.F., D'Intini, V., Ratanarat, R., De Cal, M., Bonello, M., Bordoni, V., Salvatori, G., Andrikos, E.*, et al.* (2005). Uremic toxins: a new focus on an old subject. Semin Dial *18*, 203-211.

223. Yoshida, H., and Hunter, C.A. (2015). The immunobiology of interleukin-27. Annu Rev Immunol *33*, 417-443.

224. Yoshida, H., and Miyazaki, Y. (2008). Regulation of immune responses by interleukin-27. Immunol Rev *226*, 234-247.

225. Yoshimura, T., Takeda, A., Hamano, S., Miyazaki, Y., Kinjyo, I., Ishibashi, T., Yoshimura, A., and Yoshida, H. (2006). Two-sided roles of IL-27: induction of Th1 differentiation on naive CD4+ T cells versus suppression of proinflammatory cytokine production including IL-23-induced IL-17 on activated CD4+ T cells partially through STAT3-dependent mechanism. J Immunol *177*, 5377-5385.

226. Zhang, J., He, Z., Sen, S., Wang, F., Zhang, Q., and Sun, Z. (2018). TCF-1 Inhibits IL-17 Gene Expression To Restrain Th17 Immunity in a Stage-Specific Manner. J Immunol *200*, 3397-3406.

227. Zhao, C.B., Coons, S.W., Cui, M., Shi, F.D., Vollmer, T.L., Ma, C.Y., Kuniyoshi, S.M., and Shi, J. (2008). A new EAE model of brain demyelination induced by intracerebroventricular pertussis toxin. Biochem Biophys Res Commun *370*, 16-21.

228. Zhu, J., and Paul, W.E. (2010). Peripheral CD4+ T-cell differentiation regulated by networks of cytokines and transcription factors. Immunol Rev *238*, 247-262.

229. Zuniga-Pflucker, J.C. (2004). T-cell development made simple. Nat Rev Immunol *4*, 67-72.

Figure reference:

Credit to **Figure 6**, **A**: “The-Crankshaft Publishing’s web site”,
http://what-when-how.com/acp-medicine/glomerular-diseases-part-3/
last request: October 04, 2019

Used (Gene) data banks:

PubMed, www.ncbi.nlm.ih.gov, last request: October 04, 2019

PubMed gene www.ncbi.nlm.ih.gov/gene, last request: October 04, 2019

GeneCards www.genecards.org, last request: October 04, 2019

OMIM www.omim.org, last request: October 04, 2019

The Human Protein Atlas www.proteinatlas.org, last request: October 04, 2019

ENSEMBL www.ensembl.org, last request: October 04, 2019

UniProt www.uniprot.org, last request: October 04, 2019

Auflistung der verwendeten Gefahrenstoffe nach GHS

(Gefahrensymbole, H- und P-Sätze)

Substanz	CAS-Nummer	GHS-Gefahrenstoffkennzeichnung	H- und P-Sätze
Dithtiothreitol (DTT)	3483-2-3	 Reizend	H: 302-315-319-335 P: 261 305+351+338
Eosin	17372-87-1	 Reizend	H: 319 P: 319- 305+351+338
Ethanol (EtOH)	64-17-5	 Brandfördernd  Reizend	H: 225-319 P: 210-240 305+351+338 403+33
Ethidiumbromid (EtBr)	1239-45-8	 Giftig  Gesundheitsschädlich	H 302-330-341 P: 201-260-280
Ethylendiamin-tetraessisgsäure (EDTA)	60-00-5	 Reizend	H: 319 P: 305+351+338
Hämatoxylin	51728-2	 Reizend	H: 302-315-319-355 P: 261- 305+351+338

m-Xylol **(C_8H_{10})**	95-47-6	 Brandfördernd  Gesundheitsschädlich  Reizend	H: 226-304 312+332 315-319 335-412 P: 210-261-273 301+310 302+352 312-331
Octylphenoxy-polyethoxyethanol **(*IGEPAL CA-630, NP-40*)**	9002-93-1	 Reizend  Ätzend  Gewässergefährdend	H: 302-315-318-410 P: 280 301+312+330- 305+351+338+310
Paraformaldehyd **(PFA)**	30525-89-4	 Brandfördernd  Gesundheitsschädlich  Ätzend  Reizend	H: 228-351-302-322-315-319-317-335 P: 210-261-280 305+351+338

Periodsäure (H_5IO_6)	10450-60-9	 Brandfördernd  Ätzend	H: 271-314 P: 210-211 301+330+331 305+351+338 309+310
Pristan (2,6,10,14-Tetramethyl-pentadekan)	1921-70-6	 Reizend	H: 315-319 P: 305+351+338
Schwefelsäure (H_2SO_4)	7664-93-9	 Ätzend	H: 290 314 P: 280 301+330+331 305+351+338 308+310
Trypanblau ($C_{34}H_{28}N_6O_{14}S_4$)	72-57-1	 Gesundheitsschädlich	H: 350 P: 201 308+313

Acknowledgements

First of all, I want to express my gratitude to my doctoral supervisor PD Dr. Christian F. Krebs and to Prof. Dr. Samuel Huber, who gave me the opportunity to work on this very interesting T_H17-related topic. I am very grateful for their scientific support and helpful critique.
I would like to thank Prof. Dr. Samuel Huber and Prof. Dr. Wolfram Brune for being reviewer of my dissertation.

My sincere thanks also go to the *Deutsche Forschungsgemeinschaft* (DFG) for financing this project as part of the *Sonderforschungsbereich* 1192 (Special research project, SFB 1192).

I want to acknowledge Prof. Dr. Michael Kobe, Prof. Dr. Samuel Huber and PD Dr. Markus Perbandt for being members of the board of examination during my disputation.

For histological pictures, I want to thank Prof. Dr. Thorsten Wiech.

For practical help, I am very grateful to the UKE *FACS Core Facility* and Dr. Hans-Joachim Paust (CBA), especially for helping me with very frustrating pSTAT3 experiments. Furthermore I want to thank Patricia (*S.aureus* experiments), Alina (genotyping), Christoph (RNA sequencing data processing), AG Binder (*Quibit*) and AG Panzer for providing RNA samples for NTN time kinetic and other reagents, kits and consumables (Anette + “Ha-Jo”).

My sincere thanks also go to my sister Jacqueline for her professional help with graphic design, as well as to my first and best ever chemistry school teacher, Dr. Schwarz, who triggered my interest in this subject, leading the way to this thesis.

Least but for sure not last, my **VERY** hearty thanks go to Ning Song, Dr. Anna Reinicke Vogt, Anja-Michaela Oschwald and my whole family for their helpful critique, continuous support in bright and dark times and very delightful discussions. - I will never forget.